Probing Physics Beyond Standard Model with Atomic and Molecular Phenomena

University of New South Wales

Hoang Bao Tran Tan
Supervisors: V. V. Flambaum and J. B. Berengut

April 22, 2021

🎓 Welcome to the Research Alumni Portal, Hoang Bao Tran Tan!

You will be able to download the finalised version of all thesis submissions that were processed in GRIS here.

Please ensure to include the **completed declaration** (from the Declarations tab), your **completed Inclusion of Publications Statement** (from the Inclusion of Publications Statement tab) in the final version of your thesis that you submit to the Library.

Information on how to submit the final copies of your thesis to the Library is available in the completion email sent to you by the GRS.

Thesis submission for the degree of Doctor of Philosophy

Thesis Title and Abstract | **Declarations** | **Inclusion of Publications Statement** | **Corrected Thesis and Responses**

Thesis Title

Probing Physics Beyond Standard Model with Atomic and Molecular Phenomena

Thesis Abstract

Despite its success, the Standard Model is unable to explain, for example, the nature of dark matter, which is five times more abundant than normal matter, or the matter-antimatter asymmetry, which is essential for the existence of our world. Research beyond the Standard Model to describe these phenomena has thus been at the forefront of modern physics.

The direct detection of dark matter is fundamentally problematic because its coupling to normal matter is extremely weak and because its mass is unknown, the former implies that experiments searching for dark matter must have extraordinary sensitivity and the latter means that they must scan a very large energy bandwidth. As a result, there has been no definite report of direct dark matter detection.

In this thesis, I explore several mechanisms which may enhance the dark–normal matter interactions, including axion–photon interference, dark photon–photon interference and coherent axion–photon transformation in media. These mechanisms have a common feature that the dark matter signal is linear in the small couplings to normal matter, thus offering a significant improvement over conventional searches, whose signals are quadratic in these couplings. By analysing these effects, I derived independent bounds on the dark–normal matter interactions which are comparable to or better than existing limits.

Important to explaining the matter–antimatter asymmetry is the existence of CP-odd interactions, which are often searched for in the form of elementary particles' electric dipole moments (EDMs). Among these searches are experiments on nuclear EDMs, which provide information about the nucleon EDMs and CP-odd internucleon forces. However, the EDM of an atomic or molecular nucleus is screened from static external electric fields, making it difficult to measure.

I demonstrated that oscillating electric fields are not screened and may thus be used to measure nuclear EDMs. I also considered the effects of dark-matter-induced oscillating nuclear EDMs which include measurable oscillating atomic and molecular EDMs and atomic and molecular transitions. In addition, considering the mixed electric and magnetic interaction between the nucleus and the electrons, I calculated new contributions to the static EDM of atoms and molecules induced by nucleon EDMs and CP-odd internucleon forces. Comparison of these new contributions with existing limits on molecular EDMs yielded independent bounds on hadronic CP-violating parameters.

🎓 Welcome to the Research Alumni Portal, Hoang Bao Tran Tan!

You will be able to download the finalised version of all thesis submissions that were processed in GRIS here.

Please ensure to include the **completed declaration** (from the Declarations tab), your **completed Inclusion of Publications Statement** (from the Inclusion of Publications Statement tab) in the final version of your thesis that you submit to the Library.

Information on how to submit the final copies of your thesis to the Library is available in the completion email sent to you by the GRS.

Thesis submission for the degree of Doctor of Philosophy

Thesis Title and Abstract | **Declarations** | **Inclusion of Publications Statement**

Corrected Thesis and Responses

ORIGINALITY STATEMENT

☑ I hereby declare that this submission is my own work and to the best of my knowledge it contains no materials previously published or written by another person, or substantial proportions of material which have been accepted for the award of any other degree or diploma at UNSW or any other educational institution, except where due acknowledgement is made in the thesis. Any contribution made to the research by others, with whom I have worked at UNSW or elsewhere, is explicitly acknowledged in the thesis. I also declare that the intellectual content of this thesis is the product of my own work, except to the extent that assistance from others in the project's design and conception or in style, presentation and linguistic expression is acknowledged.

COPYRIGHT STATEMENT

☑ I hereby grant the University of New South Wales or its agents a non-exclusive licence to archive and to make available (including to members of the public) my thesis or dissertation in whole or part in the University libraries in all forms of media, now or here after known. I acknowledge that I retain all intellectual property rights which subsist in my thesis or dissertation, such as copyright and patent rights, subject to applicable law. I also retain the right to use all or part of my thesis or dissertation in future works (such as articles or books).

For any substantial portions of copyright material used in this thesis, written permission for use has been obtained, or the copyright material is removed from the final public version of the thesis.

AUTHENTICITY STATEMENT

☑ I certify that the Library deposit digital copy is a direct equivalent of the final officially approved version of my thesis.

🎓 Welcome to the Research Alumni Portal, Hoang Bao Tran Tan!

You will be able to download the finalised version of all thesis submissions that were processed in GRIS here.

Please ensure to include the **completed declaration** (from the Declarations tab), your **completed Inclusion of Publications Statement** (from the Inclusion of Publications Statement tab) in the final version of your thesis that you submit to the Library.

Information on how to submit the final copies of your thesis to the Library is available in the completion email sent to you by the GRS.

Thesis submission for the degree of Doctor of Philosophy

Thesis Title and Abstract | **Declarations** | **Inclusion of Publications Statement**

Corrected Thesis and Responses

UNSW is supportive of candidates publishing their research results during their candidature as detailed in the UNSW Thesis Examination Procedure.

Publications can be used in the candidate's thesis in lieu of a Chapter provided:

- The candidate contributed **greater than 50%** of the content in the publication and are the "primary author", i.e. they were responsible primarily for the planning, execution and preparation of the work for publication.
- The candidate has obtained approval to include the publication in their thesis in lieu of a Chapter from their Supervisor and Postgraduate Coordinator.
- The publication is not subject to any obligations or contractual agreements with a third party that would constrain its inclusion in the thesis.

☑ The candidate has declared that **their thesis has publications - either published or submitted for publication - incorporated into it in lieu of a Chapter/s. Details of these publications are provided below.**.

Publication Details #1

Full Title:	Interference-assisted resonant detection of axions
Authors:	V. V. Flambaum, I. B. Samsonov, H. B. Tran Tan, Y. V. Stadnik and D. Budker
Journal or Book Name:	Physics of the Dark Universe
Volume/Page Numbers:	24/100272
Date Accepted/Published:	March 2019
Status:	submitted

The Candidate's Contribution to the Work:	The candidate is a primary author of the work and contributed more than 50% of it. The candidate performed all the calculations and analyses presented in the work. The candidate was responsible for preparing the manuscript.
Location of the work in the thesis and/or how the work is incorporated in the thesis:	The work in presented in Chapter 2 of the Thesis.

Publication Details #2

Full Title:	Coherent axion-photon transformations in the forward scattering on atoms
Authors:	V. V. Flambaum, I. B. Samsonov, H. B. Tran Tan and D. Budker
Journal or Book Name:	Physical Review D
Volume/Page Numbers:	98/095028
Date Accepted/Published:	November 2018
Status:	published
The Candidate's Contribution to the Work:	The candidate is a primary author of the work and contributed more than 50% of it. The candidate performed all the calculations and analyses presented in the work.
Location of the work in the thesis and/or how the work is incorporated in the thesis:	The work in presented in Chapter 3 of the Thesis.

Publication Details #3

Full Title:	Screening and enhancement of an oscillating electric field in molecules
Authors:	H. B. Tran Tan, V. V. Flambaum and I. B. Samsonov
Journal or Book Name:	Physical Review A
Volume/Page Numbers:	99/013430
Date Accepted/Published:	January 2019
Status:	published
The Candidate's Contribution to the Work:	The candidate is a primary author of the work and contributed more than 50% of it. The candidate performed all the calculations and analyses presented in the work. The candidate was responsible for preparing the manuscript.

Location of the work in the thesis and/or how the work is incorporated in the thesis:	The work in presented in Chapter 4 of the Thesis.

Publication Details #4

Full Title:	Oscillating nuclear electric dipole moment induced by axion dark matter produces atomic and molecular EDM
Authors:	V. V. Flambaum and H. B. Tran Tan
Journal or Book Name:	Physical Review D
Volume/Page Numbers:	100/111301(R)
Date Accepted/Published:	December 2019
Status:	published
The Candidate's Contribution to the Work:	The candidate is a primary author of the work and contributed more than 50% of it. The candidate performed all the calculations and analyses presented in the work. The candidate was responsible for preparing the manuscript.
Location of the work in the thesis and/or how the work is incorporated in the thesis:	The work in presented in Chapter 5 of the Thesis.

Publication Details #5

Full Title:	Atomic and molecular transitions induced by axions via oscillating nuclear moments
Authors:	V. V. Flambaum, H. B. Tran Tan, D. Budker and A. Wickenbrock
Journal or Book Name:	Physical Review D
Volume/Page Numbers:	101/073004
Date Accepted/Published:	April 2020
Status:	published
The Candidate's Contribution to the Work:	The candidate is a primary author of the work and contributed more than 50% of it. The candidate performed all the calculations and analyses presented in the work. The candidate was responsible for preparing the manuscript.
Location of the work in the thesis and/or how the work is incorporated in the thesis:	The work in presented in Chapter 6 of the Thesis.

Publication Details #6

Full Title:	Limits on CP-violating hadronic interactions and proton EDM from paramagnetic molecules
Authors:	V. V. Flambaum, I. B. Samsonov and H. B. Tran Tan
Journal or Book Name:	Journal of High Energy Physics
Volume/Page Numbers:	2020/77
Date Accepted/Published:	October 2020
Status:	published
The Candidate's Contribution to the Work:	The candidate is a primary author of the work and contributed more than 50% of it. The candidate performed all the calculations and analyses presented in the work. The candidate was responsible for preparing the manuscript.
Location of the work in the thesis and/or how the work is incorporated in the thesis:	The work in presented in Chapter 7 of the Thesis.

Publication Details #7

Full Title:	Effects of CP-violating internucleon interactions in paramagnetic molecules
Authors:	V. V. Flambaum, I. B. Samsonov and H. B. Tran Tan
Journal or Book Name:	Physical Review D
Volume/Page Numbers:	102/115036
Date Accepted/Published:	December 2020
Status:	published
The Candidate's Contribution to the Work:	The candidate is a primary author of the work and contributed more than 50% of it. The candidate performed all the calculations and analyses presented in the work. The candidate was responsible for preparing the manuscript.
Location of the work in the thesis and/or how the work is incorporated in the thesis:	The work in presented in Chapter 8 of the Thesis.

Publication Details #8

Full Title:	Time- and parity-violating effects of nuclear Schiff moment in molecules and solids
Authors:	V. V. Flambaum, V. A. Dzuba and H. B. Tran Tan,
Journal or Book Name:	Physical Review A

Volume/Page Numbers:	101/042501
Date Accepted/Published:	April 2020
Status:	published
The Candidate's Contribution to the Work:	The candidate is a primary author of the work and contributed more than 50% of it. The candidate performed the analytical calculations and analyses presented in the work. The candidate was responsible for preparing the manuscript.
Location of the work in the thesis and/or how the work is incorporated in the thesis:	The work in presented in Chapter 9 of the Thesis.

Candidate's Declaration

I confirm that where I have used a publication in lieu of a chapter, the listed publication(s) above meet(s) the requirements to be included in the thesis. I also declare that I have complied with the Thesis Examination Procedure.

Abstract

Despite its success, the Standard Model is unable to explain the nature of dark matter, which is five times more abundant than normal matter and the matter-antimatter asymmetry, which is essential for the existence of our world. Research beyond the Standard Model to describe these phenomena has thus been at the forefront of modern physics.

The direct detection of dark matter is fundamentally problematic because its coupling to normal matter is extremely weak and because its mass is unknown. The former implies that experiments searching for dark matter must have extraordinary sensitivity and the latter means that they must scan a very large energy bandwidth. As a result, there has been no definite report of direct dark matter detection.

In this thesis, I explore several mechanisms which may enhance the probability of detecting DM. Such mechanisms include axion-photon interference, dark photon-photon interference and coherent axion-photon transformation in media. These approaches have a common feature that the dark matter signal is linear in the small couplings to normal matter, thus offering a significant improvement over conventional searches, whose signals are quadratic in these couplings. By analysing these effects, I derived independent bounds on the dark-normal matter interactions which are comparable to or better than existing limits.

Important to explaining the matter-antimatter asymmetry is the existence of CP-odd interactions, which manifest themselves in the form of elementary particles' electric dipole moments (EDMs). Among these searches are experiments on nuclear EDMs, which provide information about the nucleon EDMs and CP-odd internucleon forces. However, the EDM of an atomic or molecular nucleus is screened from static external electric fields, making it difficult to measure.

I demonstrated that oscillating electric fields are only partially screened and may thus be used to measure nuclear EDMs. I also considered the effects of dark-matter-induced oscillating nuclear EDMs which include measurable oscillating atomic and molecular EDMs and atomic and molecular transitions. In addition, considering the mixed electric and magnetic interaction between the nucleus and the electrons, I calculated new contributions to the static EDM of atoms and molecules induced by nucleon EDMs and CP-odd internucleon forces. Comparison of these new contributions with existing limits on molecular EDMs yields independent bounds on hadronic CP-violating parameters.

List of publications

Below, I present the list of my publications written during the course of my Ph.D. studies. List of authors is usually alphabetical among UNSW co-authors in accord with a particle theory tradition.

Refereed publications

1. V. V. Flambaum, I. B. Samsonov and H. B. Tran Tan
   Effects CP-violating internucleon interactions in paramagnetic molecules
   Phys. Rev. D 102, 115036 (2020), DOI: 10.1103/PhysRevD.102.115036, arXiv:2009.07992

2. V. V. Flambaum, I. B. Samsonov and H. B. Tran Tan
   Limits on CP-violating hadronic interactions and proton EDM from paramagnetic molecules
   J. High Energ. Phys. 2020, 77 (2020), DOI: 10.1007/JHEP10(2020)077, arXiv:2004.10359

3. V. V. Flambaum, V. A. Dzuba and H. B. Tran Tan
   Time- and parity-violating effects of nuclear Schiff moment in molecules and solids
   Phys. Rev. A **101**, 042501 (2020), DOI: 10.1103/PhysRevA.101.042501, arXiv:1912.10620

4. V. V. Flambaum, H. B. Tran Tan, D. Budker and A. Wickenbrock
   Atomic and molecular transitions induced by axions via oscillating nuclear moments
   Phys. Rev. D **101**, 073004 (2020), DOI: 10.1103/PhysRevD.101.073004, arXiv:1910.07705

5. V. V. Flambaum and H. B. Tran Tan
   Oscillating nuclear electric dipole moment induced by axion dark matter produces atomic and molecular EDM
   Phys. Rev. D 100, 111301(R) (2019), DOI: 10.1103/PhysRevD.100.111301, arXiv:1904.07609

6. H. B. Tran Tan, V. V. Flambaum and I. B. Samsonov
   Screening and enhancement of an oscillating electric field in molecules
   Phys. Rev. A 99, 013430 (2019), DOI: 10.1103/PhysRevA.99.013430, arXiv:1812.03312

7. V. V. Flambaum, I. B. Samsonov and H. B. Tran Tan
   Interference-assisted detection of dark photon using atomic transitions
   Phys. Rev. D 99, 115019 (2019), DOI: 10.1103/PhysRevD.99.115019, arXiv:1904.02271

8. V. V. Flambaum, I. B. Samsonov, H. B. Tran Tan, Y. V. Stadnik and D. Budker
   Interference-assisted resonant detection of axions
   Phys. Dark Universe 24, 100272 (2019), DOI: 10.1016/j.dark.2019.100272, arXiv:1803.09388

9. V. V. Flambaum, I. B. Samsonov, H. B. Tran Tan and D. Budker
   Coherent axion-photon transformations in the forward scattering on atoms
   Phys. Rev. D 98, 095028 (2018), DOI: 10.1103/PhysRevD.98.095028, arXiv:1805.01793

Review papers

1. V. V. Flambaum, I. B. Samsonov, H. B. Tran Tan, Y. V. Stadnik and D. Budker
   Resonant detection and production of axions with atoms
   Int. J. Mod. Phys. A **33**, 31, 1844030 (2018), DOI: 10.1142/S0217751X1844030X

Submitted papers and preprints

1. V. V. Flambaum, I. B. Samsonov, H. B. Tran Tan and A. V. Viatkina
   Nuclear polarization effects in atoms and ions
   Submitted to Phys. Rev. A, January 2021

2. H. B. Tran Tan, V. V. Flambaum and J. C. Berengut
   Dark Matter near gravitating bodies
   arXiv:1808.01856v1

List of presentations

Below I present the list of my presentation at international and national conferences, workshops and competitions during the course of my Ph.D. studies.

1. **Searching for Axions and Axionic Dark Matter with Interference and Axion-induced Nuclear Moments**, TeV Particle Astrophysics Conference, University of Sydney, Sydney, Australia, December 2019

2. **Screening and Enhancement of Nuclear Electric Dipole Moments Induced by Axionic Dark Matter**, Frontiers in Quantum Matter Workshop: Electric Dipole Moments, Australian National University, Canberra, Australia, November 2019

3. **Effects of Dark Matter in atomic and molecular phenomena**, Australian Institute of Physics Postgraduate Presentation Competition, University of Technology Sydney, Sydney, Australia, October 2019

4. **Coherent axion-photon transformations in the forward scattering on atoms**, Quantum Technologies for Axion Dark Matter Detection Incubator, University of Sydney, Sydney, Australia, September 2018

5. **Detection of Axions Using Atomic Transitions Induced by Interference between Electromagnetic and Axion Fields**, Australian Institute of Physics Summer Meeting, University of New South Wales, Sydney, Australia, December 2017

Acknowledgements

As I was writing the last sentences of my thesis, a realization started to come to me that another important stage of my life was drawing to its end and that I was about to leave the institution where I have stayed for more than seven years. Such a moment inevitably engenders certain emotional ambiguity and personal ambivalence. While I was honoured by the cause of my departure, I was saddened by the fact of it. While I was excited about the new horizon that had just appeared to me, I still wanted to spend more time among the people whom I have held so dear.

In particular, I was saddened by having to leave the tutelage of a teacher without parallel in my experience. To me, Prof. Victor Flambaum has been a constant source of immeasurable knowledge, profound wisdom and everlasting inspiration. Above all, he is a true leader who knows instinctively what to do and how to achieve it. I am deeply grateful to him for imparting to me his knowledge and his way of thinking.

I would also like to thank my co-supervisor Prof Julian Berengut for his support, availability and constructive suggestions, which were determinant for the accomplishment of the work presented in this thesis.

I thank all of my co-authors, with whom I have worked on many interesting problems: Dmitry Budker, Vladimir Dzuba, Igor Samsonov, Yevgeny Stadnik and Arne Wickenbrock. Igor Samsonov is especially acknowledged for very fruitful collaborations, numerous comments and discussions and comprehensive support during my study. I am also grateful to Oleg Sushkov for many useful discussions and for his kind interest in my research.

Contents

Chapter 1

Introduction

1.1 Axion as a Dark Matter candidate

In the 1930s, Zwicky [1, 2] used the observational values for the velocities of the galaxies near the edge of the Coma Cluster to estimate the cluster's mass. He obtained a result which was some 400 times larger than the estimate based on the cluster's luminosity. This striking discrepancy led Zwicky to speculate that most of the matter in the Coma Cluster were non-luminous and existed in a form theretofore unknown. Zwicky called this new type of matter Dark Matter (DM). Zwicky's result was confirmed in several more detailed analyses performed in the 1970s by Rubin, Ford and Freeman [3, 4], who found that the orbital velocities v of galactic stars remain constant at large distances r from the galactic center, as oppose to the Kepplerian behaviour $v \sim 1/\sqrt{r}$, indicating a galactic mass distribution substantially different from its luminous profile. Further observations pointing to the existence of DM include gravitational lensing observations of the Bullet Cluster [5–7], angular fluctuations in the cosmic microwave background spectrum [8] and the need for non-baryonic matter to explain the observed structure formation of the universe [9]. Evidences from these observations also indicated that DM interacts very weakly with itself and with normal matters. It is this fact which makes the empirical discovery of DM difficult, with most detection schemes consistently giving null results.

As the existence of DM was becoming a widely accepted fact, possible answers to the questions about its nature and composition were being explored. Initially, it was thought that the Standard Model (SM) neutrino, which is known to exist and is essentially collisionless, could be unknown DM. It was quickly realized, however, that relic neutrinos abundance is not enough to account for the observed DM density. Subsequently, different non-SM candidates for DM have been proposed, including, for example, the sterile neutrinos, the gravitinos, the weakly interacting massive particles (WIMPs) and the axions, etc (for comprehensive reviews on the motivations, production mechanisms, properties and possible detection methods for these candidates, see Refs. [9, 10]).

In recent years, the axion has emerged as the object of increasing theoretical and experimental interest, with new methods being proposed to search for it in laboratories around the world. In chapters 2 and 3, I discuss two such proposals. The first one, interference-assisted resonant detection of axions, allows one to achieve axion signals which are linear in the small coupling constants to SM matter, in contrast with the signals of conventional axion searches which are quadratic or quartic in those coupling constants. The second proposal proposal, coherent axion-photon transformations in the forward scattering on atoms, allows one to measure directly the axion-electron coupling constant.

In the rest of this section, I will briefly describe the axion and its candidacy as DM.

1.1.1 The strong CP problem and the axion

The Quantum Chromodynamics (QCD) Lagrangian contains a parity (P)- and charge-parity(CP)-violating term

$$\bar{\theta}\frac{g^2}{32\pi^2}G^{a\mu\nu}\tilde{G}^a_{\mu\nu}\,, \tag{1.1}$$

where $\bar{\theta}$ is the QCD vacuum angle related to the amount of CP-violation, $g^2/4\pi$ is the strong coupling constant, $G^a_{\mu\nu}$ and $\tilde{G}^a_{\mu\nu} = \frac{1}{2}\varepsilon_{\mu\nu\rho\sigma}G^{a\rho\sigma}$ are the gluon field strengths and its dual and $a = 1, 2, ..., 8$ is the color index. In principle, $\bar{\theta}$ can take any value in the range $-\pi \leq \bar{\theta} \leq \pi$.

It is a well-known fact that the Standard Model is invariant under the combined charge, parity and time reversal (CPT) symmetry. An electric dipole moment (EDM) of an elementary particle violates both P-and T-symmetries and therefore violates also the CP-symmetry (see Sect. 1.2.1 for further details). As a result, measurements of these EDMs provide knowledge of the amount of CP-violation in QCD. Indeed, the term (1.1) gives rise, for example, to the EDMs of the neutron and the ^{199}Hg atom, which have the values

$$|d_n| = 1.2 \times 10^{-16} |\bar{\theta}| \, \mathrm{e} \times \mathrm{cm} \,, \tag{1.2a}$$

$$\left|d_{^{199}\mathrm{Hg}}\right| = 4.9 \times 10^{-20} |\bar{\theta}| \, \mathrm{e} \times \mathrm{cm} \,, \tag{1.2b}$$

Measurements of d_n [11–13] and $d_{^{199}\mathrm{Hg}}$ [14] showed that $|\bar{\theta}| \lesssim 10^{-10}$. This, in turn, indicated that QCD is, to a good degree, invariant under the CP-symmetry. This fine tuning of $\bar{\theta}$ is referred to as the strong CP problem.

In 1977, Peccei and Quinn proposed a solution to the strong CP problem [15–18]. They introduced an extra $U(1)$ global symmetry which lead to a dynamical interpretation of the vacuum angle $\bar{\theta} = a(t)/f_a$ where $a(t)$ is a time-dependent massive pseudo-scalar field [1], called the axion field, and f_a is the axion decay constant (which is also the order parameter associated with the spontaneous breaking of the introduced $U(1)$ symmetry). The invariance of the SM Lagrangian under the new $U(1)$ symmetry requires that the CP-odd term (1.1) be modified to read

$$\left(\bar{\theta} - \frac{a}{f_a}\right) \frac{g^2}{32\pi^2} G^{a\mu\nu} \tilde{G}^a_{\mu\nu} \,, \tag{1.3}$$

which produces an effective potential for the axion in the form $V_{\text{eff}} = m_a^2 f_a^2 \left[1 - \cos(\bar{\theta} - a/f_a)\right]$ where m_a is the axion mass. Minimizing this potential with respect to a gives $a = \bar{\theta} f_a$, at which value the CP-violating $\bar{\theta}$-term (1.3) vanishes, thus restoring CP-invariance.

1.1.2 The axion as a DM Candidate

Shortly after the axion was proposed as a solution to the strong CP problem, it was suggested that the axion could also be considered as a Dark Matter particle. This speculation is supported by the estimates of the axion's abundance and its couplings to SM matter.

Assuming that a/f_a is somewhat smaller than one, it is reasonable to approximate the potential V_{eff} with the quadratic term $V_{\text{eff}} \approx m_a^2 a^2/2$. The evolution of the pseudo-scalar axion field in this potential in an expanding universe is thus descibed by the equation

$$\ddot{a} + 3H(t)\dot{a} + m_a(t)^2 a = 0 \,, \tag{1.4}$$

where the dot denotes differentiation with respect to time.

In the early universe, when the temperature was higher than the QCD phase transition temperature, the Hubble constant H was much larger than the axion's mass m_a and Eq. (1.4) possesses a constant solution $a = A_0$. In contrast, in the later stage of the universe, when $H \ll m_a$, the axion field oscillates around the minimum of its potential, $a \sim \cos(m_a t)$. In this case, the energy density $\rho_a = (\dot{a}^2 + m_a^2 a^2)/2$ associated with this oscillation may be shown to have the form [19–21]

$$\rho_a \sim (f_a/10^{12}\,\mathrm{GeV})^2 (A_0/f_a)^2 \rho_c \,, \tag{1.5}$$

where $\rho_c = 3H^2/(8\pi G)$ is the critical density required for a flat universe (G is the gravitational constant). It is clear from Eq. (1.5) that if $A_0 \sim f_a \sim 10^{12}\,\mathrm{GeV}$ then axions saturate the present-day DM abundance.

The interactions between the axion and SM particles are given by

$$\mathcal{L}_{\text{int}} = \frac{C_G}{f_a} \frac{g^2}{32\pi^2} a G^a_{\mu\nu} \tilde{G}^{a\mu\nu} + \frac{C_\gamma}{f_a} \frac{e^2}{32\pi^2} a F_{\mu\nu} \tilde{F}^{\mu\nu} - \sum_{f=n,p,e} \frac{C_f}{2f_a} \partial_\mu a \bar{f} \gamma^5 \gamma^\mu f \,, \tag{1.6}$$

where g, G and $\tilde{G}$ are defined as in Sect. 1.1.1, $-e$ is the electron's electric charge, F and $\tilde{F}$ are the electromagnetic field tensors, $\bar{f}$ and f are fermionic spinors and γ^5 and γ^μ are the Dirac gamma matrices. The coefficients C_G, C_γ and C_f are model dependent but, typically, are of the order of one [22, 23], except for C_e which is about one in the DFSZ model [22, 24] but is about 10^{-3} in the KSVZ model

[1] The axion field can also have a spatial dependence.

[25, 26]. In any case, if $f_a \sim 10^{12}$ GeV so that axions saturate the DM content, the couplings between these particles and the SM sector are very weak indeed. This is in agreement with the observations mentioned in Sect. 1.1.

Recently, it was also pointed out that the axion may allow the formation of the so-called axion quark nuggets [27–31], which not only resolve the DM problem but also explain other puzzling cosmological and astrophysical observations such as the predominance of matter over antimatter in the universe [32, 33], the solar coronal heating puzzle [34], the primordial lithium problem [35, 36], the DAMA/LIBRA annual modulation [37, 38], the strange sky-quakes [39], the mysterious burst-like events observed by the Telescope Array Experiment [40, 41] and the x-ray seasonal variations observed by the XMM-Newton observatory [42]. These possibilities further improve the axion's attractiveness and a 'magical' solution to a wide range of problems, thus making its empirical detection more and more imperative.

1.2 Elementary particles' EDMs and the solution to the matter-antimatter asymmetry

Another standing puzzle for modern physics is the apparent asymmetry between matter and antimatter [43]. The Big Bang should have produced equal amounts of matter and antimatter, which would then annihilate one another off completely. The existence of the material world implies, on the other hand, that a tiny portion of matter, about five parts in ten billion, survived. A solution to this apparent asymmetry is a major part of the question that has troubled the human race since the dawn of civilization: 'Why are we here?'.

In 1967, Sakharov proposed three conditions necessary for the predominance of matter over antimatter [32]. Among these conditions is the violation of the CP-symmetry. As discussed in Sect. 1.1.1, the source for CP-violation in the QCD sector is small, too small, in fact, to completely account for the observed matter-antimatter asymmetry. Experiments searching for CP-violation in the leptonic sector by using, for example, neutrino oscillations [44–46], are ongoing. In this thesis, I investigate the possibility of searching for CP-violation in the hadronic sector, particularly, in terms of the nucleon EDMs and CP-odd nuclear forces.

1.2.1 CP-violation and elementary particles' EDMs

A EDM of an elementary particle violates both parity (P) and time reversal symmetry (T). This may be understood by considering, for example, a nucleon carrying a magnetic dipole moment $\boldsymbol{\mu}$ and an EDM $\mathbf{d}$. Under time reversal, $\boldsymbol{\mu}$ changes its sign but $\mathbf{d}$ remains the same so time invariance is violated. Under parity, $\mathbf{d}$ changes its direction, but $\boldsymbol{\mu}$ stays the same, so the parity symmetry is also violated. Due to the virtue of the CPT theorem, T-violation imply CP-violation.

The EDM of a nucleon may arise from those of its constituent quarks, but it may also arise due to the CP-odd interactions with pion [47, 48]. At the same time, the pion can also mediate CP-odd internucleon interactions, as was noted in Ref. [49]. Altogether, the nucleon EDMs and the CP-odd internucleon forces give rise to the EDM of the nucleus, which could, in principle, be detected by placing the nucleus in a combination of magnetic and electric fields and measuring the energy difference between two configurations where the fields are parallel and anti-parallel.

1.2.2 Schiff's theorem and methods to circumvent it

In measuring nuclear EDMs, it is natural to work with atoms and molecules. However, it is known that the nucleus of a neutral atom or molecule is completely shielded from any constant electric field, a result often called the Schiff's theorem [50]. This theorem may be understood if one notes that a neutral atom or molecule does not accelerate in a constant electric field, so an atomic or molecular nucleus does not accelerate either, meaning no field on the nucleus. Physically, the external electric field deforms the atomic or molecular electronic cloud in such a way that the internal electric field it creates at the nucleus exactly cancels the external field.

The Schiff's theorem forces conventional EDM experiments to measure, instead of nuclear EDMs, the related Schiff moment which arises due to the nucleus' finite size. The atomic or molecular EDM induced by this nuclear Schiff moment is typically about a thousand time smaller than the nuclear EDM itself. As a result, it would be experimentally advantageous to be able to access the nuclear EDM directly. In this thesis, I present different methods through which this goal may be achieved.

For example, I demonstrated that oscillating electric fields are not hindered by Schiff's theorem. The physical picture for this result is clear: since the electronic cloud has inertia, it does not react instantly to an oscillating electric field; it is this delayed response which allows for the penetration of the external field. This fact is even more pronounced in molecules where nuclei, which also participate in screening, have even larger inertia. These results are presented in Chapter 4.

Nuclear EDMs may also be oscillating if they are induced by axion Dark Matter [48]. I studied the effects of these oscillating nuclear EDMs on atoms and molecules. Physically, such an oscillating nuclear EDM acts as a time-dependent perturbation to the electron cloud (and other nuclei in a molecule), thus reduces its screening ability, thus inducing a non-zero atomic or molecular EDM. If one then applies an oscillating electric field, observable nuclear spin precession happens. These possibilities are presented in Chapter 5.

Chapter 6 is devoted to the study of the atomic and molecular transitions that may be induced by oscillating nuclear EDMs, Schiff moments and magnetic quadrupole moments.

Chapters 7 and 8 present another possibility to overcome Schiff's theorem, namely, by taking into account the magnetic interaction between electrons and nucleons. It will be demonstrated that a combined electric and magnetic interaction indeed gives rise to measurable atomic and molecular EDMs. Comparing the contribution of this interaction with that of the phenomenological electron-nucleon contact interaction allows ones to place independent constraints on various CP-violating hadronic parameters.

Finally, chapter 9 presents an attempt to improve the accuracy of existing computations of the Schiff moment's interaction with electrons. The result of this chapter is important for deriving bounds on the Schiff moment from results of experiments with molecules.

Bibliography

[1] F. Zwicky, Helv. Phys. Acta **6**, 110 (1933).

[2] F. Zwicky, Astrophys. J. **86**, 217 (1937).

[3] V. C. Rubin and W. K. Ford Jr, Astrophys. J. **159**, 379 (1970).

[4] V. C. Rubin, W. K. Ford Jr, and N. Thonnard, Astrophys. J. **238**, 471 (1980).

[5] M. Markevitch, A. H. Gonzalez, D. Clowe, A. Vikhlinin, W. Forman, C. Jones, S. Murray, and W. Tucker, Astrophys. J **606**, 819 (2004).

[6] D. Clowe, A. Gonzalez, and M. Markevitch, Astrophys. J. **604**, 596 (2004).

[7] D. Clowe, M. Bradač, A. H. Gonzalez, M. Markevitch, S. W. Randall, C. Jones, and D. Zaritsky, Astrophys. J. **648**, L109 (2006).

[8] G. Hinshaw, J. L. Weiland, R. S. Hill, N. Odegard, D. Larson, C. L. Bennett, J. Dunkley, B. Gold, M. R. Greason, N. Jarosik, et al., Astrophys. J., Suppl. Ser. **180**, 225 (2009).

[9] G. Bertone, D. Hooper, and J. Silk, Phys. Rep. **405**, 279 (2005).

[10] K. Olive, Chin. Phys. C **40**, 100001 (2016).

[11] C. A. Baker, D. D. Doyle, P. Geltenbort, K. Green, M. G. D. van der Grinten, P. G. Harris, P. Iaydjiev, S. N. Ivanov, D. J. R. May, J. M. Pendlebury, et al., Phys. Rev. Lett. **97**, 131801 (2006).

[12] J. M. Pendlebury et al., Phys. Rev. D **92**, 092003 (2015).

[13] C. Abel, S. Afach, N. J. Ayres, C. A. Baker, G. Ban, G. Bison, K. Bodek, V. Bondar, M. Burghoff, E. Chanel, et al., Phys. Rev. Lett. **124**, 081803 (2020).

[14] B. Graner, Y. Chen, E. G. Lindahl, and B. R. Heckel, Phys. Rev. Lett. **116**, 161601 (2016).

[15] R. D. Peccei and H. R. Quinn, Phys. Rev. Lett. **38**, 1440 (1977).

[16] R. D. Peccei, *The Strong* CP *Problem and Axions* (Springer, Berlin, Heidelberg, 2008), pp. 3–17.

[17] S. Weinberg, Phys. Rev. Lett. **40**, 223 (1978).

[18] F. Wilczek, Phys. Rev. Lett. **40**, 279 (1978).

[19] J. Preskill, M. B. Wise, and F. Wilczek, Phys. Lett. B **120**, 127 (1983).

[20] L. Abbott and P. Sikivie, Phys. Lett. B **120**, 133 (1983).

[21] M. Dine and W. Fischler, Physics Letters B **120**, 137 (1983).

[22] J. E. Kim, Phys. Rev. Lett. **43**, 103 (1979).

[23] M. Srednicki, Nucl. Phys. B **260**, 689 (1985).

[24] M. Shifman, A. Vainshtein, and V. Zakharov, Nucl. Phys. B **166**, 493 (1980).

[25] M. Dine, W. Fischler, and M. Srednicki, Phys. Lett. B **104**, 199 (1981).

[26] A. Zhitnitsky, Sov. J. Nucl. Phys. **31**, 260 (1980).

[27] D. Budker, V. V. Flambaum, X. Liang, and A. Zhitnitsky, Phys. Rev. D **101**, 043012 (2020).

[28] A. Zhitnitsky, arXiv:2008.04325 (2020).

[29] D. Budker, V. V. Flambaum, and A. Zhitnitsky, arXiv:2003.07363 (2020).

[30] S. Ge, M. S. R. Siddiqui, L. V. Waerbeke, and A. Zhitnitsky, arXiv:2009.00004 (2020).

[31] S. Ge, H. Rachmat, M. S. R. Siddiqui, L. V. Waerbeke, and A. Zhitnitsky, arXiv:2004.00632 (2020).

[32] A. Sakharov, JTEP Lett. **5**, 24 (1967).

[33] A. D. Sakharov, Sov. Phys. Usp. **34**, 392 (1991).

[34] W. Grotrian, NW **27**, 214 (1939).

[35] R. H. Cyburt, B. D. Fields, and K. A. Olive, J. Cosmo. Astropart. Phys. **2008**, 012 (2008).

[36] R. H. Cyburt, B. D. Fields, K. A. Olive, and T.-H. Yeh, Rev. Mod. Phys. **88**, 015004 (2016).

[37] R. Bernabei et al., Eur. Phys. J. C **67**, 39 (2010).

[38] R. Bernabei, P. Belli, F. Cappella, V. Caracciolo, S. Castellano, R. Cerulli, C. Dai, A. d'Angelo, S. d'Angelo, A. Di Marco, et al., Eur. Phys. J. C **73**, 2648 (2013).

[39] *The Elginfield Infrasound Array (ELFO): Interesting (non-meteoric) events detected by ELFO*, aquarid.physics.uwo.ca/research/infrasound/is_mysteriousexplosions.html, August 1, 2008.

[40] R. Abbasi et al., Phys. Lett. A **381**, 2565 (2017).

[41] T. Okuda, J. Phys. Conf. Ser. **1181**, 012067 (2019).

[42] G. Fraser, A. Read, S. Sembay, J. Carter, and E. Schyns, Mon. Not. R. Astron. Soc. **445**, 2146 (2014).

[43] L. Canetti, M. Drewes, and M. Shaposhnikov, New J. Phys. **14**, 095012 (2012).

[44] K. Dick, M. Freund, M. Lindner, and A. Romanino, Nuclear Physics B **562**, 29 (1999).

[45] H. Nunokawa, S. Parke, and J. W. Valle, Progress in Particle and Nuclear Physics **60**, 338 (2008).

[46] K. Abe, R. Akutsu, A. Ali, C. Alt, C. Andreopoulos, L. Anthony, M. Antonova, S. Aoki, A. Ariga, Y. Asada, et al., Nature **580**, 339 (2020).

[47] R. J. Crewther, P. Di Vecchia, G. Veneziano, and E. Witten, Phys. Let. B **88**, 123 (1979).

[48] P. W. Graham and S. Rajendran, Phys. Rev. D **84**, 055013 (2011).

[49] O. P. Sushkov, V. V. Flambaum, and I. B. Khriplovich, Zh. Eksp. Teor. Fiz **87**, 1521 (1984).

[50] L. I. Schiff, Phys. Rev. **132**, 2194 (1963).

Chapter 2

Interference-assisted resonant detection of axions

2.1 Overview

In this chapter, I consider a proposal to detect axion DM. This new scheme exploits the resonance of axions and photons by atoms and molecules. By arranging for the absorption amplitudes to interfere, one may achieve an axion signal that is linear in the axion-electron coupling constant, making the new scheme more advantageous than conventional axion searches.

These results are published in the following papers:

1. V. V. Flambaum, I. B. Samsonov, H. B. Tran Tan, Y. V. Stadnik and D. Budker, **Interference-assisted resonant detection of axions**, Phys. Dark Universe 24, 100272 (2019), arXiv:1803.09388,

2. V. V. Flambaum, I. B. Samsonov, H. B. Tran Tan, Y. V. Stadnik and D. Budker, **Resonant detection and production of axions with atoms**, Int. J. Mod. Phys. A **33**, 31, 1844030 (2018),

which I have presented them at one international conference, one national conference and one national competition:

1. **Searching for Axions and Axionic Dark Matter with Interference and Axion-induced Nuclear Moments**, TeV Particle Astrophysics Conference, University of Sydney, Sydney, Australia, December 2019,

2. **Effects of Dark Matter in atomic and molecular phenomena**, Australian Institute of Physics Postgraduate Presentation Competition, University of Technology Sydney, Sydney, Australia, October 2019,

3. **Detection of Axions Using Atomic Transitions Induced by Interference between Electromagnetic and Axion Fields**, Australian Institute of Physics Summer Meeting, University of New South Wales, Sydney, Australia, December 2017.

2.2 Abstract

Detection schemes for the quantum-chromodynamics axions and other axion-like particles in light-shining-through-a-wall (LSW) experiments are based on the conversion of these particles into photons in a magnetic field. An alternative scheme may involve the detection via a resonant atomic or molecular transition induced by resonant axion absorption. The signal obtained in this process is second order in the axion-electron interaction constant but may become first order if we allow interference between the axion-induced transition amplitude and the transition amplitude induced by the electromagnetic radiation that produces the axions.

2.3 Introduction

The axion is a light pseudoscalar particle proposed by Peccei and Quinn in 1977 to resolve the strong CP (charge and parity) problem in quantum chromodynamics (QCD) [1–4]. Since then, the axion and other feebly interacting pseudoscalar particles with similar properties (axion-like particles or ALPs) have been identified as possible candidates to explain the observed Dark Matter (DM). Despite numerous theoretical speculations, there is still no definitive experimental evidence for the existence of these particles. The reason for this lack of evidence is two-fold. The first difficulty arises from the fact that the coupling constants of the interactions of axions [1] with Standard-Model (SM) particles, although not known precisely, are constrained to be small. As a result, any attempt to detect axions must seek to enhance the effects of the interactions and render them observable. This task is formidable. The second difficulty is that the axion's mass is poorly constrained, so experiments that search for axions must cover a large range of frequencies. In recent years, significant efforts, both theoretical and experimental, have been made to investigate the possible parameter spaces in mass and coupling strengths.

Traditional searches for axions are based mainly on the interaction between axions and photons in the presence of a magnetic field. In such a situation, the mixing of the axion and photon states is possible and the two types of particles can interconvert with one another [5, 6]. Helioscope experiments including Sumico [7–11], CAST [12–15], SOLAX [16, 17], COSME [18], DAMA [19–21], CDMS [22–25] and IAXO [26–28] convert solar axions into photons for detection. Haloscope experiments such as ADMX [29–31], HAYSTAC [32, 33] and ORGAN [34] convert cosmic axions into photons in microwave cavities and detect these photons resonantly with SQUIDs. A notable feature of haloscope experiments is the long scanning time: since the energy of the incoming axions is not known, these experiments have to sweep a large frequency range to find a resonance. Light-shining-through-a-wall (LSW) experiments including ALPS [35–37], OSQAR [38–40] and GammeV [41] involve converting photons into axions, passing the resulting beam through a wall, which blocks all the photons but not the axions, and then converting the transmitted axions back into photons for detection on the other side of the wall. These LSW experiments do not involve frequency scanning since the energy of the axion is known from energy conservation. However, since the axion signals in these experiments scale to the fourth power in the axion-photon coupling constant (instead of to the second power as in helio- and haloscope experiments), the sensitivity is greatly compromised. Finally, experiments like PVLAS [42–44], Q & A [45] and BMV [46, 47] search for optical birefringence (difference in optical refractive indices for different polarizations) and dichroism (difference in absorption of light of different polarizations) due to interconversion with axions [48].

Recently, various new schemes for axion detection have been proposed. These include searching for axions by converting them into magnons in a ferromagnet [49, 50], by looking for parity- and time-reversal-invariance-violating effects (due to couplings of axions to SM particles) such as oscillating electric dipole moments [51–55], by using dielectric haloscopes (improved sensitivity compared to traditional haloscopes) [56–59], by using nuclear magnetic resonance to search for axion-mediated CP-violating forces [60–63], by resonantly detecting the oscillating magnetic flux sourced by the axions entering a static magnetic field [64], by using electron spin resonance in magnetized media to detect the oscillating effective magnetic field induced by axions [65], by using superconductors [66] and semiconductors [67], by using an LC circuit (Dark Matter radio) [68–70], by using Josephson junctions [71, 72], by using photon interferometry [73], by using axion-induced resonant molecular transitions [74], by using laser-spectroscopy techniques to probe axion-induced atomic and molecular tranistions [75], by looking for an axion-induced topological Casimir effect [76] and by using a photon field (instead of a magnetic field) to trigger axion-to-photon decay then detecting the product photons with Raman scattering [77]. In this paper, we explore some possible experimental schemes which are based on atomic or molecular transitions due to the absorption of axions.

The idea of using atomic transitions to produce and detect axions dates back to a 1988 paper by Zioutas and Semertzidis [78]. The authors proposed using an *M1* transition to *produce* axions which would then be detected in a microwave cavity. In 2014, Sikivie extended this idea and proposed using the axion-induced *M1* transitions to detect galactic-halo axions [79]. In Sikivie's scheme, atoms in the ground state 0 *absorb* axions and go to an excited state i. A laser is then used to further excite the atoms to the state f. This laser must be tuned so that it can only cause the $i \to f$ transition. Photons emitted when the atoms in the state f decay are then detected. Following Sikivie's paper, an experimental realization that uses Zeeman states in molecular oxygen at a temperature of 280 mK was proposed [80]. In this particular proposal, the transition frequency is scanned by applying a strong magnetic field and the

[1] In this paper, we will not distinguish between the QCD axion and other axion-like particles. The term 'axion' will refer to both.

detection is done via resonant multiphoton-ionization (REMPI) spectroscopy.

A general feature of the processes considered in the atom- or molecule-based proposals above is the quadratic dependence of the detection rate on the axion-electron coupling constant. Since this constant is small, the detection rate is minuscule. A possible enhancement of this rate may be achieved by allowing the atoms to absorb a coherent mixture of axions and photons. The detection rate will then contain a cross term due to the interference between the axion- and photon-induced atomic transition amplitudes. This cross term is linear in the axion-electron coupling constant. In this paper, we explore this idea of axion-photon interference by propopsing and studing a scheme which resembles the traditional ALPS experiment. We find that the sensitivity of our scheme may be better than that of existing helioscope experiments [14]. This fact is certainly interesting if one notes that the axions used in our scheme have to be artificially produced and are thus not as abundant in number as the solar axions detected by helioscope experiments.

The rest of this paper will be organized as follows. In Sect. 2.4, we will give a general description of the experimental set-up and target choice for our scheme. In Sect. 2.5, all relevant formulae for transition amplitudes, signal and signal-to-noise ratio for our scheme will be presented. Sect. 2.6 contains numerical estimates for some particular targets and a discussion of our scheme's sensitivity to the product $g_{aee}g_{a\gamma\gamma}$. In Sect. 2.7, we summarize our findings and provide some extra remarks. In Appendix A, for completeness, we discuss an alternative choice of target for our experiment which was not presented in the main text. Specifically, we consider in Appendix A the axion-induced $M0$ atomic transition and compare it with the $M1$ transitions presented in the main text. As it turns out, an $M0$-type experiment is not as competitive as an $M1$-type one. In Appendix B, we study, as an offshoot of the axion-induced atomic transition calculation, the possibility of using atom transitions to make axion 'lasers'.

2.4 Experimental scheme

2.4.1 General set-up

Our proposed experimental set-up to detect axions is shown in Fig. 2.1. The photons produced by

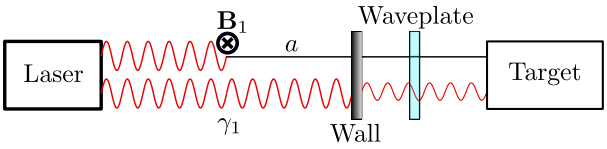

Figure 2.1: Set-up of the axion-photon interference experiment: Some of the γ_1 photons get converted into axions a in the magnetic field $\mathbf{B}_1$. The resulting axion-photon beam is passed through a thin wall which suppresses the photon amplitude. A waveplate is inserted into the path of the beam to compensate for the phase difference between the axion- and the photon-induced transition amplitudes.

a high-power monochromatic laser pass through a strong magnetic field $\mathbf{B}_1$ where some photons get converted into axions. The axion-photon beam is then passed through a thin wall which suppresses the photon amplitude while leaving the axion amplitude intact. This suppression is necessary for keeping the axion-induced effect from being completely overwhelmed by its photon-induced counterpart. The axion-photon beam then hits a target and causes atomic transitions therein.

These transitions can then be detected by using, for example, the method suggested in [79]. That is, another finely tuned laser is used to further excite the already excited atoms to some final state; the photons emitted when atoms in this final state decay are detected (these photons are not shown in Fig. 2.1). It is worth noting that in recent years, there has been significant progress in the detection of single-quantum excitation in a variety of systems, including gas, liquid (for example, rare-isotope detection) and solids (for example, a large body of work on color centers in diamond). There are many possible experimental techniques used for this type of detection. For instance, one may produce many photons from a single atomic/molecular excitation by using a cycling transition à la 'optical shelving'. However, such details go beyond the scope of this work and shall not be discussed here.

By comparing the detected signals when the magnetic field $\mathbf{B}_1$ changes sign, one can detect the axion-induced transition amplitude. The axion-photon interference contribution also changes sign and may be separated by the change of the sign of the weak field $\mathbf{B}_2$ in the detection area (see below).

There are different possible choices for the atoms in the target, corresponding to different transitions that one may be interested in. In the main text of this paper, we consider a scheme which uses $M1$

transitions, which appear to be the most advantageous choice. In the Appendix, a scheme with $M0$ transition shall be considered. It appears that the $M0$ experiment is not as advantageous as its $M1$ counterpart. Nevertheless, for completeness, we present both schemes in this paper.

2.4.2 Atomic transition

The diagram for the $M1$ atomic transition is shown in Fig. 2.2. This transition may be induced by the absorption of an axion since the axion can carry angular momentum and parity 1^+. An $M1$ transition can happen between levels that have the same quantum numbers except for their total angular momenta, e.g., between the fine-structure components of the ground state.

Since a level with total angular momentum $J \neq 0$ is degenerate (with degeneracy $2J+1$ corresponding to $2J+1$ possible values of the total angular momentum projection quantum number m), if the target atoms are not polarized, i.e., have no definite initial projection m and final projection m', one needs to average the square of the total amplitude over m and sum over m' to get the transition probability. It is easy to see that the axion-photon interference term in this total probability vanishes.

Indeed, as will be shown in Sect. 2.5.2, the axion $M1$ transition amplitude is specified by the axion propagation unit vector $\hat{\mathbf{k}}_a$ while the photon $M1$ amplitude is proportional to the vector $\hat{\mathbf{b}}_\gamma = \hat{\mathbf{k}}_\gamma \times \boldsymbol{\epsilon}$, where $\boldsymbol{\epsilon}$ is the photon polarization vector and $\hat{\mathbf{k}}_\gamma$ is the photon propagation unit vector (which is the same as $\hat{\mathbf{k}}_a$). For non-polarized atoms, due to spherical symmetry, the interference term must be proportional to $\hat{\mathbf{b}}_\gamma \cdot \hat{\mathbf{k}}_\gamma$ which is zero since these two vectors are orthogonal by construction. Of course, this can be verified by straightforward calculations.

Thus, for the interference to be nonzero, it is necessary to break this spherical symmetry. This can be achieved by applying to the target a magnetic field $\mathbf{B}_2$, which defines a quantization axis (the z-axis). The full spherical symmetry is now reduced to the rotational symmetry around this axis. This reduction of the symmetry gives a nonzero interference term.

In terms of energy levels, the field $\mathbf{B}_2$ lifts the degeneracy of the initial (total angular momentum J) and final (total angular momentum J') levels. Sublevels with the same J (J') but different m (m') are now distinct (with energy separations of the order of $\mu_0 B_2$ where μ_0 is the Bohr magneton). If one then chooses the laser frequency so that only transitions between sublevels of specific projections are induced, the axion-photon interference term should not be averaged and summed over the initial and final projections and hence no longer vanishes. We stress that the interference between the axion- and photon-induced $M1$ transition amplitudes always occurs; however, its effect averages out over the (degenerate) sublevels in non-polarized atoms. To reveal the effect of the interference, one needs to resolve these sublevels.

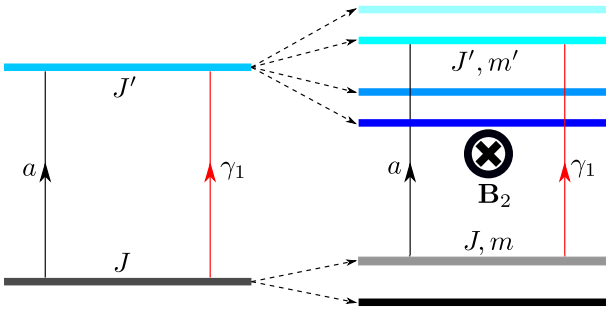

Figure 2.2: Energy levels in the target atoms in the M1 case. The absorption of axions and photons causes resonant transitions between two states with the same parity and total angular momenta differing by 0 or ± 1. Without an external field, the axion-photon interference term in the total transition probability is zero. If a magnetic field $\mathbf{B}_2$ is applied and the laser is tuned so that it induces transition between levels of specific total angular momentum projections, the axion-photon interference term can be nonzero.

2.5 Calculations

2.5.1 Photon-to-axion conversion probability

The interaction between axions and photons is described by the Lagrangian density

$$\mathcal{L}_{a\gamma\gamma} = -\frac{g_{a\gamma\gamma}}{4} a F_{\mu\nu} \tilde{F}^{\mu\nu} \,, \tag{2.1}$$

where $g_{a\gamma\gamma}$ is the axion-photon coupling constant, a is the axion field, $F_{\mu\nu}$ and $\tilde{F}^{\mu\nu}$ are the electromagnetic field tensor and its dual. This interaction is responsible for the interconversion between photons and axions in a magnetic field $\mathbf{B}_1$, with the conversion probability given in the natural units ($\hbar = c = 1$) by [81, 82]

$$\mathcal{P} = \frac{\omega}{4k_a} \left(g_{a\gamma\gamma} B_1 l_0\right)^2 F^2 \left(q\right) \,, \tag{2.2}$$

where ω is the photon energy (equal to the axion energy), k_a is the axion's momentum, l_0 is the spatial extent of the magnetic field in the direction of the axion-photon beam direction, $q = \omega - k_a$ is the momentum transferred from the photon field to the axion field and $F\left(q\right) = \int e^{-iqx} \left(B\left(x\right)/B_1 l\right) dx$ is a form factor. For a homogeneous magnetic field $\mathbf{B}_1$, formula (2.2) simplifies to

$$\mathcal{P} = \frac{\left(g_{a\gamma\gamma} B_1 l_0\right)^2}{4} \operatorname{sinc}^2 \left(\frac{M^2 l_0}{4\omega}\right) . \tag{2.3}$$

where $M^2 = m_a^2 + 2\omega^2 \left(n - 1\right)$, m_a is the axion mass, n is the photon refractive index and $\operatorname{sinc}\left(x\right) = \sin\left(x\right)/x$. We will not need these formulae explicitly in the calculations below. The only quantity we need for a numerical estimate is $\mathcal{P}$.

According to the projected sensitivity of the ALPS II experiment [83], which features $l_0 = 100\,\mathrm{m}$ and $B_1 = 5.3\,\mathrm{T}$, the upper limit on the axion-photon coupling constant $g_{a\gamma\gamma}$ ($2 \times 10^{-11}\,\mathrm{GeV}^{-1}$) corresponds to the photon-to-axion conversion probability $\mathcal{P} \sim 10^{-7}$. We will use these values in our estimates below.

Note that although not shown here, it is clear that the amplitude for the photon-to-axion conversion process is linear in B_1 (this must be true since the conversion probability is quadratic in B_1) and this amplitude will change its sign when B_1 does. We will exploit this observation to detect axions, as explained in the sections below.

2.5.2 Atomic transition amplitudes

Photon absorption amplitude

The amplitude for an atomic transition $A \to B$ induced by the absorption of a photon is given by [84–86]

$$M^\gamma = i\sqrt{2\pi n_\gamma \omega_\gamma} e^{-i\omega_\gamma t} M^\gamma_{BA} \,, \tag{2.4}$$

where ω_γ is the photon energy, n_γ is the photon number density in the beam and M^γ_{BA} is the transition matrix element. The photon energy ω_γ needs to match the difference of the energy levels $E_i - E_{^1S_0}$, corresponding to the resonant transition.

The $M1$ photon matrix element M^γ_{BA} is given by

$$M^\gamma_{BA} = \frac{e}{2m_e} \hat{\mathbf{b}}_\gamma \cdot \langle B| \mathbf{J} + \mathbf{S} \left|A\right\rangle \,, \tag{2.5}$$

where $\hat{\mathbf{b}}_\gamma = \hat{\mathbf{k}}_\gamma \times \boldsymbol{\epsilon}$ is the direction of the magnetic component of the photon field ($\hat{\mathbf{k}}_\gamma$ is the photon propagation unit vector and $\boldsymbol{\epsilon}$ is the photon polarization vector), $\mathbf{J}$ is the electron's total angular momentum and $\mathbf{S}$ is the electron's spin.

If we now fix a spherical basis $\{\mathbf{e}_{-1}, \mathbf{e}_0, \mathbf{e}_1\}$ with the quantization axis $\mathbf{e}_0$ in the direction of the applied field $\mathbf{B}_2$, we can write the components of the vector $\mathbf{b}_\gamma$ as b^q_γ where $q = -1, 0, 1$. We can also describe the states A and B by the quantum numbers n, j, l, m and n', j', l', m', respectively. The $M1$ photon matrix element thus reads

$$M^\gamma_{BA} = (-1)^{j'-m'} \hat{b}^q_\gamma \begin{pmatrix} j' & 1 & j \\ -m' & q & m \end{pmatrix} \mathfrak{J} \,, \tag{2.6}$$

where $\begin{pmatrix} j' & 1 & j \\ -m' & q & m \end{pmatrix}$ is the $3j$ symbol and $\mathfrak{J} = \frac{e}{2m_e} \langle n' j' l' \| \mathbf{J} + \mathbf{S} \| n j l \rangle$ is the reduced $M1$ matrix element. Note that here and below, summations over the repeated indices $p, q, \ldots$ are implicit.

Axion absorption amplitude

The interaction between the axion field a and the electron field ψ is described by the Lagrangian density

$$\mathcal{L}_{\text{int}} = -\frac{g_{aee}}{2m_e}\partial_\mu a\bar{\psi}\gamma^5\gamma^\mu\psi\,, \tag{2.7}$$

where g_{aee} is the axion-electron coupling constant. This coupling constant can be written as

$$g_{aee} = \frac{C_e m_e}{f_a}\,, \tag{2.8}$$

where f_a is the axion decay constant and C_e is a model-dependent parameter. Currently, there are two main models for the QCD axion: the KSVZ model [87, 88] and the DFSZ model [89, 90]. At tree-level, $C_e = 0$ for the KSVZ axion and $C_e \sim 1$ for the DFSZ axion [91] (a nonzero value $C_e \sim \alpha/2\pi \sim 10^{-3}$ appears in the former case due to radiative corrections). Generic ALPs can have any C_e value.

The amplitude for the atomic transition $A \to B$ induced by the absorption of an axion can be calculated using a method similar to that used in the case of photon absorption. We find that

$$M^a = -\sqrt{2n_a\omega_a}e^{-i(\omega_a t+\phi_a)}M^a_{BA}\,, \tag{2.9}$$

where ω_a is the axion energy (which is equal to the energy of the γ_1 photons, $\omega_a = \omega_\gamma$), ϕ_a is the axion phase (which differs from the photon phase by the phase of the field $\mathbf{B}_1$), n_a is the axion number density in the beam and the matrix element M^a_{BA} can be derived from the interaction Lagrangian (2.7). In the relativistic limit ($\omega_a \gg m_a$), the leading-order terms of M^a_{BA} are [79, 92]

$$M^a_{BA} \approx -\frac{ig_{aee}}{2m_e}\langle B|\,\hat{\mathbf{k}}_a\cdot\mathbf{S}\,|A\rangle - \frac{g_{aee}\omega_a}{2m_e}\langle B|\,\mathbf{r}\cdot\mathbf{S} - \left(\hat{\mathbf{k}}_a\cdot\mathbf{S}\right)\left(\hat{\mathbf{k}}_a\cdot\mathbf{r}\right)|A\rangle\,, \tag{2.10}$$

where $\hat{\mathbf{k}}_a = \mathbf{k}_a/\omega_a$ is the axion propagation unit vector, $\mathbf{r}$ is the electron's position vector and $\mathbf{S} = \boldsymbol{\sigma}/2$ is the electron's spin. The form of the matrix element can be qualitatively understood if we note that the relevant quantities in the problem are the electron's momentum $\mathbf{p}$ (which can be replaced by $\mathbf{r}$ by using the identity $\mathbf{p} = im_e\,[H_0, \mathbf{r}]$ where H_0 in the unperturbed nonrelativistic electronic Hamiltonian), the electron's spin $\mathbf{S}$ and the axion's momentum $\mathbf{k}_a$. The interaction Lagrangian, being a pseudoscalar, must therefore be built from the scalar products of these vectors.

It can be shown that the first term in Eq. (2.10) is of $M1$ type whereas the second term is of $M0$ type. Here, we are concerned only with the first term of Eq. (2.10). The $M0$ case will be considered in appendix A.

The axion $M1$ matrix element is thus given by

$$M^a_{BA} = \frac{ig_{aee}}{2m_e}\langle B|\,\hat{\mathbf{k}}_a\cdot\mathbf{S}\,|A\rangle = (-1)^{j'-m'}\frac{ig_{aee}}{e}\hat{k}^q_a\begin{pmatrix} j' & 1 & j \\ -m' & q & m\end{pmatrix}\mathfrak{S}\,, \tag{2.11}$$

where $\mathfrak{S} = \frac{e}{2m_e}\langle n'j'l'\|\mathbf{S}\|njl\rangle$. The second line of Eq. (2.11) is obtained by assuming the same spherical basis as above.

2.5.3 Axion signal and signal-to-noise ratio

Suppose that the source laser (laser 1) produces photons continuously at a rate of N photons per unit time. Passing through the magnetic field, $\mathcal{P}N$ of them get converted into axions where $\mathcal{P}$ is the photon-axion conversion probability given by formula (2.3). Since $\mathcal{P} \ll 1$, the number of remaining photons after conversion is approximately N. Denoting by $\mathcal{T}$ the photon-transmission coefficient of the wall, the number of incident photons per unit time is $\mathcal{T}N$. Thus, the photon number density in Eq. (2.4) is $n_\gamma \propto \mathcal{T}N$ and the axion number density n_a in Eq. (2.9) is $n_a \propto \mathcal{P}N$.

The total amplitude for the $A \to B$ transition is the sum of those given by Eqs. (2.4) and (2.9). Squaring this sum and discarding the term which is second order in the axion-electron coupling constant, we find the total transition probability

$$\mathcal{P} \propto |M^\gamma|^2 + 2\,\text{Re}\left(i\overline{M^a}M^\gamma\right) \tag{2.12}$$

(the bar denotes complex conjugation). The factor i comes from the inserted phase-compensating waveplate.

Multiplying this probability by the probability of transition from B to C (recall that to detect the atomic transitions, we further excite the atoms in the state B to some state C then detect the photons emitted when atoms in this state decay), one finds the detection probability. Multiplying the detection probability by the number of atoms in the target and the detection coefficient, which includes the probability of decay from the state C and the sensitivity of the detector, one gets the number of observed excited atoms, which we denote by S. We assume that these stages of detection, associated with counting the atoms excited to state B, have close to 100% efficiency.

We observe that as the magnetic field $\mathbf{B}_1$ changes sign, the phase ϕ_a changes by π. This corresponds to the interference term $2\,\mathrm{Re}\left(i\overline{M^a}M^\gamma\right)$ flipping sign. The same thing happens if $\mathbf{B}_2$ change its sign. Hence, the relative difference in the number of excited atoms when $\mathbf{B}_1$ or $\mathbf{B}_2$ changes sign is (here, ΔS denotes the change in S as $\mathbf{B}_1$ or $\mathbf{B}_2$ flips sign)

$$\eta = \left|\frac{4\,\mathrm{Re}\left(i\overline{M^a}M^\gamma\right)}{\overline{M^\gamma}M^\gamma}\right| = \frac{4g_{aee}}{\sqrt{\pi}e}\left|\frac{\hat{k}^p\begin{pmatrix} j' & 1 & j \\ -m' & p & m\end{pmatrix}\mathfrak{S}}{\hat{b}^q\begin{pmatrix} j' & 1 & j \\ -m' & q & m\end{pmatrix}\mathfrak{I}}\right|\sqrt{\frac{\mathcal{P}}{\mathcal{T}}}\,. \tag{2.13}$$

We will call this quantity η the axion signal. Note that η is first order in the axion-electron coupling constant.

As noted before, in the absence of the external field $\mathbf{B}_2$, the axion-photon interference term in the total transition probability (2.12) vanishes. For completeness, we prove this assertion here. According to Eq. (2.12), this term is (twice) the product of the amplitudes (2.5) and (2.11). When averaged over the initial projections m and summed over the final projections m', this term gives (up to a numerical factor)

$$\sum \hat{b}^p_\gamma \hat{k}^q_\gamma \begin{pmatrix} j' & 1 & j \\ -m' & p & m\end{pmatrix}\begin{pmatrix} j' & 1 & j \\ -m' & q & m\end{pmatrix} \propto \hat{\mathbf{b}}_\gamma \cdot \hat{\mathbf{k}}_\gamma\,, \tag{2.14}$$

where the sum is over m, m', p and q. This quantity vanishes since $\hat{\mathbf{b}}_\gamma$ is perpendicular to $\hat{\mathbf{k}}_\gamma$ by construction.

Since the axion-electron coupling constant is small, the axion signal η is also small. For this signal to be detectable, the contribution of the interference term in Eq. (2.12) to the number of excited atoms S should exceed the noise in this number. In other words, the signal-to-noise-ratio (SNR) between ΔS (the contribution of the interference term) and the noise of S should be greater than unity.

Neglecting the contribution from axions, the number of excited atoms equals the number of photons absorbed by the target after the time t of the experiment. This number is given by

$$S \approx \mathcal{T} N t l / l_a\,, \tag{2.15}$$

where l_a is the photon absorption length and l is the length of the target (this equation is only applicable when $l \ll l_a$ so that the Beer-Lambert law for absorption probability $P_{\mathrm{abs}} = 1 - \exp\left(-l/l_a\right)$ reduces to $P_{\mathrm{abs}} \approx l/l_a$).

Recall that the absorption length l_a is expressed in terms of the atom density in the target n and the photon resonant absorption cross section σ as [84, 85]

$$l_a = \frac{1}{n\sigma}\,, \qquad \sigma = \frac{4\pi}{\omega^2}\frac{\Gamma_i}{\Gamma_{\mathrm{tot}}}\,, \tag{2.16}$$

where $\omega = E_{j',m'} - E_{j,m}$, $\Gamma_i = \frac{4}{3}\omega^3\left|M^\gamma_{BA}\right|^2$ is the rate of the $M1$ transition $|j,m\rangle \to |j',m'\rangle$ and Γ_{tot} is its total width. If we assume that the target atoms are in vapor form then Γ_{tot} is approximately the Doppler width, which is given by

$$\Gamma_{\mathrm{Dop}} = 2v_0\Delta_0/\sqrt{\pi} \tag{2.17}$$

where $v_0 = \sqrt{2k_BT/m}$ is the most probable thermal speed of the target atoms, k_B is Boltzmann's constant, T is the temperature of the target and m is the atomic mass.

To sum up, the SNR is given by

$$\begin{aligned}\mathrm{SNR} = \frac{\Delta S}{\sqrt{S}} &= \frac{8g_{aee}}{e}\left|\frac{\hat{k}^p_\gamma\begin{pmatrix} j' & 1 & j \\ -m' & p & m\end{pmatrix}\mathfrak{S}}{\hat{b}^q_\gamma\begin{pmatrix} j' & 1 & j \\ -m' & q & m\end{pmatrix}\mathfrak{I}}\right|\sqrt{\frac{\mathcal{P}Nltn\Gamma_i}{\omega^2\Gamma_{\mathrm{tot}}}} \\ &\approx \frac{16\pi^{1/4}g_{aee}}{\sqrt{6}e}\left|\hat{k}^p_\gamma\begin{pmatrix} j' & 1 & j \\ -m' & p & m\end{pmatrix}\mathfrak{S}\right|\sqrt{\frac{\mathcal{P}Nltn}{v_0}}\,.\end{aligned} \tag{2.18}$$

We observe that the SNR is independent of the wall's transmission coefficient $\mathcal{T}$ but is proportional to the square root of the total number of photons Nt and the target size l. Hence, to gain a better SNR, one needs a sufficiently powerful laser and a sufficiently large target to absorb as many photons as possible.

2.6 Numerical estimates

2.6.1 The $M1$ case - vapor target

We now provide numerical estimates for the axion signal and the SNR of the axion-photon $M1$ interference experiment, Eqs. (2.13) and (2.18). As explained in [93], the most suitable elements for an experiment involving atomic $M1$ transitions are Tl, Pb and Bi. We consider for Tl the transition $6s^2 6p\,^2P_{1/2} \to 6s^2 6p\,^2P_{3/2}$, for Pb the transition $6s^2 6p^2\,^3P_0 \to 6s^2 6p^2\,^3P_1$ and for Bi the transition $6s^2 6p^3\,^4S_{3/2} \to 6s^2 6p^3\,^2D_{3/2}$. The values of the reduced matrix element $\mathfrak{J}$ for these transitions are presented in [93–95].

For simplicity of calculation, we consider for Tl the transition $|j=\frac{1}{2}, m=\frac{1}{2}\rangle \to |j'=\frac{3}{2}, m'=\frac{1}{2}\rangle$, for Pb the transition $|j=0, m=0\rangle \to |j'=1, m'=0\rangle$ and for Bi the transition $|j=\frac{3}{2}, m=\frac{3}{2}\rangle \to |j'=\frac{3}{2}, m'=\frac{3}{2}\rangle$. For these transitions, we observe that the axion signal is proportional to the ratio $\left|\hat{k}^0_\gamma/\hat{b}^0_\gamma\right|$, so by arranging the photon's direction $\hat{\mathbf{k}}_\gamma$ very close to the z-axis (which is defined by the external field $\mathbf{B}_2$), one can make the axion signal large. For numerical estimates, we assume that $\hat{k}^0_\gamma \approx 1$ and $\hat{b}^0_\gamma \approx 0.01$.

For $\mathcal{P}$ and N, we use the values that are expected at the ALPS II experiment [83]: $\mathcal{P} \sim 10^{-7}$ and $N \approx 10^{20}\,\mathrm{s}^{-1}$. We assume that $C_e \sim 1$ and $f_a = 10^9\,\mathrm{GeV}$, which corresponds to $g_{aee} \approx 5\times 10^{-13}$. For the transmission coefficient $\mathcal{T}$, we take $\mathcal{T} = 10^{-18}$ to have the photon signal sufficiently suppressed. For simplicity, we assume that the laser light is polarized in the z-direction. For the target length we take $l = 10\,\mathrm{m}$. For numerical estimates, we choose t=100 days, which is the order of magnitude for the maximal practical integration times. The appropriate values for the atom density n and temperature T for different atoms are presented in Table 2.1 (see the caption of this table for more comments on the values of n and T). The estimates of η and SNR are summarized in Table 2.1.

Atom	ω (eV)	$\mathfrak{J}$ $(e/2m_e)$	n $\left(10^{17}\,\mathrm{cm}^{-3}\right)$	η $\left(\times 10^{-4}\right)$	SNR
Tl	0.966	-1.13	6.6	4.3	8.8
Pb	0.969	-1.29	1.1	4.3	5.8
Bi	1.416	-1.69	1.5	4.3	6.0

Table 2.1: Estimates of the $M1$ interference signal η and the SNR for some target atoms. Here, ω and $\mathfrak{J}$ are the energy and $M1$ reduced matrix element of the transitions under consideration, respectively. The relevant values of $\mathfrak{J}$ are given in [93–95]. We assume that the temperature of the metal vapors is 1473 K. The densities of the vapors at this temperature are estimated using the ideal gas equation and experimentally fitted vapor pressure equations presented in [96]. The SNR corresponds to a target length of 10 m and integration time of 100 days. The signal and SNR are presented for $g_{aee} = 5\times 10^{-13}$.

We observe that for $g_{aee} = 5\times 10^{-13}$ (this constraint is compatible with the bounds obtained from considerations of White Dwarf and Red Giant stars' cooling [97–102]), the SNR can be significantly greater than unity. Thus, axion-photon interference experiments which use $M1$ transitions in post-transition metals may be sensitive to the product $g_{a\gamma\gamma}g_{aee}$ at the level of $10^{-23}\,\mathrm{GeV}^{-1}$.

2.6.2 The $M1$ case - solid target

The sensitivity to $g_{a\gamma\gamma}g_{aee}$ at the level of $10^{-23}\,\mathrm{GeV}^{-1}$ achieved with the use of $M1$ transitions in vapors can be further improved if we use, as absorption targets, some solids of high density and narrow linewidth.

Let us consider the crystal $EuCl_3 \cdot H_2O$ (the usefulness of this crystal for coherently producing axions was demonstrated in Ref. [103]), whose optical properties can be understood through the electron-shell structure of the Eu^{3+} ion which has six valence electrons on the 4f orbital [104, 105]. We consider the $M1$ transition $|^7F_0, m=0\rangle \to |^5D_1, m'=0\rangle$ with energy $\omega = 2.36\,\mathrm{eV}$. The reduced matrix element $\mathfrak{J}$ for this transition can be calculated using the spectral data of the Eu^{3+} ion [104, 105] and reads $\mathfrak{J} = \mathfrak{S} \approx 0.17 e/2m_e$. The atomic number density of Eu^{3+} in this crystal is $2.7\times 10^{21}\,\mathrm{cm}^{-3}$. We assume

that the total width of this transition is $\Gamma_{\rm tot} \approx 25\,\text{MHz}$ (this width was realized in $EuCl_3 \cdot H_2O$ for the $E1$ transition ${}^7F_0 \to {}^5D_0$ [106]; for simplicity, we assume that the width of the $M1$ transition under consideration is similar to this). Note that due to the high density and ultranarrow width, the $M1$ photon absorption length in this crystal is very small, $l_a \sim 1\,\text{cm}$, so we must use, in Eq. (2.18), $l \sim l_a$. As a result, the SNR is

$$\text{SNR}^{\rm solid} = \frac{4 g_{aee}}{\sqrt{\pi} e} \left| \frac{\hat{k}_\gamma^0}{\hat{b}_\gamma^0} \right| \sqrt{\mathcal{P} N t r}\,, \tag{2.19}$$

where $r = l/l_a$. Taking $r \approx 3$, one obtains $\text{SNR}^{\rm solid} \approx 20$ for $g_{aee} = 5 \times 10^{-13}$. Thus, an experiment using solid targets with ultranarrow linewidths can reach the sensitivity $g_{a\gamma\gamma} g_{aee} \sim 10^{-24}\,\text{GeV}^{-1}$. This is an order of magnitude better than the constraint obtained by multiplying the limits of ALPS-II and White Dwarf/Red Giant star cooling.

2.6.3 Comparison of projected sensitivities

To end this section, we provide a summary of all the assumptions that were made in our analysis and a comparison between the projected sensitivities of our proposed scheme and other existing and planned experiments.

The parameters used in our calculations are listed in Table 2.2.

<table>
<tr><td rowspan="6">Axion generation</td><td>Laser power</td><td colspan="2">10^{20} photons/second</td></tr>
<tr><td>Magnetic field strength</td><td colspan="2">$B_1 = 5.3\,\text{T}$</td></tr>
<tr><td>Magnetic field length</td><td colspan="2">$l_0 = 100\,\text{m}$</td></tr>
<tr><td rowspan="3">Photon-axion conversion probability</td><td colspan="2" rowspan="3">$\mathcal{P} = 10^{-7}$</td></tr>
<tr></tr>
<tr></tr>
<tr><td>Semi-transparent wall</td><td>Transmission coefficient</td><td colspan="2">$\mathcal{T} = 10^{-18}$</td></tr>
<tr><td rowspan="8">Target</td><td rowspan="2">Material</td><td>Vapor</td><td>Tl, Pb, Bi,...</td></tr>
<tr><td>Solid</td><td>$EuCl_3 \cdot H_2O$</td></tr>
<tr><td rowspan="2">Density</td><td>Vapor</td><td>$n \sim 10^{17}\,\text{cm}^{-3}$</td></tr>
<tr><td>Solid</td><td>$n \sim 10^{21}\,\text{cm}^{-3}$</td></tr>
<tr><td rowspan="2">Size</td><td>Vapor</td><td>$l = 10\,\text{m}$</td></tr>
<tr><td>Solid</td><td>$l \sim 3\,\text{cm}$</td></tr>
<tr><td>Integration time</td><td colspan="2">t =100 days</td></tr>
<tr><td colspan="2" rowspan="2">Projected sensitivity to $g_{a\gamma\gamma} g_{aee}$</td><td>Vapor</td><td>$\sim 10^{-23}\,\text{GeV}^{-1}$</td></tr>
<tr><td>Solid</td><td>$\sim 10^{-24}\,\text{GeV}^{-1}$</td></tr>
</table>

Table 2.2: Summary of the parameters used in the analysis of the axion signal and signal-to-noise ratio of the proposed ($M1$) axion-photon interference experiment.

A comparison between our scheme's level of sensitivity to $g_{a\gamma\gamma} g_{aee}$ with existing constraints from CAST experiment [14] and predicted sensitivity of the future IAXO experiment [27] is presented in Fig. 2.3. The exclusion curve *Axion-photon Interference with gas/liquid target* represents our scheme's sensitivity to $g_{a\gamma\gamma} g_{aee}$ if the target atoms are vapor post-transitional metals, in which the axion-induced transitions are of $M1$ type, or vapor alkali earth metals or liquid noble gases, in which the axion-induced transitions are of $M0$ type (the analysis for this latter case is presented in appendix A). The exclusion curve *Axion-photon Interference with solid target* represents our scheme's sensitivity to $g_{a\gamma\gamma} g_{aee}$ if the target is a solid with $M1$ type axion-induced transition.

As can be seen, for small axion mass $m_a \lesssim 10^{-4}\,\text{eV}$, our proposed experiment may improve on the limits of existing CAST measurements. It seems, however, not as competitive as the IAXO projections. The main reason for this is that the axions used in our scheme have to be artificially produced, and thus are not abundant in number, whereas in a helioscope experiment like IAXO, these particles come from

the Sun in a large quantity. In that respect, it is actually surprising that our proposed scheme can reach and in some case surpass CAST's sensitivity.

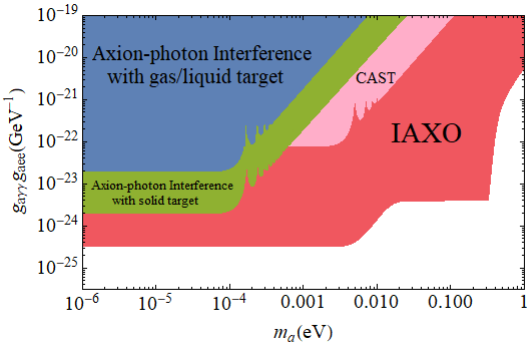

Figure 2.3: Comparison between constraints on the product $g_{a\gamma\gamma}g_{aee}$ as a function of the axion mass m_a from the CAST experiment (existing) [14], the IAXO experiment (projected) [27] and the sensitivity of the experimental scheme proposed in this paper (projected).

We note that it is possible, at least within some specific axion models, to relate the two coupling constants $g_{a\gamma\gamma}$ and g_{aee}. The latter is given in Eq. (2.8). The former may be expressed as [14]

$$g_{a\gamma\gamma} \approx \frac{\alpha}{2\pi f_a}\left(\frac{E}{N} - 1.92\right), \tag{2.20}$$

where α is the fine-structure constant and E/N is the ratio of the electromagnetic and color anomalies of the Peccei-Quinn symmetry.

If we assume that the axion is described by the KSVZ model [87, 88] then $C_e \sim \alpha/2\pi$ and $E/N = 0$. As a result, we obtain, from Eqs. (2.8) and (2.20)

$$g_{a\gamma\gamma} \approx -3.8 \times 10^3 g_{aee}\mathrm{GeV}^{-1}. \tag{2.21}$$

If, on the other hand, we assume that the axion is described by the DFSZ model [89, 90] then $C_e \sim 1$ and $E/N = 8/3$ so in this model, we have

$$g_{a\gamma\gamma} \approx 1.7 g_{aee}\mathrm{GeV}^{-1}. \tag{2.22}$$

The relations (2.21) and (2.22) allow us to convert our scheme's sensitivity to $|g_{a\gamma\gamma}g_{aee}|$ into a sensitivity to $g_{a\gamma\gamma}$ alone. This may then be compared to the projected limit on $g_{a\gamma\gamma}$ by ALPS-II [83] as presented in Fig. 2.4.

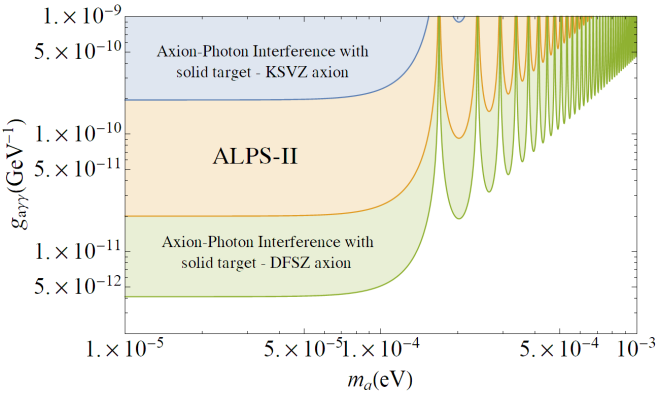

Figure 2.4: Comparison between the projected constraints on the coupling constant $g_{a\gamma\gamma}$ as a function of the axion mass m_a from the ALPS-II experiment [83] and the sensitivity of the experimental scheme using $M1$ atomic transition in a crystal proposed in this paper.

We conclude that for the DFSZ axion, our proposed scheme may have a better sensitivity to $g_{a\gamma\gamma}$ than ALPS-II. However, for the KFSZ axion, our sensitivity to $g_{a\gamma\gamma}$ is not as good as that of ALPS-II. Of course, since none of the axion models have been verified or falsified, it is not certain how g_{aee} and $g_{a\gamma\gamma}$ are related.

2.7 Conclusions

In this work, we have proposed and considered a scheme for the resonant detection of laboratory-produced axions and other axion-like particles. In this scheme, the axions are generated from photons in a magnetic field, as in current LSW experiments, and are then detected by using atomic (or molecular) transitions. The fundamental difference between this scheme and traditional LSW experiments is that instead of completely blocking the photons, we allow a small fraction of them to be absorbed by the target atoms. With such an allowance, the interference between the axion- and photon-induced transition amplitudes occurs and the experimental signal now scales linearly with the axion-electron coupling constant. This is an improvement over existing atom-based proposals whose signals have a quadratic dependence on the axion-electron coupling constant.

We have provided theoretical calculations and numerical estimates for a number of target atoms. We found that post-transition metals, in which axions induce transitions of $M1$ type, are potential candidates for experimental applications. This scheme may be realized as simple add-ons to the existing and planned ALPS experiments, with the photon-blocking wall replaced by some semi-transparent material and the axion-to-photon reconversion unit replaced by a vapor cell. Whereas ALPS and ALPS-II measure the quantity $g_{a\gamma\gamma}$ only, our scheme, as an upgrade to these experiments, allows one to also measure the product $g_{a\gamma\gamma}g_{aee}$. This means that with some relatively simple modifications, ALPS experiments can measure both $g_{a\gamma\gamma}$ and g_{aee}.

Our proposed scheme has a potential sensitivity to the product of the axion-photon and axion-electron coupling constants $g_{a\gamma\gamma}g_{aee}$ at the level of 10^{-24}–$10^{-23}\,\mathrm{GeV}^{-1}$. This level of sensitivity is at least one order of magnitude better than the existing limit of CAST. By using known relations between g_{aee} and $g_{a\gamma\gamma}$, we have shown that our proposed experiment is more sensitive to the DFSZ axion than ALPS-II.

It might be possible to increase the sensitivity to $g_{a\gamma\gamma}g_{aee}$ by using heterodyne interferometry, whose usefulness to ALPS-type experiments was studied in [107]. The authors of [107] suggested to interfere the photon signal in an ALPS-type experiment with a laser of slightly different frequency. This generates a time-varying signal, called the beat note (at the difference frequency) which is separated from the constant photon background and is detected. The authors of [107] hope to achieve a sensitivity of 10^{-6} photons per second. Following this idea, we can consider a scheme in which the axion-generating photons are blocked off completely (a completely opaque wall is used instead of a semi-transparent one) and the axion-induced transition amplitude is allowed to interfere with the amplitude of the transition caused by photons of slightly different frequency. The beat note in the total number of transitions is detected. This scheme may have some advantages over those considered in this paper. A detailed study of it will be the subject of our future work.

Acknowledgments

We thank Carlo Rizzo for asking the right questions that triggered this work and for his advice on the manuscript and Vladimir Dzuba, Max Zolotorev and Joerg Jaeckel for helpful discussions. This work was supported in part by the Australian Research Council Grant No. DP150101405, the Gutenberg Fellowship, the Humboldt Research Fellowship, the DFG Koselleck Program and the Heising-Simons and Simons Foundation. This project has also received funding from the European Research Council (ERC) under the European Union's Horizon 2020 Research and Innovative Programme (grant agreement No. 695405).

2.A Axion-photon interference with atomic transitions of $M0$ type

2.A.1 Scheme description

As discussed in Sect. 2.5.2, axions can also induce atomic transition of $M0$ type (total angular momentum is unchanged, parity is changed). In this appendix, we analyze the possibility of using $M0$ transitions to detect axions.

An $M0$ transition might be realized if the atoms are chosen to have two valence electrons, with the ground state 0 being $ns^2\,{}^1S_0$ and the first excited state being $nsnp\,{}^3P_0$ (such atoms include Mg, Ca, Sr, Ba and Hg). In such atoms, the single-photon transition from the ground state ${}^1S_0$ to the excited state ${}^3P_0$ is forbidden. On the other hand, since an axion can carry the quantum numbers (angular

momentum and parity) $0^-, 1^+, 2^-$,... [3, 78], this ${}^1S_0 \to {}^3P_0$ transition can be induced by absorption of axions (corresponding to axion angular momentum and parity 0^-).

If one applies a weak magnetic field $\mathbf{B}_2 = B_2\hat{\mathbf{z}}$ to the target atoms, the upper state ${}^3P_0$ becomes an admixture of the states ${}^3P_0$ and ${}^3P_{1,J_z=0}$:

$$|{}^3P_0\rangle \to |i\rangle = |{}^3P_0\rangle - \frac{\langle {}^3P_1|\,\boldsymbol{\mu}\cdot\mathbf{B}_2\,|{}^3P_0\rangle}{E_{{}^3P_0} - E_{{}^3P_1}}\,|{}^3P_1\rangle\ , \tag{2.23}$$

where $\boldsymbol{\mu} = \boldsymbol{\mu}_1 + \boldsymbol{\mu}_2$ is the sum of the magnetic moments of the two valence electrons. In the presence of the applied field, there will be a one-photon transition from the ground state to the state i due to the coupling between ${}^1S_0$ and ${}^3P_1$. One may choose the energy ω_γ of the photons from the laser (this energy equals that of the axions because the axions are produced from the same light field) so that it matches the energy difference $E_i - E_{{}^1S_0}$. In other words, the transition $0 \to i$ should be resonant. A diagram for the $M0$ transition in question is presented in Fig. 2.5.

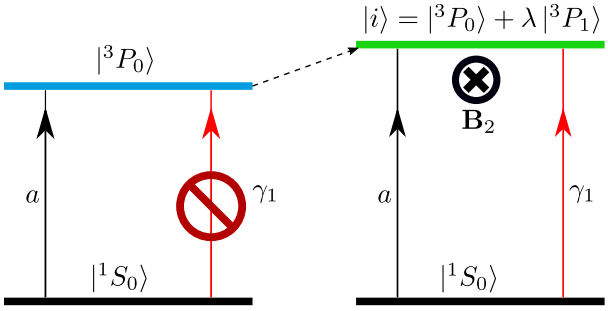

Figure 2.5: Energy levels in the target atoms in the $M0$ case. Normally, the transition ${}^1S_0 \to {}^3P_0$ due to the absorption of a photon is forbidden. If a magnetic field is applied to the target, the state ${}^3P_0$ becomes the state i which is an admixture of ${}^3P_0$ and ${}^3P_1$ and the transition due to photon absorption becomes weakly allowed. The absorption of axions and photons causes a resonant transition of the target atoms from the ground state ${}^1S_0$ to the excited state i. Interference occurs between the axion- and photon-induced transition amplitudes.

The total amplitude for the transition $0 \to i$ is the sum of the amplitudes due to axion absorption and photon absorption. The interference between these amplitudes allows us to detect axions. We note that for interference to occur, the photon and axion signals should have the same phase. However, as discussed in the next section, the photon absorption amplitude differs from the axion absorption amplitude by a factor of i which corresponds to a phase shift of a quarter of a wavelength. To compensate for this shift, the photons should be passed through a $\lambda/4$-waveplate as shown in Fig. 2.1. The phase compensation should also include photon phase shift due to the thin wall. In a realistic experiment, a phase-compensating waveplate is necessary.

We point out that the $J = 0 \to J' = 0$ (axion) transition also exists in noble gas atoms such as Xe, Ne, Kr and Ar. This transition may happen between the ground state $np^6\,{}^1S_0$ and the excited state $np^5\,{}^2P_{1/2}\,(n+1)\,s\,[1/2]_0$. The calculations for these noble gases are similar to those for the metals. We will present only the results of numerical estimates for these gases.

2.A.2 Calculations for the $M0$ case

Photon absorption amplitude

The value of the coefficient $\langle {}^3P_1, J_z = 0|\,\boldsymbol{\mu}\cdot\mathbf{B}_2\,|{}^3P_0\rangle$ in Eq. (2.23) is $\sqrt{2/3}\mu_0 B_2$. The energy difference $E_{{}^3P_0} - E_{{}^3P_1}$ in Eq. (2.23) can be conveniently written as $\Delta_0 - \Delta_1$ where $\Delta_0 = E_{{}^3P_0} - E_{{}^1S_0}$ and $\Delta_1 = E_{{}^3P_1} - E_{{}^1S_0}$. The values of these energy differences in the atoms of interest are given in [108, 109].

In the case of the transition $0 \to i$, the leading contribution to the matrix element M^γ_{BA} in Eq. (2.4) comes from the electric dipole (E1) term

$$M^\gamma_{BA} \approx e\,\langle i|\,\boldsymbol{\epsilon}\cdot\mathbf{r}\,|0\rangle = \frac{\sqrt{2}\mu_0 B_2}{3\,(\Delta_0 - \Delta_1)}\epsilon_{1z} D^P_S\ , \tag{2.24}$$

where $\boldsymbol{\epsilon}$ is, again, the photon polarization vector and $D^P_S = \langle {}^3P_1\|e\mathbf{r}\|{}^1S_0\rangle$ is the reduced E1 matrix element. The value of D^P_S can either be calculated numerically or determined from experiment. These values for the atoms of interest are presented in [108, 109].

Substituting Eq. (2.24) into Eq. (2.4), we obtain

$$M^{\gamma} \approx \frac{2i}{3}\sqrt{\pi n_{\gamma}\omega_{\gamma}}e^{-i\omega_{\gamma}t}\frac{\mu_0 B_2}{\Delta_0-\Delta_1}\epsilon_z D_S^P\,. \tag{2.25}$$

Axion absorption amplitude

For the transition $0 \xrightarrow{a} i$, only the $M0$ term contributes to the axion amplitude. Also, for this transition, it suffices to take into account only the first term in Eq. (2.23) which corresponds to the state ${}^3P_0$. In this case, the second ($M0$) term of the matrix element (2.10) can be calculated as

$$M^a_{BA} = \frac{g_{aee}\omega_a R}{3\sqrt{2}m_e}\,, \tag{2.26}$$

where $R = \int f\left(p_{1/2}\right) f\left(s_{1/2}\right) r^3 dr$. Here, $f\left(s_{1/2}\right)$ and $f\left(p_{1/2}\right)$ are the radial parts of the upper components of the $s_{1/2}$ and $p_{1/2}$ spinor wavefunctions, respectively. The coefficient R may be expressed via the reduced electric dipole matrix elements $D_S^P = \left\langle {}^3P_1\|e\mathbf{r}\|{}^1S_0\right\rangle$ and $\tilde{D}_S^P = \left\langle {}^1P_1\|e\mathbf{r}\|{}^1S_0\right\rangle$ as $R = D_S^P/e + \frac{1}{\sqrt{2}}\tilde{D}_S^P/e$ (the p electron in $nsnp\,{}^3P_1$ and $nsnp\,{}^1P_1$ states is in a linear combination of states $p_{3/2}$ and $p_{1/2}$; for R, we need only $p_{1/2}$, so a linear combination of D_S^P and $\tilde{D}_S^P$ is necessary to eliminate $p_{3/2}$). The values of D_S^P and $\tilde{D}_S^P$ for Mg, Ca and Sr are presented in [108]. The explicit values of R are given in Table 2.3.

Substituting Eq. (2.26) into Eq. (2.9), we find the resulting expression for the axion absorption amplitude

$$M^a \approx -\frac{g_{aee}n_a^{1/2}{\omega_a}^{3/2}R}{3m_e}e^{-i(\omega_\gamma t+\phi_a)}\,. \tag{2.27}$$

In contrast to the photon amplitude (2.25), the axion amplitude (2.27) does not have a factor of i. This means that the phases of these amplitudes differ by $\pi/2$ in addition to ϕ_a. To have the possibility of observing the interference between the photon and axion amplitudes, their phases need to be matched.

Axion signal and signal-to-noise ratio

The axion signal, as was defined in Sect. 2.5.3, now reads

$$\eta_{M0} \approx \frac{2g_{aee}}{\sqrt{\pi}}\frac{\Delta_0(\Delta_0-\Delta_1)R}{m_e\mu_0 B_2\epsilon_z D_S^P}\sqrt{\frac{\mathcal{P}}{\mathcal{T}}}\,. \tag{2.28}$$

To calculate the SNR, we note that in the current situation, the the rate of the $|0\rangle \to |i\rangle$ transition is given by $\Gamma_i = \frac{8}{81}\left(\frac{\mu_0 B_2}{\Delta_0-\Delta_1}\right)^2\Delta_1^3\left|D_S^P\right|^2$. Also, since we will be interested in both metal vapors and noble gases liquids, we need the total width $\Gamma_{\rm tot}$ in its general form

$$\Gamma_{\rm tot} \approx \begin{cases} \Gamma_{\rm Dop} = 2v_0\Delta_0/\sqrt{\pi} & ({\rm dv})\,, \\ \Gamma_{\rm col} = 2v_0 n\sigma_{\rm col} & ({\rm lq})\,, \end{cases} \tag{2.29}$$

where 'dv' means dilute vapor and 'lq' means liquid. Here $\Gamma_{\rm Dop}$ is the Doppler width as given in Eq. (2.17), whereas $\Gamma_{\rm col}$ is the collisional width; $v_0 = \sqrt{2k_BT/m}$ is again the most probable thermal speed of the target atoms and $\sigma_{\rm col}$ is the collisional cross section of the target atoms.

In summation, we find

$${\rm SNR}_{M0} \approx \begin{cases} \frac{8\pi^{1/4}g_{aee}\Delta_1^{3/2}R}{9\epsilon_z m_e}\sqrt{\frac{\mathcal{P}Nltn}{v_0\Delta_0}} & ({\rm dv})\,, \\ \frac{8g_{aee}\Delta_1^{3/2}R}{9\epsilon_z m_e}\sqrt{\frac{\mathcal{P}Nlt}{v_0\sigma_{\rm col}}} & ({\rm lq})\,. \end{cases} \tag{2.30}$$

Note that the SNR (2.30) is independent of the transmission coefficient $\mathcal{T}$ and the magnetic field B_2.

Note also that the first of Eqs. (2.30) has a dependence on the atom density n but the second does not. This change of behavior happens at a critical value of the atom density, e.g., that of dense gases, such that the collisional and Doppler widths are comparable. As a result, as we increase the atom density, the SNR increases then saturates. After this point, we gain no further enhancement by having denser targets.

In the idealized experiment considered so far, since the axion signal η is inversely proportional to the magnetic field B_2 whereas the SNR is independent of this quantity, one may suggest using arbitrarily

small B_2 to enhance the axion signal. However, Eq. (2.30) applies only if the photon noise makes the dominant contribution to the total noise. In practice, when the photon amplitude (proportional to B_2) becomes too small, signal-independent backgrounds will become significant, degrading the SNR. This determines the minimum usable value of B_2. Note also that close to this regime, the relative value of the interference term compared to the leading term in the transition probability is maximal.

2.A.3 Comparison with the $M1$ case

In this subsection, we provide a comparison between the two schemes which use axion-induced $M0$ and $M1$ types of atomic transition.

On the one hand, the photon-induced (as well as the axion-induced) amplitude of $M1$ type is allowed. On the other hand, when the axion-induced transition is of $M0$ type, the photon-induced transition amplitude is forbidden due to the selection rule $J = 0 \nrightarrow J' = 0$.

Nevertheless, by inspection of Eq. (2.10) for the axion-induced transition matrix element, one deduces

$$\left|\frac{M^a_{M0}}{M^a_{M1}}\right| = \left|\frac{\omega_a \langle B|\, \mathbf{r}\cdot\mathbf{S} - \left(\hat{\mathbf{k}}_a\cdot\mathbf{S}\right)\left(\hat{\mathbf{k}}_a\cdot\mathbf{r}\right)|A\rangle}{\langle B|\, \hat{\mathbf{k}}_a\cdot\mathbf{S}\,|A\rangle}\right| \sim \omega_a r \sim 10^{-4}\text{–}10^{-3}\,, \tag{2.31}$$

where ω_a is the energy of the transition ($\lesssim$ eV), r is a typical atomic radius ($\sim 2\,$Å). Thus, the axion-induced $M0$ transition amplitude is suppressed compared to its $M1$ counterpart.

This means that for some fixed set of experimental parameters, an axion-photon interference experiment which uses $M1$ transitions will generally give a larger absolute signal and SNR (which are proportional to the interference term in the total transition probability, i.e., the real part of the product of the axion- and photon-induced amplitudes) and thus might make it easier to detect axions than an experiment that uses $M0$ transitions.

2.A.4 Numerical estimates for the $M0$ case

We have derived the formulae for the signal and the SNR of the axion-photon $M0$ interference experiment, Eqs. (2.28) and (2.30), respectively. We now provide numerical estimates for these quantities.

Besides the aforementioned situations where the target atoms are metals, we also consider the noble gases. Although the electronic configurations in the latter are different from those in the former (the outermost shell is p^6 instead of s^2), the calculation presented above is still good for the purpose of an estimate. We give numerical estimates for the noble gases using the same equations (2.28) and (2.30) as for metals.

For $\mathcal{P}$, N, $\mathcal{T}$ and t, we use the same values as in Sect. (2.6). We again assume that the laser light is polarized in the z-direction.

The appropriate values for the atom density n and temperature T for different atoms are presented in Table 2.3 (see the caption of this table for more comments on the values of n and T). We take $l = 100\,$m. For B_2, we assume the value $10^{-4}\,$T, which is larger than Earth's magnetic field, so no elaborate shielding is needed. The values for the reduced electric dipole matrix elements are given in [108, 109]. The resulting quantities are summarized in Table 2.3.

We observe that for $g_{aee} = 5\times10^{-13}$, the SNR in the cases of the nobles gases can be of the order of unity. Thus, an axion-photon interference experiment that uses a noble gas as the axion and photon absorption medium is sensitive to the product $g_{a\gamma\gamma}g_{aee} \gtrsim 10^{-23}\,\text{GeV}^{-1}$. If a metal vapor is used instead of a noble gas, the sensitivity decreases by two to three orders of magnitude. However, the drawback of the noble gases is their large excitation energies Δ_0 and Δ_1, which are far beyond the optical region. Such large energies can be achieved by using high-harmonic generation, but at the expense of the number of available photons.

2.B Axion laser

As a byproduct of the atomic transition calculated performed in this paper, we can consider the possibility of using atoms to make axion 'lasers'. To the authors' knowledge this problem has not been studied before.

In principle, the $M0$ transition ${}^3P_0 \to {}^1S_0$ can be used to produce axions. Schematically, we can use a laser to resonantly excite the atoms in the ground state ${}^1S_0$ to some state with total angular momentum

Atom	Δ_0 (eV)	Δ_1 (eV)	D_S^P/e (a.u.)	$\tilde{D}_S^P/e$ (a.u.)	R (a.u.)	T (K)	$n\,(\mathrm{cm}^{-3})$	$\frac{\eta_{M0}}{10^{-3}}$	SNR_{M0}
Ca	1.879	1.886	0.03	4.93	3.52	1700	4.3×10^{18} (dv)	0.9	0.06
Sr	1.775	1.798	0.15	5.39	3.96	1600	5.1×10^{18} (dv)	0.8	0.1
Ba	1.521	1.567	0.31	5.46	4.17	2000	3.7×10^{18} (dv)	0.7	0.07
Hg	4.667	4.886	0.45	2.64	2.32	1000	2.2×10^{19} (dv)	4	0.4
Yb	2.143	2.231	0.54	4.24	3.54	1400	4.2×10^{18} (dv)	0.8	0.1
Ne	16.72	16.85	0.60	0.17	0.73	26	3.6×10^{22} (lq)	1	1
Ar	11.72	11.83	0.93	0.46	1.14	86	2.1×10^{22} (lq)	1	2
Kr	10.56	10.64	0.85	0.91	1.04	118	1.7×10^{22} (lq)	0.7	2
Xe	9.447	9.570	0.89	1.15	1.09	164	1.3×10^{22} (lq)	1	1

Table 2.3: Estimates of the $M0$ interference signal η and SNR for some target atoms. For the metals, Δ_0 and Δ_1 are the energies of the states $nsnp\,^3P_0$ and $nsnp\,^3P_1$ with respect to the ground state $ns^2\,^1S_0$. For the noble gases, Δ_0 and Δ_1 are the energies of the states $np^5\,^2P_{1/2}\,(n+1)\,s\,[1/2]_0$ and $np^5\,^2P_{1/2}\,(n+1)\,s\,[1/2]_1$ with respect to the ground state $np^6\,^1S_0$. For the metals, D_S^P and $\tilde{D}_S^P$ are the $E1$ reduced matrix elements between the ground state $^1S_0$ and the states $^3P_1$ and $^1P_1$, respectively. For the noble gases, D_S^P and $\tilde{D}_S^P$ are the $E1$ reduced matrix elements between the ground state $np^6\,^1S_0$ and the states $np^5\,^2P_{1/2}\,(n+1)\,s\,[1/2]_1$ and $np^5\,^2P_{1/2}\,(n+1)\,s\,[3/2]_1$, respectively. We assume that the temperatures of the metals vapors (except for Hg) are only slightly lower than their corresponding boiling points. The densities n of the vapors at these temperatures are estimated using the ideal gas equation and experimentally fitted vapor pressure equations presented in [96]. The temperature of the Hg vapor is taken to be 1000 K (higher than Hg's boiling point) and its density at this temperature is presented in [110]. The temperatures and densities of the noble gas liquids are presented in [111]. The SNR corresponds to a target length of 100 m and integration time of 100 days. The signal and SNR are presented for $g_{aee}=5\times10^{-13}$.

$J'=1$ then use another laser to bring the atoms in this state to the $^3P_0$ state. The state $^3P_0$ can only decay to the ground state $^1S_0$ by spontaneously emitting axions (or two photons). In this section, we give an estimate of the $^3P_0\to{}^1S_0$ transition rate due to the spontaneous emission of axions. We also provide an estimate for the cross section of the absorption of an axion by a single atom (which makes the $^3P_0\to{}^1S_0$ transition). This quantity might be of interest if one wishes to know how many axions are absorbed in the scheme proposed above.

The matrix element for the $^3P_0\to{}^1S_0$ transition is obtained from Eq. (2.27) by setting $n_a=1$. The transition rate then reads

$$\begin{aligned}\Gamma^a &= 2\pi\int\frac{\omega_1^2 d\omega_1 d\Omega}{(2\pi)^3}\delta\left(\omega_1-\Delta_0\right)\left|M^a\right|^2=\frac{\Delta_0^2}{(2\pi)^2}\left|M^a\right|^2\Big|_{\omega_1=\Delta_0}=\frac{g_{aee}^2R^2\Delta_0^5}{9\pi m_e^2}\\ &\approx\left(\frac{10^9\,\mathrm{GeV}}{f_a/C_e}\right)^2\left(\frac{\Delta_0}{1\,\mathrm{eV}}\right)^5\left(\frac{R}{1\text{ a.u.}}\right)^2\times\frac{3.86}{10^{30}\,\mathrm{s}}\,,\end{aligned}\tag{2.32}$$

where Δ_0 is the energy of the $^3P_0$ state and the value of the integral R is given in Table 2.3. Here, we take $f_a/C_e=10^9\,\mathrm{GeV}$. The transition rates in some typical atoms are presented in Table 2.4. Now suppose that one constructs an axion 'laser' using one of these elements as the gain medium. Let us estimate the number of axions produced per second per unit volume (cm^3) of the gain medium by this 'laser'. This value is obtained by multiplying the transition rates (Table 2.4) by the number of atoms per unit volume (cm^{-3}) of the corresponding elements (Table 2.3). The results are presented in the last column of Table 2.4. We observe that the number of axions produced (per unit time per unit volume) is small so an axion 'laser' using the $J=0\to J'=0$ is not efficient.

Finally, the axion absorption cross section σ_a (without interference with a photon field) is obtained by replacing Γ_i in Eq. (2.16) with the axion emission rate Γ^a (2.32). We find

$$\sigma_a=\frac{4\pi}{\Delta_0^2}\frac{\Gamma^a}{\Gamma_{\mathrm{tot}}}=\begin{cases}\frac{2\sqrt{\pi}g_{aee}^2R^2\Delta_0^2}{9m_e^2v_0} & (\mathrm{dv})\,,\\ \frac{2g_{aee}^2R^2\Delta_0^3}{9m_e^2v_0n\sigma_{\mathrm{col}}} & (\mathrm{lq})\,.\end{cases}\tag{2.33}$$

The estimate of this cross section σ_a for some atoms are presented in Table 2.4.

Atom	Axion spontaneous emission rate Γ^a (s^{-1})	Axion absorption cross section σ_a (a_B^2)	Atom density (cm^{-3})	Number of axions produced $(\mathrm{s}^{-1}\,\mathrm{cm}^{-3})$
Mg	4.8×10^{-27}	7.7×10^{-30}	4.6×10^{18}	2.2×10^{-8}
Ca	1.1×10^{-27}	6.3×10^{-30}	4.3×10^{18}	4.7×10^{-9}
Sr	1.1×10^{-27}	1.5×10^{-29}	5.1×10^{18}	5.6×10^{-9}
Ba	5.5×10^{-28}	9.7×10^{-30}	3.7×10^{18}	2.0×10^{-9}
Hg	4.6×10^{-26}	4.8×10^{-29}	2.2×10^{19}	1.0×10^{-6}
Yb	2.2×10^{-27}	1.9×10^{-29}	4.2×10^{18}	9.2×10^{-9}
Ne	2.6×10^{-24}	2.1×10^{-30}	3.6×10^{22}	9.4×10^{-4}
Ar	1.1×10^{-24}	1.7×10^{-30}	2.1×10^{22}	2.4×10^{-4}
Kr	5.5×10^{-25}	1.3×10^{-30}	1.7×10^{22}	9.5×10^{-5}
Xe	3.5×10^{-25}	1.1×10^{-30}	1.3×10^{22}	4.7×10^{-5}

Table 2.4: Estimates of the rates of the ${}^3P_0 \to {}^1S_0$ transition due to spontaneous emission of axions, the axion absorption cross section and the number of axions emitted per unit time per unit volume. The axion absorption cross section is given in the units of a_B^2, where a_B is the Bohr radius.

Bibliography

[1] R. D. Peccei and H. R. Quinn, Phys. Rev. Lett. **38**, 1440 (1977).

[2] R. D. Peccei, *The Strong* CP *Problem and Axions* (Springer, Berlin, Heidelberg, 2008), pp. 3–17, ISBN 978-3-540-73518-2.

[3] S. Weinberg, Phys. Rev. Lett. **40**, 223 (1978).

[4] F. Wilczek, Phys. Rev. Lett. **40**, 279 (1978).

[5] P. Sikivie, Phys. Rev. Lett. **51**, 1415 (1983).

[6] P. Sikivie, Phys. Rev. D **32**, 2988 (1985).

[7] S. Moriyama, M. Minowa, T. Namba, Y. Inoue, Y. Takasu, and A. Yamamoto, Phys. Lett. B **434**, 147 (1998).

[8] Y. Inoue, T. Namba, S. Moriyama, M. Minowa, Y. Takasu, T. Horiuchi, and A. Yamamoto, Phys. Lett. B **536**, 18 (2002).

[9] Y. Inoue, Y. Akimoto, R. Ohta, T. Mizumoto, A. Yamamoto, and M. Minowa, Phys. Lett. B **668**, 93 (2008).

[10] R. Ohta, Y. Akimoto, Y. Inoue, M. Minowa, T. Mizumoto, S. Moriyama, T. Namba, Y. Takasu, and A. Yamamoto, Nucl. Instr. Meth. A **670**, 73 (2012).

[11] T. Mizumoto, R. Ohta, T. Horie, J. Suzuki, Y. Inoue, and M. Minowa, J. Cosmo. Astropart. Phys. **07**, 013 (2013).

[12] K. Zioutas et al., Nucl. Instrum. Meth. A **425**, 480 (1999).

[13] E. Arik et al., J. Cosmo. Astropart. Phys. **02**, 008 (2009).

[14] K. Barth et al., J. Cosmo. Astropart. Phys. **05**, 010 (2013).

[15] V. Anastassopoulos et al. (CAST Collaboration), Nat. Phys. **13**, 584 (2017).

[16] F. T. Avignone, D. Abriola, R. L. Brodzinski, J. I. Collar, R. J. Creswick, D. E. DiGregorio, H. A. Farach, A. O. Gattone, C. K. Guérard, F. Hasenbalg, et al. (SOLAX Collaboration), Phys. Rev. Lett. **81**, 5068 (1998).

[17] A. Gattone et al., Nucl. Phys. B - Proc. Suppl. **70**, 59 (1999).

[18] A. Morales et al., Astropar. Phys. **16**, 325 (2002).

[19] R. Bernabei, P. Belli, R. Cerulli, F. Montecchia, F. Nozzoli, A. Incicchitti, D. Prosperi, C. Dai, H. He, H. Kuang, et al., Phys. Lett. B **515**, 6 (2001).

[20] R. Bernabei, P. Belli, F. Montecchia, F. Nozzoli, F. Cappella, A. Incicchitti, D. Prosperi, R. Cerulli, C. J. Dai, H. L. He, et al., Int. J. Mod. Phys. A **21**, 1445 (2006).

[21] R. Bernabei et al., Eur. Phys. J. C **67**, 39 (2010).

[22] Z. Ahmed et al. (CDMS Collaboration), Phys. Rev. Lett. **103**, 141802 (2009).

[23] Z. Ahmed et al. (CDMS Collaboration), Phys. Rev. Lett. **106**, 131302 (2011).

[24] R. Agnese et al. (CDMS Collaboration), Phys. Rev. Lett. **111**, 251301 (2013).

[25] R. Agnese et al. (SuperCDMS Collaboration), Phys. Rev. Lett. **112**, 241302 (2014).

[26] I. Irastorza et al., J. Cosmo. Astropar. Phys. **06**, 013 (2011).

[27] I. G. Irastorza et al. (IAXO Collaboration), Tech. Rep. CERN-SPSC-2013-022. SPSC-I-242, CERN, Geneva (2013).

[28] E. Armengaud et al., J. Instrum. **9**, T05002 (2014).

[29] S. J. Asztalos, G. Carosi, C. Hagmann, D. Kinion, K. van Bibber, M. Hotz, L. J. Rosenberg, G. Rybka, J. Hoskins, J. Hwang, et al., Phys. Rev. Lett. **104**, 041301 (2010).

[30] A. Wagner, G. Rybka, M. Hotz, L. J. Rosenberg, S. J. Asztalos, G. Carosi, C. Hagmann, D. Kinion, K. van Bibber, J. Hoskins, et al., Phys. Rev. Lett. **105**, 171801 (2010).

[31] J. Hoskins, J. Hwang, C. Martin, P. Sikivie, N. S. Sullivan, D. B. Tanner, M. Hotz, L. J. Rosenberg, G. Rybka, A. Wagner, et al., Phys. Rev. D **84**, 121302 (2011).

[32] S. A. Kenany et al., Nucl. Instrum. Meth. A **854**, 11 (2017).

[33] B. M. Brubaker, L. Zhong, Y. V. Gurevich, S. B. Cahn, S. K. Lamoreaux, M. Simanovskaia, J. R. Root, S. M. Lewis, S. Al Kenany, K. M. Backes, et al., Phys. Rev. Lett. **118**, 061302 (2017).

[34] B. T. McAllister, G. Flower, E. N. Ivanov, M. Goryachev, J. Bourhill, and M. E. Tobar, Phys.Dark Univ **18**, 67 (2017).

[35] K. Ehret, M. Frede, E.-A. Knabbe, D. Kracht, A. Lindner, N. T. Meyer, D. Notz, A. Ringwald, and G. Wiedemann, arXiv:0702023 (2007).

[36] K. Ehret, M. Frede, S. Ghazaryan, M. Hildebrandt, E.-A. Knabbe, D. Kracht, A. Lindner, J. List, T. Meier, N. Meyer, et al., Nucl. Instrum. Meth. A **612**, 83 (2009).

[37] K. Ehret, M. Frede, S. Ghazaryan, M. Hildebrandt, E.-A. Knabbe, D. Kracht, A. Lindner, J. List, T. Meier, N. Meyer, et al., Phys. Lett. B **689**, 149 (2010).

[38] P. Pugnat, L. Duvillaret, R. Jost, G. Vitrant, D. Romanini, A. Siemko, R. Ballou, B. Barbara, M. Finger, M. Finger, et al. (OSQAR Collaboration), Phys. Rev. D **78**, 092003 (2008).

[39] P. Pugnat et al. (OSQAR Collaboration), Eur. Phys. J. C **74**, 3027 (2014).

[40] R. Ballou, G. Deferne, M. Finger, M. Finger, L. Flekova, J. Hosek, S. Kunc, K. Macuchova, K. A. Meissner, P. Pugnat, et al. (OSQAR Collaboration), Phys. Rev. D **92**, 092002 (2015).

[41] A. S. Chou, W. Wester, A. Baumbaugh, H. R. Gustafson, Y. Irizarry-Valle, P. O. Mazur, J. H. Steffen, R. Tomlin, X. Yang, and J. Yoo, Phys. Rev. Lett. **100**, 080402 (2008).

[42] G. Cantatore, F. D. Valle, E. Milotti, L. Dabrowski, and C. Rizzo, Phys. Lett. B **265**, 418 (1991).

[43] E. Zavattini, G. Zavattini, G. Ruoso, G. Raiteri, E. Polacco, E. Milotti, V. Lozza, M. Karuza, U. Gastaldi, G. Di Domenico, et al. (PVLAS Collaboration), Phys. Rev. D **77**, 032006 (2008).

[44] F. Della Valle, A. Ejlli, U. Gastaldi, G. Messineo, E. Milotti, R. Pengo, G. Ruoso, and G. Zavattini, Eur. Phys. J. C **76**, 24 (2016).

[45] S. J. Chen, H. H. Mei, and W. T. Ni, Mod. Phys. Lett. A **22**, 2815 (2007).

[46] R. Battesti, B. Pinto Da Souza, S. Batut, C. Robilliard, G. Bailly, C. Michel, M. Nardone, L. Pinard, O. Portugall, G. Trénec, et al., Eur. Phys. J. D **46**, 323 (2008).

[47] J. Jackel, A. Lindner, and J. Redondo, eds., *Proceedings, 5th Patras Workshop on Axions, WIMPs and WISPs (AXION-WIMP 2009)*, DESY (DESY, Hamburg, Germany, 2010).

[48] L. Maiani, R. Petronzio, and E. Zavattini, Phys. Lett. B **175**, 359 (1986).

[49] R. Barbieri, M. Cerdonio, G. Fiorentini, and S. Vitale, Phys. Lett. B **226**, 357 (1989).

[50] R. Barbieri, C. Braggio, G. Carugno, C. Gallo, A. Lombardi, A. Ortolan, R. Pengo, G. Ruoso, and C. Speake, Phys. Dark Univ **15**, 135 (2017).

[51] P. W. Graham and S. Rajendran, Phys. Rev. D **84**, 055013 (2011).

[52] D. Budker, P. W. Graham, M. Ledbetter, S. Rajendran, and A. O. Sushkov, Phys. Rev. X **4**, 021030 (2014).

[53] P. W. Graham and S. Rajendran, Phys. Rev. D **88**, 035023 (2013).

[54] Y. V. Stadnik and V. V. Flambaum, Phys. Rev. D **89**, 043522 (2014).

[55] C. Abel et al., Phys. Rev. X **7**, 041034 (2017).

[56] D. Horns, J. Jaeckel, A. Lindner, A. Lobanov, J. Redondo, and A. Ringwald, J. Cosmo. Astropart. Phys. **04**, 016 (2013).

[57] J. Jaeckel and J. Redondo, Phys. Rev. D **88**, 115002 (2013).

[58] A. J. Millar, G. G. Raffelt, J. Redondo, and F. D. Steffen, J. Cosmo. Astropart. Phys **01**, 061 (2017).

[59] A. Caldwell, G. Dvali, B. Majorovits, A. Millar, G. Raffelt, J. Redondo, O. Reimann, F. Simon, and F. Steffen (MADMAX Collaboration), Phys. Rev. Lett. **118**, 091801 (2017).

[60] J. E. Moody and F. Wilczek, Phys. Rev. D **30**, 130 (1984).

[61] A. Arvanitaki and A. A. Geraci, Phys. Rev. Lett. **113**, 161801 (2014).

[62] Y. V. Stadnik, V. A. Dzuba, and V. V. Flambaum, Phys. Rev. Lett. **120**, 013202 (2018).

[63] V. A. Dzuba, V. V. Flambaum, I. B. Samsonov, and Y. V. Stadnik, Phys. Rev. D **98**, 035048 (2018).

[64] Y. Kahn, B. R. Safdi, and J. Thaler, Phys. Rev. Lett. **117**, 141801 (2016).

[65] G. Ruoso, A. Lombardi, A. Ortolan, R. Pengo, C. Braggio, G. Carugno, C. S. Gallo, and C. C. Speake, J. Phys. - Conf. Ser **718**, 042051 (2016).

[66] Y. Hochberg, T. Lin, and K. M. Zurek, Phys. Rev. D **94**, 015019 (2016).

[67] Y. Hochberg, T. Lin, and K. M. Zurek, Phys. Rev. D **95**, 023013 (2017).

[68] P. Sikivie, N. Sullivan, and D. B. Tanner, Phys. Rev. Lett. **112**, 131301 (2014).

[69] S. Chaudhuri, P. W. Graham, K. Irwin, J. Mardon, S. Rajendran, and Y. Zhao, Phys. Rev. D **92**, 075012 (2015).

[70] M. Silva-Feaver, S. Chaudhuri, H. M. Cho, C. Dawson, P. Graham, K. Irwin, S. Kuenstner, D. Li, J. Mardon, H. Moseley, et al., EEE Trans. Appl. Supercond **27**, 1 (2017).

[71] C. Beck, Phys. Rev. Lett. **111**, 231801 (2013).

[72] C. Beck, Phys. Dark Univ. **7-8**, 6 (2015).

[73] H. Tam and Q. Yang, Phys. Lett. B **716**, 435 (2012).

[74] A. Arvanitaki, S. Dimopoulos, and K. Van Tilburg, Phys. Rev. X **8**, 041001 (2018).

[75] C. Braggio et al., eds., *New detectors for axions* (Turin, Italy, 2017).

[76] C. J. Cao and A. Zhitnitsky, Phys. Rev. D **96**, 015013 (2017).

[77] M. Yoshimura and N. Sasao, arXiv:1710.11262 (2017).

[78] K. Zioutas and Y. Semertzidis, Phys. Lett. A **130**, 94 (1988).

[79] P. Sikivie, Phys. Rev. Lett. **113**, 201301 (2014).

[80] L. Santamaria, C. Braggio, G. Carugno, V. D. Sarno, P. Maddaloni, and G. Ruoso, New J. Phys. **17**, 113025 (2015).

[81] K. Van Bibber, N. R. Dagdeviren, S. E. Koonin, A. K. Kerman, and H. N. Nelson, Phys. Rev. Lett. **59**, 759 (1987).

[82] K. van Bibber, P. M. McIntyre, D. E. Morris, and G. G. Raffelt, Phys. Rev. D **39**, 2089 (1989).

[83] R. Baehre, B. Doebrich, J. Dreyling-Eschweiler, S. Ghazaryan, R. Hodajerdi, D. Horns, F. Januschek, E. A. Knabbe, A. Lindner, D. Notz, et al., J. Instrum **8**, T09001 (2013).

[84] V. B. Berestetskii, E. M. Lifshitz, and L. P. Pitaevskii, *Quantum Electrodynamics*, vol. 4 of *Course of Theoretical Physics* (Pergamon Press, Oxford, 1982).

[85] K. Gottfried and T. M. Yan, *Quantum mechanics: fundamentals* (Springer, New York, Berlin, Heidelberg, 2013).

[86] I. I. Sobelman, *Atomic spectra and radiative transitions*, vol. 12 (Springer, New York, Berlin, Heidelberg, 2012).

[87] J. E. Kim, Phys. Rev. Lett. **43**, 103 (1979).

[88] M. Shifman, A. Vainshtein, and V. Zakharov, Nucl. Phys. B **166**, 493 (1980).

[89] M. Dine, W. Fischler, and M. Srednicki, Phys. Lett. B **104**, 199 (1981).

[90] A. Zhitnitsky, Sov. J. Nucl. Phys. **31**, 260 (1980).

[91] M. Srednicki, Nucl. Phys. B **260**, 689 (1985).

[92] M. Pospelov, A. Ritz, and M. Voloshin, Phys. Rev. D **78**, 115012 (2008).

[93] I. B. Khriplovich, *Parity nonconservation in atomic phenomena* (Gordon and Breach Science Publishers, Philadelphia, 1991).

[94] O. Sushkov, V. Flambaum, and I. Khriplovich, *Report at the Conference on the Theory of Atoms and Molecules* (Vilnius, 1979).

[95] V. A. Dzuba, V. V. Flambaum, P. G. Silvestrov, and O. P. Sushkov, Phys. Rev. A **44**, 2828 (1991).

[96] C. B. Alcock, V. P. Itkin, and M. K. Horrigan, Can. Metall. Q **23**, 309 (1984).

[97] G. G. Raffelt, Phys. Lett. B **166**, 402 (1986).

[98] J. Isern, E. Garcia-Berro, S. Torres, and S. Catalan, Astrophys. J. Lett. **682**, L109 (2008).

[99] J. Isern, S. Catalan, E. Garcia-Berro, and S. Torres, J. Phys. Conf. Ser. **172**, 012005 (2009).

[100] A. H. Corsico, L. G. Althaus, M. M. Bertolami, A. D. Romero, E. Garcia-Berro, J. Isern, and S. O. Kepler, Mon. Notices Royal Astron. Soc. **424**, 2792 (2012).

[101] A. Corsico, L. Althaus, A. Romero, A. Mukadam, E. Garcia-Berro, J. Isern, S. Kepler, and M. Corti, J. Cosmo. Astropart. Phys. **2012**, 010 (2012).

[102] N. Viaux, M. Catelan, P. B. Stetson, G. G. Raffelt, J. Redondo, A. A. R. Valcarce, and A. Weiss, Phys. Rev. Lett. **111**, 231301 (2013).

[103] V. V. Flambaum, I. B. Samsonov, H. B. Tran Tan, and D. Budker, Phys. Rev. D **98**, 095028 (2018).

[104] G. S. Ofelt, J. Chem. Phys. **38**, 2171 (1963).

[105] K. Binnemans, Coord. Chem. Rev. **295**, 1 (2015).

[106] R. L. Ahlefeldt, M. R. Hush, and M. J. Sellars, Phys. Rev. Lett. **117**, 250504 (2016).

[107] Z. Bush, S. Barke, H. Hollis, G. Mueller, and D. Tanner (2017).

[108] S. G. Porsev, M. G. Kozlov, Y. G. Rakhlina, and A. Derevianko, Phys. Rev. A **64**, 012508 (2001).

[109] A. Kramida et al. (NIST ASD Team), NIST Atomic Spectra Database (2017).

[110] R. E. Drullinger, M. M. Hessel, and E. W. Smith, J. Chem. Phys. **66**, 5656 (1977).

[111] W. M. Haynes, *CRC handbook of chemistry and physics* (CRC press, Boca Raton, 2014).

Chapter 3

Coherent axion-photon transformations in the forward scattering on atoms

3.1 Overview

In this chapter, I consider the possibility of producing axions by using forward scattering on atoms in media. Conventionally, axions are produced from photons in a strong magnetic field, with the photon-to-axion conversion rate being proportional to the axion-photon coupling $g_{a\gamma\gamma}$ squared. In contrast, the mechanism investigated in this chapter has a production rate which is proportional to the axion-electron coupling g_{aee} squared. Thus, this gives us a method to measure a different interaction constant.

This results is published in the following paper:

1. V. V. Flambaum, I. B. Samsonov, H. B. Tran Tan and D. Budker, **Coherent axion-photon transformations in the forward scattering on atoms**, Phys. Rev. D 98, 095028 (2018), arXiv:1805.01793,

which I presented at the international workshop:

1. **Coherent axion-photon transformations in the forward scattering on atoms**, Quantum Technologies for Axion Dark Matter Detection Incubator, University of Sydney, Sydney, Australia, September 2018.

3.2 Abstract

In certain laboratory experiments the production and/or detection of axions is due to the photon-axion transformations in a strong magnetic field. This process is coherent, and the rate of the transformation is proportional to the length l and magnitude B of the magnetic field squared, $\sim l^2B^2$. In the present paper, we consider coherent production of axions due to the forward scattering of photons on atoms or molecules. This process may be represented as being due to an effective electromagnetic field which converts photons to axions. We present analytical expressions for such effective magnetic and electric fields induced by resonant atomic M0 and M1 transitions, as well as give some numerical estimates for these fields. The corresponding experiments would allow one to measure the electron-axion coupling constant g_{ae} in the same way as the photon-axion coupling $g_{a\gamma}$ is studied.

3.3 Introduction

The axion was introduced to explain the absence of CP violation in the strong interaction [1–9] and is considered as a probable candidate for a dark matter particle. The majority of experiments searching for axions in laboratories are based on the transformation of axions to photons (for axion detection) and photons to axions (for axion production) in a strong magnetic field [10–49]. The use of atomic and molecular transitions for the axion detection has been suggested in Refs. [50–55]. It is natural to assume

that the atomic transitions can play role of effective electromagneic field in the process of conversion of photons to axions. This paper aims to estimate such effective electric and magnetic fields induced by forward scattering of photons on atoms near atomic resonances.

The photon-to-axion conversion probability in magnetic field B is [56] (in units $\hbar = c = 1$)

$$P = \frac{\omega}{4k_a} \left(g_{a\gamma} B l\right)^2 F^2(q)\,, \tag{3.1}$$

where ω is the axion and photon energy, k_a is the axion momentum, $g_{a\gamma}$ is the axion-photon coupling constant, l is the spatial extent of the magnetic field in the direction of the axion-photon beam, $F(q) = \int dx\, e^{-iqx} B(x)/\overline{B} l$ is the form factor, $q = \omega - k_a$ is the momentum transferred from the photon field to the axion field. For a small axion mass, $m_a \ll \omega$, we have $q \approx 0$ and $F(0) \approx 1$.

Probabilities of the transformation of photons to axions and axions to photons are calculated by solving the system of Maxwell and Klein-Gordon equations coupled through the interaction term in the Lagrangian density:

$$L^{a\gamma} = g_{a\gamma}\, a\, (\mathbf{E} \cdot \mathbf{B})\,, \tag{3.2}$$

where a, E and B are the axion, electric and magnetic fields, correspondingly. A similar effective Lagrangian density appears due to the interaction between the axion field and an atom

$$L^{a\gamma}_{\text{eff}} = g_{ae}\, a\, (\mathbf{E} \cdot \mathbf{B}_{\text{eff}} + \mathbf{E}_{\text{eff}} \cdot \mathbf{B})\,, \tag{3.3}$$

where the effective magnetic $\mathbf{B}_{\text{eff}}$ and electric $\mathbf{E}_{\text{eff}}$ fields are produced by the atom, while $\mathbf{E}$ and $\mathbf{B}$ are physical electromagnetic fields of an external photon. The effective Lagrangian (3.3) includes the coupling constant g_{ae} which originates from the axion-electron (or axion-nucleon) interaction

$$L^{ae} = g_{ae}\, \partial_\mu a\, \bar{\psi}\, \gamma^5 \gamma^\mu \psi\,, \tag{3.4}$$

where ψ is the electron (or nucleon) spinor field. The aim of this paper is to derive the expressions for the effective electric and magnetic fields stipulated by the interaction (3.4).

The rest of the paper is organized as follows. In the next section we derive analytical expressions for the effective magnetic and electric fields due to the photon-axion transformation. The numerical estimates of these fields in vapor, liquid and solid media are given in Sect. 3.5. The obtained results are summarized in Sect. 3.6. In the appendices, we present the details of calculations of the effective fields.

3.4 Calculations

Allowing for the axion-electron interaction (3.4), one can consider a scattering amplitude, where a bound electron absorbs an incident photon and emits an axion. Of special interest is the scattering in forward direction since the forward scattering on multiple atoms is always coherent. If the wavelengths of the photon and axion are significantly larger than the distance between the atoms, we may treat the atomic system as a continuous medium, and the forward scattering amplitude scales linearly with the number density of atoms N_{at}. Thus, the effective Lagrangian (3.3) can be identified with the amplitude of forward scattering of photons on atoms [57]

$$L^{a\gamma}_{\text{eff}} = N_{\text{at}} \sum_n \frac{M^a_{0n} M^\gamma_{n0}}{E_0 - E_n + \omega - i\Gamma_n/2}\,, \tag{3.5}$$

where the summation goes over the atomic (or nuclear) excited states n with the energies E_n and widths Γ_n. Here ω is the energy of the incident photon, M^a_{0n} is the matrix element of the axion-electron interaction (3.4) and M^γ_{n0} is the matrix element of the interaction of atomic electrons with external electromagnetic field of the incident photon.

The matrix element M^a_{0n} in Eq. (3.5) is given by $M^a_{0n} = \langle 0|H^{ae}|n\rangle$, where the Hamiltonian H^{ae} corresponds to the interaction (3.4). For non-relativistic electrons this Hamiltonian has the form [51, 52]

$$H^{ae} = g_{ae} \left(\boldsymbol{\nabla} a \cdot \boldsymbol{\sigma} - \partial_t a \frac{\mathbf{p} \cdot \boldsymbol{\sigma}}{m_e}\right), \tag{3.6}$$

where m_e is the electron mass and $\mathbf{p}$ is its momentum. The form of this Hamiltonian can be further specified when the axion field is given by the plane wave with energy ω and wave-vector $\mathbf{k}$, $a(\mathbf{r}, t) = a_0 \sin(\omega t - \mathbf{kr})$.

Then the Hamiltonian may be represented in the form of multipole expansion with the leading terms given by (modulo the oscillating factor $e^{i\omega t}$)

$$H^{ae} = g_{ae}\, a_0 \left(H^{ae}_{\rm M0} + H^{ae}_{\rm M1} + \ldots\right), \tag{3.7}$$

$$H^{ae}_{\rm M0} = \frac{1}{2}\left(-\frac{\omega}{m_e}\mathbf{p}\cdot\boldsymbol{\sigma} + i(\mathbf{k}\cdot\mathbf{r})(\mathbf{k}\cdot\boldsymbol{\sigma})\right), \tag{3.8}$$

$$H^{ae}_{\rm M1} = -\frac{1}{2}(\mathbf{k}\cdot\boldsymbol{\sigma}). \tag{3.9}$$

The scattering amplitude (3.5) may be considered as a process, where an atom is (virtually) excited by absorbing a photon and returns back to the initial state via axion emission. Note that the M0 axions induce transitions between the states of opposite atomic parity but the same total angular momentum. Thus, M0 axions are produced when atoms absorb E1 photon which also changes the parity. Analogously, M1 axions do not change parity, and they may be produced when M1 photons are absorbed. As a result, in Eq. (3.5) the matrix element of the operator $H^{ae}_{\rm M0}$ should be coupled with the matrix element of E1 photon absorption operator $H^{\gamma}_{\rm E1} = e(\boldsymbol{\epsilon}\cdot\mathbf{r})$, while the matrix element of the operator $H^{ae}_{\rm M1}$ should be multiplied by the matrix element of M1 photon-absorption operator $H^{\gamma}_{\rm M1} = \frac{e}{2m_e}(\mathbf{n}\times\boldsymbol{\epsilon})(\mathbf{J}+\mathbf{S})$, where $\mathbf{n}$ is the propagation unit vector of the photon and $\boldsymbol{\epsilon}$ is its polarization. The former case corresponds to the effective magnetic field while the latter generates the effective electric field due to the interaction of photons with atoms,

$$B_{\rm eff} = N_{\rm at}{\rm Re}\sum_n \frac{\langle 0|H^{ae}_{\rm M0}|n\rangle\langle n|H^{\gamma}_{\rm E1}|0\rangle}{E_0 - E_n + \omega - i\Gamma_n/2}, \tag{3.10}$$

$$E_{\rm eff} = N_{\rm at}{\rm Re}\sum_n \frac{\langle 0|H^{ae}_{\rm M1}|n\rangle\langle n|H^{\gamma}_{\rm M1}|0\rangle}{E_0 - E_n + \omega - i\Gamma_n/2}. \tag{3.11}$$

The direction of the effective fields is specified by the matrix elements in Eqs. (3.10) and (3.11). In fact, as we prove in our previous paper [55], for non-polarized atoms the product of axion and photon matrix elements always sums to zero, $\sum_n \langle 0|H^{ae}|n\rangle\langle n|H^{\gamma}|0\rangle = 0$, because the excited states $|n\rangle$ with different projections of the total momentum contribute destructively. To get a non-vanishing result we have to assume that a (weak) external magnetic field B_2 is applied, which lifts the degeneracy of Zeeman sublevels such that only some of them are in resonance with the applied laser field. In this case, it is possible to show that the direction of the effective field $B_{\rm eff}$ coincides with the direction of the applied physical magnetic field B_2 while $\mathbf{E}_{\rm eff}$ is directed along $\mathbf{k}\times\mathbf{B}_2$.

A resonant atomic transition may lead to a significant photon absorption and a phase shift of the photon field (relative to the axions field) which destroys the coherence. Both effects may be seen from the complex phase in the photon field $A \propto e^{in_r\mathbf{k}\cdot\mathbf{r}}$, where

$$n_r = 1 - 2\pi N_{\rm at}\sum_n \frac{|M^{\gamma}_{n0}|^2}{E_0 - E_n + \omega - i\Gamma_n/2} \tag{3.12}$$

is the complex refractive index. One could go to the tail of resonance to suppress the photon absorption since the imaginary part of n_r decreases quadratically with $E_0 - E_n + \omega$, but the phase decreases slowly (linearly), similar to $E_{\rm eff}$ and $B_{\rm eff}$ in Eqs. (3.10) and (3.11). The phase of the photons may be corrected by placing phase-correcting transparent plates in the medium. This situation is opposite to the case of photon-axion transformation in magnetic field [58], where it was proposed to use a gas to match the photons' speed with the speed of low-mass axion. In our case the phase-correcting transparent plates may be needed if the photons' phase velocity in the medium appears less than the axion's speed. In this case the plate should add the photons' phase to equate the phase difference with axions to a multiple of 2π.

3.5 Numerical estimates

Note that the effective fields (3.10) and (3.11) are proportional to the atom density $N_{\rm at}$. Thus, a stronger effective field is produced in dense atomic systems such as solids, liquids or dense gases. In this note we consider noble gases in liquid phase and heavy metal vapors since they can be treated using the standards atomic methods. We also show that there is a significant enhancements of the effective field in crystals with narrow spectral lines.

3.5.1 Effective magnetic field in liquid xenon

Let us consider liquid xenon with atomic density $N_{\rm at} = 1.3 \times 10^{22}$ cm^{-3}. The resonant axion M0 transition is possible from the ground state 0^+ to the excited state 0^- with the energy $E_{0^-} = 9.45$ eV, while the corresponding photon transition is highly forbidden. This photon transition may be open when an external magnetic field B_2 is applied. This magnetic field causes the mixing of the states 0^- and 1^-, where the latter corresponds to the energy level $E_{1^-} = 9.57$ eV. As we demonstrate in Appendix 3.A.1, the effective magnetic field may reach the value

$$B_{\rm eff} \approx 1.2 \times 10^{-2} \text{ T}. \tag{3.13}$$

We stress that, according to Eq. (3.3), the strength of interaction of this effective field with the axion field is specified by the coupling constant g_{ae}, which is independent from the axion-photon constant $g_{a\gamma}$. Thus, although this effective field is much weaker than the physical magnetic field $B = 5.3$ T applied at the ALPS experiment [59], it may be significant in the processes of axion production or detection if $g_{ae} \gg g_{a\gamma}$.

3.5.2 Effective electric field in vapor thallium

To estimate the effective electric field (3.11) we consider a vapor of Tl atoms at temperature $T = 1200$ °C and density $N_{\rm at} = 6.6 \times 10^{17}$ cm^{-3}. This system proved useful in the study of weak-interaction-induced optical activity of heavy-metal vapors [60]. Indeed, the transition between the ground state A with $J = \frac{1}{2}$ and the nearest excited state B with $J = \frac{3}{2}$ is of M1 type. The energy difference between these states $\omega = 0.966$ eV corresponds to near-infrared region. In Appendix 3.A.2 we give an estimate of the effective electric field corresponding to such atomic transitions:

$$E_{\rm eff} \approx 1.5 \times 10^5 \, \frac{\text{V}}{\text{cm}} \, . \tag{3.14}$$

This field is still not competitive with the physical magnetic field used at ALPS experiments.

3.5.3 Effective electric field in a crystal

According to equations (3.10) and (3.11), the strong effective fields are achieved in media with high atom density $N_{\rm at}$ and small width Γ. Therefore it is natural to consider photon-to-axion transformations in crystals with narrow optical lines. One of such crystals based on $EuCl_3 \cdot 6H_2O$ compound has recently been studied in [61]. Remarkable spectral properties of this crystal are due to the 4f valence electron shell of the Eu^{3+} ion [63, 64]. In particular, in [61] it was shown that the optical $^7F_0 \to {}^5D_0$ transition in such isotopically purified crystal may be as narrow as 25 MHz. However, we cannot employ this transition for axion production since it corresponds to the induced electric dipole type and does not obey the axion-amplitude selection rules. Instead, we consider the transition $^7F_0 \to {}^5D_1$ with the energy $\omega = 2.36$ eV in the Eu^{3+} ion, which is of M1 type [63] and is allowed for both the photon and axion amplitudes. Note that the states $^7F_0$ and $^5D_1$ refer to the intermediate coupling scheme, and each of them is given by a linear combination of the LS-states according to [64].

Although there is no explicit data about the width of the $^7F_0 \to {}^5D_1$ transition in the $EuCl_3 \cdot 6H_2O$ crystal, we assume that it may be as narrow as for the $^7F_0 \to {}^5D_0$ transition, $\Gamma \sim 10^{-7}$ eV. Then, taking into account that the density of Eu atoms in this crystal is $N_{\rm at} \approx 2.7 \times 10^{21}$ cm^{-3} [61], in Appendix 3.A.3 we estimate the effective electric field due to the photon-axion transformation:

$$E_{\rm eff} \approx 1.7 \times 10^9 \, \frac{\text{V}}{\text{cm}} \, . \tag{3.15}$$

Thus, the effective field in crystals (3.15) is much stronger than that in vapor media (3.14) due to higher atom density and smaller linewidth.

We point out that Eq. (3.15) gives a rough estimate of the effective field because we do not know the exact width of the line corresponding to the $^7F_0 \to {}^5D_1$ transition in the $EuCl_3 \cdot 6H_2O$ crystal. We hope that a more accurate estimate may be given when this transition is experimentally measured.

3.6 Concluding remarks

The aim of this note is to attract the attention to the possibility to have resonance enhancement of the axion-photon transformations in a medium. Such transitions between photons and axions in atoms can be

represented via the effective electric and/or magnetic fields, similar to the interaction of the axion with physical electromagnetic fields. The crucial difference of these effective fields from the physical ones is that they couple to the axion through the independent coupling constant g_{ae} which, for general axion-like particles, may be much larger than the axion-photon coupling $g_{a\gamma}$. This motivates to set up new axion production/detection experiments where the medium plays the role of physical magnetic field in the current axion-search experiments. Such new experiments would allow one to measure the axion-electron coupling constant in the same way as the axion-photon coupling is studied. It is tempting to design such experiments and to estimate their efficiency.

We point out that the equations (3.10) and (3.11) give an important hint towards the design of future atom- and molecule-based detectors with high sensitivity to axion-like particles: They should possess narrow spectral lines at relatively high atom density. In particular, it is natural to look for crystals with ultranarrow optical or microwave transitions. Examples of such crystals with the linewidth $\Gamma \sim 10^{-7}$ eV in the optical region have recently been studied, see, e.g., [61]. In Sect. 3.5.3 we demonstrated that the use of such crystals as a media for photon-axion transformation may give a significant enhancement of the effective field which may be much stronger than the physical fields employed at the ALPS experiments, see, e.g., [65] for a review. It is tempting to design such detectors and estimate their efficiency more accurately for applications in future ALPS experiments. We leave this issue for further work.

Acknowledgments

The authors thank R. Ahlefeldt, V. Dzuba, C. Rizzo, M. Sellars, and Y. Stadnik for useful discussions. This work is supported by the Australian Research Council, the Gutenberg Fellowship, New Zealand Institute for Advanced Studies, the DFG via its Reinhardt Koselleck Program, and the European Research Council under the European Union's Horizon 2020 Research 41 and Innovative Program under Grant agreement No. 695405.

3.A Estimates of effective fields

3.A.1 Effective magnetic field produced by liquid xenon

Let us consider the excited state 0^- in Xe atom with energy $E_{0^-} \equiv \omega = 9.447$ eV. This state has zero total angular momentum, $J = 0$, and odd parity in contrast with the even-parity ground state 0^+. Therefore, the axion transition between these states is of M0 type. The corresponding matrix element for resonant axion absorption was calculated in our recent work [55]

$$M^a = \langle 0^-|H^{ae}_{\rm M0}|0^+\rangle = i\frac{\sqrt{2}}{3}\omega^2 R\,, \tag{3.16}$$

where R is the radial integral $R = \int_0^\infty f_{6s_{1/2}}(r) f_{5p_{1/2}}(r) r^3 dr$. Here $f_{6s_{1/2}}(r)$ and $f_{5p_{1/2}}(r)$ are radial parts of $6s_{1/2}$ and $5p_{1/2}$ wavefunctions, respectively (see, e.g. [60]). For Xe atom, the value of this integral may be deduced from [62], $R \approx -1.09$ a.u.

The photon transition $0^+ \leftrightarrow 0^-$ is highly forbidden. However, this transition may be opened by applying a magnetic field B_2 which provides the mixing of the excited states $|0^-\rangle$ and $|1^-\rangle$,

$$|i\rangle = |0^-\rangle - \frac{\langle 1^-|\boldsymbol{\mu}\cdot\mathbf{B}_2|0^-\rangle}{E_{0^-} - E_{1^-}}|1^-\rangle\,, \tag{3.17}$$

where $E_{1^-} = 9.57$ eV; $\boldsymbol{\mu} = -\mu_B(\mathbf{J} + \mathbf{S})$ is the electron magnetic moment operator and μ_B is the Bohr magneton. Taking into account that the matrix element $\langle 0^-|\boldsymbol{\mu}\cdot\mathbf{B}_2|1^-\rangle$ is $2/3\mu_B B_2$, the photon E1 transition amplitude between the ground state $|0^+\rangle$ and the excited state $|i\rangle$ is found to be

$$M^\gamma = \frac{2}{3}\frac{e\mu_B B_2}{E_{0^-} - E_{1^-}}\langle 1^-|\boldsymbol{\epsilon}\cdot\mathbf{r}|0^+\rangle = \frac{\sqrt{2}}{9}\frac{e\mu_B B_2 R}{E_{0^-} - E_{1^-}}\,, \tag{3.18}$$

where $\boldsymbol{\epsilon}$ is the photon polarization vector which is assumed to be along the z-axis, $\boldsymbol{\epsilon} = (0, 0, 1)$. Thus, for the product of transition amplitudes (3.16) and (3.18) we find

$$M^a M^\gamma = \frac{2i}{27}\frac{e\mu_B B_2}{E_{0^-} - E_{1^-}}\omega^2 R^2\,. \tag{3.19}$$

Note that the expression (3.19) is imaginary. Hence, the real part of the effective Lagrangian (3.5) corresponds to the resonant absorption. Note also that for liquid Xe the dominant contribution to the width of the state Γ comes from the collisional broadening, $\Gamma \approx \Gamma_{\rm col} = 2 v_0 N_{\rm at} \sigma_{\rm col}$, where $v_0 = \sqrt{2 k_B T / m_{\rm at}}$ is the most probable thermal speed of the atoms and $\sigma_{\rm col}$ is the collisional cross section. Here k_B is the Boltzmann constant and $m_{\rm at}$ is the atomic mass. Assuming that the temperature of liquid Xe is $T = 164$ K and the atom density is $N_{\rm at} = 1.3 \times 10^{22}$ cm^{-3}, the collisional width is estimated as $\Gamma_{\rm col} \approx 1.4 \times 10^{-3}$ eV. Taking into account Eq. (3.19), we find the expression for the effective magnetic field

$$B_{\rm eff} = \frac{2}{27} N_{\rm at} \frac{\mu_B B_2}{E_{0^-} - E_{1^-}} \frac{\omega^2 R^2}{\Gamma_{\rm col}} \,. \tag{3.20}$$

Assuming that the magnetic field B_2 is of order of the magnetic field applied at ALPS experiment [59], $B_2 = 5$ T, we estimate the effective magnetic field produced by the atomic transitions (3.20): $B_{\rm eff} \approx 1.2 \times 10^{-2}$ T.

3.A.2 Effective electric field produced by thallium vapor

Consider the ground and excited states of the Tl atom, $A = |L = 1, J = \frac{1}{2}\rangle$ and $B = |L = 1, J = \frac{3}{2}\rangle$, with energy difference $\omega = 0.966$ eV. The transition between these states is of M1 type. The axion and photon absorption amplitudes for this transition are

$$M^a = -\frac{1}{2} \langle B | \mathbf{k} \cdot \boldsymbol{\sigma} | A \rangle \,, \tag{3.21}$$

$$M^\gamma = \frac{e}{2 m_e} (\mathbf{n} \times \boldsymbol{\epsilon}) \langle B | \mathbf{J} + \mathbf{S} | A \rangle \,, \tag{3.22}$$

where $\mathbf{n}$ is the photon or axion propagation unit vector and $\boldsymbol{\epsilon}$ is the photon polarization vector. For unpolarized atoms, in (3.11) we have to average over the states with different z-projection of the total angular momentum M_J. After this averaging, the contribution to the effective electric field vanishes, $\sum_{M_J} M^a M^\gamma = 0$, see [55].

To get a non-vanishing result in (3.11) one can apply a magnetic field B_2, which splits the Zeeman sublevels. The laser frequency is in resonance with a transition from only one of these sublevels. In particular, we suppose that the constant magnetic field B_2 is applied along the z-axis, $\mathbf{B}_2 = B_2 \hat{\mathbf{z}}$, and the laser frequency corresponds to the energy difference of levels $A = |1, \frac{1}{2}, -\frac{1}{2}\rangle$ and $B = |1, \frac{3}{2}, \frac{1}{2}\rangle$. We assume also that the photon propagates along the y-axis and is polarized in the (x, z)-plain, $\mathbf{n} = (0, 1, 0)$, $\boldsymbol{\epsilon} = (\epsilon_x, 0, \epsilon_z)$. In this case, the axion and photon matrix elements (3.21) and (3.22) are

$$M^a = \frac{i}{3\sqrt{2}} \omega I \,, \tag{3.23}$$

$$M^\gamma = \frac{e \epsilon_z I}{6\sqrt{2} m_e} \,, \tag{3.24}$$

where I is the overlap integral for $6p_{1/2}$ and $6p_{3/2}$ wavefunctions, $I = \int_0^\infty dr\, r^2 f_{6p_{1/2}}(r) f_{6p_{3/2}}(r) \approx 0.98$.

As is shown in [60], for Tl vapor at a temperature of $T = 1473$ K, the dominant contribution to the width of the line comes from the Doppler broadening, $\Gamma \approx \Gamma_{\rm Dop} = 2 v_0 \omega / \sqrt{\pi}$, where $v_0 = \sqrt{2 k_B T / m_{\rm at}}$ is the most probable thermal speed of the atoms. The numerical estimate for this width is $\Gamma_{\rm Dop} \approx 1.3 \times 10^{-6}$ eV. Taking this into account, we have the following expression for the effective electric field

$$E_{\rm eff} = N_{\rm at} \frac{e}{18 m_e} \frac{\omega I^2 \epsilon_z}{\Gamma_{\rm Dop}} \,, \tag{3.25}$$

where the density of the vapor is $N_{\rm at} = 6.6 \times 10^{17}$ cm^{-3}.

Assuming that the polarization of the photon is such that $\epsilon_z = 1$, we estimate the effective electric field $E_{\rm eff} \approx 1.5 \times 10^5 \, \frac{\rm V}{\rm cm}$.

Note that the same result may be obtained using the optical pumping rather than applying the magnetic field B_2.

3.A.3 Effective electric field in crystals

Let us consider a $EuCl_3 \cdot 6H_2O$ crystal, where there are narrow spectral lines in the optical region, and high optical density can be achieved, see [61]. The optical properties of this crystal can be understood

through the electron-shell structure of the Eu^{3+} ion which has six valence electrons on the 4f orbital [63, 64]. We are interested in the transition between the states $A = {}^7F_0$ and $B = {}^5D_1$ corresponding to the energy $\omega = 2.36$ eV. Since this transition is of M1 type, we apply the formula (3.11) to estimate the effective electric field $E_{\rm eff}$ due to axion-photon transformation.

The relevant computation is similar to the one given in Sect. 3.A.2 for Tl vapor. In particular, it is also necessary to apply the constant magnetic field B_2 along the z-axis to lift the degeneracy of the Zeeman sub-levels of state $B = {}^5D_1$ with the total angular momentum $J = 1$. To be specific, we assume that the laser frequency is in resonance with the transition between the states $|A\rangle = |{}^7F_0; J = 0, M = 0\rangle$ and $|B\rangle = |{}^5D_1; J = 1, M = 1\rangle$. For simplicity, we also assume that the laser beam is aligned along the y-direction and is polarized in the z-direction, so that $\mathbf{n} = (0, 1, 0)$ and $\boldsymbol{\epsilon} = (0, 0, 1)$. In this case, using the equations (3.21) and (3.22) we find

$$M^a = -\frac{i}{\sqrt{6}}\omega\langle {}^5D_1||S||{}^7F_0\rangle\,, \tag{3.26}$$

$$M^\gamma = -\frac{e}{2\sqrt{6}m_e}\langle {}^5D_1||J+S||{}^7F_0\rangle\,, \tag{3.27}$$

where $\langle {}^5D_1||S||{}^7F_0\rangle$ is the reduced matrix element of the spin operator $\mathbf{S}$ and $\langle {}^5D_1||J+S||{}^7F_0\rangle = \langle {}^5D_1||S||{}^7F_0\rangle$. This matrix element may be computed using the spectral data for the Eu^{3+} ion [63, 64]: $\langle {}^5D_1||S||{}^7F_0\rangle \approx 0.17$.

To apply the equation (3.11) we need the atom density $N_{\rm at}$ and the width of the state Γ. The former may be easily estimated for the crystal $EuCl_3{\cdot}6H_2O$ described in [61]: $N_{\rm at} \approx 2.7 \times 10^{21}$ cm^{-3}. The authors of this paper claim that the width of the optical transition ${}^7F_0 \to {}^5D_0$ in this crystal is about 25 MHz. For our estimates, we can assume that the transition ${}^7F_0 \to {}^5D_1$ possesses a comparable width $\Gamma \sim 10^{-7}$ eV. For these values of the parameters, we find the effective electric field in the crystal due to the photon-axion transformation,

$$E_{\rm eff} = \frac{N_{\rm at} e\omega}{12 m_e \Gamma}|\langle {}^5D_1||S||{}^7F_0\rangle|^2 \approx 1.7 \times 10^9 \frac{\rm V}{\rm cm}\,. \tag{3.28}$$

We point out that these estimates are very rough; a more accurate estimate requires experimental measurements of the width of the line for the transition ${}^7F_0 \to {}^5D_1$ in the $EuCl_3{\cdot}6H_2O$ crystal.

Bibliography

[1] R. D. Peccei and H. R. Quinn, Phys. Rev. Lett. **38**, 1440 (1977).

[2] R. D. Peccei, in Axions: Theory, Cosmology, and Experi-mental Searches (Springer, 2008) pp. 3-17.

[3] S. Weinberg, Phys. Rev. Lett. **40**, 223 (1978).

[4] F. Wilczek, Phys. Rev. Lett. **40**, 279 (1978).

[5] J. E. Kim, Phys. Rev. Lett. **43**, 103 (1979).

[6] M. A. Shifman, A. I. Vainshtein and V. I. Zakharov, Nucl. Phys. B **166**, 493 (1980).

[7] M. Dine, W. Fischler and M. Srednicki, Phys. Lett. **104B**, 199 (1981).

[8] A. R. Zhitnitsky, Sov. J. Nucl. Phys. **31**, 260 (1980) [Yad. Fiz. **31**, 497 (1980)].

[9] M. Srednicki, Nucl. Phys. B **260**, 689 (1985).

[10] P. Sikivie, Phys. Rev. Lett. **51**, 1415 (1983) Erratum: [Phys. Rev. Lett. **52**, 695 (1984)].

[11] P. Sikivie, Phys. Rev. D **32**, 2988 (1985) Erratum: [Phys. Rev. D **36**, 974 (1987)].

[12] S. Moriyama, M. Minowa, T. Namba, Y. Inoue, Y. Takasu and A. Yamamoto, Phys. Lett. B **434**, 147 (1998).

[13] Y. Inoue, T. Namba, S. Moriyama, M. Minowa, Y. Takasu, T. Horiuchi and A. Yamamoto, Phys. Lett. B **536**, 18 (2002).

[14] Y. Inoue, Y. Akimoto, R. Ohta, T. Mizumoto, A. Yamamoto and M. Minowa, Phys. Lett. B **668**, 93 (2008).

[15] R. Ohta *et al.*, Nucl. Instrum. Meth. A **670**, 73 (2012).

[16] T. Mizumoto, R. Ohta, T. Horie, J. Suzuki, Y. Inoue and M. Minowa, JCAP **1307**, 013 (2013).

[17] K. Zioutas *et al.*, Nucl. Instrum. Meth. A **425**, 480 (1999).

[18] E. Arik *et al.* [CAST Collaboration], JCAP **0902**, 008 (2009).

[19] V. Anastassopoulos *et al.* [CAST Collaboration], Nature Phys. **13**, 584 (2017).

[20] F. T. Avignone, III *et al.* [SOLAX Collaboration], Phys. Rev. Lett. **81**, 5068 (1998).

[21] A. O. Gattone *et al.*, Nucl. Phys. Proc. Suppl. **70**, 59 (1999).

[22] A. Morales *et al.* [COSME Collaboration], Astropart. Phys. **16**, 325 (2002).

[23] R. Bernabei *et al.*, Phys. Lett. B **515**, 6 (2001).

[24] R. Bernabei *et al.*, Int. J. Mod. Phys. A **21**, 1445 (2006).

[25] R. Bernabei *et al.* [DAMA and LIBRA Collaborations], Eur. Phys. J. C **67**, 39 (2010).

[26] Z. Ahmed *et al.* [CDMS Collaboration], Phys. Rev. Lett. **103**, 141802 (2009).

[27] Z. Ahmed *et al.* [CDMS-II Collaboration], Phys. Rev. Lett. **106**, 131302 (2011).

[28] R. Agnese *et al.* [CDMS Collaboration], Phys. Rev. Lett. **111**, no. 25, 251301 (2013).

[29] R. Agnese *et al.* [SuperCDMS Collaboration], Phys. Rev. Lett. **112**, no. 24, 241302 (2014).

[30] I. G. Irastorza *et al.*, JCAP **1106**, 013 (2011).

[31] E. Armengaud *et al.*, JINST **9**, T05002 (2014).

[32] S. J. Asztalos *et al.* [ADMX Collaboration], Phys. Rev. Lett. **104**, 041301 (2010).

[33] A. Wagner *et al.* [ADMX Collaboration], Phys. Rev. Lett. **105**, 171801 (2010).

[34] J. Hoskins *et al.*, Phys. Rev. D **84**, 121302 (2011).

[35] S. Al Kenany *et al.*, Nucl. Instrum. Meth. A **854**, 11 (2017).

[36] B. M. Brubaker *et al.*, Phys. Rev. Lett. **118**, no. 6, 061302 (2017).

[37] B. T. McAllister *et al.*, Phys. Dark Univ. **18**, 67 (2017).

[38] K. Ehret et al., arXiv:0702023, (2007).

[39] K. Ehret *et al.* [ALPS Collaboration], Nucl. Instrum. Meth. A **612**, 83 (2009).

[40] K. Ehret *et al.*, Phys. Lett. B **689**, 149 (2010).

[41] P. Pugnat *et al.* [OSQAR Collaboration], Phys. Rev. D **78**, 092003 (2008).

[42] A. S. Chou *et al.* [GammeV (T-969) Collaboration], Phys. Rev. Lett. **100**, 080402 (2008).

[43] G. Cantatore, F. Della Valle, E. Milotti, L. Dabrowski and C. Rizzo, Phys. Lett. B **265**, 418 (1991).

[44] E. Zavattini *et al.* [PVLAS Collaboration], Phys. Rev. D **77**, 032006 (2008).

[45] F. Della Valle, A. Ejlli, U. Gastaldi, G. Messineo, E. Milotti, R. Pengo, G. Ruoso and G. Zavattini, Eur. Phys. J. C **76**, no. 1, 24 (2016).

[46] S. J. Chen, H. H. Mei and W. T. Ni, Mod. Phys. Lett. A **22**, 2815 (2007).

[47] R. Battesti et al., Eur. Phys. J. D **46**, 323 (2008).

[48] F. Bielsa *et al.*, arXiv:0911.4567, (2009).

[49] E. Iacopini and E. Zavattini, Phys. Lett. **85B**, 151 (1979).

[50] K. Zioutas and Y. Semertzidis, Phys. Lett. A **130**, 94 (1988).

[51] P. Sikivie, Phys. Rev. Lett. **113**, no. 20, 201301 (2014).

[52] M. Pospelov, A. Ritz and M. B. Voloshin, Phys. Rev. D **78**, 115012 (2008).

[53] L. Santamaria *et al.*, New J. Phys. **17**, 113025 (2015).

[54] A. Arvanitaki, S. Dimopoulos and K. Van Tilburg, arXiv:1709.05354, (2017).

[55] H. B. Tran Tan, V. V. Flambaum, I. B. Samsonov, Y. V. Stadnik and D. Budker, arXiv:1803.09388, (2018).

[56] K. van Bibber, N. R. Dagdeviren, S. E. Koonin, A. Kerman and H. N. Nelson, Phys. Rev. Lett. **59**, 759 (1987).

[57] L. Landau and E. Lifshitz, Quantum Mechanics (Pergammon Press, Hungary, 1969)

[58] K. van Bibber, P. M. McIntyre, D. E. Morris, G. G. Raffelt, Phys. Rev. D **39**, 2089 (1989).

[59] K. Ehret *et al.*, Phys. Lett. B **689**, 149 (2010).

[60] I. B. Khriplovich, Parity Nonconservation in Atomic Phenomena (Gordon and Breach, Amsterdam, 1991).

[61] R. L. Ahlefeldt, M. R. Hush, and M. J. Sellars, Phys. Rev. Lett. **117**, 250504 (2016).

[62] A. Kramida, Yu. Ralchenko, J. Reader and NIST ASD Team, *NIST Atomic Spectra Database* (ver. 5.5.3), [Online]. Available: `https://physics.nist.gov/asd` [2018, March 31]. National Institute of Standards and Technology, Gaithersburg, MD. (2018).

[63] K. Binnemans, Coord. Chem. Rev. **295**, 1 (2015).

[64] G. S. Ofelt, J. Chem. Phys. **38**, 2171 (1963).

[65] R. Battesti *et al.*, arXiv:1803.07547 (2018).

Chapter 4

Screening and enhancement of oscillating electric field in molecules

4.1 Overview

In this chapter, I consider the problem of screening of oscillating electric fields in molecules. It is well-known that static electric fields do not penetrate to the nucleus of a neutral atom or molecule. I showed the oscillating electric field not only reaches the nucleus, but also may be enhanced by several orders of magnitude if its frequency matches one of the atomic or molecular transition frequency. This fact is particularly useful for experiments detecting the CP-odd nuclear EDMs.

These results are published in the following paper:

1. H. B. Tran Tan, V. V. Flambaum and I. B. Samsonov, **Screening and enhancement of an oscillating electric field in molecules**, Phys. Rev. A 99, 013430 (2019), arXiv:1812.03312,

which I presented at one international conference, one international workshop and one national competition:

1. **Searching for Axions and Axionic Dark Matter with Interference and Axion-induced Nuclear Moments**, TeV Particle Astrophysics Conference, University of Sydney, Sydney, Australia, December 2019,
2. **Screening and Enhancement of Nuclear Electric Dipole Moments Induced by Axionic Dark Matter**, Frontiers in Quantum Matter Workshop: Electric Dipole Moments, Australian National University, Canberra, Australia, November 2019,
3. **Effects of Dark Matter in atomic and molecular phenomena**, Australian Institute of Physics Postgraduate Presentation Competition, University of Technology Sydney, Sydney, Australia, October 2019.

4.2 Abstract

According to the Schiff theorem, the atomic electrons completely screen the atomic nucleus from an external static electric field. However, this is not the case if the field is time-dependent. Electronic orbitals in atoms either shield the nucleus from an oscillating electric field when the frequency of the field is off the atomic resonances or enhance this field when its frequency approaches an atomic transition energy. In molecules, not only electronic, but also rotational and vibrational states are responsible for the screening of oscillating electric fields. As will be shown in this paper, the screening of a low-frequency field inside molecules is much weaker than it appears in atoms owing to the molecular ro-vibrational states. We systematically study the screening of oscillating electric fields inside diatomic molecules in different frequency regimes,i.e., when the field's frequency is either of order of ro-vibrational or electronic transition frequencies. In the resonance case, we demonstrate that the microwave-frequency electric field may be enhanced up to six orders in magnitude due to ro-vibrational states. We also derive the general formulae for the screening and resonance enhancement of oscillating electric field in polyatomic molecules. Possible applications of these results include nuclear electric dipole moment measurements and stimulation of nuclear reactions by laser light.

4.3 Introduction

It is well-known that the Standard Model of elementary particles predicts small electric dipole moments (EDMs) for the electron and nucleon, see, e.g., Refs. [1–3] for recent reviews. Different extensions of SM such as axion or supersymmetry predict, however, different values for the EDMs of elementary particles. Therefore, it is a challenge for modern experimental physics to measure the EDMs of the electron and neutron in order to verify (or falsify) these models. Presently, there are several groups pursuing this goal, although the sensitivity of current experiments does not allow one to make firm conclusions.

One of the difficulties encountered in measuring the EDMs of nuclei in atoms and molecules is the screening of the external electric field by the electron shells in these systems. Indeed, according to a theorem by Schiff [4], the atomic nucleus of a neutral atom is completely screened from any *static* external electric field. EDMs of diamagnetic atoms are produced by the interaction of electrons with the nuclear Schiff moment [5–9]. For light atoms, atomic EDMs produced by the Schiff moment are very small, while they appear significant for heavy atomic species ($\sim 10^{-3} d_n$; d_n is the EDM of neutron). Thus, the electron screening makes the detection of the nuclear EDMs difficult.

A possible way to overcome this difficulty is to use ions instead of neutral atoms, where the screening of external fields is incomplete [10]. However, since a charged particle is not stationary in an electric field, it is problematic to preform precise measurements on such particle.

The behavior of atoms in an *oscillating* electric field is drastically different from that in the static case. It is natural to expect that the screening of alternating electric field in atoms and molecules is incomplete since the particles constituting an atom or a molecule respond to the changes in the field with some delay. Recently, it has been shown that when the frequency of the external electric field is far from atomic resonances, the resulting electric field at the center of an atom is proportional to the dynamical atomic polarizability [11]. Numerical tests of these results were performed in Ref. [12]. However, when the frequency of the external field approaches the energy of atomic transition, there may be a significant enhancement (up to 10^5) of the field [13].

The extension of the static Schiff theorem to molecules was considered in Ref. [14]. The derivation therein used the Ehrenfest theorem and resorted to classical mechanics to relate the acceleration of each nucleus to that of the whole molecule. Although this approach proved fruitful in the static case, it becomes inefficient in the dynamic case since the classical motion of a molecule in an oscillating field is itself difficult to describe. This paper aims at developing a general and fully quantum mechanical method for computing the electric field inside atoms and molecules which is applicable both for static and oscillating electric fields.

Note that the quantum mechanical description of molecules has some important features as compared with the atomic case. In molecules, it is necessary to separate the relative motion of the constituent nuclei from the motion of the common center of mass while in atoms this separation is not essential, i.e., the atomic nucleus may be considered as fixed in space. This relative motion of the nuclei in a molecule is described by the rotational and vibrational modes. As a result, the molecular spectra appear to have a very rich structure with rotational, vibrational and electronic states. As will be shown in this paper, these states give rise to new terms in the formula for the resulting electric field in the molecule as compared with the atomic case studied in [11]. All these new terms play an important role in the screening of the external electric field in molecules.

The rest of this paper is organized as follows. In Sect. 4.4, the problem of calculating the field at the nuclei in a diatomic molecule in an external electric field is discussed. The cases of a static field, of an oscillating field off resonance with the molecular transitions and of an oscillating field on resonance with a molecular transition will be examined. In Sect. 4.5, we will consider examples of some diatomic molecules and present the estimates of screening and resonance enhancement of electric field at nuclei. Sect. 4.6 is devoted to the generalization of the diatomic-molecule case to systems of arbitrary number of nuclei. Sect. 4.7 contains a summary of the results and discussion of their potential application.

Throughout this paper, we employ the atomic units in which $\hbar = e = m_e = 4\pi\epsilon_0 = 1$. This makes the intermediate formulae more compact. The final results, for convenience, will be presented in arbitrary units with all fundamental constants given explicitly.

4.4 Screening of electric field in diatomic molecules

In this section, we derive the general formulae for the screening of both static and alternating external electric fields inside diatomic molecules. To make our presentation self-consistent, we begin with a review of the molecular Hamiltonian in the center-of-mass coordinates frame.

4.4.1 The diatomic molecule Hamiltonian in the center-of-mass frame

Consider a diatomic molecule with L electrons in an external electric field $\mathbf{E}_{\text{ext}}$. Let M_I and Z_I be the masses and charges of the nuclei, respectively (the subscript $I = 1, 2$ labels the nuclei). The position and momentum operators of the nuclei in the laboratory frame will be denoted by $\mathbf{R}_I$ and $\mathbf{P}_I$, respectively. The electron positions and momenta operators will be denoted by $\mathbf{r}_i$ and $\mathbf{p}_i$ (the subscript $i = 1, \ldots, L$ labels the electrons).

The Hamiltonian of the diatomic molecule in the laboratory frame has the standard form

$$H_{\text{mol}} = K + V_0 + V \,, \tag{4.1a}$$

$$K = \frac{\mathbf{P}_1^2}{2M_1} + \frac{\mathbf{P}_2^2}{2M_2} + \sum_{i=1}^{L} \frac{\mathbf{p}_i^2}{2} \,, \tag{4.1b}$$

$$V_0 = \frac{Z_1 Z_2}{R_{12}} - \sum_{i=1}^{L} \left(\frac{Z_1}{R_{1i}} + \frac{Z_2}{R_{2i}} \right) + \sum_{i<j}^{L} \frac{1}{r_{ij}} \,, \tag{4.1c}$$

$$V = -\mathbf{E}_{\text{ext}} \cdot \left(Z_1 \mathbf{R}_1 + Z_2 \mathbf{R}_2 - \sum_{i=1}^{L} \mathbf{r}_i \right) \,, \tag{4.1d}$$

where $R_{Ii} = |\mathbf{R}_I - \mathbf{r}_i|$, $r_{ij} = |\mathbf{r}_i - \mathbf{r}_j|$ and $R_{IJ} = |\mathbf{R}_I - \mathbf{R}_J|$. Recall that we are using the atomic unit system in which $e = m_e = 1$. Here, for simplicity, we consider the non-relativistic Hamiltonian for spinless particles.

It is convenient to define the total nuclear mass $M_N = M_1 + M_2$, the total nuclear charge $Z_N = Z_1 + Z_2$, the total molecular mass $M_T = M_N + L$ and the total molecular charge $Z_T = Z_N - L$ ($Z_T = 0$ for a neutral molecule).

To separate the molecule's center-of-mass motion from the relative dynamics of the electrons and nuclei, we perform the change of variables $(\mathbf{R}_I, \mathbf{r}_i) \to (\mathbf{S}_T, \mathbf{S}, \mathbf{s}_i)$

$$\begin{aligned} \mathbf{S}_T &= \frac{1}{M_T} \left(M_1 \mathbf{R}_1 + M_2 \mathbf{R}_2 + \sum_{i=1}^{L} \mathbf{r}_i \right) \,, \\ \mathbf{S} &= \mathbf{R}_1 - \mathbf{R}_2 \,, \\ \mathbf{s}_i &= \mathbf{r}_i - \frac{M_1 \mathbf{R}_1 + M_2 \mathbf{R}_2}{M_N} \,. \end{aligned} \tag{4.2}$$

where $\mathbf{S}_T$ is the position operator of the molecular center of mass, $\mathbf{S}$ defines the molecular axis and $\mathbf{s}_i$ are the positions of the electrons with respect to the nuclear center of mass.

The conjugated momenta of the coordinates $(\mathbf{S}_T, \mathbf{S}, \mathbf{s}_i)$ will be denoted by $(\mathbf{Q}_T, \mathbf{Q}, \mathbf{q}_i)$. These momenta are related to the original momenta $(\mathbf{P}_I, \mathbf{p}_i)$ via

$$\begin{aligned} \mathbf{P}_I &= -\frac{M_I}{M_N} \sum_{i=1}^{L} \mathbf{q}_i - (-1)^I \mathbf{Q} + \frac{M_I}{M_T} \mathbf{Q}_T \,, \\ \mathbf{p}_i &= \mathbf{q}_i + \frac{1}{M_T} \mathbf{Q}_T \,. \end{aligned} \tag{4.3}$$

The change of variables (4.2) and (4.3) in the Hamiltonian (4.1) allows us to isolate the dynamics of the center-of-mass from the relative motion,

$$H_{\text{mol}} = H_T + H_{\text{rel}} \,, \tag{4.4}$$

where

$$H_T = \frac{\mathbf{Q}_T^2}{2M_T} - Z_T \mathbf{E}_{\text{ext}} \cdot \mathbf{S}_T \tag{4.5}$$

is the center-of-mass Hamiltonian and H_{rel} is the Hamiltonian describing the relative dynamics

$$H_{\text{rel}} = H_0 + V_{\text{rel}} \,, \tag{4.6a}$$

$$H_0 = \sum_{i=1}^{L} \frac{\mathbf{q}_i^2}{2\mu_e} + \sum_{i<j}^{L} \frac{\mathbf{q}_i \mathbf{q}_j}{M_N} + \frac{\mathbf{Q}^2}{2\mu_N} + V_0 \,, \tag{4.6b}$$

$$V_{\text{rel}} = V + Z_T \mathbf{E}_{\text{ext}} \cdot \mathbf{S}_T \equiv -\mathbf{d} \cdot \mathbf{E}_{\text{ext}} \,. \tag{4.6c}$$

Here

$$\mu_N = \frac{M_1 M_2}{M_N}\,, \qquad \mu_e = \frac{M_N}{1+M_N} \tag{4.7}$$

are the reduced nuclear and electron masses, respectively, and $\mathbf{d}$ is the electric dipole moment with respect to the molecular center of mass,

$$\mathbf{d} = -\zeta_e \sum_{i=1}^{L} \mathbf{s}_i + \zeta_N \mathbf{S}\,. \tag{4.8}$$

Here we introduced the notations for the reduced electron charge ζ_e and reduced nuclear charge ζ_N:

$$\zeta_e = \frac{M_N + Z_N}{M_T}\,, \tag{4.9}$$

$$\zeta_N = \frac{M_2 Z_1 - M_1 Z_2}{M_N}\,. \tag{4.10}$$

Note that the Hamiltonian (4.6) contains the potential V_0 defined in Eq. (4.1c). Here it is assumed that this potential is expressed in terms of the new variables $\mathbf{S}$ and $\mathbf{s}_i$.

We point out that this section presents no new results. It only describes the standard change of variables in the molecular Hamiltonian (4.1) which allows one to isolate the dynamics of the center of mass of the molecule from the relative dynamics.

4.4.2 Screening of a static external electric field

Let us consider the screening of a static homogeneous electric field $\mathbf{E}_{\rm ext} = \mathbf{E}_0$ at the position $\mathbf{R}_I$ of the $I^{\rm th}$ nucleus. The operator of the electric field induced by the other nucleus and the electrons reads

$$\mathbf{E}'_I = -\frac{1}{Z_I}\nabla_{\mathbf{R}_I} V_0 = -\frac{i}{Z_I}\left[\mathbf{P}_I, H_0\right]\,, \tag{4.11}$$

where the Hamiltonian H_0 is given in Eq. (4.6).

Note that the Hamiltonian H_0 defined in Eq. (4.6) is independent from the center-of-mass coordinate $\mathbf{S}_T$. As a consequence, $[\mathbf{Q}_T, H_0] = 0$, and Eq. (4.11) may be put in the form

$$\mathbf{E}'_I = -\frac{i}{Z_I}\left[\mathbf{\Pi}_I, H_0\right]\,, \tag{4.12}$$

where $\mathbf{\Pi}_I$ denotes the truncated momentum operator

$$\mathbf{\Pi}_I \equiv \mathbf{P}_I - \frac{M_I}{M_T}\mathbf{Q}_T = -(-1)^I \mathbf{Q} - \frac{M_I}{M_N}\sum_{i=1}^{L}\mathbf{q}_i\,. \tag{4.13}$$

Using Eqs. (4.8) and (4.9), one can prove the following commutator relation between $\mathbf{\Pi}_I$ and the potential $V_{\rm rel}$ given in Eq. (4.6c)

$$\left(1 - \frac{M_I Z_T}{M_T Z_I}\right)\mathbf{E}_0 = -\frac{i}{Z_I}\left[\mathbf{\Pi}_I, -\mathbf{d}\cdot\mathbf{E}_0\right]\,. \tag{4.14}$$

The composition of Eqs. (4.12) and (4.14) yields

$$\mathbf{E}'_I + \left(1 - \frac{M_I Z_T}{M_T Z_I}\right)\mathbf{E}_0 = -\frac{i}{Z_I}\left[\mathbf{\Pi}_I, H_{\rm rel}\right]\,. \tag{4.15}$$

Let ψ be a stationary-state wavefunction describing the molecule in the center-of-mass frame, namely

$$H_{\rm rel}\psi = \mathcal{E}\psi\,. \tag{4.16}$$

The expectation value of the commutator on the right-hand side of Eq. (4.15) with respect to ψ vanishes. This allows us to find the expectation value of the operator $\mathbf{E}'_I$ on the left-hand side of Eq. (4.15), $\langle\mathbf{E}'_I\rangle \equiv \langle\psi|\mathbf{E}'_I|\psi\rangle$, so the total electric field at $I^{\rm th}$ nucleus $\langle\mathbf{E}_I\rangle$ is

$$\langle\mathbf{E}_I\rangle \equiv \langle\mathbf{E}'_I\rangle + \mathbf{E}_0 = \frac{M_I Z_T}{M_T Z_I}\mathbf{E}_0\,. \tag{4.17}$$

This result, derived in a fully quantum mechanical way, agrees with that obtained in Ref. [14] with the use of the Ehrenfest theorem. Note that for a neutral molecule, $Z_T = 0$ so the nuclei are completely screened from the static external field, $\langle \mathbf{E}_I \rangle = 0$. In deriving this result we explicitly assumed that the nuclei are point-like particles. For real molecules, this screening is incomplete due to the finite-size effects of the nuclei which are accounted for by the Schiff moment operator [5–9]. In this paper, however, we do not consider Schiff moment corrections.

4.4.3 Off-resonance screening of an oscillating external electric field

We now consider the case of an oscillating external electric field with frequency ω [1]

$$\mathbf{E}_{\rm ext} = \mathbf{E}_0 \cos\omega t \,. \tag{4.18}$$

When this field is sufficiently weak, the time-dependent perturbation theory may be applied to the Hamiltonian (4.6) with

$$V_{\rm rel}(t) = -\mathbf{d}\cdot\mathbf{E}_0 \cos\omega t \tag{4.19}$$

treated as the perturbation.

Let $|n\rangle$ be a complete set of eigenstates of the unperturbed Hamiltonian H_0, namely

$$H_0|n\rangle = \mathcal{E}_n|n\rangle \,. \tag{4.20}$$

Up to the first order in perturbation theory, the evolution of the ground state $|0\rangle$ is described by the wavefunction

$$\psi(t) = e^{-i\mathcal{E}_0 t}\left[|0\rangle - i\sum_n \int^t d\tau\, e^{-i\omega_{n0}(t-\tau)}|n\rangle\langle n|V_{\rm rel}(\tau)|0\rangle\right] , \tag{4.21}$$

where $\omega_{n0} = \mathcal{E}_n - \mathcal{E}_0$. In this formula, we assume that the frequency of the external field ω is not in resonance with any transition with energy ω_{n0}. In this case, it is safe to discard the widths of these states. The resonant case will be addressed in the next subsection.

Substituting the potential (4.19) into Eq. (4.21), we find the expectation value of the operator $\mathbf{E}'_I$ describing the induced electric field at the $I^{\rm th}$ nucleus due to the other nucleus and the electrons,

$$\langle \mathbf{E}'_I\rangle \equiv \langle\psi(t)|\mathbf{E}'_I|\psi(t)\rangle = 2\cos\omega t \sum_n \frac{\omega_{n0}{\rm Re}\langle 0|\mathbf{E}'_I|n\rangle\langle n|\mathbf{d}\cdot\mathbf{E}_0|0\rangle}{\omega_{n0}^2-\omega^2} \,. \tag{4.22}$$

Making use of the identity (4.12), one may cast Eq. (4.22) in the form

$$\langle \mathbf{E}'_I\rangle = \frac{2\cos\omega t}{Z_I}\sum_n \frac{\omega_{n0}^2 {\rm Im}\left[\langle 0|\mathbf{\Pi}_I|n\rangle\langle n|\mathbf{d}\cdot\mathbf{E}_0|0\rangle\right]}{\omega_{n0}^2-\omega^2} \,, \tag{4.23}$$

where the operator $\mathbf{\Pi}_I$ is defined as in Eq. (4.13).

Using the identity $\frac{\omega_{n0}^2}{\omega_{n0}^2-\omega^2} = 1 + \frac{\omega^2}{\omega_{n0}^2-\omega^2}$, the completeness of the set of states $|n\rangle$ and the relation (4.15), we find the total electric field at the position of $I^{\rm th}$ nucleus

$$\langle \mathbf{E}_I\rangle \equiv \langle \mathbf{E}'_I\rangle + \mathbf{E}_0\cos\omega t = \frac{M_I Z_T}{M_T Z_I}\mathbf{E}_0\cos\omega t + \frac{2\omega^2\cos\omega t}{Z_I}\sum_n \frac{{\rm Im}\left[\langle 0|\mathbf{\Pi}_I|n\rangle\langle n|\mathbf{d}\cdot\mathbf{E}_0|0\rangle\right]}{\omega_{n0}^2-\omega^2} \,. \tag{4.24}$$

We point out that Eq. (4.24) is valid not only for the Schrödinger Hamiltonian (4.6b), but also for the case when the kinetic term for electrons is described by the Dirac Hamiltonian. In the latter case, the relativistic corrections due to the Dirac equation are included in the energies ω_{n0} and states $|n\rangle$.

Using the explicit form of the Hamiltonian H_0 given in Eq. (4.6), one may prove the following identity for the operator (4.13):

$$\mathbf{\Pi}_I = \frac{iM_I}{\zeta_e M_T}\left[-\mathbf{d} + \mathcal{M}_I\mathbf{S}, H_0\right] , \tag{4.25}$$

where

$$\mathcal{M}_I = (-1)^I\left(M_N - M_I + Z_N - Z_I\right) , \tag{4.26}$$

[1] An oscillating electric field $\mathbf{E}_{\rm ext} = \mathbf{E}_0\cos\omega t$ generates an oscillating magnetic field $\mathbf{B}_{\rm ext} = \mathbf{B}_0\cos\omega t$ where $\mathbf{B}_0$ is orthogonal to $\mathbf{E}_0$. This field however does not contribute to the resulting electric field at nuclei due to the parity selection rules. Therefore in what follows we focus on the external electric field only.

and the quantities $\mathbf{d}$ and ζ_e are given in Eqs. (4.8) and (4.9), respectively.

The identity (4.25) allows us to represent the formula (4.24) for the resulting electric field at the I^{th} as

$$\langle \mathbf{E}_I \rangle = \left[\frac{M_I Z_T}{M_T Z_I} - \frac{\omega^2 M_I}{\zeta_e M_T Z_I} \left(\overleftrightarrow{\boldsymbol{\alpha}} - \overleftrightarrow{\boldsymbol{\beta}}_I \right) \right] \mathbf{E}_0 \cos \omega t \,, \tag{4.27}$$

where

$$\overleftrightarrow{\boldsymbol{\alpha}} = 2 \sum_n \frac{\omega_{n0}}{\omega_{n0}^2 - \omega^2} \langle 0|\mathbf{d}|n\rangle\langle n|\mathbf{d}|0\rangle \tag{4.28}$$

is the molecule's polarizability tensor and

$$\overleftrightarrow{\boldsymbol{\beta}}_I = 2\mathcal{M}_I \sum_n \frac{\omega_{n0}}{\omega_{n0}^2 - \omega^2} \langle 0|\mathbf{S}|n\rangle\langle n|\mathbf{d}|0\rangle \,. \tag{4.29}$$

Eq. (4.27) describes the screening of an oscillating electric field inside a diatomic molecule in the case when the frequency of the field is off resonance from any molecular transition. Let us discuss the terms in this formula.

The first term in the brackets has the same form as for the screening of static electric field (4.17). This term is proportional to the total charge of the molecule Z_T which is vanishing for neutral molecules.

The second term in the brackets is specified by the molecular polarizability tensor $\overleftrightarrow{\boldsymbol{\alpha}}$. This term has the same structure as that in the formula for screening of electric fields in atoms derived in Ref. [11].

The last term in Eq. (4.27) is described by the tensor $\overleftrightarrow{\boldsymbol{\beta}}_I$ defined in Eq. (4.29). This tensor depends on the matrix element of the inter-nuclear distance operator $\mathbf{S}$ which has no analogy in the atomic case. As we will show in the next section, this term plays a significant role in the screening of the external field in molecules. In fact, due to the large ratio of nuclear and electron mass $|\mathcal{M}_I| \approx (M_N - M_I)/m_e \gg 1$, $\overleftrightarrow{\boldsymbol{\beta}}_I$ usually dominates over $\overleftrightarrow{\boldsymbol{\alpha}}$. As will be discussed in Sect. 4.5.2, if the external field's frequency is in the rotational or vibrational regimes ($10^{-5} - 10^{-3}$ a.u.) then $|\overleftrightarrow{\boldsymbol{\beta}}_I| \gg \overleftrightarrow{\boldsymbol{\alpha}}$. Only the case where the field's frequency is in the electronic transition regime (~ 0.1 a.u.) that $\overleftrightarrow{\boldsymbol{\beta}}_I$ and $\overleftrightarrow{\boldsymbol{\alpha}}$ become comparable.

In conclusion of this section, we rewrite our results (4.27)–(4.29) with the fundamental constants $\hbar$, e and m_e explicitly shown

$$\langle \mathbf{E}_I \rangle = \left[\frac{M_I Z_T}{M_T Z_I} - \frac{\omega^2 m_e M_I}{e^2 \zeta_e M_T Z_I} \left(\overleftrightarrow{\boldsymbol{\alpha}} - \overleftrightarrow{\boldsymbol{\beta}}_I \right) \right] \mathbf{E}_{\text{ext}} \,, \tag{4.30a}$$

$$\overleftrightarrow{\boldsymbol{\alpha}} = \frac{2}{\hbar} \sum_n \frac{\omega_{n0}}{\omega_{n0}^2 - \omega^2} \langle 0|\mathbf{d}|n\rangle\langle n|\mathbf{d}|0\rangle \,, \tag{4.30b}$$

$$\overleftrightarrow{\boldsymbol{\beta}}_I = \frac{2\mathcal{M}_I}{\hbar} \sum_n \frac{\omega_{n0} \langle 0|e\mathbf{S}|n\rangle\langle n|\mathbf{d}|0\rangle}{\omega_{n0}^2 - \omega^2} \,, \tag{4.30c}$$

where $\mathcal{M}_I = (-1)^I \left[m_e^{-1}(M_N - M_I) + Z_N - Z_I \right]$, $\zeta_e = M_T^{-1} \left(M_N + m_e Z_N \right)$ and $\mathbf{d} = -\zeta_e e \sum_{i=1}^{L} \mathbf{s}_i + \zeta_N e \mathbf{S}$.

Since $m_e \ll M_I$, one can make the (good) approximations $\zeta_e \approx 1$, $\mathcal{M}_1 \approx -M_2/m_e$, $\mathcal{M}_2 \approx M_1/m_e$ and $M_T \approx M_N$. Note that, with these approximations, the final term in the bracket in Eq. (4.30a) may be written as

$$\frac{\omega^2 m_e M_I}{e^2 \zeta_e M_T Z_I} \overleftrightarrow{\boldsymbol{\beta}}_I \approx \frac{2(-1)^I \omega^2 \mu_N}{e^2 \hbar Z_I} \sum_n \frac{\omega_{n0} \langle 0|e\mathbf{S}|n\rangle\langle n|\mathbf{d}|0\rangle}{\omega_{n0}^2 - \omega^2} \,, \tag{4.31}$$

where μ_N is the reduced nuclear mass defined in Eq. (4.7).

4.4.4 Resonance enhancement of an oscillating external electric field

When the frequency of the external electric field (4.18) approaches one of the molecular transition frequencies, $\omega = \omega_{n0}$, the width of this state Γ_n cannot be ignored in perturbative calculations. In this case, the wavefunction (4.21) should be modified to read

$$\psi(t) = e^{-i\mathcal{E}_0 t} \left[|0\rangle - i \sum_k \int^t \left(d\tau e^{-i(\omega_{k0} - i\Gamma_k/2)(t-\tau)} |k\rangle\langle k|V_{\text{rel}}(\tau)|0\rangle \right) \right] . \tag{4.32}$$

Using the explicit form of the potential (4.19), we find the expectation value of the operator $\mathbf{E}'_I$ describing the electric field at the I^{th} nucleus induced by the electrons and the other nucleus

$$\langle \mathbf{E}'_I \rangle = \sum_k [-\cos(\omega t) f_k(\omega) + \frac{\Gamma_k}{2} \sin(\omega t) g_k(\omega)] \mathrm{Re} \langle 0|\mathbf{E}'_I|k\rangle\langle k| - \mathbf{d}\cdot\mathbf{E}_0|0\rangle \,, \tag{4.33}$$

where

$$f_k(\omega) = \frac{\omega_{k0}+\omega}{(\omega_{k0}+\omega)^2 - (\Gamma_k/2)^2} + \frac{\omega_{k0}-\omega}{(\omega_{k0}-\omega)^2 - (\Gamma_k/2)^2} \,, \tag{4.34a}$$

$$g_k(\omega) = \frac{1}{(\omega_{k0}+\omega)^2 - (\Gamma_k/2)^2} - \frac{1}{(\omega_{k0}-\omega)^2 - (\Gamma_k/2)^2} \,. \tag{4.34b}$$

Note that in Eq. (4.33), we keep only the terms which are not suppressed by the small factor $e^{-\Gamma_k t/2}$.

It is natural to assume that all linewidths Γ_k are much smaller than the corresponding energies, $\Gamma_k \ll \omega_{k0}$. Under this assumption, the leading term in the functions $f_k(\omega)$ and $g_k(\omega)$ are

$$f_k(\omega) = \begin{cases} 1/2\omega \,, & k = n \\ 2\omega_{k0}/\left(\omega_{k0}^2 - \omega^2\right) \,, & k \neq n \end{cases} \,, \tag{4.35a}$$

$$g_k(\omega) = \begin{cases} -4/\Gamma_n^2 \,, & k = n \\ -4\omega_{k0}\omega/(\omega_{k0}^2 - \omega^2)^2 \,, & k \neq n \end{cases} \,. \tag{4.35b}$$

Substituting these functions into Eq. (4.33) and using the identity (4.12), we find the total field at the I^{th} nucleus $\langle \mathbf{E}_I \rangle \equiv \mathbf{E}_0 \cos(\omega t) + \langle \mathbf{E}'_I \rangle$,

$$\begin{aligned} \langle \mathbf{E}_I \rangle = {} & \frac{M_I Z_T}{M_T Z_I} \mathbf{E}_0 \cos\omega t + \frac{2\omega^2 \cos\omega t}{Z_I} \sum_{k\neq n} \frac{\mathrm{Im}\left[\langle 0|\mathbf{\Pi}_I|k\rangle\langle k|\mathbf{d}\cdot\mathbf{E}_0|0\rangle\right]}{\omega_{k0}^2 - \omega^2} \\ & - \frac{3\cos\omega t}{2Z_I} \mathrm{Im}\left[\langle 0|\mathbf{\Pi}_I|n\rangle\langle n|\mathbf{d}\cdot\mathbf{E}_0|0\rangle\right] - \frac{2\omega \sin\omega t}{Z_I \Gamma_n} \mathrm{Im}\left[\langle 0|\mathbf{\Pi}_I|n\rangle\langle n|\mathbf{d}\cdot\mathbf{E}_0|0\rangle\right] \,. \end{aligned} \tag{4.36}$$

In deriving this result, we have employed the identity (4.14) and taken into account the completeness of the set of states $|k\rangle$.

Different terms in the expression (4.36) play different role in the screening or resonant enhancement of the electric field at the I^{th} nucleus in the molecule. Let us discuss them separately.

The term in the first line of Eq. (4.36) is present only for charged molecules with $Z_T \neq 0$. In the rest of this subsection we consider neutral molecules for which this term vanishes.

The term in the second line is responsible for the screening of the external field due to the states which are off resonance with frequency ω. Strictly speaking, this term cannot be expressed via the tensors (4.30b) and (4.30c) since the sum does not contain the state $|n\rangle$, which is on resonance with the external field.

The terms in the last two lines arise from this state $|n\rangle$ which is in resonance with the external field. Between these terms, the last one dominates because the width is typically much smaller than the energy, $\Gamma_n \ll \omega$. Moreover, if $|n\rangle$ is a rotational or vibrational state then Γ_n is typically very small and the factor ω/Γ_n in the last term of Eq. (4.36) makes it to dominate over all other terms. We can thus write (with the constant e and m_e restored)

$$\langle \mathbf{E}_I \rangle \approx \frac{\omega^2 m_e M_I}{\zeta_e e^2 Z_I M_T \Gamma_n} \overleftrightarrow{\gamma}_I \mathbf{E}_0 \sin\omega t \,, \tag{4.37}$$

where we have introduced the tensor

$$\overleftrightarrow{\gamma}_I = 2\langle 0|\mathbf{d}|n\rangle\langle n|\mathbf{d}|0\rangle - 2\mathcal{M}_I \langle 0|\mathbf{S}|n\rangle\langle n|\mathbf{d}|0\rangle \,. \tag{4.38}$$

In deriving Eq. (4.37) we applied the identity (4.25).

The electric field at the I^{th} nucleus (4.37) has the following features: (i) The external field may be enhanced by many orders of magnitude due to the resonance factor ω/Γ. (ii) The phase of the resulting field is shifted by $\pi/2$ with respect to the applied field. This is a typical resonance phase shift which occurs in damped driven oscillations. Both these features are already known for an atom in an oscillating electric field [13]. Here we establish similar results for molecules.

We note that although in the resonance case, the external field may be significantly enhanced thanks to the smallness of the width Γ_n, it certainly does not mean that one can induce an arbitrarily large field at a nucleus by using an arbitrarily strong external field. This is because for strong fields, perturbation theory, in the framework of which the results of this section were derived, breaks down. The condition for the applicability of perturbation theory reads

$$\Omega \ll \Gamma_n \,, \tag{4.39}$$

where $\Omega \equiv |\langle 0|\mathbf{d}\cdot\mathbf{E}_0|n\rangle|$ is the Rabi frequency (see Ref. [13] for more detail).

If the condition $\Omega \ll \Gamma_n$ is not met then $\langle \mathbf{E}_I\rangle$ may be calculated non-perturbatively by considering the states $|0\rangle$ and $|n\rangle$ as forming a two-level quantum system. The result is

$$\langle \mathbf{E}_I\rangle \approx \frac{\omega^2 m_e M_I}{\zeta_e e^2 Z_I M_T}\frac{\Gamma_n}{\Gamma_n^2+2\Omega^2}\overleftrightarrow{\gamma}_I \mathbf{E}_0 \sin\omega t \,. \tag{4.40}$$

We note that for the weak external field E_0 such that $\Omega \ll \Gamma_n$, Eq. (4.40) reduces to Eq. (4.37) derived perturbatively. For a strong external field such that $\Omega \gg \Gamma_n$ the resulting electric field at nucleus $\langle \mathbf{E}_I\rangle$ becomes inversely proportional to the applied field E_0.

According to Eq. (4.40), the field $\langle \mathbf{E_I}\rangle$, considered as a function of E_0 reaches its maximum at

$$E_0 = E_{\rm crit} \equiv \frac{\Gamma_n}{\sqrt{2}d} \,, \tag{4.41}$$

where $d = |\langle 0|\mathbf{d}\cdot\hat{\mathbf{k}}|n\rangle|$. Here, $\hat{\mathbf{k}}$ is the unit vector in the direction of $\mathbf{E}_0$. The maximal value of $E_I \equiv |\langle \mathbf{E_I}\rangle|$, corresponding to $E_0 = E_{\rm crit}$ is

$$E_I^{\rm max} \approx \frac{\omega^2 m_e M_I}{\sqrt{8}\zeta_e e^2 Z_I M_T d}|\overleftrightarrow{\gamma}_I\hat{\mathbf{k}}| \sin\omega t \,. \tag{4.42}$$

It is important to note that this field is independent of the width of the excited state Γ_n.

4.5 Numerical estimates for diatomic molecules

In this section, the screening of an electric field in some diatomic molecules will be considered. To find the total electric field at the $I^{\rm th}$ nucleus (4.27), one needs to evaluate the tensors $\overleftrightarrow{\boldsymbol{\alpha}}$, $\overleftrightarrow{\boldsymbol{\beta}}_I$ and $\overleftrightarrow{\boldsymbol{\gamma}}_I$ given in Eqs. (4.28), (4.29) and (4.38). In general, to accurately compute these tensors one needs to apply sophisticated numerical methods. Our goal is, however, to give crude semi-analytic estimates of some leading contributions to these tensors. For this purpose, we first develop a representation of these tensors in the Born-Oppenheimer approximation and then present numerical estimates for some simple molecules.

4.5.1 Molecular polarizability in the Born-Oppenheimer approximation

The leading contributions to the tensors (4.28), (4.29) and (4.38) may be estimated in the Born-Oppenheimer approximation. In this approximation, the motion of the molecule in any state $|n\rangle$ may be separated into rotational, vibrational and electronic modes. The rotational motion is described by the Wigner D-matrix $D^{J_n}_{M_n\Lambda_n}(\Theta)$ depending on the set of Euler angles Θ which describes the molecule's orientation with respect to the fixed laboratory frame (J_n is the molecule's total angular momentum quantum number, M_n is the projection of this angular momentum onto the laboratory z-axis and Λ_n is the projection of the electronic angular momentum onto the inter-nucler axis) whereas the vibrational and electronic motions may be described by the ket $|\mu_n\Lambda_n\nu_n\rangle$ (ν_n is the vibrational quantum number which, generally, depends on J_n, $\nu_n = \nu_n(J_n)$, and μ_n denotes all other quantum numbers). We write

$$|n\rangle = \sqrt{\frac{2J_n+1}{8\pi^2}}D^{J_n}_{M_n\Lambda_n}(\Theta)|\mu_n\Lambda_n\nu_n\rangle \,. \tag{4.43}$$

where the coefficient $\sqrt{(2J_n+1)/8\pi^2}$ is the normalization constant for the Wigner D-matrix. The ket $|\mu_n\Lambda_n\nu_n\rangle$ is assumed to be properly normalized.

The ket $|\mu_n\Lambda_n\nu_n\rangle$ may be considered as a wavefunction of the molecule in the rotating frame. This wavefunction factorizes into the vibrational $\psi^{\mu_n\Lambda_n}_{\nu_n}(S)$ and electronic $\phi_{\mu_n\Lambda_n}(S,\mathbf{s}_i)$ parts,

$$|\mu_n\Lambda_n\nu_n\rangle = S^{-1}\psi^{\mu_n\Lambda_n}_{\nu_n}(S)\phi_{\mu_n\Lambda_n}(S,\mathbf{s}_i) \,. \tag{4.44}$$

In this representation, we ignore all spins of electrons and nuclei. This approximation usually gives acceptable accuracy for low rotational levels [15].

In literature, the polarizablity tensor $\overleftrightarrow{\boldsymbol{\alpha}}$ is often calculated in the frame rotating with the molecule (this frame is defined with respect to the laboratory by the angular coordinates Θ). However, the external electric field is naturally defined with respect to the laboratory frame. Thus, one needs to express the laboratory-frame components of the molecular polarizability tensor via its rotating-frame components.

The spherical components of the vector $\mathbf{d}$ in the laboratory (l) and rotating (r) frames will be denoted by $d_q^{(l)}$ and $d_q^{(r)}$ ($q = 0, \pm 1$), respectively. They are related to each other by the formula [15]

$$d_p^{(l)} = \sum_q (-1)^{p-q} D^1_{pq}(\Theta) d_q^{(r)} \,. \tag{4.45}$$

This formula, together with Eq. (4.43) and the standard identity for the Wigner D-matrices [16, 17]

$$\frac{1}{8\pi^2} \int \bar{D}^{J'}_{M'\Lambda'}(\Theta) D^j_{pq}(\Theta) D^J_{M\Lambda}(\Theta) d\Theta = (-1)^{2J'-M'-\Lambda'} \begin{pmatrix} J' & j & J \\ -M' & p & M \end{pmatrix} \begin{pmatrix} J' & j & J \\ -\Lambda' & q & \Lambda \end{pmatrix} , \tag{4.46}$$

allows us to relate the laboratory-frame components of the tensor $\langle 0|\mathbf{d}|n\rangle\langle n|\mathbf{d}|0\rangle$ to its rotating-frame components

$$\begin{aligned} &\langle 0|d_p^{(l)}|n\rangle\langle n|\bar{d}_q^{(l)}|0\rangle = \delta_{pq}\,(2J_0+1)\,(2J_n+1) \\ &\times \begin{pmatrix} J_0 & 1 & J_n \\ -M_0 & p & M_n \end{pmatrix}^2 \begin{pmatrix} J_0 & 1 & J_n \\ -\Lambda_0 & \Lambda_0 - \Lambda_n & \Lambda_n \end{pmatrix}^2 \left| \langle \mu_0 \Lambda_0 \nu_0 | d^{(r)}_{\Lambda_0 - \Lambda_n} | \mu_n \Lambda_n \nu_n \rangle \right|^2 . \end{aligned} \tag{4.47}$$

If the molecule is non-polarized in the ground state, the expression (4.47) should be averaged over the quantum number M_0 and summed over the quantum number M_n. In this case, the molecular polarizability tensor (4.28) has only the scalar part $\alpha(\omega)$, namely

$$\overleftrightarrow{\boldsymbol{\alpha}}(\omega) = \alpha(\omega) \mathbf{1}_{3\times 3} \,. \tag{4.48}$$

Physically, this implies that the induced electric field in the non-polarized molecule can only be parallel to the external electric field.

Without loss of generality, it may be assumed that the external field $\mathbf{E}_{\text{ext}}$ is directed along the laboratory z-axis. For simplicity, it will also be assumed that the ground state is in the Σ ($\Lambda = 0$) configuration and has total angular momentum $J_0 = 0$ (this assumption forces $M_0 = 0$ and $J_n = 1$). Under these assumptions, the only relevant component of the tensor (4.47) is

$$\langle 0|d_0^{(l)}|n\rangle\langle n|\bar{d}_0^{(l)}|0\rangle = \delta_{0M_n} \begin{pmatrix} 0 & 1 & 1 \\ 0 & -\Lambda_n & \Lambda_n \end{pmatrix}^2 \left| \langle \mu_0 \Sigma \nu_0 | d^{(r)}_{-\Lambda_n} | \mu_n \Lambda_n \nu_n \rangle \right|^2 , \tag{4.49}$$

where the vibrational quantum number ν_0 corresponds to the total momentum quantum number $J = 0$ whereas ν_n is attributed to $J = 1$.

Substituting Eq. (4.49) into Eq. (4.28), we obtain the expression for the polarizability tensor in the laboratory frame via the components of this tensor in the molecular (rotating) frame

$$\alpha(\omega) = \frac{1}{3} \left[\alpha^{\parallel}_{\text{el}}(\omega) + 2\alpha^{\perp}_{\text{el}}(\omega) + \alpha^{\parallel}_{\text{vib}}(\omega) + \alpha^{\parallel}_{\text{rot}}(\omega) \right] , \tag{4.50}$$

where $\alpha^{\parallel}_{\text{el}}$ and $\alpha^{\perp}_{\text{el}}$ are the parallel and perpendicular components with respect to the molecular axis arising due to electronic excitations; $\alpha^{\parallel}_{\text{vib}}$ and $\alpha^{\parallel}_{\text{rot}}$ are the terms originating from the vibrational and rotational states. Explicitly, these quantities read

$$\alpha^{\parallel}_{\text{el}}(\omega) = \sum_{\substack{\mu_n \neq \mu_0 \\ \nu_n}} \frac{2\omega_{n0}}{\omega_{n0}^2 - \omega^2} \left| \langle \mu_0 \Sigma \nu_0 | \, d_0^{(r)} \, | \mu_n \Sigma \nu_n \rangle \right|^2 , \tag{4.51a}$$

$$\alpha^{\perp}_{\text{el}}(\omega) = \sum_{\mu_n, \nu_n} \frac{2\omega_{n0}}{\omega_{n0}^2 - \omega^2} \left| \langle \mu_0 \Sigma \nu_0 | \, d_{-1}^{(r)} \, | \mu_n \Pi \nu_n \rangle \right|^2 , \tag{4.51b}$$

$$\alpha^{\parallel}_{\text{vib}}(\omega) = \sum_{\nu_n \neq \nu_0} \frac{2\omega_{n0}}{\omega_{n0}^2 - \omega^2} \left| \langle \mu_0 \Sigma \nu_0 | \, d_0^{(r)} \, | \mu_0 \Sigma \nu_n \rangle \right|^2 , \tag{4.51c}$$

$$\alpha^{\parallel}_{\text{rot}}(\omega) = \frac{2\omega_{\nu_0 \nu_0'}}{\omega_{\nu_0 \nu_0'}^2 - \omega^2} \left| \langle \mu_0 \Sigma \nu_0 | \, d_0^{(r)} \, | \mu_0 \Sigma \nu_0' \rangle \right|^2 , \tag{4.51d}$$

where the vibrational quantum numbers ν_0 and ν_0' correspond to $J = 0$ and $J = 1$, respectively.

As we will show in the end of this section, the representation for the molecular polarizablity (4.50) appears useful, as the values of the quantities (4.51) may be either easily calculated or found in literature. Similar representations may be developed for the tensors (4.29) and (4.38). Following the same procedure as above, it is possible to prove that each of these tensors is proportional to the unit matrix,

$$\overleftrightarrow{\boldsymbol{\beta}}_I(\omega) = \beta_I(\omega)\mathbf{1}_{3\times 3}\,, \qquad \overleftrightarrow{\boldsymbol{\gamma}}_I(\omega) = \gamma_I(\omega)\mathbf{1}_{3\times 3}\,. \tag{4.52}$$

For the quantity $\beta_I(\omega)$ we find

$$\beta_I(\omega) = \frac{\mathcal{M}_I}{3}\left[\beta^{\parallel}_{\rm vib}(\omega) + \beta^{\parallel}_{\rm rot}(\omega)\right]\,, \tag{4.53}$$

where

$$\beta^{\parallel}_{\rm vib}(\omega) = 2\sum_{\nu_n\neq\nu_0}\frac{\omega_{n0}}{\omega_{n0}^2-\omega^2}\,\langle\mu_0\Sigma\nu_0|\,S\,|\mu_0\Sigma\nu_n\rangle\,\langle\mu_0\Sigma\nu_n|\,d_0^{(r)}\,|\mu_0\Sigma\nu_0\rangle\,, \tag{4.54a}$$

$$\beta^{\parallel}_{\rm rot}(\omega) = \frac{2\omega_{\nu_0\nu_0'}}{\omega^2_{\nu_0\nu_0'}-\omega^2}\,\langle\mu_0\Sigma\nu_0|\,S\,|\mu_0\Sigma\nu_0'\rangle\,\langle\mu_0\Sigma\nu_0'|\,d_0^{(r)}\,|\mu_0\Sigma\nu_0\rangle\,. \tag{4.54b}$$

In contrast to the quantities (4.28) and (4.29), there is no summation over states in the formula of the γ-tensor (4.38) since only one pair of states is in resonance with the external field.

It is of interest to consider the external electric field in resonance with the lowest rotational state. In this case, we have

$$\gamma_I(\omega) = \frac{2}{3}\left|\langle\mu_0\Sigma\nu_0|\,d_0^{(r)}\,|\mu_0\Sigma\nu_n\rangle\right|^2 - \frac{2}{3}\mathcal{M}_I\,\langle\mu_0\Sigma\nu_0|\,S\,|\mu_0\Sigma\nu_n\rangle\,\langle\mu_0\Sigma\nu_n|\,d_0^{(r)}\,|\mu_0\Sigma\nu_0\rangle\,. \tag{4.55}$$

In this formula, the second term on the right-hand side dominates over the first one since $|\mathcal{M}_I| \gg 1$,

$$\gamma_I(\omega) \approx -\frac{2}{3}\mathcal{M}_I\,\langle\mu_0\Sigma\nu_0|\,S\,|\mu_0\Sigma\nu_n\rangle\,\langle\mu_0\Sigma\nu_n|\,d_0^{(r)}\,|\mu_0\Sigma\nu_0\rangle\,. \tag{4.56}$$

We point out, however, that the first term in Eq. (4.55) cannot be ignored if the external electric field is in resonance with electronic transitions in the molecule. In this case, the second term in Eq. (4.55) vanishes so the sole contribution to $\gamma_I\,(\omega)$ comes from its first term.

4.5.2 Screening of the external electric field in different frequency regimes

Recall that the molecular spectra have three typical frequency scales: $\omega_{\rm rot}$ associated with the rotational transitions, $\omega_{\rm vib}$ associated with the vibrational transitions and $\omega_{\rm el}$ associated with the electronic transitions. Normaly, $\omega_{\rm rot} \ll \omega_{\rm vib} \ll \omega_{\rm el}$. It is interesting to consider the screening of external electric fields with frequencies in these three different regimes.

As was shown in the previous subsection, the induced electric field at the $I^{\rm th}$ nucleus is parallel to the external electric field. The magnitude of this field may be written as

$$E_I = \sigma_I(\omega)E_0\cos\omega t\,, \tag{4.57}$$

where the suppression factor σ_I is defined as

$$\sigma_I(\omega) = \frac{M_I Z_T}{M_T Z_I} - \frac{\omega^2 M_I}{\zeta_e M_T Z_I}\left[\alpha(\omega) - \beta_I(\omega)\right]\,. \tag{4.58}$$

The first term here is ω-independent and is non-vanishing only for charged molecules. Although this term is important in the total formula for the suppression factor, it is more interesting to analyze the other terms in Eq. (4.58) which are non-vanishing both for charged and neutral molecules and are ω-dependent. Therefore, to the end of this subsection we will restrict ourselves to the case $Z_T = 0$. We will also work in the limit $m_e \ll M_I$ in which $\zeta_e \approx 1$, $\mathcal{M}_I \approx (-1)^I\,(M_N - M_I)$ and $M_T \approx M_N$.

Screening of rotational-range-frequency fields

Let us consider an external electric field with frequency of order of the lowest rotational transition frequencies, $\omega \sim \omega_{\nu_0\nu_0'}$. In this case, because the factor $\omega_{n0}/\left(\omega_{n0}^2-\omega^2\right)$ in Eq. (4.28) scales as energy inverse, the dominant contribution to $\alpha(\omega)$ comes from Eq. (4.51d) and the dominant contribution to $\beta_I(\omega)$ comes from Eq. (4.54b). Since the matrix elements $\langle\mu_0\Sigma\nu_0|\,S\,|\mu_0\Sigma\nu_0'\rangle$ and $\langle\mu_0\Sigma\nu_0|\,d_0^{(r)}\,|\mu_0\Sigma\nu_0'\rangle$ are of the same order, and since $|\mathcal{M}_I| \gg 1$, the dominant contribution to the suppression factor (4.58) comes from $\beta_I(\omega)$. Thus, the leading contribution to the suppression factor (4.58) is given by the term (4.54b), namely

$$\sigma_I^{\rm rot}\left(\omega\right) \approx (-1)^I\,\frac{2\omega^2\mu_N}{3Z_I}\,\frac{\bar\omega\bar S\bar d}{\bar\omega^2-\omega^2}\,, \tag{4.59}$$

where

$$\bar\omega \equiv \omega_{\nu_0\nu_0'} = \frac{1}{\mu_N\bar S^2} \tag{4.60}$$

is the rotational energy with $J=1$,

$$\bar S = \langle\mu_0\Sigma\nu_0|\,S\,|\mu_0\Sigma\nu_0\rangle \tag{4.61}$$

is the ground state mean inter-nuclear distance and

$$\bar d = \langle\mu_0\Sigma\nu_0|\,d_0^{(r)}\,|\mu_0\Sigma\nu_0\rangle \tag{4.62}$$

is the ground state mean electric dipole (in the direction of $\mathbf{S}$). Note that we have invoked the rigid-rotor approximation which allows us to replace ν_0' by ν_0 in the definition of $\bar S$ and $\bar d$. We have also made the approximation $M_I\mathcal{M}_I/M_T \approx (-1)^I\mu_N$.

Screening of vibrational-range-frequency fields

In the case where ω is of the order of a vibrational energy, $\omega \sim \omega_{\rm vib}$, contributions to $\alpha(\omega)$ from $\alpha_{\rm el}^{\parallel}$ and $\alpha_{\rm el}^{\perp}$ are negligible whereas the terms $\alpha_{\rm vib}^{\parallel}$ and $\alpha_{\rm rot}^{\parallel}$ are significant. In the expression (4.53) for β_I, both terms $\beta_{\rm vib}^{\parallel}$ and $\beta_{\rm rot}^{\parallel}$ contribute. Again, since $|\mathcal{M}_I| \gg 1$, β_I dominates over α. Thus, in this case, the leading contributions to the suppression factor (4.58) are

$$\sigma_I(\omega) = \sigma_I^{\rm vib}(\omega) + \sigma_I^{\rm rot}(\omega)\,, \tag{4.63a}$$

$$\sigma_I^{\rm vib}(\omega) \approx (-1)^I\,\frac{2\omega^2\mu_N}{3Z_I}\sum_{\nu_n\neq\nu_0}\frac{\omega_{n0}S_{\nu_0}^{\nu_n}\,(d_0^r)_{\nu_n}^{\nu_0}}{\omega_{n0}^2-\omega^2}\,, \tag{4.63b}$$

where $\bar\omega$, $\bar S$ and $\bar d$ are given in Eqs. (4.60), (4.61) and (4.62), respectively, and the quantities $S_{\nu_0}^{\nu_n}$ and (d_0^r) are defined by

$$S_{\nu_0}^{\nu_n} = \langle\mu_0\Sigma\nu_0|\,S\,|\mu_0\Sigma\nu_n\rangle \tag{4.64}$$

and

$$(d_0^r)_{\nu_n}^{\nu_0} = \langle\mu_0\Sigma\nu_n|\,d_0^{(r)}\,|\mu_0\Sigma\nu_0\rangle\ . \tag{4.65}$$

The quantity $\sigma_I^{\rm rot}(\omega)$ in Eq. (4.63a) is defined in Eq. (4.59). Note, however, that since the field's frequency, being in the vibrational regime, is much larger than the rotational frequency, we have $\frac{\omega^2\bar\omega}{\bar\omega^2-\omega^2} \approx -\bar\omega$. As a result, this term $\sigma_I^{\rm rot}(\omega)$ becomes independent of ω.

The quantity $S_{\nu_0}^{\nu_n}$ may be roughly estimated assuming that the vibrational mode is purely harmonic, i.e., vibrational wavefunctions are harmonic oscillator wavefunctions. The operator $d_0^{(r)}$ may be written as $-\sum_{i=1}^L s_i^{\parallel} + \zeta_N S$ where $s_i^{\parallel}$ is the projection of $\mathbf{s}_i$ onto the molecular axis. The quantity $(d_0^r)_{\nu_n}^{\nu_0}$ may be approximated by $-f_{\nu_n}^{\nu_0}\bar s^{\parallel} + \zeta_N S_{\nu_n}^{\nu_0}$ where $f_{\nu_n}^{\nu_0} = \langle\nu_n|\nu_0\rangle$ is the Franck-Condon factor and $\bar s^{\parallel} = \langle\mu_0\Sigma|\sum_{i=1}^L s_i^{\parallel}|\mu_0\Sigma\rangle$. If one takes, approximately, $f_{\nu_n}^{\nu_0} \approx \delta_{\nu_n}^{\nu_0}$ then the electronic part drops out when summed over all $\nu_n \neq \nu_0$. In this case, $(d_0^r)_{\nu_n}^{\nu_0} \approx \zeta_N S_{\nu_n}^{\nu_0}$. Typically, $S_{\nu_n}^{\nu_0}$ decreases rapidly as ν_n increases. Thus, only the term with $\nu_n = \nu_0 \pm 1$ makes dominant contribution to the sum in Eq. (4.63).

Screening of electronic-range-frequency fields

In the case where ω is of the order of an electronic energy, $\omega \sim \omega_{\rm el}$, the dominant contributions to the scalar polarizability (4.50) come from the electronic terms (4.51a) and (4.51b). Due to the factor $\mathcal{M}_I$, the contribution β_I to the suppression factor (4.58) is also significant. Thus, in this case, we have

$$\sigma_I = \sigma_I^{\rm el}(\omega) + \sigma_I^{\rm vib}(\omega) + \sigma_I^{\rm rot}(\omega)\,, \tag{4.66a}$$

$$\sigma_I^{\rm el}(\omega) \approx -\frac{\omega^2 M_I}{3 M_N Z_I}\left[\alpha_{\rm el}^{\parallel}(\omega) + 2\alpha_{\rm el}^{\perp}(\omega)\right]\,, \tag{4.66b}$$

where the quantities $\bar{\omega}$, $\bar{S}$, $\bar{d}$, $S_{\nu_0}^{\nu_n}$ and $(d_0^r)_{\nu_n}^{\nu_0}$ are as given in Eqs. (4.60), (4.61), (4.62), (4.64) and (4.65), respectively. We point out that the expression (4.66b) is analogous to the screening factor for the oscillating electric field in atoms found in [11].

The quantities $\sigma_I^{\rm rot}(\omega)$ and $\sigma_I^{\rm vib}(\omega)$ are defined in Eqs. (4.59) and (4.63a), respectively. Note that just as in the vibrational energy regime, here, $\sigma_I^{\rm rot}(\omega)$ and $\sigma_I^{\rm vib}(\omega)$ is independent of ω.

Summary on different contributions to the screening coefficient

In the rotational energy regime ($\omega \sim 10^{-5}$ a.u.), only $\sigma_I^{\rm rot}$ given by Eq. (4.59) contributes to σ_I. As we move up to the vibrational energy regime ($\omega \sim 10^{-3}$ a.u.), $\sigma_I^{\rm vib}(\omega)$ defined in Eq. (4.63b) becomes comparable to $\sigma_I^{\rm rot}$ and $\sigma_I^{\rm el}$, on the other hand, is still negligible. In the electronic energy regime ($\omega \sim 0.1$ a.u.), $\sigma_I^{\rm el}$ from Eq. (4.66b) becomes comparable to its rotational and vibrational counterpart; now all three terms contribute to σ_I.

In Fig. 4.1, we plot the behaviour of the three quantities $\sigma_I^{\rm rot}(\omega)$, $\sigma_I^{\rm vib}(\omega)$ and $\sigma_I^{\rm el}(\omega)$ as functions of frequency ω. The change is the significance of these terms as one moves up the frequency scale is clearly demonstrated.

Note that each of the three plots shows a single resonance (the spikes in the case of $\sigma_I^{\rm rot}$ and $\sigma_I^{\rm vib}$, the upward tail of $\sigma_I^{\rm el}$) due to the applied approximations. In reality, $\sigma_I^{\rm rot}$ and $\sigma_I^{\rm vib}$ should have many more resonances. However, since we assumed that the molecule is in the ground state when the external field is absent and the contribution to $\sigma_I^{\rm vib}$ of all states with vibrational quantum number large than 1 is negligible, $\sigma_I^{\rm rot}$ and $\sigma_I^{\rm vib}$ each has, under these approximations, a single resonance. On the other hand, $\sigma_I^{\rm el}$ possesses many resonances which we do not include in Fig. 4.1 (these resonances are at frequencies higher than the range plotted in Fig. 4.1).

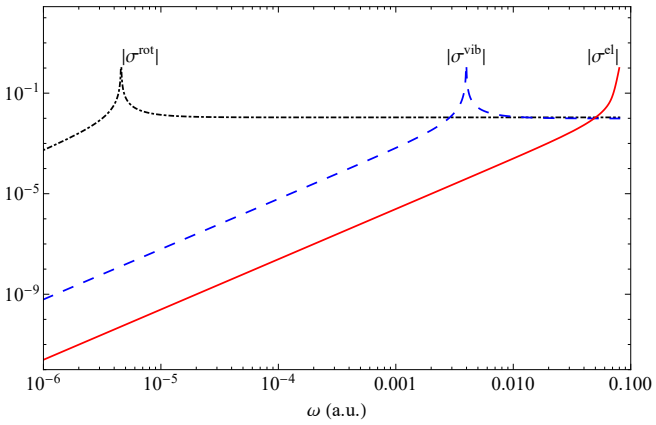

Figure 4.1: Comparison of the magnitudes of the three contributions to σ_I: $\sigma_I^{\rm rot}$, $\sigma_I^{\rm vib}$ and $\sigma_I^{\rm el}$ in CaF molecule. The frequency ω is presented in atomic units. For low frequency in the rotational regime, $\sigma_I^{\rm rot}$ dominates. For frequency in the vibrational regime, both $\sigma_I^{\rm rot}$ and $\sigma_I^{\rm vib}$ contribute; $\sigma_I^{\rm el}$ is still negligible. For large frequency in the electronic regime, each of the three terms is comparable to other two.

4.5.3 Resonance enhancement from the lowest rotational transition

In this subsection, we consider the resonance enhancement of an oscillating electric field in a diatomic molecule by the lowest rotational level. This case may be of interest for experimental applications because the energy of this level is in the microwave region and is thus quite accessible experimentally.

Since the $\overleftrightarrow{\gamma}_I$ tensor contains only the scalar part γ_I as in Eq. (4.52), the formula (4.37) for the enhancement of the electric field may by rewritten as

$$E_I = \epsilon_I(\omega) E_0 \sin\omega t\,, \tag{4.67}$$

where ϵ_I denotes the enhancement factor,

$$\epsilon_I(\omega) = \frac{\omega^2 M_I \gamma_I}{\zeta_e Z_I M_T \Gamma}\,. \tag{4.68}$$

When the frequency of the external field is equal to the lowest rotational state frequency (4.60), $\omega = \bar{\omega}$, the equation (4.56) yields $\gamma_I = -\frac{2}{3}(-1)^I \mathcal{M}_I \bar{S}\bar{d}$, where $\bar{S}$ and $\bar{d}$ are given in Eqs. (4.61) and (4.62), respectively. The width of this transition may be approximated by the electric-dipole one-photon decay rate, $\Gamma \approx \frac{4}{3}\bar{\omega}^3\bar{d}^2$. In this case, the enhancement factor (4.68) reads (in the limit $m_e \ll M_I$)

$$\epsilon_I = -\,(-1)^I\,\frac{\mu_N \bar{S}}{2 Z_I \bar{\omega}\bar{d}}\,. \tag{4.69}$$

This factor gives a large enhancement of the electric field owing to the small quantity $\bar{\omega}$ in the denominator.

The formula (4.69) is applicable only for sufficiently weak electric field, i.e., when the Rabi frequency $\Omega = \langle 0|\mathbf{d}\cdot\mathbf{E}_0|n\rangle$ satisfies the condition $\Omega \ll \Gamma$. If this condition is not met, the enhancement of the electric field is described by the non-perturbative formula (4.40). In this case, instead of Eq. (4.69) we have a more general expression for the enhancement factor

$$\epsilon_I = -\,(-1)^I\,\frac{4\mu_N \bar{\omega}^5 \bar{S}\bar{d}}{Z_I\left(8\bar{\omega}^6\bar{d}^2 + 9E_0^2\right)}\,. \tag{4.70}$$

Note that Eq. (4.70) reduces to Eq. (4.69) if $E_0 \ll \bar{\omega}^3\bar{d}$.

According to Eq. (4.41), the magnitude of the induced field, E_I, reaches its maximum at $E_0 = E_{\rm crit} \equiv \sqrt{8}\bar{\omega}^3\bar{d}/3$. The value $\epsilon_I(E_{\rm crit})$ is given by

$$\epsilon_I(E_{\rm crit}) = -(-1)^I\,\frac{\mu_N \bar{S}}{4 Z_I \bar{\omega}\bar{d}}\,, \tag{4.71}$$

and the corresponding value of E_I is

$$E_I^{\rm max} = -(-1)^I\,\frac{\mu_N \bar{\omega}^2 \bar{S}}{3\sqrt{2} Z_I}\,. \tag{4.72}$$

Note that here, for simplicity, we have assumed that Γ_n is the natural width of the state $|n\rangle$. In reality, there may be other, possibly larger, contributions to Γ_n such as Doppler width, collison width, etc. Nevertheless, as proved in Eq. (4.42), the formula (4.72) for $E_I^{\rm max}$ has the same form regardless of which Γ_n is assumed. The critical field E_0, however, depends linearly on Γ_n.

4.5.4 Numerical results

In this subsection, we present numerical estimates for the suppression and enhancement factors σ_I and ϵ_I given by Eqs. (4.59), (4.63), (4.66), (4.69) and (4.70) for various frequency regimes and different strengths of the external electric field. These estimates will be given for some simple diatomic molecules with well-studied polarizability properties: lithium hydride (LiH), sodium hydride (NaH), boron fluorine (BF) and calcium fluorine (CaF).

For our numerical estimates, we take the values of the mean electric dipole parameter $\bar{d}$ from Refs. [18–20]. The mean values of the inter-nuclear distance $\bar{S}$ for the molecules under consideration are available in the NIST database [21]. The quantity $S^{\nu_n}_{\nu_0}$ may be roughly estimated assuming that the vibrational mode is purely harmonic. The quantity $(d_0^r)^{\nu_0}_{\nu_n}$ is approximately given by $\zeta_N S^{\nu_0}_{\nu_n}$.

As noted above, the sums in Eqs. (4.63) and (4.66) contain effectively one term corresponding to $\nu_0 = 0$ and $\nu_n = 1$. The values of the parallel $\alpha_{\rm el}^{\parallel}$ and perpendicular $\alpha_{\rm el}^{\perp}$ electronic polarizabilities for the molecules under inspection are presented in Ref. [22].

For the estimates of the suppression factor σ_I we consider three frequency regimes: low-frequency regime, where the frequency of the external field is taken to be half of the first rotational frequency, $\omega = \bar{\omega}/2$; intermediate-frequency regime with $\omega = \omega_e/2$, where ω_e is the ground state vibrational constant;

electronic-transition range $\omega \approx \omega_{\rm el}$ where $\omega_{\rm el}$ is the lowest E1 electronic transition frequency. The value of ω_e may be found in the NIST database [21]) while the electronic-range frequency $\omega_{\rm el}$ is available in Ref. [22].

Recall that the index I labels the nuclei in the diatomic molecule. Without loss of generality we assume that $I = 1$ stands for the lighter nucleus while $I = 2$ for the heavier one. The values of the suppression factors of the electric field at these nuclei in different frequency regimes are presented in Table 4.1. The values of the enhancement factors ϵ_1 are given in Table 4.2 for a weak $E_0 \ll E_{\rm crit}$ and strong $E_0 = E_{\rm crit}$ external field in resonance with the first rotational level. Here $E_{\rm crit} = \sqrt{8}\bar{\omega}^3\bar{d}/3$ is a the value of the of the electric field E_0 at which the induced field E_I reaches its maxium. Incidentally, $E_{\rm crit}$ also serves as a rough marker above which the general formula (4.70) applies while under this value a simplified formula (4.69) gives sufficient accuracy.

	$\bar{S}$	$\bar{d}$	$\bar{\omega}(\times 10^{-5})$	$\omega_e(\times 10^{-3})$	ω	σ_1	σ_2
LiH	3.0	-2.3	6.9	6.4	3.4×10^{-5}	-0.17	0.06
					3.2×10^{-3}	0.70	-0.23
					0.12	0.37	0.20
NaH	3.6	-2.6	4.5	5.3	2.2×10^{-5}	-0.16	0.02
					2.7×10^{-3}	0.51	-0.05
					0.11	0.35	0.23
BF	2.4	0.4	1.4	6.4	7.0×10^{-6}	0.01	-0.004
					3.2×10^{-3}	-0.02	0.01
					0.22	0.38	0.38
CaF	3.7	1.2	0.5	2.6	2.5×10^{-6}	0.01	-0.004
					1.3×10^{-3}	-0.05	0.01
					0.075	1.4	1.3

Table 4.1: Estimates of the suppression factors for the electric field on the lighter (σ_1) and heavier (σ_2) nuclei in the molecules LiH, NaH, BF and CaF. $\bar{S}$ is the ground state mean inter-nuclear distance, $\bar{d}$ is the ground state mean electric dipole, $\bar{\omega}$ is the rigid-rotor rotational energy with angular momentum 1 and ω_e is the ground state first vibrational constant. All quantities are presented in atomic units. For the convenience of unit conversion, we recall that one atomic unit of length (Bohr) is equivalent to 0.529 Å, one atomic unit of electric dipole moment is equivalent to 0.393 Debye and one atomic unit of energy (Hartree) is equivalent to 27.21 eV or 6.58×10^6 GHz or 2.19×10^5 cm^{-1}. The suppression factors $\sigma_{1,2}$ are, of course, dimensionless.

	$E_{\rm crit}$(V/cm)	ϵ_1 ($E_0 \ll E_{\rm crit}$)	ϵ_1 ($E_0 = E_{\rm crit}$)	$E_1^{\rm max}$(V/cm)
LiH	3.7×10^{-3}	-1.5×10^7	-7.7×10^6	-2.9×10^4
NaH	1.1×10^{-3}	-2.7×10^7	-1.4×10^7	-1.5×10^4
BF	5.3×10^{-6}	5.5×10^8	2.8×10^8	1.5×10^3
CaF	7.3×10^{-7}	1.1×10^9	5.3×10^8	3.9×10^2
	$E_{\rm crit}$(V/cm)	ϵ_2 ($E_0 \ll E_{\rm crit}$)	ϵ_2 ($E_0 = E_{\rm crit}$)	$E_2^{\rm max}$(V/cm)
LiH	3.7×10^{-3}	5.1×10^6	2.6×10^6	9.5×10^3
NaH	1.1×10^{-3}	2.5×10^6	1.2×10^6	1.4×10^3
BF	5.3×10^{-6}	-3.1×10^8	-1.5×10^8	-8.2×10^2
CaF	7.3×10^{-7}	-2.7×10^8	-1.3×10^8	-9.6×10^1

Table 4.2: Estimates of the enhancement factors ϵ_1 and ϵ_2 in the molecules LiH, NaH, BF and CaF.

4.6 Screening and enhancement of electric field in polyatomic molecules

In this section, we derive the analogs of the equations (4.27) and (4.40) for the screening and resonant enhancement of alternating electric fields in polyatomic molecules.

4.6.1 The polyatomic molecule Hamiltonian in the center-of-mass frame

In this subsection we consider the Hamiltonian of a polyatomic molecule in the center-of-mass frame. This subsection contains no new results and serves mainly to specify the notation for the next subsection. For a more extensive discussion of the separation of the nuclear and electronic motions in molecules, see, for example, Ref. [23].

Consider a molecule composed of H (for "heavy") nuclei and L (for "light") electrons in an external electric field $\mathbf{E}_{\rm ext}$. The masses and charges of the nuclei will be denoted by M_I and Z_I respectively; the nuclear positions and momenta operators are $\mathbf{R}_I$ and $\mathbf{P}_I$, respectively. The electrons positions and momenta are denoted by $\mathbf{r}_i$ and $\mathbf{p}_i$, respectively. Here we use capital letters $I, J = 1, \ldots, H$ to label the nuclei, and small letters are attributed to the electrons $i, j = 1, \ldots, L$.

The Hamiltonian of a polyatomic molecule has the standard form

$$\begin{aligned} H_{\rm mol} &= K + V_0 + V\,, \\ K &= \sum_{I=1}^{H} \frac{\mathbf{P}_I^2}{2M_I} + \sum_{i=1}^{L} \frac{\mathbf{p}_i^2}{2}\,, \\ V_0 &= \sum_{I<J}^{H} \frac{Z_I Z_J}{R_{IJ}} - \sum_{I=1}^{H}\sum_{i=1}^{L} \frac{Z_I}{R_{Ii}} + \sum_{i<j}^{L} \frac{1}{r_{ij}}\,, \\ V &= -\mathbf{E}_{\rm ext}\cdot\left(\sum_{I=1}^{H} Z_I \mathbf{R}_I - \sum_{i=1}^{L} \mathbf{r}_i\right)\,, \end{aligned} \tag{4.73}$$

where $R_{IJ} = |\mathbf{R}_I - \mathbf{R}_J|$, $R_{Ij} = |\mathbf{R}_I - \mathbf{r}_j|$ and $r_{ij} = |\mathbf{r}_i - \mathbf{r}_j|$. In this Hamiltonian, we ignore all spins of particles.

Following the same steps as in the case of diatomic molecules, Sect. 4.4.1, we introduce the parameters of total nuclear mass $M_N = \sum_{I=1}^{H} M_I$ and the total nuclear charges $Z_N = \sum_{I=1}^{H} Z_I$. The total molecular mass and charge are $M_T = M_N + L$, $Z_T = Z_N - L$, respectively. Using these notation, we perform a change of variables $(\mathbf{R}_I, \mathbf{r}_i) \to (\mathbf{S}_T, \mathbf{S}_I, \mathbf{s}_i)$ similar to Eqs. (4.2):

$$\mathbf{S}_T = \sum_{J=1}^{H} U_N^{HJ} \mathbf{R}_J + \frac{1}{M_T}\sum_{i=1}^{L} \mathbf{r}_i\,, \tag{4.74a}$$

$$\mathbf{S}_I = \sum_{J=1}^{H} U_N^{IJ} \mathbf{R}_J \qquad (I = 1, \ldots H-1)\,, \tag{4.74b}$$

$$\mathbf{s}_i = \mathbf{r}_i - \frac{1}{M_N}\sum_{I=1}^{H} M_I \mathbf{R}_I\,, \tag{4.74c}$$

where U_N is an $H \times H$ invertible matrix whose bottom-row elements have the form $U_N^{HJ} = M_J/M_T$. The inverse of U_N is denoted by U_N^{-1} and has elements on the last column of the form $\left(U_N^{-1}\right)^{IH} = M_T/M_N$.

The condition $U_N^{HJ} = M_J/M_T$ means that the vector $\mathbf{S}$ in Eq. (4.74a) is the coordinates of the molecule's center of mass. The submatrix U_N^{IJ}, with $I, J = 1, \ldots, H-1$, in Eq. (4.74b) specifies the relative coordinates of the nuclei in the center-of-mass frame. Physical quantities, such as the (expectation value of) total electric field at a nucleus in the molecule, must be independent of U_N^{IJ}.

It should also be noted that the equation (4.74c) defines the coordinates of electrons $\mathbf{s}_i$ with respect to the nuclear center of mass.

The conjugated momenta for the coordinates $(\mathbf{S}_T, \mathbf{S}_I, \mathbf{s}_i)$ are denoted by $(\mathbf{Q}_T, \mathbf{Q}_I, \mathbf{q}_i)$. The original momenta $\mathbf{P}_I$ and $\mathbf{p}_i$ may be expressed in terms of the new ones

$$\mathbf{p}_i = \mathbf{q}_i + \frac{1}{M_T}\mathbf{Q}_T\,, \tag{4.75a}$$

$$\mathbf{P}_I = \sum_{J=1}^{H-1} U_N^{JI} \mathbf{Q}_J - \frac{M_I}{M_N}\sum_{i=1}^{L} \mathbf{q}_i + \frac{M_I}{M_T}\mathbf{Q}_T\,. \tag{4.75b}$$

Upon this transformation the Hamiltonian (4.73) acquires the form (4.4) with the center-of-mass

Hamiltonian H_T given by Eq. (4.5) and the relative motion Hamiltonian given by

$$H_{\rm rel} = H_0 + V_{\rm rel}\,, \tag{4.76a}$$

$$H_0 = \sum_{i=1}^{L} \frac{\mathbf{q}_i^2}{2\mu_e} + \sum_{i<j}^{L} \frac{\mathbf{q}_i \mathbf{q}_j}{M_N} + \frac{1}{2} \sum_{I,J=1}^{H-1} \left(\mu_N^{-1}\right)^{IJ} \mathbf{Q}_I \mathbf{Q}_J + V_0\,, \tag{4.76b}$$

$$V_{\rm rel} = -\mathbf{d} \cdot \mathbf{E}_{\rm ext}\,. \tag{4.76c}$$

Here μ_e is the reduced electron mass (4.7) and μ_N^{-1} is the inverse reduced nuclear mass $H \times H$-matrix with elements

$$\left(\mu_N^{-1}\right)^{IJ} = \sum_{K=1}^{H} M_K^{-1} U_N^{KI} U_N^{KJ}\,. \tag{4.77}$$

It is straightforward to show that μ_N^{-1} has the following properties

$$\begin{aligned} &\left(\mu_N^{-1}\right)^{IH} = \left(\mu_N^{-1}\right)^{HI} = 0 \qquad (I = 1, \ldots, H-1)\,, \\ &\left(\mu_N^{-1}\right)^{HH} = M_T^{-1}\,. \end{aligned} \tag{4.78}$$

The interaction potential (4.76c) involves the molecule's electric dipole moment $\mathbf{d}$ with respect to the center of mass $\mathbf{S}_T$. This EDM is described by the analog of Eq. (4.8)

$$\mathbf{d} = -\zeta_e \sum_{i=1}^{L} \mathbf{s}_i + \sum_{I=1}^{H-1} \zeta_N^I \mathbf{S}_I\,, \tag{4.79}$$

where ζ_e is the reduced electron charge (4.9) and ζ_N^I is the reduced nuclear charge

$$\zeta_N^I = \sum_{J=1}^{H} \left(U_N^{-1}\right)^{JI} Z_J \qquad (I = 1, \ldots, H-1)\,. \tag{4.80}$$

The representation (4.76) allows us to apply perturbation theory with $V_{\rm rel}$ considered as a perturbation. The unperturbed wavefunctions $|n\rangle$ are defined with respect to the Hamiltonian H_0 given in Eq. (4.76b), i.e., $H_0|n\rangle = \mathcal{E}_n|n\rangle$. The evolution of the ground state $|0\rangle$ shall be described by the wavefunction (4.21) (in the off resonance case) or (4.32). We will use these wavefunctions to find the expectation value of the operator of electric field at the $I^{\rm th}$ nucleus.

4.6.2 Off-resonance screening of an oscillating external electric field

Let us assume that the frequency ω of the oscillating electric field (4.18) is far from any molecular transition frequency ω_{n0}. When the magnitude of this field is sufficiently weak, the time-dependent perturbation theory may be applied to compute the expectation value of the operator of electric field at the $I^{\rm th}$ nucleus (4.11). This procedure is the same as presented in Sect. 4.4.3. As a result, for the electric field at $I^{\rm th}$ nucleus we arrive at the same expression (4.24)

$$\langle \mathbf{E}_I \rangle = \frac{M_I Z_T}{M_T Z_I} \mathbf{E}_0 \cos\omega t + \frac{2\omega^2 \cos\omega t}{Z_I} \sum_n \frac{\mathrm{Im}\,[\langle 0|\mathbf{\Pi}_I|n\rangle\langle n|\mathbf{d}\cdot\mathbf{E}_0|0\rangle]}{\omega_{n0}^2 - \omega^2}\,, \tag{4.81}$$

where $\mathbf{\Pi}_I$ is the truncated momentum operator of $I^{\rm th}$ nucleus. This operator is defined by the expression (4.75b) with the center-of-mass term removed, namely

$$\mathbf{\Pi}_I \equiv \mathbf{P}_I - \frac{M_I}{M_T}\mathbf{Q}_T = \sum_{J=1}^{H-1} U_N^{JI} \mathbf{Q}_J - \frac{M_I}{M_N} \sum_{i=1}^{L} \mathbf{q}_i\,. \tag{4.82}$$

Using the expressions of the Hamiltonian H_0 in Eq. (4.76b) and molecular EDM operator (4.79), it is possible to show that the operator (4.82) may be represented in the form

$$\mathbf{\Pi}_I = \frac{i M_I}{\zeta_e M_T} \left[-\mathbf{d} + \sum_{J=1}^{H-1} \mathcal{M}^{IJ} \mathbf{S}_J, H_0 \right]\,, \tag{4.83}$$

where

$$\mathcal{M}^{IJ} = \zeta_N^J - (M_N + Z_N)\left(U_N^{-1}\right)^{IJ} \tag{4.84}$$

is a generalization of the quantity $\mathcal{M}_I$ in Eq. (4.26).

Substituting Eq. (4.83) into Eq. (4.81), one finds that the electric field at I^{th} nucleus is given by the expression similar to Eq. (4.27),

$$\langle \mathbf{E}_I \rangle = \left[\frac{M_I Z_T}{M_T Z_I} - \frac{\omega^2 M_I}{\zeta_e M_T Z_I} \left(\overleftrightarrow{\boldsymbol{\alpha}} - \overleftrightarrow{\boldsymbol{\beta}}_I \right) \right] \mathbf{E}_0 \cos \omega t \,, \tag{4.85}$$

where $\overleftrightarrow{\boldsymbol{\alpha}}$ is the molecule's polarizability tensor

$$\overleftrightarrow{\boldsymbol{\alpha}} = 2 \sum_n \frac{\omega_{n0}}{\omega_{n0}^2 - \omega^2} \langle 0|\mathbf{d}|n\rangle\langle n|\mathbf{d}|0\rangle \,, \tag{4.86}$$

and $\overleftrightarrow{\boldsymbol{\beta}}_I$ is the polyatomic analog of the tensor (4.29),

$$\overleftrightarrow{\boldsymbol{\beta}}_I = 2 \sum_n \frac{\omega_{n0}}{\omega_{n0}^2 - \omega^2} \langle 0| \sum_{J=1}^{H-1} \mathcal{M}^{IJ} \mathbf{S}_J |n\rangle\langle n|\mathbf{d}|0\rangle \,. \tag{4.87}$$

We point out that the results (4.85)–(4.87) reduce to the analogous results (4.27)–(4.29) for diatomic molecules given in Sect. 4.4.3 upon the special choice of the matrix $U_N = M_T^{-1} \begin{pmatrix} M_T & -M_T \\ M_1 & M_2 \end{pmatrix}$.

It is important to note that the value of the electric field at nucleus (4.85) is independent of the choice of the matrix U_N in Eq. (4.74). To demonstrate this, it is sufficient to prove that the tensors (4.86) and (4.87) are independent of this matrix.

As follows from Eqs. (4.75b) and (4.77), the Hamiltonian (4.76b) is independent of the matrix U_N when expressed in terms of the coordinates $\mathbf{r}_i$ and $\mathbf{R}_I$ and momenta $\mathbf{p}_i$ and $\mathbf{P}_I$. Thus, the eigenstates $|n\rangle$ of this Hamiltonian are also independent of the matrix U_N when expressed in terms of the coordinates $\mathbf{r}_i$ and $\mathbf{R}_I$. Taking into account Eqs. (4.74b) and (4.80) one can easily see that the molecular EDM (4.79) is also independent of the matrix U_N in the coordinates $\mathbf{r}_i$ and $\mathbf{R}_I$. Since these coordinates are integrated out in the matrix elements in Eq. (4.86), we conclude that the molecular polarizability tensor $\overleftrightarrow{\boldsymbol{\alpha}}$ is independent of the choice of the matrix U_N.

Using Eqs. (4.74b), (4.80) and (4.84) one may check the edientity $\sum\limits_{J=1}^{H-1} \mathcal{M}^{IJ} \mathbf{S}_J = \sum\limits_{J=1}^{H} (M_J + Z_J)\,\mathbf{R}_J - (M_N + Z_N)\,\mathbf{R}_I$. Thus, the quantity $\sum\limits_{J=1}^{H-1} \mathcal{M}^{IJ} \mathbf{S}_J$ is independent of the matrix U_N in the coordinates $\mathbf{r}_i$ and $\mathbf{R}_I$. As a corollary, all matrix elements in Eq. (4.87) are independent of the matrix U_N. This completes the proof that the expression for the electric field at nucleus (4.85) is independent of the choice of the matrix U_N.

The independence of the result (4.85) on U_N means that one is free to define the relative nuclear coordinates in any convenient way. Once a particular matrix U_N is chosen, one can then solve for the states n and proceed to calculating the fields as in Eq. (4.85). The results one obtains this way will be the same as those obtained if some different U_N was chosen.

4.6.3 Resonance enhancement of an oscillating electric field

Let us now assume that the frequency of the external electric field is in resonance with one of the molecular transition frequency, $\omega = \omega_{n0}$, associated with some excited state $|n\rangle$ with width Γ_n. Theoretically, due to the resonance, the magnitude of the electric field at nucleus infinitely grows with time if one discards the spontaneous decay rate of the excited state. Physically, this field can grow only up to the lifetime of the excited state, $\tau = 1/\Gamma_n$. Therefore, the resonance enhancement of the electric field in the molecule is due to the factor $1/\Gamma_n$ which is large for lowest rotational and vibrational states. The off-resonance states, however, provide partial screening of the electric field in the same way as is described in Sect. 4.4.4. We stress that Eq. (4.36) describing the resonance enhancement of the electric field in diatomic molecules holds for polyatomic molecules as well. Indeed, the derivation of this equation is purely formal and is not limited to the diatomic case.

Since the lowest ro-vibrational states in molecules possess very large lifetime, the resonance enhancement due to the factor $1/\Gamma_n$ becomes significantly larger than the screening due to the off-resonance states. In this case, the electric field is described by the analog of Eq. (4.37)

$$\langle \mathbf{E}_I \rangle \approx \frac{\omega^2 m_e M_I}{\zeta_e e^2 Z_I M_T \Gamma_n} \overleftrightarrow{\gamma}_I \mathbf{E}_0 \sin \omega t \,, \tag{4.88}$$

where the tensor $\overleftrightarrow{\gamma}_I$ reads now

$$\overleftrightarrow{\gamma}_I = 2\langle 0|\mathbf{d}|n\rangle\langle n|\mathbf{d}|0\rangle - 2\langle 0| \sum_{J=1}^{H-1} \mathcal{M}^{IJ} \mathbf{S}_J |n\rangle\langle n|\mathbf{d}|0\rangle \,. \tag{4.89}$$

Here $\mathcal{M}^{IJ}$ is given in Eq. (4.84).

We point out that the expression (4.88) for the enhancement of the electric field at nucleus is valid for a weak external field since it is obtained in perturbation theory. The condition of the applicability of perturbation theory reads $\Omega \ll \Gamma_n$, where $\Omega = |\langle 0|\mathbf{d}\cdot\mathbf{E}_0|n\rangle|$ is the Rabi frequency. For a stronger electric field one is to apply a more general formula derived non-perturbatively in [13]:

$$\langle \mathbf{E}_I \rangle = \frac{\omega^2 m_e M_I}{\zeta_e e^2 Z_I M_T} \frac{\Gamma_n}{\Gamma_n^2 + 2\Omega^2} \overleftrightarrow{\gamma}_I \mathbf{E}_0 \sin \omega t \,. \tag{4.90}$$

This formula has the same form as in the case of diatomic molecules (4.40) except for the tensor $\overleftrightarrow{\gamma}_I$ given by Eq. (4.89). As a result, the formulae for the critical field $E_{\rm crit}$ and the maximal field $E_I^{\rm max}$ are the same as given in Eqs. (4.41) and (4.42) but with $\overleftrightarrow{\gamma}_I$ given by Eq. (4.89).

4.7 Summary and discussion

In this paper, we derived the general formulae for the screening (4.30) and resonance enhancement (4.40) of an oscillating electric field at a nucleus in a diatomic molecule.

The screening formula (4.30) applies when the frequency of external electric field is far from any transition frequency in the molecule. This formula may be considered, on the one hand, as a generalization of the screening of a static electric field in molecules [14] and, on the other hand, as an extension of the screening formula of oscillating electric field in atoms [11]. For molecules, the screening of electric field exhibits some important features. Similarly to the atomic case [11], Eq. (4.30) contains the term with dynamical polarizability $\overleftrightarrow{\boldsymbol{\alpha}}$. However, there are extra terms (described by the tensor $\overleftrightarrow{\boldsymbol{\beta}}$) in Eq. (4.30), which have no analogs in the atomic case.

To uncover the role of the new terms in Eq. (4.30), we considered the examples of some diatomic molecules in the electric field in different frequency regimes. We found that when the frequency of the electric field is of order of the frequency of ro-vibrational transitions in a molecule, the $\overleftrightarrow{\boldsymbol{\beta}}$-tensor in Eq. (4.30) gives dominant contribution to the resulting electric field at nucleus since it is enhanced by the ratio M_I/m_e. This parameter makes the screening of the low-frequency electric field in molecules very different from that in atoms.

When the frequency of the external field approaches the energies of electronic transitions, the contributions from both tensors $\overleftrightarrow{\boldsymbol{\alpha}}$ and $\overleftrightarrow{\boldsymbol{\beta}}$ become significant. Thus, the molecules exhibit different screening behaviour in different frequency ranges. The typical dependence on the frequency of different contributions to the suppression coefficient is presented at Fig. 4.1. In particular, the screening of the field in molecules in the microwave regime appears not as strong as it is in atoms [11]. The summary of suppression coefficients σ_I for some molecules in various frequency regimes is given in Table 4.1.

When the frequency of the external electric field approaches one of the transition frequency, the resonant excited state in the molecule is responsible for the linear-in-time growth of the electric field at nucleus up to the life-time of the excited state. The off-resonant states, however, provide partial screening of this electric field as is shown in Eq. (4.36). The resonance enhancement may be up to the factor 10^9 due to a small width of the state Γ, so it becomes dominating over the suppression factors as in Eq. (4.37).

The advantage molecules have over atoms is that they possess ro-vibrational states with energies in the microwave or even radio-frequency region. These states in molecules typically have very narrow spectral lines that makes the resonance enhancement of the oscillating electric field at nucleus very large.

However, we caution the readers against using the resonance enhancement formula (4.37) for the electric field at nucleus: Since this result is derived within the perturbatie approach, it is applicable only

for sufficiently weak electric field under the constraint (4.39). For a stronger electric field, one should apply the non-perturbative formula (4.40) which was derived in [13]. Physically, this formula tells us that even in the resonance one cannot produce the electric field at nucleus stronger than the Coulomb field inside the molecule. The point of the perturbative formula (4.36) is that one can take a very weak electric field in resonance with the molecular transition to produce sufficiently large oscillating electric field at nucleus. Some particular examples of such weak fields and their amplification factors ϵ_I are presented in Table 4.2.

Although our main results (4.30) and (4.40) are derived for the case of diatomic molecules, we present a generalization of these formulae to the polyatomic molecules in Sect. 4.6.

The results of this paper may have various physical applications since they represent a way out from the shielding of a static electric field at nucleus due to the Schiff theorem [4]. In particular, it would be interesting to develop a technique for measuring nuclear EDM using an oscillating electric field in resonance with molecular transition. Many diatomic molecules possess Ω-doubling of states with splitting of order of 100 MHz. Such molecules have already proved useful for measuring electron's EDM, see, e.g., [24–26]. One can apply the electric field in resonance with this transition to induce a large electric field at nucleus which may be used to measure nuclear EDM. Another use of the results of this paper may be related to application of laser beams to stimulate nuclear transitions such as the neutron capture in the ^{139}La nucleus proposed in [27–29]. These issues deserve separate studies.

Acknowledgments

This work is supported by the Australian Research Council Grant No. DP150101405 and by a Gutenberg Fellowship.

Bibliography

[1] T. Chupp, P. Fierlinger, M. Ramsey-Musolf, and J. Singh, arXiv:1710.02504 (2017).

[2] N. Yamanaka, B. K. Sahoo, N. Yoshinaga, T. Sato, K. Asahi, and B. P. Das, Eur. Phys. J. **A53**, 54 (2017).

[3] M. S. Safronova, D. Budker, D. DeMille, D. F. J. Kimball, A. Derevianko, and C. W. Clark, Rev. Mod. Phys. **90**, 025008 (2018).

[4] L. I. Schiff, Phys. Rev. **132**, 2194 (1963).

[5] P. G. H. Sandars, Phys. Rev. Lett. **19**, 1396 (1967).

[6] E. A. Hinds and P. G. H. Sandars, Phys. Rev. A **21**, 471 (1980).

[7] O. P. Sushkov, V. V. Flambaum, and I. B. Khriplovich, Zh. Exp. Teor. Fiz. **87**, 1521 (1984).

[8] V. Flambaum, I. Khriplovich, and O. Sushkov, Phys. Lett. B **162**, 213 (1985).

[9] V. Flambaum, I. Khriplovich, and O. Sushkov, Nuclear Physics A **449**, 750 (1986).

[10] V. Dzuba, V. Flambaum, P. Silvestrov, and O. Sushkov, Phys. Lett. A **118**, 177 (1986).

[11] V. V. Flambaum, Phys. Rev. A **98**, 043408 (2018).

[12] V. A. Dzuba, J. C. Berengut, J. S. M. Ginges, and V. V. Flambaum, Phys. Rev. A **98**, 043411 (2018).

[13] V. V. Flambaum and I. B. Samsonov, Phys. Rev. **A98**, 053437 (2018).

[14] V. V. Flambaum and A. Kozlov, Phys. Rev. A **85**, 022505 (2012).

[15] M. Brieger, Chem. Phys. **89**, 275 (1984).

[16] M. Mizushima et al., *Theory of rotating diatomic molecules* (Wiley, 1975).

[17] A. R. Edmonds, *Angular momentum in quantum mechanics* (Princeton university press, 2016).

[18] F. Grimaldi, A. Lecourt, and C. Moser, Symp. Faraday Soc. **2**, 59 (1968).

[19] K. A. Peterson and R. C. Woods, J. Chem. Phys. **87**, 4409 (1987).

[20] W. Childs, G. Goodman, and L. Goodman, J. Mol. Spectrosc. **115**, 215 (1986).

[21] *NIST chemistry WebBook, SRD 69* (2018).

[22] E. V. Akindinova, V. E. Chernov, I. Y. Kretinin, and B. A. Zon, Phys. Rev. A **81**, 042517 (2010).

[23] B. Sutcliffe (Wiley-Blackwell, 2007), pp. 1–121, ISBN 9780470141731.

[24] J. Baron et al. (ACME), Science **343**, 269 (2014).

[25] S. Eckel, P. Hamilton, E. Kirilov, H. W. Smith, and D. DeMille, Phys. Rev. A **87**, 052130 (2013).

[26] S. Bickman, P. Hamilton, Y. Jiang, and D. DeMille, Phys. Rev. A **80**, 023418 (2009).

[27] D. Zaretskii and V. Lomonosov, Pis'ma Zh. Eksp. Teor. Fiz. **30**, 541 (1979).

[28] D. Zaretskii and V. Lomonosov, Zh. Eksp. Teor. Fiz. **81**, 429 (1981).

[29] A. Y. Dzyublik, Zh. Eksp. Teor. Fiz. **102**, 120 (1992).

Chapter 5

Oscillating nuclear electric dipole moment induced by axion dark matter produces atomic and molecular EDMs and nuclear spin rotation

5.1 Overview

Schiff's theorem states that a static nuclear EDM does not induce atomic or molecular EDM. In this chapter, I demonstrate that an oscillating nuclear EDM does produce measurable atomic and molecular EDMs. Moreover, if one applies an oscillating electric field whose frequency matches that of the oscillating nuclear EDM then nuclear spin precession happens. By manipulating the atomic or molecular spectrum so that a level is on resonance with both the field and the nuclear EDM, the effect may be further enhanced. The nuclear spin precession may reach 10^{-6} radian per second. In terms of energy, this is about five orders of magnitude larger than the energy typically measured in the ^{199}Hg experiment.

These results are published in the following paper:

1. V. V. Flambaum and H. B. Tran Tan, **Oscillating nuclear electric dipole moment induced by axion dark matter produces atomic and molecular EDM**, Phys. Rev. D 100, 111301(R) (2019), DOI: 10.1103/PhysRevD.100.111301, arXiv:1904.07609,

which I presented at one international conference, one international workshop and one national competition:

1. **Searching for Axions and Axionic Dark Matter with Interference and Axion-induced Nuclear Moments**, TeV Particle Astrophysics Conference, University of Sydney, Sydney, Australia, December 2019,

2. **Screening and Enhancement of Nuclear Electric Dipole Moments Induced by Axionic Dark Matter**, Frontiers in Quantum Matter Workshop: Electric Dipole Moments, Australian National University, Canberra, Australia, November 2019,

3. **Effects of Dark Matter in atomic and molecular phenomena**, Australian Institute of Physics Postgraduate Presentation Competition, University of Technology Sydney, Sydney, Australia, October 2019.

5.2 Abstract

According to the Schiff theorem, a static nuclear electric dipole moment (EDM) does not produce atomic and molecular EDMs. However, interaction with the axion dark matter field generates nuclear

EDMs $\mathbf{d}_N = \mathbf{d}_N^0 \cos(\omega t)$ which oscillate with the frequency $\omega = m_a c^2/\hbar$. These oscillating nuclear EDMs generate atomic and molecular EDMs proportional to ω^2. The resulting atomic and molecular EDMs do not, however, lead to nuclear spin rotation in constant external electric fields. On the other hand, an oscillating electric field penetrates atoms and molecules and can interact with nuclear EDMs. Moreover, if the nuclear EDM oscillation frequency is in resonance with the external field, nuclear spin rotation happens, with the rotation angle growing linearly with time.

5.3 Introduction

It was suggested in Ref. [1] that interaction with the axionic dark matter produces oscillating neutron and thus oscillating nuclear electric dipole moments (EDMs). We show that such oscillating EDMs will not be limited by the Schiff theorem [2] and will produce oscillating atomic and molecular EDMs calculated below. However, a constant electric field does not penetrate to the nucleus so there is no interaction with the nuclear EDM, i.e., there will be no nuclear spin rotation for both static and oscillating nuclear EDMs.

Observable atomic and molecular EDMs are actually produced by the nuclear Schiff moment which is suppressed compared to EDM by an additional second power of the nuclear radius which is very small on the atomic scale [3–7] (see also [8–14] for other effects producing atomic and molecular EDM). The effects produced by the axion-induced Schiff moment have been considered in Ref. [15]. A corresponding experiment in solids has been proposed in Ref. [16]. The first results of the oscillating neutron EDM and Hg atom's EDM measurements are presented in Ref. [17] where the limits on the low-mass axion interaction constant with matter have been improved up to three orders of magnitude.

In this paper, we consider the situation when both the nuclear EDM and the external field are oscillating. In such cases, the external field penetrates to the atomic and molecular nucleus [18–20] and can interact with the nuclear EDM. We demonstrate that in the case where the frequency of the external field matches the frequency of the nuclear EDM oscillation, nuclear spin rotation happens with the rotation angle growing linearly with time. This effect is, in principle, observable.

We will also present the result for the atomic and molecular EDMs induced by nuclear EDMs. It will be observed that the molecular EDM is larger than its atomic counterpart, due to the fact that nuclei move much slower than electrons so their screening effect is much weaker. As a result, the residual, partly screened EDMs in molecules are M_N/m_e times larger than those in atoms. Here M_N is the nuclear mass and m_e is the electron mass. Additional M_N/m_e appears due to the small energy intervals between rotational states in molecule.

5.4 Screening theorem for time-dependent electric fields and EDMs

As known, a nucleus in a neutral system (atom or molecule) is completely screened from a constant electric field [2]. We will here present a derivation of this fact following the Appendix in Ref. [21]. For definiteness, we assume that the system in question is a neutral atom in a static homogeneous external electric field of an arbitrary strength (we ignore the possibility of atomic ionization and effects of magnetic fields).

The Hamiltonian of an atom placed in a static homogeneous external electric field $\mathbf{E}_0$ is

$$H = \sum_i \left[K_i - e\phi_0\left(\mathbf{r}_i\right) + e\mathbf{r}_i \cdot \mathbf{E}_0\right] + \sum_{i>j} \frac{e^2}{|\mathbf{r}_i - \mathbf{r}_j|} - \mathbf{d} \cdot \mathbf{E}_0, \tag{5.1}$$

where K_i and $\mathbf{r}_i$ are the kinetic energy and coordinates of the electrons, $\mathbf{d}$ is the static nuclear EDM and $\phi_0\left(\mathbf{r}_i\right)$ is the electrostatic nuclear potential given by

$$\phi_0\left(\mathbf{r}_i\right) = e\int \frac{\rho\left(\mathbf{r}\right) d^3\mathbf{r}}{|\mathbf{r}_i - \mathbf{r}|}, \tag{5.2}$$

where ρ is the nuclear charge distribution. We consider here the case of an infinitely heavy nucleus. The nuclear recoil correction is not enough to generate an atomic EDM [2].

We add to H an auxiliary term

$$V = \mathbf{d} \cdot \mathbf{E}_0 - \frac{1}{Ze} \sum_i \mathbf{d} \cdot \nabla_i \phi_0\left(\mathbf{r}_i\right), \tag{5.3}$$

which, in the linear approximation in $\mathbf{d}$, does not produce any energy shift, $\langle V\rangle = 0$. Indeed, we have

$$\frac{i}{m}\left[\sum_i \mathbf{p}_i, H\right] = -e\sum_i \nabla_i\phi_0\left(\mathbf{r}_i\right) + Ze\mathbf{E}_0, \tag{5.4}$$

where we have taken into account the fact that the total electron momentum $\sum_i \mathbf{p}_i$ commutes with the electron-electron interaction term. Using Eq. (5.3) and the fact that

$$\frac{i}{m}\langle\psi|\left[\sum_i \mathbf{p}_i, H\right]|\psi\rangle \propto \left(E_\psi - E_\psi\right) = 0 \tag{5.5}$$

(ψ is the wavefunction of the Hamiltonian H), we obtain

$$\langle V\rangle = \left\langle \mathbf{d}\cdot\mathbf{E}_0 - \frac{1}{Ze}\sum_i \mathbf{d}\cdot\nabla_i\phi_0\left(\mathbf{r}_i\right)\right\rangle = 0. \tag{5.6}$$

To find an EDM one needs to measure a linear energy shift in an external electric field. Since V does not contribute to this shift we can add it to the Hamiltonian

$$\tilde{H} \equiv H + V = \sum_i \left[K_i - e\phi\left(\mathbf{r}_i\right) + e\mathbf{r}_i\cdot\mathbf{E}_0\right] + \sum_{i>j}\frac{e^2}{|\mathbf{r}_i - \mathbf{r}_j|}, \tag{5.7}$$

where

$$\phi\left(\mathbf{r}_i\right) = \phi_0\left(\mathbf{r}_i\right) + \frac{1}{Ze}\mathbf{d}\cdot\nabla_i\phi_0\left(\mathbf{r}_i\right). \tag{5.8}$$

Note that the Hamiltonian $\tilde{H}$ does not contain the direct interaction $\mathbf{d}\cdot\mathbf{E}_0$ between the nuclear EDM and external field (Schiff theorem). The dipole term is also canceled out in the multipole expansion of $\phi\left(\mathbf{r}_i\right)$.

Let us now consider the case where the nuclear EDM is time-dependent $\mathbf{d} = \mathbf{d}\left(t\right)$. In this case, Eq. (5.5) becomes

$$\frac{i}{m}\left\langle\left[\sum_i \mathbf{p}_i, H\right]\right\rangle = -\frac{1}{m}\frac{d}{dt}\left\langle\sum_i \mathbf{p}_i\right\rangle = \frac{1}{m}\frac{d\left\langle\mathbf{p}_{\rm nuc}\right\rangle}{dt} \propto \mathbf{d}\,. \tag{5.9}$$

Therefore, the contribution due to $\langle V\rangle$ is zero in the first order in $\mathbf{d}$. As a result, just as in the case of a static nuclear EDM, there is no direct interaction between a time-dependent nuclear EDM and a static external electric field, hence, no nuclear spin rotation. Indeed, the external electric field does not penetrate to the nucleus (since an atom and its nucleus are not accelerated by a static homogeneous electric field), so the nuclear EDM has nothing to interact with.

Now consider the case of a time-dependent electric field. In this case, we have

$$\frac{1}{m}\frac{d\left\langle\mathbf{p}_{\rm nuc}\right\rangle}{dt} \propto \mathbf{E}_0\,, \tag{5.10}$$

since the external field now penetrates to the nucleus [18–20]. Indeed, the external electric field forces the electron shells to oscillate and since the atom's center of mass stays at rest, the nucleus must move, so the electric field on it is not zero. Therefore, the nuclear EDM interacts with this electric field and nuclear spin rotation happens.

Note that the absence of nuclear spin rotation in the case of a static electric field does not mean that the oscillating nuclear EDM does not produce any effect. An oscillating nuclear EDM excites the electrons and produces atomic and molecular EDMs (as demonstrated below). This effect is particularly clear in the case where the nuclear EDM's frequency of oscillation is in resonance with some atomic or molecular frequency, in which case the electronic wavefunciton is a linear combination of two states of opposite parities and thus gives rise to oscillating atomic and molecular EDMs. Oscilalting nuclear EDMs may also be detected using the atomic and molecular transitions they induced, as investigated in Refs. [22–24].

The case where both the nuclear EDM and the external electric field are time-dependent, particularly when they are oscillating, is of special interest. As demonstrated in Refs. [18–20], an external electric field which oscillates with a frequency Ω, $\mathbf{E}_0 \sim \cos\Omega t$, induces an electric field on the nucleus which oscillates with the same frequency. The interaction of this field with a nuclear EDM which itself oscillates with a frequency ω, $\mathbf{d}_N \sim \cos\omega t$, is proportional to $\cos\omega t\cos\Omega t$. If $\omega = \Omega$ then this interaction contains a time-independent component and the nuclear spin rotation angle grows linearly with time (see below).

5.5 Nuclear EDMs produced by the axion dark matter field

It has been noted in Ref. [25] that the neutron EDM may be produced by the QCD θ term. Numerous references and recent results for the neutron and proton EDMs are summarised in Ref. [26]:

$$\begin{aligned} d_n &= -(2.7 \pm 1.2) \times 10^{-16} \theta \, e \, \mathrm{cm} \,, \\ d_p &= (2.1 \pm 1.2) \times 10^{-16} \theta \, e \, \mathrm{cm} \,. \end{aligned} \tag{5.11}$$

Calculations of the nuclear EDM produced by the P,T-odd nuclear forces have been performed in the Refs. [5–7, 27]. For a general estimate of the nuclear EDM it is convenient to use a single-valence-nucleon formula from Ref. [5] and express the result in terms of θ following Ref. [28]:

$$d \approx e \left(q - \frac{Z}{A} \right) (1 - 2q) \, \xi \, \langle \sigma \rangle \,, \tag{5.12}$$

where $\xi = 7 \times 10^{-16} \theta \mathrm{cm}$.

Here $q = 1$ for the valence proton, $q = 0$ for the valence neutron, the nuclear spin matrix element $\langle \sigma \rangle = 1$ if $I = l + 1/2$ and $\langle \sigma \rangle = -I/(I+1)$ if $I = l - 1/2$. Here, I and l are the total and orbital momenta of the valence nucleon.

It was noted in Ref. [1] that the axion dark matter field may be an oscillating θ term and thus generates the oscillating neutron EDM. To reproduce the density of dark matter, following Ref. [15], we may substitute $\theta(t) = \theta_0 \cos(\omega t)$ where $\theta_0 = 4 \times 10^{-18}$, $\omega = m_a c^2/\hbar$ and m_a is the axion mass.

5.6 Evolution of an osclillating nuclear EDM in an oscillating electric field

In this section, we investigate the behavior of an oscillating nuclear EDM $\mathbf{d}_N \cos \omega t$ when an oscillating external electric field $\mathbf{E}_0 \cos \Omega t$ is applied to an atom. It was shown in Refs. [18–20] that the field $\mathbf{E}_0 \cos \Omega t$ induces on the nucleus an electric field of frequency Ω and amplitude

$$\mathbf{E}_N^{\mathrm{off-res}} = -\frac{\Omega^2 m_e \alpha(\Omega)}{Z e^2 \hbar^2} \mathbf{E}_0 \,, \tag{5.13}$$

where α is the atomic polarizabiliy.

This result applies in the case where Ω is far away from any atomic transition frequency. In the case where Ω matches the transition frequency ω_{n0} from the ground state $|0\rangle$ to some state $|n\rangle$, $\mathbf{E}_N$ is resonantly enhanced

$$\mathbf{E}_N^{\mathrm{on-res}} = -\frac{2 m_e}{\hbar e^2 Z} \frac{\Omega^2}{\Gamma} \left| \langle 0 | \, D_z \, | n \rangle \right|^2 \mathbf{E}_0 \,, \tag{5.14}$$

where Γ is the width of the state $|n\rangle$ and D_z is the atom's electric dipole operator. Typically, $\Gamma \ll \omega_{n0} = \Omega$ so $E_N^{\mathrm{off-res}} \ll E_N^{\mathrm{on-res}}$.

In any case, the interaction of the nuclear EDM $\mathbf{d}_N \cos \omega t$ with the field $\mathbf{E}_N \cos \Omega t$ may be written as

$$V = -\mathbf{d}_N \cdot \mathbf{E}_N \cos \Omega t \cos \omega t = -\frac{\mathbf{d}_N \cdot \mathbf{E}_N}{2} \cos(\Omega + \omega) t - \frac{\mathbf{d}_N \cdot \mathbf{E}_N}{2} \cos(\Omega - \omega) t \,. \tag{5.15}$$

The evolution of the nuclear spin $\mathbf{I}$ under the influence of this interaction (without magnetic fields) is

$$\langle \mathbf{I} \rangle = \langle \mathbf{I} \rangle_0 + d_N \, \mathrm{Im} \, \langle \mathbf{I} \, [\mathbf{I} \cdot \mathbf{E}_N] \rangle_0 \frac{\sin(\Omega + \omega) t}{\Omega + \omega} + d_N \, \mathrm{Im} \, \langle \mathbf{I} \, [\mathbf{I} \cdot \mathbf{E}_N] \rangle_0 \frac{\sin(\Omega - \omega) t}{\Omega - \omega} \,, \tag{5.16}$$

where $\langle . \rangle_0$ means the expectation value with respect to the original state of the nuclear spin.

If $\Omega, \omega \neq 0$ then the second term in Eq. (5.16) is sinusoidal and thus averages to zero. However, in the case where $\omega = \Omega$, the third term in Eq. (5.16) is proportional to t.

If we assume that the nucleus carries spin 1/2, which initially points in the x-direction and that $\mathbf{E}_0 = E_0 \hat{\mathbf{z}}$ then in the case where $\Omega = \omega$, Eq. (5.16) reads (neglecting the oscillating term)

$$\langle \mathbf{I} \rangle = \frac{1}{2} \hat{\mathbf{x}} - \frac{1}{4} d_N E_N t \hat{\mathbf{y}} \,, \tag{5.17}$$

which shows that $\mathbf{I}$ starts to rotate in the xy-plane and the rotation angle is $\theta \sim d_N E_N t/2$. In fact, since the result (5.16) was obtained using perturbation theory, it only holds, in the case where $\Omega = \omega$, if t is small. For large t, we should write (neglecting the oscillating term)

$$\langle \mathbf{I} \rangle = \frac{1}{2} \cos \frac{d_N E_N t}{2} \hat{\mathbf{x}} - \frac{1}{2} \sin \frac{d_N E_N t}{2} \hat{\mathbf{y}} \,. \tag{5.18}$$

Note that E_N in Eq. (5.18) may take the off-resonance value (5.13) or the resonance value (5.14). The latter is of particular interest since in that case E_N is enhanced by several orders of magnitude. This situation requires $\Omega = \omega = \omega_{n0}$. When such 'double resonance' condition is met, nuclear spin rotation may be much more significant.

Note that although the analysis of this section was performed for an atom, the same conclusion holds if a molecule was considered. In fact, molecules have several advantages over atoms. In molecules, nuclei also participate in the screening of an external electric field and since nuclei move much slower than electrons, their screening effect of an oscillating electric field is weaken. As a result, the induced field on a molecular nucleus is enhanced by a factor of $M_N/m_e \lesssim 10^5$ in comparison with the field on an atomic nucleus. A further enhancement to the field on a molecular nucleus comes from the small energy intervals between rotational levels in molecules which appear in the denominator [20]. Finally, since molecules have rich spectra with small energy intervals which are in the expected range of axion mass, the 'double resonance' condition may be more easily satisfied in molecules than in atoms. Achieving this entails tuning the energy interval between the states $|0\rangle$ and $|n\rangle$ (using Stark and Zeeman shifts) and the frequency of the external electric field to match the nuclear EDM oscillation frequency.

5.7 Oscillating atomic EDMs induced by oscillating nuclear EDMs

As remarked earlier, an oscillating nuclear EDM $\mathbf{d}_N \cos \omega t$ induces oscillating atomic EDMs. In this section, we provide the calculation for the atomic EDM induced by a nuclear EDM.

The Hamiltonian of an atom in the field of an oscillating nuclear EDM $\mathbf{d} = \mathbf{d}_0 \cos(\omega t)$ may be written as

$$V = e \sum_{k=1}^{N_e} \frac{\mathbf{d} \cdot \mathbf{r}_k}{r_k^3} = \frac{i}{Ze\hbar} [\mathbf{P} \cdot \mathbf{d}, H_0] \,, \tag{5.19}$$

where H_0 is the Schrödinger or the Dirac Hamiltonian for the atomic electrons in the absence of $\mathbf{d}$, N_e is the number of electrons, Ze is the nuclear charge, $Z_i = Z - N_e$, $-e$ is the electron charge, r_k is the electron position relative to the nucleus, $\mathbf{P} = \sum_{k=1}^{N_e} \mathbf{p_k}$ is the total momentum of all atomic electrons (which commutes with the electron-electron interaction but not with the nuclear-elect interaction $U = -\sum_{k=1}^{N_e} Ze^2/r_k$: $[\mathbf{P}, H_0] = [\mathbf{P}, U] = -i\hbar Ze^2 \sum_{k=1}^{N_e} \nabla \frac{1}{r_k}$). Here we assumed that the nuclear mass is infinite and neglect very small effects of the Breit and magnetic interactions.

Using $H_0 |n\rangle = E_n |n\rangle$ we obtain the matrix element of V between atomic states $|n\rangle$ and $|m\rangle$

$$\langle n| V |m\rangle = \frac{iE_{nm}}{Ze\hbar} \langle n| \mathbf{P} \cdot \mathbf{d} |m\rangle \,, \tag{5.20}$$

where $E_{nm} = E_n - E_m$.

Using the time dependent perturbation theory [29] for the oscillating perturbation $V = V_0 \cos \omega t$ and Eq. (5.20) we obtain a formula for the induced atomic EDM

$$\mathbf{D}_{\rm ind} = 2 \sum_n \frac{E_{0n} \mathrm{Re} \left(\langle 0| V |n\rangle \langle n| \mathbf{D} |0\rangle \right)}{E_{0n}^2 - \epsilon^2} = \frac{2}{Ze\hbar} \sum_n \frac{E_{0n}^2 \mathrm{Im} \left(\langle 0| \mathbf{P} \cdot \mathbf{d} |n\rangle \langle n| \mathbf{D} |0\rangle \right)}{E_{0n}^2 - \epsilon^2} \,, \tag{5.21}$$

where $\epsilon = \hbar\omega$ and $\mathbf{D} = -e \sum_{k=1}^{N_e} \mathbf{r_k}$.

The energy dependent factor may be presented as

$$\frac{E_{0n}^2}{E_{0n}^2 - \epsilon^2} = 1 + \frac{\epsilon^2}{E_{0n}^2 - \epsilon^2} \,. \tag{5.22}$$

The energy independent term 1 on the right hand side allows us to sum over states $|n\rangle$ in Eq. (5.21). Using the closure condition and the commutator relation $[\mathbf{P}, \mathbf{D}] = -ie\hbar N_e$, this term gives

$$\mathbf{D}_{\rm atom} = \mathbf{d} + \mathbf{D}_{\rm ind} = \frac{Z_i}{Z} \mathbf{d} + \frac{2}{Ze\hbar} \sum_n \frac{\epsilon^2 \mathrm{Im} \left(\langle 0| \mathbf{P} \cdot \mathbf{d} |n\rangle \langle n| \mathbf{D} |0\rangle \right)}{E_{0n}^2 - \epsilon^2} \,. \tag{5.23}$$

We observe that, in agreement with the Schiff theorem, the atomic electric dipole moment $\mathbf{D}_{\rm atom}$ vanishes in a neutral atom ($Z_i = Z - N_e = 0$) with static nuclear EDM ($\epsilon = \hbar\omega = 0$).

Assume that nuclear EDM d is directed along the z-axis. Using the non-relativistic commutator relation $\mathbf{P} = -\frac{im_e}{e\hbar}[H_0, \mathbf{D}]$ (where m_e is the electron mass), we can express the atomic EDM in terms of the atomic dynamical polarisability $\alpha_{zz}(\omega)$

$$D^z_{\rm atom} = \frac{d_z}{Z}\left(Z_i - \frac{m_e\epsilon^2\alpha_{zz}}{e^2\hbar^2}\right), \quad \alpha_{zz} = 2\sum_n \frac{E_{n0}\left|\langle 0|\, D_z\, |n\rangle\right|^2}{E_{n0}^2 - \epsilon^2}\,. \tag{5.24}$$

The axion field oscillation frequency may be very small on the atomic scale, therefore, we may use static polarisabilities in this expression which are known for all atoms. The formula (5.24) may be rewritten, with the energy and the polarizabilty expressed in atomic units $\tilde\epsilon = \frac{\epsilon}{e^2/a_B}$ and $\tilde\alpha_{zz} = \frac{\alpha_{zz}}{a_B^3}$ (where a_B is the Bohr radius), as:

$$D^z_{\rm atom} = \frac{Z_i - \tilde\epsilon^2\tilde\alpha_{zz}}{Z} d_z \tag{5.25}$$

Since the atomic EDM $D_{\rm atom}$ is proportional to $1/Z$, it appears that the shielding is stronger in heavy atoms. This, however, is not necessary the case since, for example in hydrogen and helium $\tilde\alpha_{zz} \sim 1$ whereas $\tilde\alpha_{zz} \sim 400$ in caesium (Z=55). Indeed, the numerical value of the polarizability $\tilde\alpha_{zz}$ in atomic units often exceeds the value of the nuclear charge Z, therefore, the suppression of EDM in a neutral atom mainly comes from the small frequency of the dark matter field oscillations in atomic units, $\tilde\epsilon$.

5.8 Oscillating molecular EDMs induced by oscillating nuclear EDMs

We see from the first line in Eq. (5.24) that the residual EDM in a neutral system ($Z_i = 0$) is proportional to the mass m of the particle which produces the screening of the nuclear EDM $\mathbf{d}$. Masses of nuclei M_N in a molecule are up to 5 orders of magnitude larger than the mass of electron m_e. In addition, the interval between molecular rotational energy levels ($\sim m_e/M_N$ atomic units) are many orders of magnitude smaller than typical energy intervals in atoms and this may give an additional enormous advantage, see the denominator in the second line in Eq. (5.24). Finally, since the molecular spectra are very rich, the energy intervals are small and may be tuned by electric and magnetic fields, it is easier to bring them into resonance with the small oscillation frequency of the axion dark matter field.

Calculations presented in the Supplemental Material give the following results for the induced electric dipole of a neutral diatomic molecule when ϵ is smaller or of the order of the first rotational energy $E_{\rm rot}$

$$\mathbf{D}^{\rm EDM}_{\rm mol} \approx \frac{2\mu_N \bar X \bar d E_{\rm rot}}{3e\hbar^2}\frac{\epsilon^2}{E_{\rm rot}^2 - \epsilon^2}\left(\frac{\mathbf{d}_1}{Z_1} - \frac{\mathbf{d}_2}{Z_2}\right), \tag{5.26}$$

where $\mu_N = M_1M_2/(M_1+M_2)$ is the reduced nuclear mass, $\bar X$ is the ground state inter-nuclear distance, $\bar d$ is the ground state intrinsic electric dipole of a polar molecule and $E_{\rm rot} \approx \hbar^2\mu_N^{-1}\bar X^{-2}$ is the energy of the first rotational state and $\mathbf{d}_{1,2}$ are the nuclear EDMs. In writing Eq. (5.26), we have assumed that the molecular ground state has total angular momentum 0.

For $d_1 \sim d_2$, we see that the lighter nucleus gives dominating contribution. In other words, if $Z_1 \ll Z_2$ then the term $\mathbf{d}_2/Z_2$ drops out. We assume this is the case. In the limits $\epsilon \ll E_{\rm rot}$ and $\epsilon \gg E_{\rm rot}$, Eq. (5.26) gives

$$\frac{\mathbf{D}^{\rm EDM}_{\rm mol}}{\mathbf{d}_1} \approx \begin{cases} \frac{2\epsilon^2\mu_N^2\bar X^3\bar d}{3e\hbar^4 Z_1} & \epsilon \ll E_{\rm rot}\,, \\ \frac{2\bar d}{3eZ_1\bar X} & \epsilon \gg E_{\rm rot}\,. \end{cases} \tag{5.27}$$

We see that in the small axion mass limit ($\epsilon = m_ac^2 \ll E_{\rm rot}$), heavy molecules have an advantage (μ_N^2/Z_1). In the large axion mass limit ($\epsilon = m_ac^2 \gg E_{\rm rot}$), the ratio of the EDMs is independent of ϵ and has asymptotic value $2\bar d/\left(3eZ_1\bar X\right) < 2/\left(3Z_1\right) \le 2/3$ ($\bar d \sim e\bar X$ for polar molecule) so molecules with at least one light nucleus are more advantageous.

The result (5.26) applies for the off-resonance case. If $\epsilon = E_{\rm rot}$ then we have the following relation between the oscillation amplitudes of $\mathbf{D}^{\rm EDM}_{\rm mol}$ and $\mathbf{d}_1$;

$$D^{\rm EDM}_{\rm mol} \approx \frac{2\bar d}{3eZ_1\bar X}\frac{E_{\rm rot}}{\Gamma} d_1\,, \tag{5.28}$$

which is the large axion mass asymtotic value in Eq. (5.27) multiplied by the resonace enhancement factor $E_{\rm rot}/\Gamma$ where Γ is the width. Again, we see that molecules with at least one light nucleus give bigger effect.

There may be different contributions to Γ: natural width (which is typically small), Doppler width, collision width and time of flight (if the experiment is done with molecular beam). If, however, the experiment uses a trapped molecule then Γ is mainly due to the velocity distribution of the axion: $\Gamma/E_{\rm rot} \approx \langle v\rangle^2/c^2 \sim 10^{-6}$ where $\langle v\rangle$ is the mean axion velocity.

We remark that some molecules have $^3\Delta_1$ as their ground or metastable state and thus have doublets of opposite parities and very small energy gaps (which may be manipulated by external electric and magnetic fields to scan for resonance with the axionic dark matter field). Accordingly, if the axion mass ϵ is of the order of these doublet splittings, the coefficient 2/3 in the results (5.26)–(5.28) should be replaced by 1/2 and the first rotational energy $E_{\rm rot}$ by the energy $E_{\rm dbt}$ of the $^3\Delta_1$ doublet splitting. Examples of this type will be presented in Table. 5.1.

In Figs. 5.1 and 5.2 below, we show the behavior of $D^{\rm EDM}_{\rm mol}/d_1$ in LiF and TlF (the solid lines). For comparison, we also presented the ratio $D^{\rm EDM}_{\rm mol}/D^{\rm SCHIFF}_{\rm mol}$ between the molecular EDM induced by a nuclear EDM with that induced by a nuclear Schiff moment. The large ϵ asymptotic value and resonance value of $D^{\rm EDM}_{\rm mol}/d_1$ and the position of the first resonances (rotation or doublet) in some example molecules are summarized in Table. 5.1. Note that we have assumed that $E_{\rm rot,dbt}/\Gamma \approx 10^6$ (trapped molecule, Γ is due to axion velocity distribution).

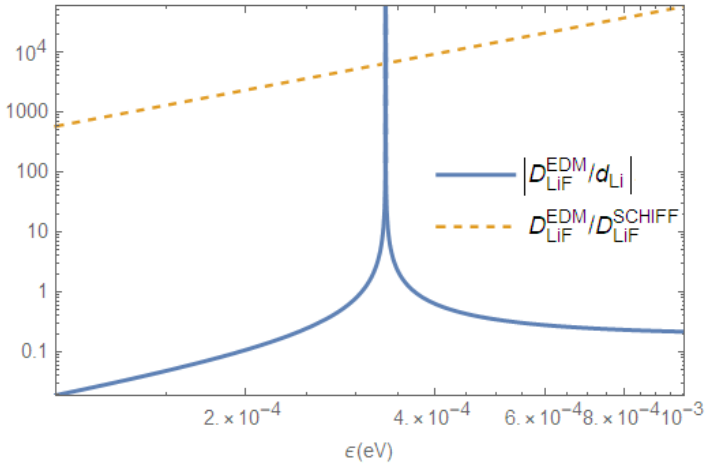

Figure 5.1: Ratios of molecular EDM induced by nuclear EDM with the nuclear EDM and with the molecular EDM induced by nuclear Schiff moment in LiF.

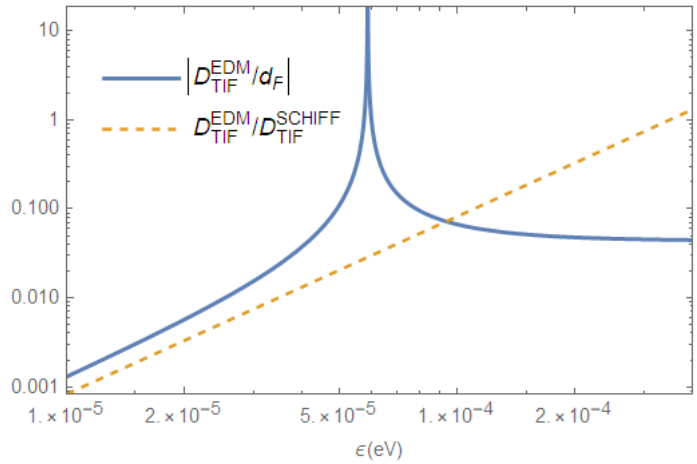

Figure 5.2: Ratios of molecular EDM induced by nuclear EDM with the nuclear EDM and with the molecular EDM induced by nuclear Schiff moment in TlF.

	Resonance position (eV)	Large ω value	Resonance value
HF ($^1\Sigma^+$)	5.2×10^{-3}	0.8	8×10^5
LiF ($^1\Sigma^+$)	3.4×10^{-4}	0.2	2×10^5
YbF ($^2\Sigma^+$)	6.0×10^{-5}	0.04	4×10^4
BaF ($^2\Sigma^+$)	5.3×10^{-5}	0.02	2×10^4
TlF ($^1\Sigma^+$)	5.6×10^{-5}	0.06	6×10^4
HfF$^+$ ($^1\Sigma^+$)	7.5×10^{-5}	0.04	4×10^4
HfF$^+$ ($^3\Delta_1$)	4.1×10^{-11}	0.06	6×10^4
ThF$^+$ ($^1\Sigma^+$)	5.8×10^{-5}	0.04	4×10^4
ThF$^+$ ($^3\Delta_1$)	2.9×10^{-10}	0.06	6×10^4
ThO ($^1\Sigma^+$)	7.6×10^{-5}	0.03	3×10^4
ThO ($^3\Delta_1$)	7.7×10^{-10}	0.05	5×10^4
WC ($^3\Delta_1$)	4.1×10^{-12}	0.08	8×10^4

Table 5.1: Position of the resonance(rotational or Ω-doublet), large axion mass asymptotic and resonance values of the ratio $\left|D_{\rm mol}^{EDM}/d_1\right|$ between the magnitude of the molecular EDM induced by the oscillating nuclear EDM $\mathbf{d}_1$ and d_1 in several molecules.

5.9 Conclusion

We have presented in this paper the possibility of observing axion-induced oscillating nuclear EDMs with oscillating external electric fields. We found that if the frequencies of the external field and the nuclear EDM are the same then nuclear spin rotation appears with the rotation angle growing linearly with time. Moreover, if the two frequencies also equal some transition frequency in atoms or molecules then the effect is resonantly enhanced. We also presented the atomic and molecular EDMs induced by oscillating EDMs. Although these quantities do exist as expectation values of electric dipole operators, they do not produce nuclear spin rotation in a constant external electric field.

On the other hand, if the electric field is oscillating but the nuclear EDM is constant then there is nuclear spin rotation about the direction of the electric field. However, in this case, atomic and molecular EDMs remain zero since, in accordance with Schiff theorem, a static nuclear EDM is completely shielded by electrons. Nevertheless, the rotation of the nuclear spin is observable because the nucleus carries a magnetic moment which produces a rotating magnetic field.

Acknowledgment

This work is supported by the Australian Research Council, Gutenberg Fellowship and New Zealand Institute for Advanced Study. We thank Igor Samsonov and Oleg Sushkov for helpful discussions.

Bibliography

[1] P. W. Graham and S. Rajendran, Phys. Rev. D **84**, 055013 (2011).

[2] L. I. Schiff, Phys. Rev. **132**, 2194 (1963).

[3] P. G. H. Sandars, Phys. Rev. Lett. **19**, 1396 (1967).

[4] E. A. Hinds and P. G. H. Sandars, Phys. Rev. A **21**, 471 (1980).

[5] O. P. Sushkov, V. V. Flambaum and I. B. Khriplovich. Zh. Exp. Teor. Fiz. **87**, 1521 (1984) [Sov. JETP **60**, 873 (1984)].

[6] V. V. Flambaum, I. B. Khriplovich and O. P. Sushkov, Phys. Lett. B **162**, 213 (1985).

[7] V. V. Flambaum, I.B. Khriplovich and O. P. Sushkov. Nucl. Phys. A **449**, 750 (1986).

[8] I. B. Khriplovich, *Parity Nonconservation in Atomic Phenomena* (Gordon & Breach, Amsterdam, 1991).

[9] N. Auerbach, V. V. Flambaum, and V. Spevak, Phys. Rev. Lett. **76**, 4316 (1996).

[10] S. G. Porsev, J. S. M. Ginges, and V. V. Flambaum, Phys. Rev. A **83**, 042507 (2011).

[11] V. V. Flambaum and A. Kozlov Phys. Rev. A **85**, 022505 (2012).

[12] P. G. H. Sandars, Phys. Lett. **14**, 194 (1965).

[13] V. V. Flambaum. Yad. Fiz. **24** , 383 (1976) [Sov. J. Nucl. Phys. **24**, 199 (1976)].

[14] O. P. Sushkov and V. V. Flambaum, Zh. Exp. Teor. Fiz. **75**, 1208, (1978) [Sov. JETP **48**, 608 (1978)].

[15] Y. V. Stadnik and V. V. Flambaum, Phys. Rev. D **89**, 043522 (2014).

[16] D. Budker, P. W. Graham, M. Ledbetter, S. Rajendran and A. O. Sushkov, Phys. Rev. X **4**, 021030 (2014).

[17] C. Abel, N. J. Ayres, G. Ban, G. Bison, K. Bodek, V. Bondar, M. Daum, M. Fairbairn, V. V. Flambaum *et al*, Phys. Rev. X **7**, 041034 (2017).

[18] V. V. Flambaum, Phys. Rev. A **98**, 043408 (2018).

[19] V. V. Flambaum and I. B. Samsonov, Phys. Rev. A **98**, 053437 (2018).

[20] H. B. Tran Tan, V. V. Flambaum and I. B. Samsonov, Phys. Rev. A **99**, 013430 (2019).

[21] V. Spevak, N. Auerbach and V. V. Flambaum, Phys. Rev. C **56**, 1357 (1997).

[22] V. V. Flambaum, A, Wickenbrock and D. Budker, arXiv:1909.04970 (2019)

[23] V. V. Flambaum, H. B. Tran Tan, A, Wickenbrock and D. Budker, arXiv:1910.07705 (2019).

[24] A. Arvanitaki, S. Dimopoulos and K. Van Tilburg, Phys. Rev. X 8, 041001 (2018).

[25] R. J. Crewther, P. di Vecchia, G. Veneziano and E. Witten. Phys. Lett. B **91**, 487 (1980).

[26] N. Yamanaka, B. K. Sahoo, N. Yoshinaga, T. Sato and K. Asahi, B. P. Das. Eur. Phys. J **53**, 54 (2017).

[27] W. C. Haxton and E. M. Henley, Phys. Rev. Lett. **51**, 1937 (1983).

[28] V. V. Flambaum, D. DeMille and M. G. Kozlov, Phys. Rev. Lett. **113**, 103003 (2014).

[29] L. D. Landau and E. M. Lifshitz, *Quantum Mechanics* (Pergamon press, Oxford, 1965).

Chapter 6

Atomic and molecular transitions induced by axions via oscillating nuclear moments

6.1 Overview

In the presence of a periodic perturbation a quantum mechanical system undergoes transition. A familiar example is the atomic and molecular transitions induced by external electromagnetic fields. However, it is worth noting that the perturbation does not have to come from outside to have such an effect. In this chapter, I consider the transitions induced by various oscillating CP-violating nuclear moments inside atoms and molecules. These oscillating nuclear moments may be induced by axion Dark Matter. I demonstrate that these transitions are, in principle, observable.

As the result of this research, I have published a paper:

1. V. V. Flambaum, H. B. Tran Tan, D. Budker and A. Wickenbrock, **Atomic and molecular transitions induced by axions via oscillating nuclear moments**, Phys. Rev. D **101**, 073004 (2020), DOI: 10.1103/PhysRevD.101.073004, arXiv:1910.07705,

and presented it at one international conference, one international workshop and one national competition:

1. **Searching for Axions and Axionic Dark Matter with Interference and Axion-induced Nuclear Moments**, TeV Particle Astrophysics Conference, University of Sydney, Sydney, Australia, December 2019,

2. **Screening and Enhancement of Nuclear Electric Dipole Moments Induced by Axionic Dark Matter**, Frontiers in Quantum Matter Workshop: Electric Dipole Moments, Australian National University, Canberra, Australia, November 2019,

3. **Effects of Dark Matter in atomic and molecular phenomena**, Australian Institute of Physics Postgraduate Presentation Competition, University of Technology Sydney, Sydney, Australia, October 2019.

6.2 Abstract

The interaction of standard model's particles with the axionic Dark Matter field may generate oscillating nuclear electric dipole moments (EDMs), oscillating nuclear Schiff moments and oscillating nuclear magnetic quadrupole moments (MQMs) with a frequency corresponding to the axion's Compton frequency. Within an atom or a molecule an oscillating EDM, Schiff moment or MQM can drive transitions between atomic or molecular states. The excitation events can be detected, for example, via subsequent fluorescence or photoionization. Here we calculate the rates of such transitions. If the nucleus has octupole deformation or quadrupole deformation then the transition rate due to Schiff moment and MQM can be up to 10^{-16} transition per molecule per year. In addition, an MQM-induced transition may be of

M2-type, which is useful for the elimination of background noise since M2-type transitions are suppressed for photons.

6.3 Introduction

The nature of dark matter (DM) remains unknown. The axion is a prominent dark matter candidate originally introduced in the 1970s to explain the apparent charge-parity (CP) symmetry of the strong interactions [1–4]. Traditional searches for axion and axion-like particles (ALPs)[1] rely on the conversion between axion and photon in a strong magnetic field [5, 6]. Helioscope experiments including Sumico [7–11], CAST [12–15], SOLAX [16, 17], COSME [18], CDMS [19–22] and IAXO [23–25] convert solar axions into photons for detection. Haloscope experiments such as ADMX [26–28], HAYSTAC [29, 30] and ORGAN [31] convert cosmic axions into photons in microwave cavities and detect these photons resonantly with SQUIDs. Light-shining-through-a-wall (LSW) experiments including ALPS [32–34], OSQAR [35–37] and GammeV [38] convert photons into axions, use a wall to block all the photons but not the axions, and then convert the axions back into photons for detection behind the wall. Finally, experiments like PVLAS [39–41], Q & A [42] and BMV [43, 44] search for optical birefringence (difference in optical refractive indices for different polarizations) and dichroism (difference in absorption of light of different polarizations) due to interconversion with axions [45].

Other proposals to search for axion DM include converting axions into magnons in a ferromagnet [46, 47], using dielectric haloscopes with improved sensitivity [48–51], using nuclear magnetic resonance to search for axion-mediated CP-violating forces [52–55], detecting the oscillating magnetic flux sourced by the axions entering a static magnetic field [56], using electron spin resonance in magnetized media to detect the oscillating effective magnetic field induced by axions [57], using superconductors [58] and semiconductors [59], using an LC circuit (Dark Matter radio) [60–62], using Josephson junctions [63, 64], using photon interferometry [65], using axion-induced resonant molecular transitions [66], using laser-spectroscopy techniques to probe axion-induced atomic and molecular tranistions [67], looking for an axion-induced topological Casimir effect [68], using a photon field (instead of a magnetic field) to trigger axion-to-photon decay then detecting the product photons with Raman scattering [69] and using the interference of axion and photon absorption in atoms and molecules [70].

Recently, a new class of experiments have also been proposed to look for parity- and time-reversal-invariance-violating (P,T-odd) effects due to couplings of axions to Standard Model (SM) particles [71–75]. Assuming that the dark matter in the Milky Way consists of axions , the dark matter field can be described as a field oscillating at a frequency close to the Compton frequency of the axion. The interaction of SM particles with this oscillating axion field induces oscillating electric dipole moments (EDMs), oscillating Schiff moments and an oscillating magnetic quadrupole moments (MQMs) of fundamental particles, nuclei, atoms, and molecules [71, 74]. These resulting moments then cause the precession of particle's spins due to gradients in the axion field (the axion-wind effect) [76] and may thus, in principle, be detected. The CASPEr experiments [72] search for spin precession due to the oscillating nuclear Schiff moment, which is related to the nucleon EDMs and axion-induced P,T-odd nuclear forces, and axion wind with nuclear magnetic resonance. First results constraining the axion-nucleon couplings have been published by CASPEr [77, 78], as well as by other experiments re-analyzing existing data obtained in the neutron-EDM [79] and atomic co-magnetometer experiments [80] and trapped anti-proton experiment [81].

In this paper, we analyze the effect of an axion-induced oscillating nuclear EDM, an oscillating nuclear Schiff moment and an oscillating nuclear MQM in atoms and molecules. Such oscillating moments may induce transitions in the atom or molecule if the transition frequency matches the axion oscillation frequency. In fact, nuclear-EDM-induced atomic and molecular transitions were already discussed in Ref. [82]. In this work, we extend the discussion to the case of Schiff-moment-induced- and nuclear-MQM-induced transitions whose rates, as we will demonstrate, may be several orders of magnitude larger than that of an EDM-induced transitions.

The rest of the paper is organized as follows. In Sect. 6.4, we provide a brief revision of the nuclear EDM, nuclear Schiff moment, nuclear MQM and how these moments might be produced by an oscillating axion DM field. In Sects. 6.5 and 6.6, we estimate the rates of the atomic and molecular transitions induced by the oscillating nuclear moments and discuss the scaling of these rates with respect to relevant atomic and molecular parameters. Sect. 7.7 contains a brief summary of our finding and several comments

[1] ALPs are pseudoscalar particles like the axion that do not, however, solve the strong-CP problem; we refer to both axions and ALPs as 'axions' in this paper.

on the feasibility of experimental observation of the effects.

6.4 Nuclear moments produced by the axion dark matter field

In this section, we give a brief overview of three nuclear moments which give rise to P,T-odd interactions with the electrons. These are the nuclear EDM, nuclear Schiff moment and the nuclear MQM. The first two moments arise due to P,T-odd-interaction-induced charge distribution inside the nucleus whereas the last moment arises due to P,T-odd-interaction-induced current distribution inside the nucleus. We will also explain the connection between an oscillating axion DM field and the oscillating nuclear moments.

6.4.1 Nuclear EDM

The P,T-odd interaction of the atomic electrons with a nuclear EDM $\mathbf{d}$ has the familiar form

$$V_{\rm EDM} = e\sum_{k=1}^{N_e}\frac{\mathbf{d}\cdot\mathbf{r}_k}{r_k^3}\,, \tag{6.1}$$

where N_e is the number of the electrons, $-e$ is the electron charge and $\mathbf{r}_k$ is the electron position relative to the nucleus.

The EDM $\mathbf{d}$ of a nucleus arises from the inherent EDMs of the nucleons and from the P,T-odd interactions between the nucleons. As noted in Ref. [1–4, 83], a neutron EDM may be produced by the so-called 'QCD θ-term', where the parameter θ is the axion field strength. Numerous references and recent results for the neutron and proton EDMs are summarised in the review [84]

$$\begin{aligned} d_n &= -(2.7\pm 1.2)\times 10^{-16}\theta\, e\,{\rm cm}\,,\\ d_p &= (2.1\pm 1.2)\times 10^{-16}\theta\, e\,{\rm cm}\,. \end{aligned} \tag{6.2}$$

Apart from contribution from the neutron and proton EDMs (6.2), the EDM of a nucleus also receives contributions arising from P,T-odd interactions between nucleons. Calculations of the EDM of a nucleus with more than one nucleon produced by the P,T-odd nuclear forces were performed in Refs. [85–102]. For a general estimate of such a nuclear EDM, it is convenient to use a single-valence-nucleon model in which the P,T-odd interaction between the valence nucleon with the nuclear core is given by [86]

$$H_{PT} = \frac{G}{\sqrt{2}}\frac{\eta}{2m_p}\boldsymbol{\sigma}\cdot\nabla\rho\left(\mathbf{r}\right)\,, \tag{6.3}$$

where G is the Fermi weak interaction constant, η is a constant which characterizes the strength of the P,T-odd nucleon-nucleon interaction, $\boldsymbol{\sigma}$ is the nuclear spin operator, $\rho\left(\mathbf{r}\right)$ is the density of the nuclear core and m_p is the proton mass. The nuclear EDM in this case is that of the valence nucleon, given by

$$\mathbf{d} = e\left(q - Z/A\right)\langle\mathbf{r}\rangle \tag{6.4}$$

where $\mathbf{r}$ is the position operator of the valence nucleon with respect to the nuclear core, $q = 1$ for the valence proton and $q = 0$ for the valence neutron. The effective charge $e\left(q - Z/A\right)$ appears due to recoil effect.

Using Eqs. (6.3) and (6.4) and expressing the result in terms of θ following Ref. [103], we obtain the PT-odd force contribution to the nuclear EDM

$$d \approx 7\times 10^{-16}\left(q - \frac{Z}{A}\right)\left(1-2q\right)\langle\sigma\rangle\theta\, e\,{\rm cm}\,, \tag{6.5}$$

where the nuclear spin matrix element is $\langle\sigma\rangle = 1$ if $j = l + 1/2$ and $\langle\sigma\rangle = -j/\left(j+1\right)$ if $j = l - 1/2$. Here, j and l are the total and orbital momenta of the valence nucleon.

There are many specific results for the ^{2}H and ^{3}He EDMs, see, e.g., reviews [100, 104]. Within the error bars, the deuterium EDM is consistent with zero due to the cancellation between the proton and neutron contributions. The ^{3}He nucleus contains an unpaired neutron. Using the calculation of the P,T-odd nuclear force contribution from Refs. [97–99] $(-1.5\times 10^{-16}\theta\, e\,{\rm cm})$ and the value of the neutron EDM from Eq. (6.2), we obtain for the ^{3}He EDM

$$d(^3{\rm He}) = (-4.2\pm 1.5)\times 10^{-16}\theta\, e\,{\rm cm}\,, \tag{6.6}$$

which is close to the estimate obtained using Eq. (9.12d), which gives $d(^3{\rm He}) = -4.7\times 10^{-16}\theta\, e\,{\rm cm}$, even though the latter does not include the contribution of the neutron EDM.

6.4.2 Nuclear Schiff moment

According a theorem by Schiff [105], a static nuclear EDM does not induce an atomic or molecular EDM in a neutral atom or molecule. This reduces to the fact that the P,T-odd interaction between an electron and the nucleus must have the form [86, 106]

$$V(\mathbf{R}) = -Ze^2 \left[\int \frac{\rho(\mathbf{r})\, d^3r}{|\mathbf{R}-\mathbf{r}|} + \langle \mathbf{r} \rangle \cdot \nabla \int \frac{\rho(\mathbf{r})\, d^3r}{|\mathbf{R}-\mathbf{r}|} \right] \tag{6.7}$$

where $\mathbf{R}$ is the electron position operator, $\rho(\mathbf{r})$ is the nuclear charge density normalized to $\int \rho(\mathbf{r})\, d^3r = 1$ and $\langle \mathbf{r} \rangle = Z \int \rho(\mathbf{r})\, \mathbf{r} d^3r$.

The dipole term of this interaction reads[2] [86]

$$V_{\text{SCHIFF}} = 4\pi \mathbf{S} \cdot \boldsymbol{\nabla} \rho(\mathbf{R}) \,, \tag{6.8}$$

where $\mathbf{S}$ is the Schiff moment of the nucleus, defined by

$$\mathbf{S} = \frac{e}{10} \left[\langle r^2 \mathbf{r} \rangle - \frac{5}{3Z} \langle r^2 \rangle \langle \mathbf{r} \rangle \right] , \tag{6.9}$$

where $\langle r^n \rangle = Z \int \rho(\mathbf{r})\, r^n d^3r$ are the moments of the nuclear charge density and $\mathbf{r}$ is measured from the nuclear center of mass ($n = 2, 3$ is relevant in Eq. (6.9)).

For a spherical nucleus with one unpaired nucleon, we can use the model Eq. (6.3), in which Eq. (6.9) gives

$$\begin{aligned} \mathbf{S} &= S\mathbf{I}/I \,, \\ S &= -7 \times 10^{-7} \theta e q \left[\left(\langle \sigma \rangle + \frac{1}{I+1} \right) \langle r^2 \rangle - \frac{5}{3} \langle \sigma \rangle r_q^2 \right] , \end{aligned} \tag{6.10}$$

where $\mathbf{I}$ is the nuclear spin, q and $\langle \sigma \rangle$ are defined as in Eq. (9.12d) and r_q^2 is the mean square charge radius. Approximately, $\langle r^2 \rangle \approx r_q^2 \approx (3/5) R^2$ where $R = r_0 A^{1/3}$ is the mean bound-state radius of the nucleus ($r_0 \approx 1.5\,\text{fm}$ and A is the nuclear mass number).

It is observed from Eq. (6.9) that the Schiff moment is a result of adding two terms of opposite sign. These two terms are often not known with sufficient accuracy so the result of calculating the Schiff moment becomes unreliable. Also, the Schiff moment is determined by the charge distribution of the protons. However, it is directed along the nuclear spin which, for example in ^{199}Hg, is carried by the valence neutron, so the Schiff moment is determined by the many-body effects which are harder to calculate. The calculation of nuclear EDMs, on the other hand, does not suffer from these problems (such as the difference of two nearly equal terms) and thus have certain computational advantages.

Despite of these difficulties, numerical calculations of the Schiff moments do exist. Some numerically computed values for the Schiff moments of spherical nuclei with one unpaired nucleon are [86–88, 107–111]

$$\begin{aligned} S\left(^{205}\text{Tl}\right) &\approx -0.027\theta\, e\, \text{fm}^3 \,, \\ S\left(^{199}\text{Hg}\right) &\approx -0.005\theta\, e\, \text{fm}^3 \,. \end{aligned} \tag{6.11}$$

We note in passing that there are experimental limits on the static Schiff moments of ^{205}Tl and ^{199}Hg, e.g., $\left|S_{^{199}\text{Hg}}\right| \lesssim 3.1 \times 10^{-13} e\,\text{fm}^3$ corresponding to $|\theta| \lesssim 10^{-10}$ [112–114].

In nuclei with octupole deformation, the nuclear Schiff moments may be enhanced by 100 to 1000 times (thanks to the small energy differences of nuclear levels with opposite parity and collective effects) [106, 111, 115–118]

$$\begin{aligned} S\left(^{153}\text{Eu}\right) &\approx 3.7\,\theta\, e\, \text{fm}^3 \,, \\ S\left(^{225}\text{Ra}\right) &\approx \theta\, e\, \text{fm}^3 \,, \\ S\left(^{227}\text{Ac}\right) &\approx 10\,\theta\, e\, \text{fm}^3 \,, \\ S\left(^{229}\text{Th}\right) &\approx 2\,\theta\, e\, \text{fm}^3 \,, \\ S\left(^{235}\text{U}\right) &\approx 3\,\theta\, e\, \text{fm}^3 \,, \\ S\left(^{237}\text{Np}\right) &\approx 6\,\theta\, e\, \text{fm}^3 \,. \end{aligned} \tag{6.12}$$

[2] A better form for this interaction which takes into account the finite size of the nucleus is available, see Ref. [107]; for our estimate, the form (6.26) is sufficient.

It should also be mentioned that for the Schiff moment of a nucleus with octuple deformation, the aforementioned problem with the cancellation of two nearly equal terms does not arise since the first term in Eq. (6.9) is significantly enhanced whereas the second term is not (it is zero for similar distribution of protons and neutrons) and the result is stable. The calculation of the Schiff moment is, in this case, reduced to that of the expectation value of the P,T-odd interaction over intrinsic states of the deformed nucleus.

6.4.3 Nuclear MQM

Since there exists nucleon currents inside a nucleus, apart from electric interaction, the nucleus can also have magnetic interactions with electrons. The most familiar of such interaction, the magnetic dipole interaction, is P,T-even and is thus of no interest to us. The first P,T-odd magnetic interaction is thus between the electron and the MQM of the nucleus, given by [86, 119]

$$V_{\mathrm{MQM}} = -\frac{M}{4I\,(2I-1)} T_{ij} A_{ij}\,, \tag{6.13}$$

(summation over the indices i, j is implied) where the tensor T_{ij} is defined by ($\mathbf{I}$ is again the nuclear spin)

$$T_{ij} = I_i I_j + I_j I_i - \frac{2}{3}\delta_{ij} I\,(I+1)\,, \tag{6.14}$$

and the tensor A_{ij} by

$$A_{ij} = \epsilon_{nmi}\alpha_n \partial_m \partial_j \frac{1}{r}\,. \tag{6.15}$$

Here, M is the magnitude of the MQM, α_n are the Dirac alpha matrices and r the distance from the electron to the nucleus.

The MQM of a spherical nucleus with one unpaired nucleon is given by [86, 103, 120]

$$M = \left[d - 6\times 10^{-16}\theta\,(\mu - q)\,(e\,\mathrm{cm})\right]\lambda_p\,(2I-1)\,\langle\sigma\rangle\,, \tag{6.16}$$

where d is the valence nucleon's EDM, μ is its magnetic dipole moment in nuclear magnetons, q, σ, I are as defined in Eqs. (9.12d) and (6.9) and $\lambda_p = \hbar/m_p c = 2.1\times 10^{-14}\,\mathrm{cm}$ (m_p is the proton mass).

Some values for the MQM of spherical nuclei are [86]

$$\begin{aligned} M\left(^{131}\mathrm{Xe}\right) &\approx -3\times 10^{-29}\theta\, e\,\mathrm{cm}^2\,,\\ M\left(^{201}\mathrm{Hg}\right) &\approx 5\times 10^{-29}\theta\, e\,\mathrm{cm}^2\,. \end{aligned} \tag{6.17}$$

If the nucleus in question has quadrupole deformation, collective effects generally enhance the nuclear MQM by one order of magnitude [103, 120–122]

$$\begin{aligned} M\left(^{173}\mathrm{Yb}\right) &\approx -9\times 10^{-28}\theta\, e\,\mathrm{cm}^2\,,\\ M\left(^{177}\mathrm{Hf}\right) &\approx -1\times 10^{-27}\theta\, e\,\mathrm{cm}^2\,,\\ M\left(^{179}\mathrm{Hf}\right) &\approx -2\times 10^{-27}\theta\, e\,\mathrm{cm}^2\,,\\ M\left(^{181}\mathrm{Ta}\right) &\approx -2\times 10^{-27}\theta\, e\,\mathrm{cm}^2\,,\\ M\left(^{229}\mathrm{Hf}\right) &\approx -1\times 10^{-27}\theta\, e\,\mathrm{cm}^2\,. \end{aligned} \tag{6.18}$$

6.4.4 Effects of an oscillating axion DM field

Reference [71] discussed the possibility that the dark matter field is, in fact, an oscillating axion field which generates neutron EDMs. This axion field may also generate oscillating nuclear EDMs, oscillating nuclear Schiff moments and oscillating nuclear MQMs [74]. In short, the parameter θ, which is the axion field strength, is now periodic with respect to time instead of being static. Relating the value of the axion field to the local dark matter density (Ref. [74]), we may substitute $\theta(t) = \theta_0\cos(\omega t)$ where $\theta_0 = 4\times 10^{-18}$, $\omega = m_a c^2/\hbar$ and m_a is the axion mass[3]. It is important to keep in mind that ALPs inducing larger dipole moments are also among viable DM candidates, so an experiment with sensitivity less than that necessary to detect axionic DM could already be sensitive to DM composed of such ALPs.

[3] It is worth mentioning that axions are a stochastic field with a finite coherence times $\tau_c \approx \frac{10^{-6}\hbar}{m_a c^2}$, see, for example Ref. [123]. In this paper, by θ_0 we mean $\sqrt{\langle\theta_0^2\rangle}$.

6.5 Atomic transitions induced by oscillating nuclear moments

We have presented in the last section the possibility of having oscillating nuclear EDMs, Schiff moments and MQMs. The interactions of these moments with the atomic electrons may cause electronic transitions. In what follows, we provide estimates of the transition rates due to the interactions with these moments.

6.5.1 Nuclear EDM contribution

The interaction of the atomic electrons with a nuclear EDM (6.1) may also be written as

$$V_{\rm atom}^{\rm EDM} = e\sum_{k=1}^{N_e}\frac{\mathbf{d}\cdot\mathbf{r}_k}{r_k^3} = \frac{i}{Ze\hbar}[\mathbf{P}\cdot\mathbf{d}, H_0]\,, \tag{6.19}$$

where H_0 is the (Schrödinger or Dirac) Hamiltonian for the atomic electrons in the absence of $\mathbf{d}$ and $\mathbf{P} = \sum_{k=1}^{N_e}\mathbf{p}_k$ is the total momentum of all atomic electrons.

The second equal sign in Eq. (6.19) holds because we have assumed that the nuclear mass is infinite and neglected the small effects of the Breit and magnetic interactions. The operator $\mathbf{P}$ commutes with the electron-electron interaction but does not commute with U, the potential energy due to the interaction with the nucleus

$$U = -\sum_{k=1}^{N_e} Ze^2/r_k\,, \tag{6.20}$$

so we have

$$[\mathbf{P}, H_0] = [\mathbf{P}, U] = -i\hbar Ze^2\sum_{k=1}^{N_e}\nabla\frac{1}{r_k} = i\hbar Ze^2\sum_{k=1}^{N_e}\frac{\mathbf{r}_k}{r_k^3}\,. \tag{6.21}$$

Using the nonrelativistic relation

$$\mathbf{P} = -\frac{im}{e\hbar}[H_0, \mathbf{D}]\,, \tag{6.22}$$

where m_e is the electron's mass and $\mathbf{D} = -e\sum_{k=1}^{N_e}\mathbf{r}_k$ is the atomic electric dipole moment, the matrix element of $V_{\rm atom}^{\rm EDM}$ may be written as [82]

$$\langle f|\, V_{\rm atom}^{\rm EDM}\,|i\rangle = -\frac{\omega^2 m_e}{Ze^2}\mathbf{d}\cdot\langle f|\,\mathbf{D}\,|i\rangle\,, \tag{6.23}$$

where ω is the frequency of the axion field, which must matches the transition frequency $(E_f - E_i)/\hbar$.

The scalar operator $V_{\rm atom}^{\rm EDM}$ conserves the total atomic angular momentum F. For the electron variables the selection rules are identical to that for E1 amplitudes.

In accordance with the Schiff theorem, which states that the static EDM of a subatomic point particle is unobservable in the nonrelativistic limit, the matrix element (6.23) is propotional to ω^2 and thus vanishes for $\omega = 0$. This ω^2 suppression should not appear for the transitions induced by oscillating Schiff moments and MQMs which we shall consider below.

The transition probability $W \propto \left|\langle i|\, V_{\rm atom}^{\rm EDM}\,|f\rangle\right|^2$ is inversely proportional to the squared nuclear charge, $W \propto 1/Z^2$, i.e., light atoms like H, He, Li are more advantageous for experiments. The origin of this factor may be related to the extended Schiff theorem for ion: the screening factor for an external electric field scales as $1/Z$.

Note that the transition probability is not suppressed for high electron waves j, l. The reason is that the matrix element of $V \sim 1/r^2$ does not converge at small distances. Indeed, an estimate of the contribution of the small distances $\int(\psi_1^+\psi_2/r^2)r^2dr = \int\psi_1^+\psi_2 dr \sim r^{l_1+l_2+1}$ actually converges on the atomic size. This is also the reason why the relativistic corrections are not important (except for in the values of energies E_1, E_2).

Note also that the matrix element rapidly decreases with the electron principal quantum number n since $\omega_{fi} \sim (n_f - n_i)/n^3$, $\langle i|\,\mathbf{D}\,|f\rangle \sim n^2$, i.e., $\langle i|\,V\,|f\rangle \sim 1/n^4$ (we assume that $n_f \approx n_i \approx n$).

The probability of the transition on resonance for the stationary case (time $t \gg 1/\Gamma$ with Γ being the dominant decoherence mechanism) for the perturbation $V_{\rm atom}^{\rm EDM} = V^0\cos(\omega t)$ is given by the following expression [124]:

$$W_{fi} = \frac{|\,\langle f|\, V_{\rm atom}^{\rm EDM}\,|i\rangle\,|^2 t}{\hbar\Gamma}\,. \tag{6.24}$$

In our case Γ may be the width of the axion energy distribution ($\Gamma \sim 10^{-6} m_a c^2 = 10^{-6}\hbar\omega$) if the atomic level width is smaller than the axion energy distribution width (or the atomic energy level width Γ in the opposite case).

Inserting Eq. (6.23) into Eq. (6.24), we obtain the approximate time for one transition to happen

$$t_{\rm atom}^{\rm EDM} \approx \frac{2\times 10^{22}}{N} Z^2 \left(\frac{1{\rm eV}}{\omega}\right)^3 \left|\frac{3ea_B}{\langle f|\, D_z\, |i\rangle}\right|^2 \left(\frac{4\times 10^{-16}\theta_0\, e\,{\rm cm}}{d}\right)^2 {\rm years}\,, \tag{6.25}$$

where N is the number of atoms and a_B is the Bohr radius. We have presented the result for the maximal projection of the atomic angular momentum ($F_z = F = j + I$, where j is the electron angular momentum and I is the nuclear spin) and normalized the result to an atomic scale energy of 1 eV, a typical value of E1-amplitude $|\,\langle f|\, D_z\, |i\rangle\,| = 3ea_B$ and a typical value of nuclear EDM $d_0 = 4\times 10^{-16}\theta\, e\,{\rm cm}$.

Note that for the hydrogen atom and transitions between highly excited Rydberg states of electron, there are analytical expressions [125] for the transition frequencies (between states with principal quantum numbers n_i and n_f) $\omega \sim (n_i - n_f)/n^3$ and E1 amplitudes $\langle f|\, D_z\, |i\rangle \sim n^2 a$. Altogether we have $t \propto Z^2 n^5$.

6.5.2 Nuclear Schiff moment contribution

The effective Hamiltonian for the interaction between a nuclear Schiff moment and an atomic electron is given by (see Eq. (6.8))

$$V_{\rm atom}^{\rm SCHIFF} = 4\pi \mathbf{S}\cdot\boldsymbol{\nabla}\rho\,. \tag{6.26}$$

The matrix element for this interaction reads

$$\langle f|\, V_{\rm atom}^{\rm SCHIFF}\, |i\rangle = \langle f|4\pi\frac{\partial\rho}{\partial z}|i\rangle S\,, \tag{6.27}$$

where we have assumed maximal projection of the nuclear spin and that the wavefunction of the system factorizes into nuclear and atomic parts.

Inserting Eq. (6.27) into an analog of Eq. (6.24), we find the time for detection of one transition

$$t_{\rm atom}^{\rm SCHIFF} \approx \frac{2\times 10^{22}}{N} \left(\frac{\omega}{1{\rm eV}}\right) \left(\frac{50000\frac{e}{a_B^4}}{\langle f|4\pi\frac{\partial\rho}{\partial z}|i\rangle}\right)^2 \left(\frac{\theta_0\, e\,{\rm fm}^3}{S}\right)^2 {\rm years}\,, \tag{6.28}$$

where we have normalized the result to the atomic transition energy scale 1 eV, a typical value of the matrix element $\langle f|4\pi\frac{\partial\rho}{\partial z}|i\rangle \sim 50000 a_B^{-4}$ [126] and a typical value of the nuclear Schiff moment of a nucleus with octupole deformation $S \sim \theta_0\, e\,{\rm fm}^3$. If a maximal value of $S = 10\,\theta_0\, e\,{\rm fm}^3$ (^{227}Ac) was used then the result is two order of magnitudes better than (6.28).

We observe that unlike $t_{\rm atom}^{\rm EDM}$, which is proportional to ω^{-3}, $t_{\rm atom}^{\rm SCHIFF} \propto \omega$. This is because the matrix element (6.23) is proportional to ω^2 whereas the matrix element (6.27) does not depend on ω. The factor ω in Eq. (6.28) comes from the width Γ which is assumed to be $10^{-6}\omega$.

As noted in Sect. 6.4, for a typical spherical nucleus with one unpaired nucleon, the Schiff moment is two to three orders of magnitude smaller than that in Eq. (6.28). As a result, the 'waiting' time if such nuclei are used is from four to six orders of magnitude larger than that in Eq. (6.28).

Note also that the matrix element (6.27) is subjected to E1 selection rules (the matrix element $\langle f|\, 4\pi\frac{\partial\rho}{\partial z}\, |i\rangle$ contains the factor $\begin{pmatrix} j_f & 1 & j_i \\ -m_f & 0 & m_i \end{pmatrix} \xi\,(l_f + l_i + 1)$ where $\xi\,(x) = 1$ if x is even and $\xi\,(x) = 0$ if x is odd, see, e.g., [126]).

6.5.3 Nuclear magnetic quadrupole moment contribution

The interaction of an atomic electron with a nuclear MQM has the form (see Eq. (6.13))

$$V_{\rm atom}^{\rm MQM} = -\frac{M}{4I\,(2I-1)} T_{ij} A_{ij}\,. \tag{6.29}$$

The matrix element of this interaction reads (assuming maximal projection of the nuclear spin)

$$\langle f|\, V_{\rm atom}^{\rm MQM}\, |i\rangle = -\frac{I+1}{6\,(2I-1)}\,\langle f|\, A_{zz}\, |i\rangle\, M\,, \tag{6.30}$$

so the time for the detection of one transition is

$$t_{\rm atom}^{\rm MQM} \approx \frac{10^{22}}{N}\left(\frac{2I-1}{I+1}\right)^2\left(\frac{\omega}{1{\rm eV}}\right)\left(\frac{10\frac{e}{a_B^3}}{\langle f|A_{zz}|i\rangle}\right)^2\left(\frac{10^{-27}\theta_0\, e\,{\rm cm}^2}{M}\right)^2 {\rm years}\,, \tag{6.31}$$

where we have normalized the result to the atomic transition energy scale 1 eV, a typical value of the matrix element $\langle f|A_{zz}|i\rangle \sim 10\frac{e}{a_B^3}$ [126] and a typical value of the nuclear MQM for a nucleus with quadrupole deformation $M \sim 10^{-27}\theta_0\, e\,{\rm cm}^2$. If the value $2\times 10^{-27}\theta_0\, e\,{\rm cm}^2$ is used for M (e.g., ^{179}Hf) then the result is better by a factor of four.

For a nucleus with no deformation, as noted in Sect. 6.4, the MQM is generally an order of magnitude smaller than that presented in Eq. (6.31). As a result, the 'waiting' time in such case is about two orders of magnitude larger than in Eq. (6.31).

Note that the matrix element (6.30) is of M2 type (the matrix element $\langle f|\, A_{zz}\,|i\rangle$ contains the factor $\begin{pmatrix} j_f & 2 & j_i \\ -m_f & 0 & m_i\end{pmatrix}\xi\,(l_f+l_i+1)$). As a result, an MQM-induced transition, unlike an EDM-induced or a Schiff-moment-induced one, may be strongly suppressed for photons (in cases where E1-type transitions are impossible). This might prove useful for minimizing the effects of background processes.

6.6 Molecular transitions induced by oscillating nuclear moments in diatomic molecule

In Sect. 6.5, we presented the estimates for the atomic transitions induced by various oscillating nuclear moments. These transitions are suitable for searching for axion with mass in the eV region. For axion mass in the $10^{-5}-10^{-1}$ eV region (the value $m_a = 26.2\,\mu$eV was recently predicted in Ref. [127]; see also [128, 129]), molecules appear to be better suited, with the region $10^{-5}-10^{-1}$ eV coinciding with the typical separation between rovibrational states. In what follows, we present estimates for low-frequency transitions in diatomic molecules induced by oscillating nuclear moments.

6.6.1 Nuclear EDM contribution

Let us now consider a diatomic molecule consisting of two nuclei of masses M_I, charges Z_I and nuclear EDMs $\mathbf{d}_I$ (the subscript $I=1,2$ labels the nuclei) and N_e electrons. As above, the position and momentum operators of the electrons in the laboratory frame are denoted by $\mathbf{r}_k$ and $\mathbf{p}_k$. The position and momentum operators of the nuclei in the laboratory frame will be denoted by $\mathbf{R}_I$ and $\mathbf{P}_I$, respectively.

The interaction between the nuclear EDMs and the nuclei and electrons in the molecule may be presented as

$$V_{\rm mol}^{\rm EDM} = \frac{\mathbf{d}_1\cdot\nabla_{\mathbf{R}_1}V_0}{Z_1 e} + \frac{\mathbf{d}_2\cdot\nabla_{\mathbf{R}_2}V_0}{Z_2 e}\,, \tag{6.32}$$

where

$$V_0 = \frac{Z_1Z_2e^2}{R_{12}} - \sum_{k=1}^{N_e}\left(\frac{Z_1e^2}{R_{1k}}+\frac{Z_2e^2}{R_{2k}}\right) + \sum_{i\neq j}^{N_e}\frac{e^2}{r_{ij}}\,, \tag{6.33}$$

is the Coulomb potential between the constituent particles of the molecule. Here, $R_{Ik} = |\mathbf{R}_I - \mathbf{r}_k|$, $r_{hk} = |\mathbf{r}_h - \mathbf{r}_k|$ and $R_{IJ} = |\mathbf{R}_I - \mathbf{R}_J|$.

As shown in Appendix A, the matrix element of $V_{\rm mol}^{\rm EDM}$ has the form

$$\langle f|\, V_{\rm mol}^{\rm EDM}\,|i\rangle = \frac{\omega^2\mu_N}{e\sqrt{Z_1Z_2}}\,\langle f|\,\boldsymbol{\delta}\cdot\mathbf{X} - \boldsymbol{\Delta}\cdot\sum_{i=1}^{N_e}\mathbf{x}_i\,|i\rangle\,, \tag{6.34}$$

where $\mathbf{X} = \mathbf{R}_1 - \mathbf{R}_2$ is the inter-nuclear distance, $\mathbf{x}_k = \mathbf{r}_k - (M_1\mathbf{R}_1 + M_2\mathbf{R}_2)/(M_1+M_2)$ is the relative position of the electrons with respect to the nuclear center of mass and $\mu_N = M_1M_2/(M_1+M_2)$ is the reduced nuclear mass. The moments $\boldsymbol{\delta}$ and $\boldsymbol{\Delta}$ are defined as

$$\boldsymbol{\delta} = \sqrt{Z_1Z_2}\left(\frac{\mathbf{d}_1}{Z_1} - \frac{\mathbf{d}_2}{Z_2}\right)\,, \tag{6.35}$$

and

$$\boldsymbol{\Delta} \approx \frac{m_e\,(M_1Z_2\mathbf{d}_1 + M_2Z_1\mathbf{d}_2)}{M_1M_2\sqrt{Z_1Z_2}}\,, \tag{6.36}$$

where in Eq. (6.36) we retain only the lowest-order term in the small parameters $m_e \ll M_{1,2}$. Here, ω is again the frequency of the axion field which matches the transition frequency $(E_f - E_i)/\hbar$.

To estimate the matrix element (6.34), it is convenient to use the Born-Oppenheimer approximation, in which the molecular wavefunction can be written as

$$\psi_n = \sqrt{\frac{2J_n+1}{8\pi^2}} D^{J_n}_{m_n\Omega_n}(\Theta) \frac{\phi^{\rm vib}_n(X)\,\varphi^e_{\kappa_n\Omega_n}(X,\mathbf{s}_i)}{X}\,, \tag{6.37}$$

where $\sqrt{(2J+1)/(8\pi^2)}D^J_{m\Omega}$, $\phi^{\rm vib}/X$ and $\varphi^e_{\mu\Lambda}$ are, respectively, the rotational, vibrational, electronic wavefunctions. Here J is the molecule's total angular momentum, m is the projection of J on a quantization axis (it is customary to use M for this quantity; here we use m to avoid confusion with the nuclear MQM), Ω is the projection of the electrons' total angular momentum on the molecular axis $\mathbf{X}$ and κ stands for any other quantum numbers not listed so far. The rotational wavefunction $D^J_{m\Omega}(\Theta)$ is the Wigner D matrix depending on the set of Euler angles Θ which descibes the molecule's orientation with respect to some laboratory-fixed frame.

As mentioned, an advantage of molecules over atoms is the existence of rovibrational states whose small energy spacing is convenient for searching for sub-eV dark matter. In this paper, we provide estimates for the transitions between such states. Also, in anticipation of the parity selection rules for the EDM, Schiff and MQM operators (see Sect. 6.5), we assume that the states f and i have opposite parities, that is, $|f\rangle = \left(|J',m,\Omega\rangle - (-1)^{J'-\Omega}|J',m,-\Omega\rangle\right)/\sqrt{2}$ and $|i\rangle = \left(|J,m,\Omega\rangle + (-1)^{J-\Omega}|J,m,-\Omega\rangle\right)/\sqrt{2}$ (here we assume that $\Omega \neq 0$, the result for the case where $\Omega = 0$ is similar). We also assume that f and i have the same electronic configuration.

Note that due to the small parameters $m_e/M_{1,2}$, we can assume for the moment that $|\boldsymbol{\Delta}| \ll |\boldsymbol{\delta}|$. Thus, if $\langle f|\,\mathbf{X}\,|i\rangle \neq 0$ then the term $\boldsymbol{\Delta}\cdot\sum_{i=1}^{N_e}\mathbf{x}_i$ may be dropped from Eq. (6.34). Also, if we are only interested in transitions between states within a single electronic configuration then the term $\boldsymbol{\Delta}\cdot\sum_{i=1}^{N_e}\mathbf{x}_i$ is zero. In such cases, we are left with

$$\langle f|\,V^{\rm EDM}_{\rm mol}\,|i\rangle \approx \frac{\omega^2\mu_N}{e}\langle f|\,\boldsymbol{\delta}\cdot\mathbf{X}\,|i\rangle = (-1)^{2J'-m-\Omega}B^{J'm\Omega}_{Jm\Omega}\frac{\omega^2\mu_N\delta X_{fi}}{e\sqrt{Z_1Z_2}}\,, \tag{6.38}$$

(assuming maximal projection for $\boldsymbol{\delta}$) where

$$B^{J'm\Omega}_{Jm\Omega} = \sqrt{(2J'+1)(2J+1)}\begin{pmatrix} J' & 1 & J\\ -m & 0 & m\end{pmatrix}\begin{pmatrix} J' & 1 & J\\ -\Omega & 0 & \Omega\end{pmatrix}, \tag{6.39}$$

and

$$X_{fi} = \int \bar{\phi}^{\rm vib}_f X \phi^{\rm vib}_i dX\,. \tag{6.40}$$

We note that in the case where $\mathbf{d}_2 = 0$, the result (6.38) reduces to that presented in Ref. [82].

The time for the detection of one transition due to an oscillating nuclear EDM is (assuming that the dominant contribution to the width is due to the axion frequency distribution $\Gamma \approx 10^{-6}\hbar\omega$) is

$$t^{\rm EDM}_{\rm mol} \approx \frac{6\times10^{30}}{N}\frac{Z_1Z_2}{\left(B^{J'm\Omega}_{Jm\Omega}\right)^2}\left(\frac{m_p}{\mu_N}\right)^2\left(\frac{\omega_\Omega}{\omega}\right)^3\left(\frac{3a_B}{X_{fi}}\right)^2\left(\frac{4\times10^{-16}\theta_0\ e\times{\rm cm}}{\delta}\right)^2{\rm year}\,, \tag{6.41}$$

where we have normalized our result to a typical Ω-doublet separation $\omega_\Omega = 10^{-5}$eV, a typical inter-nuclear distance of $3a_B$ and a typical value for nulear EDM $4\times10^{-16}\theta_0\ e\times$cm.

Comparing Eqs. (6.23) and (6.38), we see that for the same transition energy in the region of 10^{-5} eV, the molecular transition probability is enhanced by a factor of $(\mu_N/m_e)^2 \gtrsim 10^8$. This enhancement factor arises from the fact that because the nuclei mover slower than the electrons, the field created by the oscillating EDM of one nucleus on the other one is only partially screened by the electrons, see Ref. [130]. Note also that the matrix element (6.38) is subjected to E1 selection rules.

6.6.2 Nuclear Schiff moment contribution

The effective Hamiltonian for the interaction between the nuclear Schiff moment and the molecular axis $\mathbf{N} = \mathbf{X}/X$ of a diatomic molecule is given by [86]

$$V^{\rm SCHIFF}_{\rm mol} = W_S\mathbf{S}\cdot\mathbf{N}\,, \tag{6.42}$$

where W_S is the interaction constant.

Using the Born-Oppenheimer wavefunction (6.37) and assuming maximal projection of the nuclear spin, we obtain

$$\langle f|\, V_{\rm mol}^{\rm SCHIFF}\,|i\rangle \approx (-1)^{2J'-m-\Omega} B_{Jm\Omega}^{J'm\Omega} W_S S\,, \tag{6.43}$$

where $B_{Jm\Omega}^{J'm\Omega}$ is defined as in Eq. (6.39). The time for the detection of one transition due to an oscillating nuclear Schiff moment is thus

$$t_{\rm mol}^{\rm SCHIFF} \approx \frac{2\times 10^{17}}{N}\frac{1}{\left(B_{Jm\Omega}^{J'm\Omega}\right)^2}\frac{\omega}{\omega_\Omega}\left(\frac{50000\,\frac{e}{a_B^4}}{W_S}\right)^2\left(\frac{\theta_0\, e\,\mathrm{fm}^3}{S}\right)^2 \text{ years}\,, \tag{6.44}$$

where W_S is normalized to a typical value of $50000\frac{e}{a_B^4}$ [131] and S to the typical value of $\theta_0\, e\,\mathrm{fm}^3$ (for a nucleus with octupole deformation). Using the maximal value of $S = 10\,\theta_0\, e\,\mathrm{fm}^3$ (^{227}Ac) results in a two orders of magnitudes shorter time than that of Eq. (6.44).

We observe that, for the benchmark values of the parameters shown in Eqs. (6.41) and (6.44), the result (6.44) is thirteen orders of magnitude better than the result (6.41). If nuclei with no deformation are used instead, the results are still seven to nine order of magnitude better than those of using EDMs. Hence, for small axion frequency ($\omega \lesssim 10^{-3}$eV), Schiff moments appear to be more advantageous than EDMs.

6.6.3 Nuclear magnetic quadrupole moment contribution

The effective Hamiltonian for the interaction between the nuclear MQM and the molecule is given by [86]

$$V_{\rm mol}^{\rm MQM} = -\frac{W_M M}{2I\,(2I-1)}\mathbf{S}'\hat{\mathbf{T}}\mathbf{N}\,, \tag{6.45}$$

where $\mathbf{S}' = \left(S'_\xi, S'_\psi, S'_\zeta\right)$ is an effective spin defined by the equations $S'_\zeta\,|\Omega\rangle = \Omega\,|\Omega\rangle$, $S'_\pm\,|\pm\Omega\rangle = 0$, $S'_\pm\,|\mp\Omega\rangle = |\pm\Omega\rangle$ and $S'_\pm = S'_\xi \pm S'_\psi$ where the coordinates (ξ,ψ,ζ) form the molecular frame of reference with the ζ-axis directed along the vector $\mathbf{N}$ [132–134]. The tensor $\hat{\mathbf{T}}$ is defined as in Eq. (6.14). The factor W_M is the coupling constant of the MQM interaction.

The matrix element of this interaction (assuming maximal projection of the nuclear spin) is

$$\langle f|\, V_{\rm mol}^{\rm MQM}\,|i\rangle \approx (-1)^{2J'-m-\Omega}\, C_{Jm\Omega}^{J'm\Omega} W_M M\,, \tag{6.46}$$

where

$$C_{Jm\Omega}^{J'm\Omega} = -\,(2/3)\,\sqrt{(2J'+1)\,(2J+1)}\begin{pmatrix} J' & 2 & J \\ -m & 0 & m\end{pmatrix}\begin{pmatrix} J' & 2 & J \\ -\Omega & 0 & \Omega\end{pmatrix}. \tag{6.47}$$

Thus, the time for the detection of one transition due to an oscillating nuclear magnetic quadrupole moment is

$$t_{\rm mol}^{\rm MQM} \approx \frac{8\times 10^{17}}{N}\frac{1}{\left(C_{Jm\Omega}^{J'm\Omega}\right)^2}\left(\frac{\omega}{\omega_\Omega}\right)\left(\frac{10^{33}\,\frac{\rm Hz}{e\,\mathrm{cm}^2}}{W_M}\right)^2\left(\frac{10^{-27}\theta_0\, e\,\mathrm{cm}^2}{M}\right)^2 \text{ years}\,, \tag{6.48}$$

where W_M is normalized to a typical value of $10^{33}\frac{\rm Hz}{e\,\mathrm{cm}^2}$ [103] and M to the typical value of $10^{-27}\theta_0\, e\,\mathrm{cm}^2$ (for a nucleus with quadrupole deformation). If the value $2\times 10^{-27}\theta_0\, e\,\mathrm{cm}^2$ is used for M (e.g., ^{179}Hf) then the result is better by a factor of four.

We observe that, for the benchmark values of the parameters, the result (6.48) is thirteen orders of magnitude better than (6.41). If the nucleus in question has no quadrupole deformation, the result is still about eleven orders of magnitude better than using EDMs. Note also that the MQM-induced transition (6.46) is of M2 type, which is convenient for suppressing photon backgrounds (if $J' = J \pm 2$).

6.7 Discussion and Conclusion

In this paper, we presented the possibility of searching for axionic dark matter by means of atomic and molecular transitions induced by oscillating nuclear EDMs, nuclear Schiff moments and nuclear MQMs. While the search would be limited to axion frequencies closely corresponding to resonant atomic

or molecular transitions, the latter can be tuned by using Zeeman and Stark effects. In addition, the transitions are 'dense' in the region of Rydberg excitations, so complete coverage of a frequency interval is, in principle, possible. Molecules also have dense spectra and may present additional advantages for this kind of experiments.

From our estimates, it appears that for a transition frequency $\omega \sim 1\,\mathrm{eV}$, the contribution due to the nuclear Schiff moment (in a nucleus with octupole deformation) and nuclear MQM are comparable to that of the EDM.

On the other hand, in molecular rovibrational transitions, the contribution due to Schiff moment (in a nucleus with octupole deformation) and MQM is many orders of magnitude larger than that due to EDM. This is because MQM and Schiff moment matrix elements are not suppressed by the factor ω^2 like EDM matrix elements (in this respect, atoms with small-ω transitions suffer from the same suppression of the EDM matrix elements). Also, an MQM-induced transition, unlike an EDM-induced or a Schiff-moment-induced one, which must be of E1 type and hence susceptible to photon background, can be of M2 type. Since M2-type transitions are strongly suppressed for photons, the effects of background processes may be limited. Thus, overall, MQMs are better suited for the detection of axions using atomic and molecular transition.

We note that the smallness of the rotational transition frequencies in molecules may pose a problem for the detection of axion signals if one is interested in this frequency range, with black body radiation potentially dominating the counts in the photon detector used to capture fluorescence light emitted when the molecules excited by axion-induced nuclear moments decay. This issue might be overcome by further exciting the excited molecules to a higher electronic state and then detecting the fluorescence emitted when the molecules in this final state relax back to the ground state. Since the frequency of an electronic transition is typically in the eV range, the fluorescence signal registered in the photon detector will not be dominated by black body radiation counts. We note also that this problem may arise only in the detection stage of the experiment. If the initial transition is induced by a nuclear MQM and is of $M2$-type then, as mentioned earlier, the background effects at this stage may be effectively suppressed. We note in passing that one may also explore the possibility of separating the axion induced signal from background noise using the diurnal and annual modulation of the axion field. In short, due the relative motion and orientation of the Sun, Earth and the galaxy, the axion field strength have diurnal and annual modulations with known frequency. if the axion signal can be accumulated over a large period of time, these modulations may be searched for even if background noises exceed the expected signal. For detailed discussions on this topic, we refer the readers to Refs. [135–138].

Finally, we point out that in our considerations, we implicitly assumed that the atoms and molecules in the sample are originally in the ground state. If the sample is in the gaseous phase at a temperature $T \sim 100\,\mathrm{K}$ (we focus on gases to avoid complications arising from the modification of atomic and molecular spectra in liquids and in solids; molecules in noble gas matrices are also a possible candidate) this assumption is reasonable if one targets the axion mass and thus axion-induced transition frequency $\omega \gtrsim 0.1\,\mathrm{eV}$, i.e., using vibrational or electronic transitions (thermal population of the states which lie at $\gtrsim 0.1\,\mathrm{eV}$ is small at this temperature). If, however, one is interested in scanning the small axion mass regime $\omega \sim 10^{-6} - 10^{-3}\,\mathrm{eV}$ with molecules then at $T \sim 100\,\mathrm{K}$, most of the low-lying rotational states have non-negligible thermal populations, which poses a challenge for axion signal discrimination. One approach to improve upon this situation is to use trapped molecules which may be cooled down to μK or even nK (see, e.g., [139] and references therein), assuring that only the ground state is populated. The drawback of this approach is that the relatively small number of trapped molecules N may degrade the statistical sensitivity to the axion. More modern technologies may some day allow us to cool a sufficiently large number particle down to a sufficiently small internal temperatures (see, e.g., [140] and the references therein). Still, the central experimental issue will be separating the axion related signal from the backgrounds, Here, two powerful tools are available for discriminating the useful signal: the M2 character of the axion/MQM induced transition as discussed above and the fact that the axion related signal should represent a sharp resonance with a relative frequency spread of a part per million or smaller, while the photon backgrounds are expected to be broad and non-resonant.

We note finally that the relatively long coherence time of the axion suggests another possibility, in principle, to discriminate axion signals. Here one would apply a resonant laser field weakly driving the transition that is supposed to be driven by the axion-induced oscillating nuclear moments. The probability of the pure photon-induced transition does not depend on the phase of the driving field. However, the axion- and photon-induced amplitudes interfere, and the interference term should reverse with an appropriate phase reversal of the photon field. Since the axion phase is 'reset' every coherence time, the overall interference signature should correspondingly change on the coherence-timescale of the

axion. This peculiar signature is generally not expected from the background signal. An additional benefit of the interference scheme is an enhancement of the signal: the interference term in the transition probability is bilinear in the axion- and photon-induced amplitudes and the latter can be made reasonably large. A brief discussion of interference is presented in Appendix B.

Acknowledgment

The authors thank Mikhail G. Kozlov, Derek F. Jackson Kimball, Alexander O. Sushkov and Igor. B. Samsonov for helpful discussions. This work is supported by the Australian Research Council, the Gutenberg Fellowship and the New Zealand Institute for Advanced Study. It has also received support from the European Research Council (ERC) under the European Union Horizon 2020 Research and Innovation Program (grant agreement No. 695405), from the DFG Reinhart Koselleck Project and the Heising-Simons Foundation.

6.A EDM transition matrix element

In this appendix, we provide the derivation for Eq. (6.34).

The total Hamiltonian of a diatomic molecule with the interaction with nuclear EDMs included is given by

$$\begin{aligned} H &= \frac{\mathbf{P}_1^2}{2M_1} + \frac{\mathbf{P}_2^2}{2M_2} + \sum_{i=1}^{N_e} \frac{\mathbf{p}_i^2}{2m_e} + V_0 + V_{\text{atom}}^{\text{EDM}}\,, \\ V_0 &= -\sum_{i=1}^{N_e} \frac{Z_1 e^2}{|\mathbf{r}_i - \mathbf{R}_2|} - \sum_{i=1}^{N_e} \frac{Z_2 e^2}{|\mathbf{r}_i - \mathbf{R}_2|} + \sum_{i>j}^{N_e} \frac{e^2}{|\mathbf{r}_i - \mathbf{r}_j|} + \frac{Z_2 Z_1 e^2}{|\mathbf{R}_2 - \mathbf{R}_1|}\,, \\ V_{\text{atom}}^{\text{EDM}} &= \frac{\mathbf{d}_1 \cdot \nabla_{\mathbf{R}_1} V_0}{Z_1 e} + \frac{\mathbf{d}_2 \cdot \nabla_{\mathbf{R}_2} V_0}{Z_2 e}\,, \end{aligned} \tag{6.49}$$

where the nuclear positions $\mathbf{R}_{1,2}$, nuclear momenta $\mathbf{P}_{1,2}$, electrons position $\mathbf{r}_i$ and electron momenta $\mathbf{p}_i$ are defined in the laboratory frame.

A change of coordinates to the center-of-mass frame as described in Ref. [130], gives, after discarding the free motion of the molecule

$$\begin{aligned} H &= H_0 + V_{\text{atom}}^{\text{EDM}}\,, \\ H_0 &= \frac{\mathbf{Q}^2}{2\mu_N} + \sum_{i=1}^{N_e} \frac{\mathbf{q}_i^2}{2\mu_e} + \sum_{i\neq j}^{N_e} \frac{\mathbf{q}_i \mathbf{q}_j}{M_N} + V_0\,, \end{aligned} \tag{6.50}$$

where V_0 and $V_{\text{atom}}^{\text{EDM}}$ are now functions of the new variables $\mathbf{X} = \mathbf{R}_1 - \mathbf{R}_2$ and $\mathbf{x}_i = \mathbf{r}_i - (M_1\mathbf{R}_1 + M_2\mathbf{R}_2)/M_N$. The momenta $\mathbf{Q}$ and $\mathbf{q}_i$ are conjugate to $\mathbf{X}$ and $\mathbf{x}_i$, respectively. For convenience, we have defined $M_N = M_1 + M_2$, $M_T = M_N + N_e m_e$, $\mu_N = M_1 M_2/M_N$ and $\mu_e = M_N m_e/\left(M_N + m_e\right)$.

We may then write

$$\begin{aligned} V_{\text{atom}}^{\text{EDM}} &= \frac{\mathbf{d}_1 \cdot \nabla_{\mathbf{R}_1} V_0}{Z_1 e} + \frac{\mathbf{d}_2 \cdot \nabla_{\mathbf{R}_2} V_0}{Z_2 e} = \frac{i\mathbf{d}_1 \cdot [\mathbf{P}_1, H_0]}{Z_1 e\hbar} + \frac{i\mathbf{d}_2 \cdot [\mathbf{P}_2, H_0]}{Z_2 e\hbar} \\ &= \frac{i\mathbf{d}_1 \cdot \left[\mathbf{Q} - \frac{M_1}{M_N}\sum_{i=1}^{N_e} \mathbf{q}_i, H_0\right]}{Z_1 e\hbar} - \frac{i\mathbf{d}_2 \cdot \left[\mathbf{Q} + \frac{M_2}{M_N}\sum_{i=1}^{N_e} \mathbf{q}_i, H_0\right]}{Z_2 e\hbar}\,, \end{aligned} \tag{6.51}$$

so

$$\langle f|\, V_{\text{atom}}^{\text{EDM}}\, |i\rangle = -\frac{i\omega \mathbf{d}_1 \cdot \langle f|\, \mathbf{Q} - \frac{M_1}{M_N}\sum_{i=1}^{N_e} \mathbf{q}_i\, |i\rangle}{Z_1 e\hbar} + \frac{i\omega \mathbf{d}_2 \cdot \langle f|\, \mathbf{Q} + \frac{M_2}{M_N}\sum_{i=1}^{N_e} \mathbf{q}_i\, |i\rangle}{Z_2 e\hbar}\,. \tag{6.52}$$

Using the relations

$$\mathbf{Q} + \left(-1^I\right) \frac{M_I}{M_N} \sum_{i=1}^{N_e} \mathbf{q}_i = \frac{i}{\hbar}\left[H_0, \mu_N \mathbf{X} + \left(-1^I\right) \frac{M_I \mu_e}{M_T} \sum_{i=1}^{N_e} \mathbf{x}_i\right] \tag{6.53}$$

we obtain

$$\langle f|\, V_{\rm mol}^{\rm EDM}\,|i\rangle = \frac{\omega^2\mu_N}{e\sqrt{Z_1Z_2}}\,\langle f|\,\boldsymbol{\delta}\cdot\mathbf{X} - \boldsymbol{\Delta}\cdot\sum_{i=1}^{N_e}\mathbf{x}_i\,|i\rangle\ , \tag{6.54}$$

where

$$\boldsymbol{\delta} = \frac{Z_2\mathbf{d}_1 - Z_1\mathbf{d}_2}{\sqrt{Z_1Z_2}}\,, \tag{6.55}$$

and

$$\boldsymbol{\Delta} = \frac{\mu_e\,(M_1Z_2\mathbf{d}_1 + M_2Z_1\mathbf{d}_2)}{M_T\mu_N\sqrt{Z_1Z_2}} \approx \frac{m_e\,(M_1Z_2\mathbf{d}_1 + M_2Z_1\mathbf{d}_2)}{M_1M_2\sqrt{Z_1Z_2}}\,. \tag{6.56}$$

6.B Interference-assisted detection of rotational transitions

In this appendix, we briefly discuss the possibility of using interference to assist the detection of rotational transitions driven by axion-induced oscillating nuclear MQM.

The photon-induced MQM transition amplitude is given by

$$M_\gamma = \frac{\sqrt{\pi n_\gamma}Ze\omega^{3/2}}{\sqrt{2}Am_p}\,\langle f|\left(\hat{\mathbf{k}}\cdot\mathbf{r}\right)\hat{\mathbf{b}}\cdot(g_R\mathbf{J} + g_N\mathbf{I})\,|i\rangle\ , \tag{6.57}$$

where n_γ is the photon number density, $\hat{\mathbf{k}}$ is the photon propagation unit vector, $\hat{\mathbf{b}} = \hat{\mathbf{k}}\times\hat{\boldsymbol{\epsilon}}$ is the direction of the magnetic component of the photon field, $\mathbf{J}$ is the nucleus' total angular momentum, $\mathbf{I}$ is the nuclear spin and g_R and g_N are the g-factor associated with $\mathbf{J}$ and $\mathbf{I}$. We estimate the transition amplitude (6.57) as

$$M_\gamma \sim \frac{\sqrt{n_\gamma}Ze\omega^{3/2}\bar{X}}{Am_p}\,. \tag{6.58}$$

Note that the photon density may be expressed in terms of the number of photons emitted by the source per unit time P and the cross section σ_γ of the photon beam as $n = P/(c\sigma_\gamma)$.

The ratio between the change in the signal as the axion phase resets and the total signal is

$$r \approx 4\,|M_a/M_\gamma|\ , \tag{6.59}$$

where M_a is the MQM amplitude (6.46). The factor of 4 appears because the cross term contains a factor of 2 and the effect of reversing the axion phase contains another factor of 2.

Substituting Eqs. (6.46) and (6.58) into Eq. (6.59), we obtain

$$r \approx 10^{-4}\frac{A}{Z}\left(\frac{10^{-4}\,\text{eV}}{\omega}\right)^{3/2}\left(\frac{10^{20}/\text{s}}{P}\right)^{1/2}\left(\frac{\sigma_\gamma}{1\,\text{cm}^2}\right)^{1/2}\left(\frac{3a_B}{\bar{X}}\right)\left(\frac{W_M}{10^{33}\,\frac{\text{Hz}}{e\,\text{cm}^2}}\right)\left(\frac{M}{10^{-27}\theta_0\,e\,\text{cm}^2}\right)\,. \tag{6.60}$$

We are also interested in the total number of transitions induced in one axion coherence-time τ_a, which may be approximated by the total number of photons absorbed by the target. The latter may be expressed as

$$N_\gamma = \eta P\tau_a l/l_{\rm abs} = \eta P\tau_a l n_{\rm mol}\sigma_{\rm abs}\,, \tag{6.61}$$

where l is the length of the sample in the direction of photon propagation, $l_{\rm abs} = 1/(n_{\rm mol}\sigma_{\rm abs})$ is the photon absorption length, $n_{\rm mol}$ is the molecular density in the target and $\sigma_{\rm abs}$ is the photon absorption cross section. We have included in Eq. (6.61) the factor η to accommodate the possibility of using a cavity to boost the photon flux.

The axion coherence-time may be written as

$$\tau_a = 10^6\times\frac{2\pi}{m_a} = 10^6\times\frac{2\pi}{\omega}\,, \tag{6.62}$$

where we have imposed the condition that the axion mass is in resonance with the transition frequency.

The cross section $\sigma_{\rm abs}$ is given by [see Eq. (6.58)]

$$\sigma_{\rm abs} = \frac{4\pi}{\omega^2}\frac{\Gamma_{\rm abs}}{\Gamma_{\rm tot}}\ ,\quad \Gamma_{\rm abs} = \frac{\omega^2}{(2\pi)^2}\left(\frac{Ze\omega^{3/2}\bar{X}}{Am_p}\right)^2\ , \tag{6.63}$$

where $\Gamma_{\rm tot}$ is the total width of the transition driven by the photons and the axion-induced oscillating nuclear MQM.

Substituting Eqs. (6.62) and (6.63) into Eq. (6.61), we obtain

$$N_\gamma = 2\times 10^6\,\frac{\eta P l n_{\rm mol}}{\Gamma_{\rm tot}}\left(\frac{Ze\omega\bar{X}}{Am_p}\right)^2\,, \tag{6.64}$$

which gives

$$N_\gamma \approx 1.7\times 10^3\left(\frac{Z}{A}\right)^2\left(\frac{\eta}{10^6}\right)\left(\frac{P}{10^{20}\,{\rm s}^{-1}}\right)\left(\frac{l}{1\,{\rm m}}\right)\left(\frac{10^{-10}\,{\rm eV}}{\Gamma_{\rm tot}}\right)\left(\frac{n_{\rm mol}}{10^{18}\,{\rm cm}^{-3}}\right)\left(\frac{\bar{X}}{3a_B}\right)^2\left(\frac{\omega}{10^{-4}\,{\rm ev}}\right)^2\,. \tag{6.65}$$

We note finally that ultimately, the feasibility of the interference scheme discussed here requires at least one axion-induced transition to occur per axion coherence-time. From Eqs. (6.48) and (6.62), we observe that this, in turn, requires a sample which contains some 10^{30} molecules. Achieving such a large number of molecules while maintaining a reasonable sample size is a challenge which may be overcome with future development in experimental techniques.

Bibliography

[1] R. D. Peccei and H. R. Quinn, Phys. Rev. Lett. **38**, 1440 (1977).

[2] R. D. Peccei, *The Strong* CP *Problem and Axions* (Springer, Berlin, Heidelberg, 2008), pp. 3–17.

[3] S. Weinberg, Phys. Rev. Lett. **40**, 223 (1978).

[4] F. Wilczek, Phys. Rev. Lett. **40**, 279 (1978).

[5] P. Sikivie, Phys. Rev. Lett. **51**, 1415 (1983).

[6] P. Sikivie, Phys. Rev. D **32**, 2988 (1985).

[7] S. Moriyama, M. Minowa, T. Namba, Y. Inoue, Y. Takasu, and A. Yamamoto, Phys. Lett. B **434**, 147 (1998).

[8] Y. Inoue, T. Namba, S. Moriyama, M. Minowa, Y. Takasu, T. Horiuchi, and A. Yamamoto, Phys. Lett. B **536**, 18 (2002).

[9] Y. Inoue, Y. Akimoto, R. Ohta, T. Mizumoto, A. Yamamoto, and M. Minowa, Phys. Lett. B **668**, 93 (2008).

[10] R. Ohta, Y. Akimoto, Y. Inoue, M. Minowa, T. Mizumoto, S. Moriyama, T. Namba, Y. Takasu, and A. Yamamoto, Nucl. Instr. Meth. A **670**, 73 (2012).

[11] T. Mizumoto, R. Ohta, T. Horie, J. Suzuki, Y. Inoue, and M. Minowa, J. Cosmo. Astropart. Phys. **07**, 013 (2013).

[12] K. Zioutas et al., Nucl. Instrum. Meth. A **425**, 480 (1999).

[13] E. Arik et al., J. Cosmo. Astropart. Phys. **02**, 008 (2009).

[14] K. Barth et al., J. Cosmo. Astropart. Phys. **05**, 010 (2013).

[15] V. Anastassopoulos et al. (CAST Collaboration), Nat. Phys. **13**, 584 (2017).

[16] F. T. Avignone, D. Abriola, R. L. Brodzinski, J. I. Collar, R. J. Creswick, D. E. DiGregorio, H. A. Farach, A. O. Gattone, C. K. Guérard, F. Hasenbalg, et al. (SOLAX Collaboration), Phys. Rev. Lett. **81**, 5068 (1998).

[17] A. Gattone et al., Nucl. Phys. B - Proc. Suppl. **70**, 59 (1999).

[18] A. Morales et al., Astropar. Phys. **16**, 325 (2002).

[19] Z. Ahmed et al. (CDMS Collaboration), Phys. Rev. Lett. **103**, 141802 (2009).

[20] Z. Ahmed et al. (CDMS Collaboration), Phys. Rev. Lett. **106**, 131302 (2011).

[21] R. Agnese et al. (CDMS Collaboration), Phys. Rev. Lett. **111**, 251301 (2013).

[22] R. Agnese et al. (SuperCDMS Collaboration), Phys. Rev. Lett. **112**, 241302 (2014).

[23] I. Irastorza et al., J. Cosmo. Astropar. Phys. **06**, 013 (2011).

[24] I. G. Irastorza et al. (IAXO Collaboration), Tech. Rep. CERN-SPSC-2013-022. SPSC-I-242, CERN, Geneva (2013).

[25] E. Armengaud et al., J. Instrum. **9**, T05002 (2014).

[26] S. J. Asztalos, G. Carosi, C. Hagmann, D. Kinion, K. van Bibber, M. Hotz, L. J. Rosenberg, G. Rybka, J. Hoskins, J. Hwang, et al., Phys. Rev. Lett. **104**, 041301 (2010).

[27] A. Wagner, G. Rybka, M. Hotz, L. J. Rosenberg, S. J. Asztalos, G. Carosi, C. Hagmann, D. Kinion, K. van Bibber, J. Hoskins, et al., Phys. Rev. Lett. **105**, 171801 (2010).

[28] J. Hoskins, J. Hwang, C. Martin, P. Sikivie, N. S. Sullivan, D. B. Tanner, M. Hotz, L. J. Rosenberg, G. Rybka, A. Wagner, et al., Phys. Rev. D **84**, 121302 (2011).

[29] S. A. Kenany et al., Nucl. Instrum. Meth. A **854**, 11 (2017).

[30] B. M. Brubaker, L. Zhong, Y. V. Gurevich, S. B. Cahn, S. K. Lamoreaux, M. Simanovskaia, J. R. Root, S. M. Lewis, S. Al Kenany, K. M. Backes, et al., Phys. Rev. Lett. **118**, 061302 (2017).

[31] B. T. McAllister, G. Flower, E. N. Ivanov, M. Goryachev, J. Bourhill, and M. E. Tobar, Phys.Dark Univ **18**, 67 (2017).

[32] K. Ehret, M. Frede, E.-A. Knabbe, D. Kracht, A. Lindner, N. T. Meyer, D. Notz, A. Ringwald, and G. Wiedemann, arXiv:0702023 (2007).

[33] K. Ehret, M. Frede, S. Ghazaryan, M. Hildebrandt, E.-A. Knabbe, D. Kracht, A. Lindner, J. List, T. Meier, N. Meyer, et al., Nucl. Instrum. Meth. A **612**, 83 (2009).

[34] K. Ehret, M. Frede, S. Ghazaryan, M. Hildebrandt, E.-A. Knabbe, D. Kracht, A. Lindner, J. List, T. Meier, N. Meyer, et al., Phys. Lett. B **689**, 149 (2010).

[35] P. Pugnat, L. Duvillaret, R. Jost, G. Vitrant, D. Romanini, A. Siemko, R. Ballou, B. Barbara, M. Finger, M. Finger, et al. (OSQAR Collaboration), Phys. Rev. D **78**, 092003 (2008).

[36] P. Pugnat et al. (OSQAR Collaboration), Eur. Phys. J. C **74**, 3027 (2014).

[37] R. Ballou, G. Deferne, M. Finger, M. Finger, L. Flekova, J. Hosek, S. Kunc, K. Macuchova, K. A. Meissner, P. Pugnat, et al. (OSQAR Collaboration), Phys. Rev. D **92**, 092002 (2015).

[38] A. S. Chou, W. Wester, A. Baumbaugh, H. R. Gustafson, Y. Irizarry-Valle, P. O. Mazur, J. H. Steffen, R. Tomlin, X. Yang, and J. Yoo, Phys. Rev. Lett. **100**, 080402 (2008).

[39] G. Cantatore, F. D. Valle, E. Milotti, L. Dabrowski, and C. Rizzo, Phys. Lett. B **265**, 418 (1991).

[40] E. Zavattini, G. Zavattini, G. Ruoso, G. Raiteri, E. Polacco, E. Milotti, V. Lozza, M. Karuza, U. Gastaldi, G. Di Domenico, et al. (PVLAS Collaboration), Phys. Rev. D **77**, 032006 (2008).

[41] F. Della Valle, A. Ejlli, U. Gastaldi, G. Messineo, E. Milotti, R. Pengo, G. Ruoso, and G. Zavattini, Eur. Phys. J. C **76**, 24 (2016).

[42] S. J. Chen, H. H. Mei, and W. T. Ni, Mod. Phys. Lett. A **22**, 2815 (2007).

[43] R. Battesti, B. Pinto Da Souza, S. Batut, C. Robilliard, G. Bailly, C. Michel, M. Nardone, L. Pinard, O. Portugall, G. Trénec, et al., Eur. Phys. J. D **46**, 323 (2008).

[44] J. Jackel, A. Lindner, and J. Redondo, eds., *Proceedings, 5th Patras Workshop on Axions, WIMPs and WISPs (AXION-WIMP 2009)*, DESY (DESY, Hamburg, Germany, 2010).

[45] L. Maiani, R. Petronzio, and E. Zavattini, Phys. Lett. B **175**, 359 (1986).

[46] R. Barbieri, M. Cerdonio, G. Fiorentini, and S. Vitale, Phys. Lett. B **226**, 357 (1989).

[47] R. Barbieri, C. Braggio, G. Carugno, C. Gallo, A. Lombardi, A. Ortolan, R. Pengo, G. Ruoso, and C. Speake, Phys. Dark Univ **15**, 135 (2017).

[48] D. Horns, J. Jaeckel, A. Lindner, A. Lobanov, J. Redondo, and A. Ringwald, J. Cosmo. Astropart. Phys. **04**, 016 (2013).

[49] J. Jaeckel and J. Redondo, Phys. Rev. D **88**, 115002 (2013).

[50] A. J. Millar, G. G. Raffelt, J. Redondo, and F. D. Steffen, J. Cosmo. Astropart. Phys **01**, 061 (2017).

[51] A. Caldwell, G. Dvali, B. Majorovits, A. Millar, G. Raffelt, J. Redondo, O. Reimann, F. Simon, and F. Steffen (MADMAX Collaboration), Phys. Rev. Lett. **118**, 091801 (2017).

[52] J. E. Moody and F. Wilczek, Phys. Rev. D **30**, 130 (1984).

[53] A. Arvanitaki and A. A. Geraci, Phys. Rev. Lett. **113**, 161801 (2014).

[54] Y. V. Stadnik, V. A. Dzuba, and V. V. Flambaum, Phys. Rev. Lett. **120**, 013202 (2018).

[55] V. A. Dzuba, V. V. Flambaum, I. B. Samsonov, and Y. V. Stadnik, Phys. Rev. D **98**, 035048 (2018).

[56] Y. Kahn, B. R. Safdi, and J. Thaler, Phys. Rev. Lett. **117**, 141801 (2016).

[57] G. Ruoso, A. Lombardi, A. Ortolan, R. Pengo, C. Braggio, G. Carugno, C. S. Gallo, and C. C. Speake, J. Phys. - Conf. Ser **718**, 042051 (2016).

[58] Y. Hochberg, T. Lin, and K. M. Zurek, Phys. Rev. D **94**, 015019 (2016).

[59] Y. Hochberg, T. Lin, and K. M. Zurek, Phys. Rev. D **95**, 023013 (2017).

[60] P. Sikivie, N. Sullivan, and D. B. Tanner, Phys. Rev. Lett. **112**, 131301 (2014).

[61] S. Chaudhuri, P. W. Graham, K. Irwin, J. Mardon, S. Rajendran, and Y. Zhao, Phys. Rev. D **92**, 075012 (2015).

[62] M. Silva-Feaver, S. Chaudhuri, H. M. Cho, C. Dawson, P. Graham, K. Irwin, S. Kuenstner, D. Li, J. Mardon, H. Moseley, et al., EEE Trans. Appl. Supercond **27**, 1 (2017).

[63] C. Beck, Phys. Rev. Lett. **111**, 231801 (2013).

[64] C. Beck, Phys. Dark Univ. **7-8**, 6 (2015).

[65] H. Tam and Q. Yang, Phys. Lett. B **716**, 435 (2012).

[66] A. Arvanitaki, S. Dimopoulos, and K. Van Tilburg, Phys. Rev. X **8**, 041001 (2018).

[67] C. Braggio et al., eds., *New detectors for axions* (Turin, Italy, 2017).

[68] C. J. Cao and A. Zhitnitsky, Phys. Rev. D **96**, 015013 (2017).

[69] M. Yoshimura and N. Sasao, arXiv:1710.11262 (2017).

[70] H. T. Tan, V. Flambaum, I. Samsonov, Y. Stadnik, and D. Budker, Phys. Dark Univ. **24**, 100272 (2019).

[71] P. W. Graham and S. Rajendran, Phys. Rev. D **84**, 055013 (2011).

[72] D. Budker, P. W. Graham, M. Ledbetter, S. Rajendran, and A. O. Sushkov, Phys. Rev. X **4**, 021030 (2014).

[73] P. W. Graham and S. Rajendran, Phys. Rev. D **88**, 035023 (2013).

[74] Y. V. Stadnik and V. V. Flambaum, Phys. Rev. D **89**, 043522 (2014).

[75] C. Abel et al., Phys. Rev. X **7**, 041034 (2017).

[76] P. W. Graham and S. Rajendran, Phys. Rev. D **88**, 035023 (2013).

[77] A. Garcon et al., arXiv:1902.04644 (2019).

[78] T. Wu, J. W. Blanchard, D. F. Jackson Kimball, M. Jiang, and D. Budker, Phys. Rev. Lett. **121**, 023202 (2018).

[79] C. Abel, N. J. Ayres, G. Ban, G. Bison, K. Bodek, V. Bondar, M. Daum, M. Fairbairn, V. V. Flambaum, P. Geltenbort, et al., Phys. Rev. X **7**, 041034 (2017).

[80] I. M. Bloch, Y. Hochberg, E. Kuflik, and T. Volansky, arXiv:1907.03767 (2019).

[81] C. Smorra, Y. Stadnik, P. Blessing, M. Bohman, M. Borchert, J. Devlin, S. Erlewein, J. Harrington, T. Higuchi, A. Mooser, et al., Nature **575**, 310 (2019).

[82] A. Arvanitaki, S. Dimopoulos, and K. Van Tilburg, Phys. Rev. X **8**, 041001 (2018).

[83] R. Crewther, P. D. Vecchia, G. Veneziano, and E. Witten, Physics Letters B **88**, 123 (1979).

[84] N. Yamanaka, B. K. Sahoo, N. Yoshinaga, T. Sato, K. Asahi, and B. P. Das, Eur. Phys. J. A **53**, 54 (2017).

[85] W. C. Haxton and E. M. Henley, Phys. Rev. Lett. **51**, 1937 (1983).

[86] O. Sushkov, V. Flambaum, and I. Khriplovich, Sov. Phys. - JETP **60**, 1521 (1984).

[87] V. Flambaum, I. Khriplovich, and O. Sushkov, Phys. Letts. B **162**, 213 (1985).

[88] V. Flambaum, I. Khriplovich, and O. Sushkov, Nucl. Phys. A **449**, 750 (1986).

[89] I. Khriplovich and R. Korkin, Nuclear Physics A **665**, 365 (2000).

[90] N. Yoshinaga, K. Higashiyama, and R. Arai, Prog. Theor. Phys. **124**, 1115 (2010).

[91] E. Mereghetti, J. de Vries, W. Hockings, C. Maekawa, and U. van Kolck, Phys. Letts. B **696**, 97 (2011).

[92] J. de Vries, E. Mereghetti, R. G. E. Timmermans, and U. van Kolck, Phys. Rev. Lett. **107**, 091804 (2011).

[93] J. de Vries, R. Higa, C.-P. Liu, E. Mereghetti, I. Stetcu, R. G. E. Timmermans, and U. van Kolck, Phys. Rev. C **84**, 065501 (2011).

[94] A. Wirzba, Nuclear Physics A **928**, 116 (2014).

[95] W. Dekens, J. de Vries, J. Bsaisou, W. Bernreuther, C. Hanhart, U.-G. Meißner, A. Nogga, and A. Wirzba, J. High Energy Phys. **2014**, 69 (2014).

[96] N. Yoshinaga, K. Higashiyama, R. Arai, and E. Teruya, Phys. Rev. C **89**, 045501 (2014).

[97] J. Bsaisou, J. de Vries, C. Hanhart, S. Liebig, U.-G. Meißner, D. Minossi, A. Nogga, and A. Wirzba, J. High Energy Phys. **2015**, 104 (2015).

[98] J. de Vries, E. Mereghetti, and A. Walker-Loud, Phys. Rev. C **92**, 045201 (2015).

[99] N. Yamanaka and E. Hiyama, Phys. Rev. C **91**, 054005 (2015).

[100] N. Yamanaka, Int. J. Mod. Phys. A **26**, 1730002 (2017).

[101] N. Yamanaka, T. Yamada, E. Hiyama, and Y. Funaki, Phys. Rev. C **95**, 065503 (2017).

[102] N. Yamanaka, T. Yamada, and Y. Funaki, arXiv:1907.08091 (2019).

[103] V. V. Flambaum, D. DeMille, and M. G. Kozlov, Phys. Rev. Lett. **113**, 103003 (2014).

[104] T. E. Chupp, P. Fierlinger, M. J. Ramsey-Musolf, and J. T. Singh, Rev. Mod. Phys. **91**, 015001 (2019).

[105] L. I. Schiff, Phys. Rev. **132**, 2194 (1963).

[106] V. Spevak, N. Auerbach, and V. V. Flambaum, Phys. Rev. C **56**, 1357 (1997).

[107] V. V. Flambaum and J. S. M. Ginges, Phys. Rev. A **65**, 032113 (2002).

[108] J. H. deJesus and J. Engel, Phys. Rev. C **72**, 045503 (2005).

[109] V. F. Dmitriev and R. A. Sen'kov, Phys. Rev. Lett. **91**, 212303 (2003).

[110] S. Ban, J. Dobaczewski, J. Engel, and A. Shukla, Phys. Rev. C **82**, 015501 (2010).

[111] V. V. Flambaum and H. Feldmeier, Phys. Rev. C **101**, 015502 (2020).

[112] D. Cho, K. Sangster, and E. A. Hinds, Phys. Rev. A **44**, 2783 (1991).

[113] W. C. Griffith, M. D. Swallows, T. H. Loftus, M. V. Romalis, B. R. Heckel, and E. N. Fortson, Phys. Rev. Lett. **102**, 101601 (2009).

[114] B. Graner, Y. Chen, E. G. Lindahl, and B. R. Heckel, Phys. Rev. Lett. **116**, 161601 (2016).

[115] N. Auerbach, V. V. Flambaum, and V. Spevak, Phys. Rev. Lett. **76**, 4316 (1996).

[116] J. Engel, M. Bender, J. Dobaczewski, J. H. deJesus, and P. Olbratowski, Phys. Rev. C **68**, 025501 (2003).

[117] J. Dobaczewski, J. Engel, M. Kortelainen, and P. Becker, Phys. Rev. Lett. **121**, 232501 (2018).

[118] V. V. Flambaum and V. A. Dzuba, arXiv:1912.03598 (2019).

[119] I. Khriplovich, Zh. Ehks. Teor. Fiz. **71**, 51 (1976 [Sov. Phys. JETP **44**, 25 (1976)).

[120] L. V. Skripnikov, A. V. Titov, and V. V. Flambaum, Phys. Rev. A **95**, 022512 (2017).

[121] V. Flambaum, Physics Letters B **320**, 211 (1994).

[122] B. G. C. Lackenby and V. V. Flambaum, Phys. Rev. D **98**, 115019 (2018).

[123] G. P. Centers et al., arXiv: 1905.13650 (2019).

[124] L. Landau and E. Lifshitz, *Quantum Mechanics* (Pergamon press, Oxford, 1965).

[125] H. Bethe and E. Salpeter, *Quantum Mechanics of One- and Two-Electron Atoms* (Springer, 1957).

[126] V. A. Dzuba, V. V. Flambaum, and J. S. M. Ginges, Phys. Rev. A **61**, 062509 (2000).

[127] V. B. Klaer and G. D. Moore, J. Cosmol. Astropart. Phys. **2017**, 049 (2017).

[128] M. Buschmann, J. W. Foster, and B. R. Safdi, arXiv: 1906.00967 (2019).

[129] M. Gorghetto, E. Hardy, and G. Villadoro, J. High Energy Phys. **2018**, 151 (2018).

[130] H. B. Tran Tan, V. V. Flambaum, and I. B. Samsonov, Phys. Rev. A **99**, 013430 (2019).

[131] V. V. Flambaum, Phys. Rev. C **99**, 035501 (2019).

[132] M. G. Kozlov, V. I. Fomichev, Y. Y. Dmitriev, L. N. Labzovsky, and A. V. Titov, J. Phys. B **20**, 4939 (1987).

[133] Y. Dmitriev, Y. Khait, M. Kozlov, L. Labzovsky, A. Mitrushenkov, A. Shtoff, and A. Titov, Phys. Letts. A **167**, 280 (1992).

[134] M. G. Kozlov and L. N. Labzowsky, J. Phys. B **28**, 1933 (1995).

[135] R. Bernabei, P. Belli, R. Cerulli, F. Montecchia, F. Nozzoli, A. Incicchitti, D. Prosperi, C. Dai, H. He, H. Kuang, et al., Phys. Lett. B **515**, 6 (2001).

[136] R. Bernabei, P. Belli, F. Montecchia, F. Nozzoli, F. Cappella, A. Incicchitti, D. Prosperi, R. Cerulli, C. J. Dai, H. L. He, et al., Int. J. Mod. Phys. A **21**, 1445 (2006).

[137] R. Bernabei et al., Eur. Phys. J. C **67**, 39 (2010).

[138] D. Budker, V. V. Flambaum, X. Liang, and A. Zhitnitsky, Phys. Rev. D **101**, 043012 (2020).

[139] L. Anderegg, B. L. Augenbraun, Y. Bao, S. Burchesky, L. W. Cheuk, W. Ketterle, and J. M. Doyle, Nat. Phys. **14**, 890 (2018).

[140] S. M. Rochester, K. Szymański, M. Raizen, S. Pustelny, M. Auzinsh, and D. Budker, Phys. Rev. A **94**, 043416 (2016).

Chapter 7

Limits on CP-violating hadronic interactions and nucleon EDMs from paramagnetic molecules

7.1 Overview

Oscillating electric fields and nuclear EDMs are not the only mechanisms through which Schiff's theorem may be overcome. In fact, since Schiff's theorem only applies to systems that interact electrically, one may expect that when magnetic interactions are taken into account, the difficulty posed by Schiff's theorem no longer persists. In this chapter, I show that a static nuclear EDM can induce an atomic EDM via the combined interactions of the nucleon EDMs and magnetic dipole moments with the electrons. It is important to note that this effect takes place even in paramagnetic atoms which have no nuclear magnetic dipole moment. From this analysis, I derive independent bounds on nucleon EDMs and other hadronic CP-violating parameters.

As a result of my research, I have published this paper:

1. V. V. Flambaum, I. B. Samsonov and H. B. Tran Tan
   Limits on CP-violating hadronic interactions and proton EDM from paramagnetic molecules
   J. High Energ. Phys. 2020, 77 (2020), DOI: 10.1007/JHEP10(2020)077, arXiv:2004.10359.

7.2 Abstract

Experiments with paramagnetic ground or metastable excited states of molecules (ThO, HfF^+, YbF, YbOH, BaF, PbO, etc.) provide strong constraints on electron electric dipole moment (EDM) and coupling constant C_{SP} of contact semileptonic interaction. We compute new contributions to C_{SP} arising from the nucleon EDMs due to combined electric and magnetic electron-nucleon interaction. This allows us to improve limits from the experiments with paramagnetic molecules on the CP-violating parameters, such as the proton EDM, $|d_p| < 1.1 \times 10^{-23} e\cdot$cm, the QCD vacuum angle, $|\bar{\theta}| < 1.4 \times 10^{-8}$, as well as the quark chromo-EDMs and π-meson-nucleon couplings. Our results may also be used to search for the axion dark matter which produces oscillating $\bar{\theta}$.

7.3 Introduction

The Standard Model of elementary particles naturally incorporates the sources for CP (charge and parity) violation represented by the Cabibbo–Kobayashi–Maskawa (CKM) matrix [1, 2] and the QCD vacuum angle [3–5] (see also Refs. [6, 7] and further references therein). While the elements of the CKM matrix are measured to a high accuracy, the exact value of the QCD vacuum angle $\bar{\theta}$ is not known. In recent years, the precision in modern atomic and molecular EDM experiments has been improved to such a level that constraints on $\bar{\theta}$ and other CP-violating parameters imposed by these experiments are approaching or even exceeding those of particle physics [8–14]. For example, experiments with diamagnetic

atoms and molecules targeting the nuclear Schiff moments have placed significant bounds on the nucleon EDMs [8, 12, 14–26] whereas those using paramagnetic polar molecules [10, 27–31] give rise to the most stringent constraints on the electron EDM.

In paramagnetic atoms, an atomic EDM may be induced by the following contact CP-odd semileptonic operators

$$\mathcal{L} = \frac{G_F}{\sqrt{2}} C_{SP}^p \, \bar{e} i\gamma_5 e \, \bar{p}p + \frac{G_F}{\sqrt{2}} C_{SP}^n \, \bar{e} i\gamma_5 e \, \bar{n}n \,, \tag{7.1}$$

where G_F is the Fermi coupling constant, e, p and n are respectively the electron, proton and neutron fields; C_{SP}^p and C_{SP}^n are the electron couplings to the proton and neutrons, respectively. The subscript SP denotes the nucleon-scalar and electron pseudoscalar two-fermion bilinears.

In polarised polar molecules, the interaction (7.1) induces shifts of energy levels. The measurement of these shifts places constraints on the value of $C_{SP} \equiv C_{SP}^p Z/A + C_{SP}^n N/A$, where A and Z are the nuclear mass and charge numbers, and $N = A - Z$ is the number of neutrons. The most stringent constraint on C_{SP} is placed by the ACME collaboration [31], which used the molecule ^{232}ThO, (90% C.L.)

$$|C_{SP}|_{\rm Th} < 7.3 \times 10^{-10} \,. \tag{7.2}$$

The coupling constant C_{SP} receives contributions from various sources, which include interactions with the nucleon EDM $d_{p,n}$. The parameters $d_{p,n}$ may, in turn, be expressed in terms of more fundamental ones, namely, the CP-odd π-meson-nucleon coupling constants $\bar{g}_{\pi NN}^{(0,1)}$, the quark chromo-EDMs $\tilde{d}_{d,u}$ and the QCD vacuum angle $\bar{\theta}$. Our aim is to determine the leading dependence of C_{SP} on the parameters $d_{p,n}$, $\bar{g}_{\pi NN}^{(0,1)}$, $\tilde{d}_{d,u}$ and $\bar{\theta}$ for ^{232}Th and several other atoms of experimental interest, including Ba, Yb, Hf, Pb and Ra. Note that CP-violating effects rapidly increase with nuclear charge (see next sections). Therefore, in molecules the effects come from the heaviest nucleus.

In a recent paper [32], the contributions to C_{SP} from the two-photon and π, η-meson exchanges between electrons and nucleons were calculated. These contributions led to a limit on the QCD vacuum angle $|\bar{\theta}| \lesssim 3 \times 10^{-8}$. In this paper, we take into account additional contributions to C_{SP} which are comparable or even bigger than those calculated in Ref. [32], namely, contribution of nucleon transitions in discrete spectrum (which are enhanced by small energy denominators in perturbation theory). We take into account the effect of the Coulomb interaction in intermediate electron states. In heavy atoms like thorium with $Z = 90$, the parameter $Z\alpha \sim 1$ and the Coulomb interaction is important.

As we will demonstrate further, the addition of the new contributions allows us to significantly improve the limits on the QCD vacuum angle and other CP-violating hadronic parameters. We stress that these results play important role in the search of axion-like dark matter [33] which manifests itself as oscillating $\bar{\theta}$-term (see, e.g., Ref. [34]).

It is important to note that, according to a theorem by Schiff [35], atomic electrons completely shield the nuclear EDM. However, it can be measured through the nuclear Schiff moments and magnetic quadrupole moments [36–38], or by means of applying an oscillating electric field and observing nuclear spin rotations as argued in the Refs. [39–43]. However, since the Schiff theorem applies only to a system which interacts electrically, the interaction of the atomic electrons with the magnetic dipole moment of the nucleus allows for a non-zero atomic EDM induced by a nuclear EDM [35]. This paper is devoted to the study of the mechanism for the production of the atomic EDM from the combined electric and magnetic interactions between the atomic electrons and the nucleus.

In Ref. [44], it was argued that for atoms with vanishing nuclear spins there are no non-vanishing contributions to the atomic EDM from CP-violating nuclear scalar polarizability. However, the analysis of Ref. [44] did not take into account specific near-nucleus electronic contributions which cannot be reduced to the CP-violating nuclear scalar polarizability and are significantly enhanced by relativistic effects in heavy atoms. Indeed, since the electronic s and p Dirac wave functions for a point-like nucleus are singular at the origin, the electronic matrix elements between these states are formally divergent and thus make significant contributions to the induced atomic EDM. In this paper, we will systematically analyze the contributions to the atomic EDM from such matrix elements in atoms with vanishing nuclear spins and compare them with those arising from the contact electron-nucleon interaction (7.1). This will allow us to obtain the leading-order dependence $C_{SP} = C_{SP}(d_{p,n}, \bar{g}_{\pi NN}^{(0,1)}, \tilde{d}_{d,u}, \bar{\theta})$ for several atoms of experimental interest and deduce improved limits on the CP-violating hadronic parameters.

The rest of the paper is organized as follows. In Sect. 7.4, we present an estimate for the atomic EDM arising from the contact electron-nucleon interaction. Section 7.5 is devoted to the computation of the atomic EDM induced by nucleon permanent EDMs. In Sect. 7.6, we compare the contributions to the atomic EDM from the contact electron-nucleon interaction and the nucleon permanent EDMs and

find relations between the constant C_{SP} and CP-violating hadronic parameters. In Sect. 7.7 we give a summary of our results and provide some comments on assumptions and precision. Technical details of calculations of electronic and nuclear matrix elements are collected in appendices.

Throughout this paper we use natural units with $c = \hbar = 1$.

7.4 Atomic EDM due to contact electron-nucleon interaction

In an atom, the CP-odd interaction (7.1) between a valence electron and the nucleus is described by the Hamiltonian [45]

$$H_{\rm cont} = \frac{iG_F}{\sqrt{2}} A C_{SP} \gamma_0 \gamma_5 \rho(\mathbf{R}) \,, \tag{7.3}$$

where $\gamma_0 = \begin{pmatrix} \mathbb{1}_{2\times2} & 0 \\ 0 & -\mathbb{1}_{2\times2} \end{pmatrix}$ and $\gamma_5 = \begin{pmatrix} 0 & -\mathbb{1}_{2\times2} \\ -\mathbb{1}_{2\times2} & 0 \end{pmatrix}$ are the Dirac matrices, $\mathbf{R}$ is the position vector of the electron and $\rho(\mathbf{R})$ is the normalized nuclear charge density. In the leading approximation, $\rho(\mathbf{R})$ is constant inside the nucleus of radius R_0 and vanishes outside, $\rho(\mathbf{R}) = 3\theta(R_0 - R)/(4\pi R_0^3)$, where $\theta(x)$ is the Heaviside step function.

Matrix elements of the operator (7.3) receive non-vanishing contributions only from small distances, where the nuclear density $\rho(\mathbf{R})$ is different from zero. In heavy nuclei, the $s_{1/2}$ and $p_{1/2}$ electron wave functions have large relativistic enhancement inside the nucleus, as compared with other wave functions corresponding to higher angular momenta l which are negligible at the nucleus ($\propto R^l$) [45]. As a result, the atomic EDM receives dominant contributions from the matrix element of the operator (7.3) with the $s_{1/2}$ and $p_{1/2}$ states,

$$\mathbf{d} \approx 2 \frac{\langle s_{1/2}| \, e\mathbf{R} \, |p_{1/2}\rangle \, \langle p_{1/2}| \, H_{\rm cont} \, |s_{1/2}\rangle}{E_{p_{1/2}} - E_{s_{1/2}}} \,, \tag{7.4}$$

where $E_{s_{1/2}}$ and $E_{p_{1/2}}$ are the energies of the $s_{1/2}$ and $p_{1/2}$ states, respectively, and $-e$ is the electron charge.

Here, we will estimate the matrix element $\langle p_{1/2}| \, H_{\rm cont} \, |s_{1/2}\rangle$ for heavy atoms. In subsequent sections, this matrix element will be compared with those of CP-odd operators originating from nucleon EDMs.

For an atom with a point-like nucleus, the $s_{1/2}$ and $p_{1/2}$ valence electron wave functions have simple analytic expressions, see Eqs. (7.42). For an extended nucleus model with constant charge density, it is sufficient to consider a simple continuation of the wave functions (7.42) to the region inside the nucleus as

$$|s_{1/2}\rangle = c_{s_{1/2}} \frac{R_0^{\gamma-1}}{\Gamma(2\gamma+1)} \left(\frac{2Z}{a_B}\right)^{\gamma} \begin{pmatrix} -(\gamma+1)\Omega_\mu^{-1} \\ \frac{iZ\alpha R}{R_0}\Omega_\mu^1 \end{pmatrix} , \tag{7.5a}$$

$$|p_{1/2}\rangle = c_{p_{1/2}} \frac{R_0^{\gamma-1}}{\Gamma(2\gamma+1)} \left(\frac{2Z}{a_B}\right)^{\gamma} \begin{pmatrix} \frac{(1-\gamma)R}{R_0}\Omega_\mu^1 \\ iZ\alpha\Omega_\mu^{-1} \end{pmatrix} , \tag{7.5b}$$

where Ω_μ^κ is the spherical spinor, a_B is the Bohr radius, $\gamma = \sqrt{1 - Z^2\alpha^2}$ is the relativistic factor and $\alpha \approx 1/137$ is the fine structure constant. The values of the normalization constants $c_{s_{1/2}}$, $c_{p_{1/2}}$ are not specified here, as our final results will be independent from these constants.

With the wave functions (7.5), the matrix element of the operator (7.3) reads

$$\langle p_{1/2}| \, H_{\rm cont} \, |s_{1/2}\rangle = -c_{s_{1/2}} c_{p_{1/2}} \frac{G_F C_{SP}}{10\sqrt{2}\pi} \frac{1+4\gamma}{\Gamma(2\gamma+1)^2} \frac{AZ\alpha}{R_0^2} \left(\frac{2ZR_0}{a_B}\right)^{2\gamma} . \tag{7.6}$$

For heavy nuclei, this matrix element is significantly enhanced due to the factor $AZ^{2\gamma+1}$. Since we will compare Eq. (7.6) with the contribution from nucleon EDMs, which is not enhanced that strongly, it appears that for the ratio of the effects (which is the contribution from nucleon EDMs to the effective constant C_{SP}) lighter nuclei may have bigger C_{SP} than heavy ones.

7.5 Contribution to the atomic EDM from nucleon permanent EDMs

In this section, we calculate the contribution to the atomic EDM originating from permanent nucleon EDMs. Since electric interactions alone cannot give rise to atomic EDMs due to the Schiff theorem [35],

such a contribution can only arise when both the electric and magnetic electron-nucleon interactions are taken into account. We start with the review of the effective Hamiltonian of this interaction and in subsequent subsections calculate the nuclear and electronic matrix elements of this Hamiltonian.

7.5.1 Effective Hamiltonian for the CP-odd electron-nucleon interaction

Let $\mathbf{d}_i = d_i \boldsymbol{\sigma}_i$ and $\boldsymbol{\mu}_i = \mu_0(g_i^l \mathbf{l}_i + g_i^s \mathbf{s}_i)$ be the operators of electric and magnetic dipole moments of the i-th nucleon in the nucleus. Here $d_i = d_{p,n}$ are the proton and neutron permanent EDMs, μ_0 is the nuclear magneton, $g_i^l = g_{p,n}^l$ and $g_i^s = g_{p,n}^s$ are the orbital and spin g-factors of the nucleons. The operators $\mathbf{d}_i$ and $\boldsymbol{\mu}_i$ couple with the electric and magnetic fields of the valence electron, yielding the interaction Hamiltonian[1]

$$H = -\sum_{i=1}^{A} \left(H_i^d + H_i^\mu\right) , \tag{7.7a}$$

$$H_i^d = \frac{e\,\mathbf{d}_i \cdot (\mathbf{R} - \mathbf{r}_i)}{|\mathbf{R} - \mathbf{r}_i|^3} , \tag{7.7b}$$

$$H_i^\mu = \frac{e\,\boldsymbol{\mu}_i \cdot [(\mathbf{R} - \mathbf{r}_i) \times \boldsymbol{\alpha}]}{|\mathbf{R} - \mathbf{r}_i|^3} , \tag{7.7c}$$

where $\mathbf{r}_i$ are the position vectors of the nucleons and $\boldsymbol{\alpha} = \left(\begin{smallmatrix} 0 & \boldsymbol{\sigma} \\ \boldsymbol{\sigma} & 0 \end{smallmatrix}\right)$ are Dirac matrices acting on electron wave functions.

The unperturbed atomic states will be denoted by $|mm'\rangle = |m\rangle|m'\rangle$, where $|m\rangle$ and $|m'\rangle$ are electronic and nuclear states, respectively.[2] The first-order contributions to the atomic EDM due to the interaction Hamiltonian (7.7) vanish for spinless nuclei which we consider in this paper, $\langle 0'|\mathbf{s}|0'\rangle = 0$. The leading non-vanishing contributions to the atomic EDM arise in the second order of the perturbation theory (see Ref. [44] for further details),

$$\mathbf{d} = -2 \sum_{m,n,n'} \frac{\langle 0|\, e\mathbf{R}\,|m\rangle\,\langle 0'm|\, H\,|nn'\rangle\,\langle n'n|\, H\,|00'\rangle}{(E_m - E_0)\,[\Delta E_n + \mathrm{sgn}(E_n)\Delta E_{n'}]} , \tag{7.8}$$

where the sum is taken over the excited states with $m \neq 0$ and $nn' \neq 00'$. Here, E_n and $E_{n'}$ are energies of electronic and nuclear excitations, respectively, whereas $\Delta E_n \equiv E_n - E_0$ and $\Delta E_{n'} \equiv E_{n'} - E_{0'}$. Note that the sum over the intermediate electronic states $|n\rangle$ includes both positive and negative energy levels which are inherent in Dirac's theory. The negative energy states contribute to Eq. (7.8) with opposite sign of $\Delta E_{n'}$ because they may be interpreted as blocking contributions for the electrons from the Dirac sea which cannot be excited to the occupied electron orbitals. Therefore, contribution of the transitions from the Dirac sea must be subtracted. (See also Refs. [47–49] for analogous account of the negative energy states within the problem of atomic energy shift due to nuclear polarizability.)

As is argued in Sect. 7.4, the atomic EDM (7.8) receives leading contributions from the matrix elements with $|0\rangle = |s_{1/2}\rangle$ and $|m\rangle = |p_{1/2}\rangle$. As a result, Eq. (7.8) may be cast in the form (7.4), with the contact interaction operator H_{cont} replaced with an effective interaction Hamiltonian H_{eff} defined by

$$H_{\mathrm{eff}} \equiv -\sum_{nn' \neq 00'} \frac{|m\rangle\,\langle 0'm|\, H\,|nn'\rangle\,\langle n'n|\, H\,|00'\rangle\,\langle 0|}{\Delta E_n + \mathrm{sgn}(E_n)\Delta E_{n'}} . \tag{7.9}$$

Substituting the operators (7.7) into Eq. (7.9) and keeping only linear in $\mathbf{d}_i$ terms we find

$$\langle p_{1/2}|\, H_{\mathrm{eff}}\,|s_{1/2}\rangle = -\sum_{n' \neq 0'} \sum_{i,j=1}^{A} \mathcal{M}_{ij}^{n'} , \tag{7.10}$$

where $\mathcal{M}_{ij}^{n'}$ is

$$\mathcal{M}_{ij}^{n'} = \sum_n \frac{\langle p_{1/2}0'|\, H_i^\mu\,|n'n\rangle\,\langle nn'|\, H_j^d\,|0's_{1/2}\rangle}{\Delta E_n + \mathrm{sgn}(E_n)\Delta E_{n'}} + (s_{1/2} \leftrightarrow p_{1/2}) . \tag{7.11}$$

In subsequent subsections, we will compute the nuclear and electronic matrix elements in this expression and present the results for the matrix element (7.10).

[1] In general, in addition to the nucleon EDMs, there are other CP-violating operators at hadronic level including three-pion and four-nucleon couplings. In Ref. [46], contributions to the nuclear EDM due to these operators were found for some light nuclei. In this paper, we focus only on the contributions to the atomic EDM due to the nucleon permanent EDMs.

[2] In what follows, the nuclear quantum number will be distinguished from the electronic ones with the apostrophe.

7.5.2 Integration over radial nuclear coordinates

The form of the nuclear matrix elements $\langle 0'|\, H_i^\mu \,|n'\rangle$ and $\langle 0'|\, H_i^d \,|n'\rangle$ depends on the specific nuclear model. To compute these matrix elements we consider an approximation in which the nuclear wave functions are given by

$$|n'\rangle = \prod_{i=1}^{A} R_{n'}(r_i)\Theta_{n'}(\hat{\mathbf{r}}_i)\,, \tag{7.12}$$

where $\hat{\mathbf{r}}_i = \mathbf{r}_i/r_i$ is the unit vector pointing in the direction of $\mathbf{r}_i$ and $R_{n'}(r_i)$ is the radial wave function.

The function $\Theta_{n'}(\hat{\mathbf{r}}_i)$ in Eq. (7.12) specifies the angular dependence of $|n'\rangle$. For a spherical nucleus, it is convenient to use the spherical basis, in which the nucleon states have definite total angular momenta $j_i^{n'}$ and total magnetic quantum numbers $\mu_i^{n'}$. In this case, one may take $\Theta_{n'}(\hat{\mathbf{r}}_i) = \Omega^{\kappa_i^{n'}}_{\mu_i^{n'}}(\hat{\mathbf{r}}_i)$ where $\Omega^{\kappa_i^{n'}}_{\mu_i^{n'}}$ is the two-component spherical spinor. On the other hand, for deformed nuclei, one usually employs the Nilsson basis [50], in which nucleon states have orbital magnetic quantum numbers $m_i^{n'}$ and spin projections $s_i^{n'} = \pm 1/2$.

In the spin-flip matrix elements produced by the nucleon magnetic moment and EDM operators, the radial wave functions in the bra and ket states are the same and we may average over their oscillations, taking[3]

$$|R_{n'}(r_i)|^2 = \frac{3}{R_0^3}\theta(R_0 - r_i)\,. \tag{7.13}$$

Using the radial function (7.13), one may integrate over the radial variable r_i in the matrix elements $\langle 0'|\, H_i^\mu \,|n'\rangle$ and $\langle 0'|\, H_i^d \,|n'\rangle$, keeping only the leading dipole terms with respect to the electronic coordinate $\mathbf{R}$. For that purpose, we note that the operators (7.7b) and (7.7c) depend on the function

$$\frac{\mathbf{R} - \mathbf{r}_i}{|\mathbf{R} - \mathbf{r}_i|^3} = -\nabla_{\mathbf{R}} \frac{1}{|\mathbf{R} - \mathbf{r}_i|} = -\nabla_{\mathbf{R}} \sum_{L=0}^{\infty} \frac{r_<^L}{r_>^{L+1}} P_L(\cos\varphi)\,, \tag{7.14}$$

where $r_< \equiv \min(R, r_i)$, $r_> \equiv \max(R, r_i)$ and φ is the angle between $\mathbf{R}$ and $\mathbf{r}_i$. In this expansion, it is sufficient to keep only the $L = 0$ term which reads $\theta(R - r_i)/R + \theta(r_i - R)/r_i$, because after applying the derivative $\nabla_{\mathbf{R}}$ it amounts to the dipole term with respect to the electronic coordinate $\mathbf{R}$. Taking into account only this term and integrating over the nuclear coordinates r_i, one may cast the nuclear matrix elements $\langle 0'|\, H_i^\mu \,|n'\rangle$ and $\langle 0'|\, H_i^d \,|n'\rangle$ in the form

$$\langle 0'|\, H_i^\mu \,|n'\rangle = e\mathbf{M} \cdot \langle \Theta_{0'}|\, \boldsymbol{\mu}_i \,|\Theta_{n'}\rangle\,, \tag{7.15a}$$

$$\langle 0'|\, H_i^d \,|n'\rangle = e\mathbf{D} \cdot \langle \Theta_{0'}|\, \mathbf{d}_i \,|\Theta_{n'}\rangle\,, \tag{7.15b}$$

where the operators $\mathbf{M}$ and $\mathbf{D}$ act only on electronic variables

$$\mathbf{M} \equiv \left[\theta(R - R_0)\frac{1}{R^2} + \theta(R_0 - R)\frac{R}{R_0^3}\right](\hat{\mathbf{R}} \times \boldsymbol{\alpha})\,, \tag{7.16a}$$

$$\mathbf{D} \equiv \left[\theta(R - R_0)\frac{1}{R^2} + \theta(R_0 - R)\frac{R}{R_0^3}\right]\hat{\mathbf{R}}\,. \tag{7.16b}$$

Here $\hat{\mathbf{R}} = \mathbf{R}/R$ is the unit vector pointing in the direction of $\mathbf{R}$.

Substituting Eqs. (7.15) into Eq. (7.11), one may factorize the matrix element $\mathcal{M}_{ij}^{n'}$ into nuclear and electronic parts as

$$\mathcal{M}_{ij}^{n'} = c_{s_{1/2}} c_{p_{1/2}} d_i\, \Xi_i^{n'} M(\Delta E_{n'}) \delta_{ij}\,, \tag{7.17a}$$

$$\Xi_i^{n'} = \langle \Theta_{0'}|\, \boldsymbol{\mu}_i \,|\Theta_{n'}\rangle \langle \Theta_{n'}|\, \boldsymbol{\sigma}_i \,|\Theta_{0'}\rangle\,, \tag{7.17b}$$

$$M(\Delta E_{n'}) = \frac{\alpha}{3 c_{s_{1/2}} c_{p_{1/2}}} \sum_n \frac{\langle p_{1/2}|\, \mathbf{M} \,|n\rangle \langle n|\, \mathbf{D} \,|s_{1/2}\rangle}{\Delta E_n + \mathrm{sgn}(E_n)\Delta E_{n'}} + (s_{1/2} \leftrightarrow p_{1/2})\,, \tag{7.17c}$$

[3] We stress that the function (7.13) is needed only to generalize the point-like interaction operators (7.7) to the model with extended nucleus. Upon averaging the operators (7.7) over nuclear density (7.13) the short-distance singularity of the electronic operators is spread and effectively regularized. Physically this means that the electron interacts with a nuclear charge distribution which has no singularity at the origin. One could model the nuclear charge distribution with the more realistic Woods-Saxon formula. However, we have checked that the use of the Woods-Saxon formula changes the electronic matrix elements by about 1% which is not essential within this work.

where we have separated the normalization constants $c_{s_{1/2}}$ and $c_{p_{1/2}}$ out of the electronic matrix element $M(\Delta E_{n'})$.

Equations (7.17) deserve some comments. First, we note that the matrix element (7.17a) is represented by a diagonal matrix with respect to nucleon indices ij. Indeed, the two matrix elements in the right-hand side of Eq. (7.17b) should involve the same nucleon because they both have the same initial and final nuclear states $|0'\rangle$ and $|n'\rangle$. Secondly, in passing from Eqs. (7.15) to Eqs. (7.17), we have implemented the substitution $(\mathbf{M}\cdot\boldsymbol{\mu})(\mathbf{D}\cdot\mathbf{d}) \to \frac{1}{3}(\mathbf{M}\cdot\mathbf{D})(\boldsymbol{\mu}\cdot\mathbf{d})$ which is applicable inside the matrix elements. Note that the nuclear matrix element (7.17b) is scalar for spinless nuclei which we consider in this paper.

For each nuclear energy $\Delta E_{n'}$, the value of the function $M(\Delta E_{n'})$ in Eq. (7.17c) is calculated by directly summing over the intermediate electronic states $|n\rangle$, which occupy both the discrete and continuum spectra. The contribution from the discrete spectrum appears negligible as compared with the continuum one (see Refs. [47, 49] for analogous calculations). Therefore, in what follows, we will consider intermediate electronic states $|n\rangle$ from the continuum spectrum represented by Dirac-Coulomb wave functions described in Appendix 7.B.2.

7.5.3 Nuclear spin-flip matrix elements for spherical and deformed nuclei

The nuclear matrix elements (7.17b) correspond to M1 spin-flip nuclear transitions. The computations of these matrix elements slightly differ for spherical and deformed nuclei. For the former, one uses $\Theta_{n'}(\hat{\mathbf{r}}_i) = \Omega^{\kappa_i^{n'}}_{\mu_i^{n'}}(\hat{\mathbf{r}}_i)$ and the matrix elements of the total momentum $\mathbf{j}_i$ vanish for fine structure doublets. As a result, substituting the operators $\mathbf{d}_i$ and $\boldsymbol{\mu}_i$ into Eq. (7.17b) and using the identity $\mathbf{l} = \mathbf{j} - \mathbf{s}$, the nuclear matrix elements may be written as $\Xi_i^{n'} = 2\mu_0(g_i^s - g_i^l)\,|\langle\Theta_{n'}|\,\mathbf{s}_i\,|\Theta_{0'}\rangle|^2$. For deformed nuclei, the angular functions may be chosen as $\Theta_{n'}(\hat{\mathbf{r}}_i) = Y^{l_i^{n'}}_{m_i^{n'}}(\hat{\mathbf{r}})\zeta_{\pm1/2}$, where $Y^{l_i^{n'}}_{m_i^{n'}}(\hat{\mathbf{r}})$ are spherical harmonics and $\zeta_{\pm1/2}$ is a two-component unit spinor. In this case, one may verify that $\langle\Theta_{0'}|\,\mathbf{l}_i\,|\Theta_{n'}\rangle\,\langle\Theta_{n'}|\,\mathbf{s}_i\,|\Theta_{0'}\rangle = 0$. Thus, for deformed nuclei, in Eq. (7.17b) we have $\Xi_i^{n'} = 2\mu_0 g_i^s\,|\langle\Theta_{n'}|\,\mathbf{s}_i\,|\Theta_{0'}\rangle|^2$. These two cases may be combined in one expression

$$\Xi_i^{n'} = 2\mu_0\left(g_i^s - \epsilon g_i^l\right)|\,\langle\Theta_{0'}|\,\mathbf{s}_i\,|\Theta_{n'}\rangle\,|^2\,, \tag{7.18}$$

where

$$\epsilon = \begin{cases} 1 & \text{for spherical nuclei} \\ 0 & \text{for deformed nuclei.} \end{cases} \tag{7.19}$$

In Eq. (7.18), the values of the g-factors for the proton and neutron are $g_p^l = 1$, $g_p^s = 5.586$, $g_n^l = 0$ and $g_n^s = -3.826$, respectively. The energies $\Delta E_{n'}$ and matrix elements $\langle\Theta_{0'}|\,\mathbf{s}_i\,|\Theta_{n'}\rangle$ of the M1 spin-flip transitions are listed in Appendix 7.A for different nuclei of interest.

7.5.4 Matrix element of the effective Hamiltonian

It is convenient to denote the energies and matrix elements for proton M1 spin-flip transitions as ΔE_p and $\langle 0'|\,\mathbf{s}\,|n'\rangle_p$, and for neutron transitions as ΔE_n and $\langle 0'|\,\mathbf{s}\,|n'\rangle_n$. Substituting the nuclear matrix elements (7.18) into Eq. (7.17a), the matrix element (7.10) may be presented in the form

$$\langle p_{1/2}|\,H_{\text{eff}}\,|s_{1/2}\rangle = -2c_{s_{1/2}}c_{p_{1/2}}\mu_0\left[d_p(g_p^s - \epsilon g_p^l)M_p + d_n(g_n^s - \epsilon g_n^l)M_n\right]\,, \tag{7.20}$$

where the quantities M_p and M_n are defined by

$$M_p \equiv \sum_{\Delta E_p} |\,\langle 0'|\,\mathbf{s}\,|n'\rangle_p\,|^2 M(\Delta E_p)\,, \tag{7.21a}$$

$$M_n \equiv \sum_{\Delta E_n} |\,\langle 0'|\,\mathbf{s}\,|n'\rangle_n\,|^2 M(\Delta E_n)\,. \tag{7.21b}$$

Note that for deformed nuclei Eqs. (7.20) and (7.21) simplify, because in the Nilsson basis $|\,\langle 0'|\,\mathbf{s}\,|n'\rangle_{p,n}\,|^2 = 1$ and $\epsilon = 0$.

The details of the numerical computations of the coefficients M_p and M_n are given in Appendix 7.B and the results are presented in Table 7.5. In particular, for ^{180}Hf and ^{232}Th they are:

$$\begin{aligned} &^{180}\text{Hf}: \quad M_p = 121a_B^{-1}\,, \quad M_n = 114a_B^{-1}\,, \\ &^{232}\text{Th}: \quad M_p = 244a_B^{-1}\,, \quad M_n = 385a_B^{-1}\,. \end{aligned} \tag{7.22}$$

Substituting these values into Eq. (7.20), we find

$$\langle p_{1/2}|\, H_{\rm eff}\, |s_{1/2}\rangle_{^{180}{\rm Hf}} = -2c_{s_{1/2}}c_{p_{1/2}}\frac{\mu_0}{a_B}(673.7d_p - 436.2d_n)\,, \tag{7.23a}$$

$$\langle p_{1/2}|\, H_{\rm eff}\, |s_{1/2}\rangle_{^{232}{\rm Th}} = -2c_{s_{1/2}}c_{p_{1/2}}\frac{\mu_0}{a_B}(1363d_p - 1473d_n)\,. \tag{7.23b}$$

In Sect. 7.6, we will compare these quantities with the matrix element of the contact interaction (7.6) and will find the limits on the nucleon EDMs implied by the experimental constraints on C_{SP}. However, before proceeding further, let us make a few comments about the details and the accuracy of our calculation of the matrix elements (7.23).

The leading contributions to the atomic EDM from nucleon EDMs arise from $s_{1/2}$ - $p_{1/2}$ electron matrix elements, because these states are significantly enhanced near the nucleus by the absence of the centrifugal barrier and relativistic effects [51]. Therefore, we ignore contributions from matrix elements with higher-l wave functions which are very small near the nucleus ($\propto r^l$).

We call attention to the fact that the effective electron-nucleon interactions (7.16) fall with the distance (similar to the effect of the ordinary nuclear polarizability) because they have dipole nature. These interactions give the main contributions to the matrix elements at distances from about nuclear radius to hundreds of nuclear radii. Thus, it is localised in the near-nucleus region with $R \ll a_B/Z^{1/3}$, where a_B is the Bohr radius. It is important to note that in this region the inter-electron interaction and screening are negligible, and we can use approximate electron wave functions (7.41) for $s_{1/2}$ and $p_{1/2}$ bound states. The virtual excited electronic states are described by Dirac-Coulomb wave functions in the continuum spectrum (7.45) while the excited states in the discrete spectrum give negligible contributions. For those radial wave functions, which are singular at the origin for a point-like nucleus, we consider their regular polynomial continuation inside the nucleus such that at the origin they behave similarly to the solutions for the Dirac particle inside of a constantly charged ball. This approximation does not break the accuracy of our results.

The radial integrals in the electronic matrix elements are calculated numerically. To control the accuracy of numerical integration, we checked our numerical methods by calculating the energy shifts (contributions to the Lamb shifts) in heavy one-electron ions due to the nuclear polarizability. The error in this calculation does not exceed 5% as compared with earlier calculations for Th, U, Pu, Cm and other heavy atoms [47, 49]. Technically, this energy shift is characterised by electronic matrix elements with electric electron-nucleon interaction while in our work we have similar matrix elements with combined electric and magnetic interaction. This comparison serves as a good check of the accuracy of our numerical methods in the electronic part of the calculations. However, the main error in Eq. (7.23) stems from the quantities M_p and M_n where we expect the errors of our calculations for the nuclear matrix elements and corresponding energies to be under 50%. This estimate is based on the comparison of the reduced transition probabilities for M1 spin-flip transitions calculated within the single-particle nuclear shell model employed in our work with the results of more sophisticated nuclear calculations presented in Ref. [52] for some heavy nuclei (see comments at the end of Appendix 7.A). Thus, we conclude that the error in our calculation of the matrix elements (7.23) is within 50% for all atoms. This level of accuracy is typical for most of calculations of CP-violating hadronic effects quoted, e.g., in Eqs. (7.34) and (7.35). Further errors originating from relations between hadronic CP-violating parameters will be introduced into the calculation later when we derive relations between C_{SP} and these parameters. Note also that constraints on hadronic CP-violating parameters in heavy atoms have usually logarithmic scale where the accuracy of up to a factor of two is acceptable.

7.6 Constraints on CP-odd hadronic parameters

In this section, we will compare the matrix element (7.20) with the corresponding matrix element of the contact interaction (7.6). This will allow us to determine the dependence of the coupling constant C_{SP} on the nucleon permanent EDMs d_p and d_n. Then, employing the experimental constraint (7.2) we will determine the limits on the parameters d_p and d_n originating from the EDM experiments with paramagnetic molecules. We will also present the constraints on other hadronic parameters, which follow from the obtained ones.

7.6.1 Limits on nucleon EDMs

In Eq. (7.20), we computed the contributions to the atomic EDM (7.4) due to the nucleon EDMs. It is natural to compare these contributions with that due to the contact interaction $H_{\rm cont}$. Equating the matrix elements of these interactions (7.6) and (7.20) we find the relation between the constant C_{SP} and the parameters d_p and d_n:

$$C_{SP}^{(d)} = \frac{20\sqrt{2}}{G_F}\frac{\Gamma(2\gamma+1)^2}{1+4\gamma}\frac{\pi\mu_0 R_0^2}{AZ\alpha}\left(\frac{a_B}{2ZR_0}\right)^{2\gamma}\left[d_p(g_p^s-\epsilon g_p^l)M_p + d_n(g_n^s-\epsilon g_n^l)M_n\right] . \tag{7.24}$$

We point out that the right-hand side of Eq. (7.24) is independent of the wave functions normalization constants $c_{s_{1/2}}$ and $c_{p_{1/2}}$.

We stress that the contribution to C_{SP} (7.24) originates from discrete nuclear intermediate excited states while the authors of Ref. [32] found analogous contributions due to virtual nuclear excitations to continuum spectrum,

$$C_{SP}^{(c)} = \frac{8\sqrt{2}m_e\alpha^2\ln(A)}{G_F p_F m_N}\left(\frac{Z}{A}\frac{\mu_p}{\mu_0}\frac{d_p}{e} + \frac{N}{A}\frac{\mu_n}{\mu_0}\frac{d_n}{e}\right) . \tag{7.25}$$

Here $p_F \approx 250$ MeV is the Fermi momentum of the nucleus, m_N is the nucleon mass and μ_p, μ_n are the nucleon magnetic moments ($\mu_p/\mu_0 = 2.793$, $\mu_n/\mu_0 = -1.913$). The superscripts (d) and (c) in Eqs. (7.24) and (7.25) refer to the contributions of discrete and continuum intermediate nuclear states, respectively.

Combining the two contributions (7.24) and (7.25), we find the leading-order dependence of $C_{SP} = C_{SP}^{(d)} + C_{SP}^{(c)}$ on nucleon EDMs,

$$C_{SP} = (\lambda_1 d_p + \lambda_2 d_n) \times \frac{10^{13}}{e\cdot\text{cm}} , \tag{7.26}$$

where the numerical values of the coefficients λ_1 and λ_2 for several atoms of interest are presented in Table 7.1.

The relation (7.26) represents the central results of this paper. It allows us to place limits on the nucleon EDMs. Taking into account the most recent constraints on $|C_{SP}|$ from the ^{180}HfF$^+$ [29] and ^{232}ThO [31] EDM experiments (see also Ref. [53]), we obtain the limits on d_p and d_n. These results are collected in Table 7.2 at the end of this section.

We note that since the quantities $\lambda_{1,2}$ and the corresponding limits on $d_{p,n}$ are directly linked to the effective matrix elements $M_{p,n}$, the errors in these quantities are similar to those incurred in the computation of $M_{p,n}$, i.e., around 50%.

7.6.2 Limits on CP-odd pion-nucleon coupling constants

The nucleon EDM may appear due to more fundamental interactions. In this subsection, we assume that the dominant contribution to the nucleon EDM is stipulated by the CP-odd pion-nucleon interaction.

The CP-odd pion-nucleon interactions with coupling constants $\bar{g}^{(0)}_{\pi NN}$ and $\bar{g}^{(1)}_{\pi NN}$ may induce atomic EDMs through different mechanisms: (i) they contribute to the nucleon EDMs via one-loop quantum corrections [54] and (ii) they contribute to the effective nucleon-electron interaction through one- and two-loop contributions to the nucleon polarizability [32]. In this section, we revisit all these contributions and combine them with those from d_p and d_n found in the previous subsection. This will allow us to find the constraints on $\bar{g}^{(0)}_{\pi NN}$ and $\bar{g}^{(1)}_{\pi NN}$ originating from the EDM experiments with paramagnetic atoms and molecules.

We recall that the coupling constants $\bar{g}^{(0)}_{\pi NN}$ and $\bar{g}^{(1)}_{\pi NN}$ enter the CP-odd pion-nucleon interaction as follows:

$$\mathcal{L}_{\pi NN} = \bar{g}^{(0)}_{\pi NN}\bar{N}\tau^a N\pi^a + \bar{g}^{(1)}_{\pi NN}\bar{N}N\pi^0 , \tag{7.27}$$

where N is the nucleon doublet, π^a, π^0 are the pion fields, and τ^a are isospin Pauli matrices. This interaction is responsible for the one-loop quantum correction to the nucleon EDM which were originally estimated in Ref. [55] and revisited in subsequent papers [56–58],

$$d_n \approx \frac{eg_A\bar{g}^{(0)}_{\pi NN}}{8\pi^2 F_\pi}\left(2\ln\frac{m_p}{m_\pi} + \frac{\pi}{2}\frac{m_\pi}{m_p} - 1\right) \approx 1.1\times10^{-14}\bar{g}^{(0)}_{\pi NN}\, e\cdot\text{cm} , \tag{7.28a}$$

$$d_p \approx \frac{eg_A\bar{g}^{(0)}_{\pi NN}}{8\pi^2 F_\pi}\left(1 - 2\pi\frac{m_\pi}{m_p} - 2\ln\frac{m_p}{m_\pi}\right) \approx -1.3\times10^{-14}\bar{g}^{(0)}_{\pi NN}\, e\cdot\text{cm} , \tag{7.28b}$$

where $g_A \approx 1.3$ is the axial triplet coupling constant, $F_\pi \approx 93$ MeV is the pion decay constant, $m_\pi \approx 135$ MeV is the pion mass and $m_p \approx m_n \approx 938$ MeV is the nucleon mass. In Eqs. (7.28) we keep only the terms originating from the meson cloud and omit the (counter)terms corresponding to short-distance effects (see, e.g., [6, 57, 58]). The latter terms depend on low-energy constants with unknown values which bring a high level of uncertainty in the relations (7.28). An accurate study of these short-distance effects goes beyond the scope of this paper.

There are one- and two-loop quantum contributions to the nucleon polarizability $\beta_{p,n} = \beta^{(1)}_{p,n} + \beta^{(2)}_{p,n}$, which involve interaction vertices (7.27) [32] [4]:

$$\beta^{(1)}_p = -\frac{\alpha}{\pi F_\pi m_\pi^2}\left(\bar{g}^{(1)}_{\pi NN} + \bar{g}^{(0)}_{\pi NN} + \frac{5}{\sqrt{3}}\frac{m_\pi^2}{m_\eta^2}\bar{g}^{(0)}_{\pi NN}\right), \tag{7.29a}$$

$$\beta^{(1)}_n = -\frac{\alpha}{\pi F_\pi m_\pi^2}\left(\bar{g}^{(1)}_{\pi NN} - \bar{g}^{(0)}_{\pi NN} + \frac{5}{\sqrt{3}}\frac{m_\pi^2}{m_\eta^2}\bar{g}^{(0)}_{\pi NN}\right), \tag{7.29b}$$

$$\beta^{(2)}_p = -\frac{\alpha g_A \bar{g}^{(0)}_{\pi NN}}{4F_\pi m_n m_\pi}\frac{\mu_n}{\mu_0}, \tag{7.29c}$$

$$\beta^{(2)}_n = \frac{\alpha g_A \bar{g}^{(0)}_{\pi NN}}{4F_\pi m_p m_\pi}\frac{\mu_p}{\mu_0}. \tag{7.29d}$$

Note that these relations contain only the leading terms which preserve the isospin symmetry. The nucleon polarizability corrections (7.29) amount to the following contributions to the effective coupling constant C_{SP}

$$C^{(\beta)}_{SP} = -\frac{\sqrt{2}}{G_F}\left(\frac{Z}{A}\beta_p + \frac{N}{A}\beta_n\right)\frac{3\alpha m_e}{2\pi}\ln\frac{\Lambda}{m_e}, \tag{7.30}$$

where the renormalization scale $\Lambda = m_\rho \approx 775$ MeV for one-loop corrections and $\Lambda = m_\pi \approx 135$ MeV for the two-loop ones (see [32] for detail).

Now we substitute the relation (7.28) into Eq. (7.24) or (7.26) and add also the contribution (7.30). As a result, we find the leading-order relation between the constant C_{SP} and CP-violating pion-nucleon couplings

$$C_{SP} = \lambda_3 \bar{g}^{(0)}_{\pi NN} + \lambda_4 \bar{g}^{(1)}_{\pi NN}, \tag{7.31}$$

where the numerical values of the coefficients λ_3 and λ_4 are collected in Table 7.1 for different atoms. The corresponding limits on these couplings originating from the experimental constraints are given in Table 7.2 below. We stress that these limits are based on the assumption that the CP-odd pion interaction (7.27) gives dominant contribution to the atomic EDM.

Unfortunately, we cannot accurately estimate computational errors of our results for the coefficients λ_3 and λ_4 because they are based on the relations (7.28) and (7.29) with unknown errors. However, by comparing with other analogous calculations (e.g., [58]) it is natural to expect that the errors in Eqs. (7.28) and (7.29) may be of order $30\% - 100\%$. Nevertheless, our relation (7.31) is still useful for comparison with other results for CP-violation in heavy nuclei, in particular, with the atomic EDMs produced by the nuclear Schiff moments, which do not contain estimates of the theoretical errors in the nuclear calculations and should be understood on the logarithmic scale.

7.6.3 Limits on quark chromo-EDM

In this subsection, we consider the chromo-EDM of up and down quarks denoted by $\tilde{d}_u$ and $\tilde{d}_d$, respectively. Assuming that these quantities are the only sources of the nucleon EDM and CP-violating internucleon forces, the authors of Refs. [54, 59–62] established the following relations:

$$d_p = -(2.1 \pm 1.1)e(\tilde{d}_u + 0.125\tilde{d}_d), \tag{7.32a}$$

$$d_n = (1.1 \pm 0.6)e(\tilde{d}_d + 0.5\tilde{d}_u), \tag{7.32b}$$

$$g\bar{g}^{(0)}_{\pi NN} = (0.8 \pm 0.4) \times 10^{15}(\tilde{d}_u + \tilde{d}_d)\text{cm}^{-1}, \tag{7.32c}$$

$$g\bar{g}^{(1)}_{\pi NN} = (4.0 \pm 2.0) \times 10^{15}(\tilde{d}_u - \tilde{d}_d)\text{cm}^{-1}. \tag{7.32d}$$

[4] In Eqs. (7.29a) and (7.29b), the last terms account for the contributions from η meson exchange with the mass m_η. These mesons have CP-odd meson-nucleon interaction with coupling constant $\bar{g}_{0,\eta} \approx 5\bar{g}_{0,\pi}$.

		λ_1	λ_2	λ_3	λ_4	λ_5	λ_6	λ_7
Spherical	$^{138}_{56}$Ba	6.4	-7.2	-2.3	2.2	0.4	-0.8	5.1
	$^{206}_{82}$Pb	5.5	-6.2	-2.1	2.2	0.5	-0.8	4.6
	$^{208}_{82}$Pb	5.5	-5.3	-2.0	2.2	0.5	-0.8	4.4
Deformed	$^{172}_{70}$Yb	9.4	-8.4	-2.8	2.2	0.4	-0.8	6.0
	$^{174}_{70}$Yb	9.3	-9.7	-3.0	2.2	0.4	-0.8	6.3
	$^{176}_{70}$Yb	9.2	-8.6	-2.8	2.2	0.4	-0.8	6.1
	$^{178}_{72}$Hf	12	-8.2	-3.1	2.2	0.3	-0.8	6.5
	$^{180}_{72}$Hf	12	-9.0	-3.2	2.2	0.3	-0.8	6.7
	$^{226}_{88}$Ra	5.7	-5.7	-2.1	2.2	0.5	-0.8	4.6
	$^{232}_{90}$Th	6.4	-6.9	-2.3	2.2	0.4	-0.8	5.1

Table 7.1: The results of numerical computations of the coefficients $\lambda_1, \ldots, \lambda_7$ in Eqs. (7.26), (7.31), (7.33) and (7.36).

	^{232}ThO	^{180}HfF$^+$
$\lvert C_{SP}\rvert$	7.3×10^{-10} [31]	1.8×10^{-8} [29, 53]
$\lvert d_p\rvert$	$1.1 \times 10^{-23} e \cdot$ cm	$1.5 \times 10^{-22} e \cdot$ cm
$\lvert d_n\rvert$	$1.0 \times 10^{-23} e \cdot$ cm	$2.0 \times 10^{-22} e \cdot$ cm
$\lvert \bar{g}^{(0)}_{\pi NN}\rvert$	3.1×10^{-10}	5.6×10^{-9}
$\lvert \bar{g}^{(1)}_{\pi NN}\rvert$	3.3×10^{-10}	8.2×10^{-9}
$\lvert \tilde{d}_d\rvert$	9.3×10^{-25}cm	2.2×10^{-23}cm
$\lvert \tilde{d}_u\rvert$	1.7×10^{-24}cm	5.8×10^{-23}cm
$\lvert \theta\rvert$	1.4×10^{-8}	2.7×10^{-7}

Table 7.2: Limits on absolute values of CP-violating hadronic parameters arising from the relations (7.26), (7.31), (7.33) and (7.36) upon implementing the constraints on the constant C_{SP} from the ^{180}HfF$^+$ [29, 53] and ^{232}ThO [31] experiments.

These equations should be substituted into the sum of Eqs. (7.24) and (7.30), giving the leading-order dependence of C_{SP} on $\tilde{d}_u$ and $\tilde{d}_p$ as

$$C_{SP} = (\lambda_5 \tilde{d}_u + \lambda_6 \tilde{d}_d) \times 10^{15} \text{cm}^{-1} \,. \tag{7.33}$$

The numerical values of the coefficients λ_5 and λ_6 are given in Table 7.1. The corresponding constraints on the values of quark chromo-EDMs are presented in Table 7.2 below. These constraints are based on the assumption that the quark chromo-EDMs are the dominant sources of nucleon EDM and the CP-odd pion-nucleon interaction (7.27).

In order to estimate the uncertainty in the coefficients $\lambda_{5,6}$ and the corresponding limits on $\tilde{d}_{u,d}$, we note that the relations (7.32) all have 50% uncertainty (the error bars of the relations (7.32c) and (7.32d) were estimated in Ref. [6]). Combining these with the 50% error bars in $\lambda_{1,2}$ and assuming that the relations (7.29) have a 100% uncertainty, we find that the values of λ_5 and $\tilde{d}_u$ are accurate up to a factor of 3 wheres the values of λ_6 and $\tilde{d}_d$ are accurate up to a factor of 2.

7.6.4 Limit on QCD vacuum angle $\bar{\theta}$

The QCD vacuum angle $\bar{\theta}$ is the fundamental CP-odd parameter which can induce the nucleon (and atomic) EDM. In this subsection, we find the limit on $\bar{\theta}$ in the assumption that the nucleon EDM is dominated by contributions from the QCD vacuum angle.

The dependence of the nucleon EDMs on $\bar{\theta}$ was originally estimated in Ref. [55] and refined in subsequent papers [59, 63–65]:

$$d_p = (2.1 \pm 1.2) \times 10^{-16} \bar{\theta}\, e \cdot \text{cm} \,, \qquad d_n = -(2.7 \pm 1.2) \times 10^{-16} \bar{\theta}\, e \cdot \text{cm} \,. \tag{7.34}$$

The pion-nucleon coupling constants $\bar{g}^{(0)}_{\pi NN}$ and $\bar{g}^{(1)}_{\pi NN}$ can also be expressed via $\bar{\theta}$ as [54, 63, 66] (see also Refs. [6, 65] for reviews[5])

$$\bar{g}^{(0)}_{\pi NN} = -(15.5 \pm 2.5) \times 10^{-3}\,\bar{\theta}\,, \qquad \bar{g}^{(1)}_{\pi NN} = (3.4 \pm 2) \times 10^{-3}\,\bar{\theta}\,. \tag{7.35}$$

Substituting these relations into the sum of Eqs. (7.24) and (7.30) we represent C_{SP} in terms of $\bar{\theta}$

$$C_{SP} = \lambda_7 \times 10^{-2}\bar{\theta}\,, \tag{7.36}$$

where the value of the constant λ_7 is given in Table 7.1 for different atoms. In particular, with the use of the corresponding value for ^{232}Th, the experimental constraint on C_{SP} (7.2) implies

$$|\bar{\theta}| < 1.4 \times 10^{-8}\,. \tag{7.37}$$

This constraint is close to the result advocated in the recent paper [32].

Using the uncertainties in Eqs. (7.34) and (7.35) and assuming that the relations (7.29) have a 100% uncertainty, we find that the error bars in the relation (7.36) and the corresponding limit (7.37) are about $40\% - 50\%$.

7.7 Summary and discussion

In this paper, we demonstrated that the experiments measuring the electron electric dipole moment with paramagnetic atoms and molecules are also sensitive to nucleon EDMs. Dominant contributions to the atomic EDM in such atoms arise from the combined electric and magnetic electron-nucleus interaction. Taking into account nuclear structure effects, we derived the leading-order relations (7.26) between the electron-nucleus contact interaction constant C_{SP} and nucleon permanent EDMs d_p and d_n. As a result, the constraint (7.2) on the parameter C_{SP} allows us to find limits on nucleon EDMs arising from the experiments with paramagnetic molecules:

$$|d_p| < 1.1 \times 10^{-23} e \cdot \mathrm{cm}\,, \qquad |d_n| < 1.0 \times 10^{-23} e \cdot \mathrm{cm}\,. \tag{7.38}$$

It is instructive to compare these limits with the currently accepted ones. In particular, our limit on the neutron EDM obtained from the results of experiments with paramagnetic molecules is almost three order of magnitude weaker than the recent experimental measurements of EDM of neutron $|d_n| < 1.8 \times 10^{-26} e \cdot$cm [67]. However, for the proton EDM our limit (7.38) is just about 20 times weaker than the recent constraint on this parameter $|d_p| < 5 \times 10^{-25} e \cdot$ cm [68] which was based on the measurements on EDM of ^{199}Hg atom [14].[6] Remarkably, the constraint (7.38) on the proton EDM is nearly 30 times more stringent than that found in recent ^{129}Xe EDM experiments [70, 71]. This sensitivity of eEDM experiments to hadronic CP-violating parameters is actually very impressive. We expect that further improvement of accuracy in the experiments with paramagnetic molecules would push these limits.

The nucleon EDM may be expressed via more fundamental CP-violating parameters such as CP-odd pion-nucleon coupling constants $\bar{g}^{(0,1)}_{\pi NN}$, quark chromo-EDMs $\tilde{d}_{u,d}$ and the QCD vacuum angle $\bar{\theta}$. This allows us to find the leading-order dependence of the contact interaction coupling constant C_{SP} on these parameters. The results are represented by Eqs. (7.31), (7.33) and (7.36) with coefficients $\lambda_3, \ldots, \lambda_7$ given in Table 7.1. The corresponding limits arising on these parameters from the experiments [29] and [31] are presented in Table 7.2. In particular, the QCD vacuum angle is limited as $|\bar{\theta}| < 1.4 \times 10^{-8}$ which is approximately two orders of magnitude weaker than the currently accepted constraint from neutron and Hg atom EDM experiments $|\bar{\theta}| < 10^{-10}$ [72], but is nearly three times more stringent than the corresponding bounds from ^{129}Xe EDM experiments [70, 71]. Note that the limits presented above do not include theoretical errors which often are unknown (see, e.g., calculation of the ^{199}Hg nuclear Schiff moment in Ref. [73] where different interaction models give different sign of the result). Our error estimates are presented after corresponding formulas. In particular, for the limit on the nucleon EDMs $d_{p,n}$ and the QCD angle $\bar{\theta}$, the error is about 40-50% while the limit on the up quark chromo-EDM d_u is correct up to a factor of 3 and the limit on the down quark chromo-EDM is correct up to a factor of 2.

We stress that obtained in this paper contributions to C_{SP} from nucleon EDMs are independent from and additional to those found in Ref. [32], although they originate from the same combined electric and

[5] We point out that the signs in the relations (103) and (104) between $\bar{g}^{(0,1)}_{\pi NN}$ and $\bar{\theta}$ quoted in Ref. [6] are inconsistent with the definition of $\mathcal{L}_{\pi NN}$ presented in that review.

[6] Note that this constraint is approximately two times weaker than that in Ref. [69] because the authors of Ref. [68] revisited earlier calculations of nuclear Shiff moments.

magnetic electron-nucleon interaction. Indeed, the authors of the paper [32] took into account virtual nuclear transitions from bound states to *continuum* for all nucleons in the nucleus, so it increases with the nucleon number A. In our paper, in contrast, we consider virtual nuclear transitions to excited *bound* nuclear states for several external shell nucleons which can flip their spins. This contribution is enhanced by the small energy denominators and large matrix elements of the spin operator between the spin-orbit doublet components. As we demonstrate in this paper, accounting these M1 nuclear spin-flip transitions approximately doubles the results presented in Ref. [32].

To conclude, we expect that the obtained in this paper results may place more stringent limits on CP-violating hadronic parameters once improved constraints on C_{SP} are available from next generations of eEDM experiments [10, 11, 29–31, 74]. Note that the sensitivity in these experiments improved by two orders of magnitude during the last decade.

Acknowledgements

This work was supported by the Australian Research Council Grants No. DP150101405 and DP200100150 and the Gutenberg Fellowship. We thank Vladimir Dmitriev, Maxim Pospelov, Adam Ritz, Yevgeny Stadnik and Anna Viatkina for useful discussions.

7.A Nuclear energies and matrix elements

In this appendix, we estimate the matrix elements and corresponding energies of nuclear M1 spin-flip single-particle transitions. The details of these computations slightly differ for (nearly) spherical and deformed nuclei. Therefore, we consider these two cases separately.

7.A.1 Spherical nuclei

In this section, we focus on the ^{208}Pb, ^{206}Pb and ^{138}Ba nuclei, which are nearly spherical, i.e., they have deformation $\delta < 0.1$. For these nuclei, proton and neutron single-particle states may be labeled as $|n, l, j, m\rangle$, where n is the oscillator quantum number, l and j are the orbital and total momentum numbers, m is magnetic quantum number. In this basis, the nuclear spin operator $\mathbf{s}$ provides transitions between fine structure doublets.

In the ^{208}Pb nucleus, the non-vanishing matrix elements of the spin operator are $\langle 5h\frac{9}{2}|\mathbf{s}|5h\frac{11}{2}\rangle$ for protons and $\langle 6i\frac{11}{2}|\mathbf{s}|6i\frac{13}{2}\rangle$ for neutrons. The isotope ^{206}Pb has additional contributions from the $\langle 5p\frac{1}{2}|\mathbf{s}|5p\frac{3}{2}\rangle$ neutron matrix elements. For ^{138}Ba, non-vanishing proton contributions arise from the matrix elements $\langle 4d\frac{3}{2}|\mathbf{s}|4d\frac{5}{2}\rangle$ and $\langle 4g\frac{9}{2}|\mathbf{s}|4g\frac{7}{2}\rangle$ whereas neutron contributions come from $\langle 5h\frac{9}{2}|\mathbf{s}|5h\frac{11}{2}\rangle$. All these matrix elements may be calculated using the properties of spherical spinors (see, e.g., Ref. [75]). The energies of all these transitions may be estimated with the use of Fig. 5 in Ref. [76]. When the energies are (nearly) degenerate, we give the sum of matrix elements corresponding to the same energy. In Table 7.3 below, we collect the values of such matrix elements with the corresponding energies for ^{208}Pb, ^{206}Pb and ^{138}Ba. The value of the nuclear radius R_0 is calculated according to the empirical formula:

$$R_0 = 1.2A^{1/3}\,\mathrm{fm}\,. \tag{7.39}$$

For reference, the values of the deformation parameter δ are also presented.

7.A.2 Deformed nuclei

For deformed heavy nuclei with $\delta > 0.1$, it is convenient to use the Nilsson basis [50, 76], wherein proton and neutron single-particle states are labeled with $|n_3, n_\perp, \Lambda, \Omega\rangle$, where n_3 and $n_\perp$ are the oscillator quantum numbers, Λ and Ω are the projections of angular and total momenta on the deformation axis. Note that $\Omega = \Lambda + \Sigma$ where Σ is the projection of the nucleon's spin on the deformation axis. The dependence of the energy levels on the deformation parameter δ in this model may be inferred from Fig. 5 in Ref. [76]. From such dependence, one may estimate the energies of the spin-flip transitions. Note that in the basis $|n_3, n_\perp, \Lambda, \Omega\rangle$, each M1 spin-flip matrix element is $\langle m'|\, s_+ \,|0'\rangle = 1$, and the corresponding energy level is doubly degenerate since each quantum number Σ corresponds to $\pm\Lambda$.

The single-nucleon spin-flip M1 transition energies $\Delta E_{n'}$, the deformation parameters δ and the nuclear radii R_0 for several nuclei of interest are presented in Table 7.4.

	Proton transitions		Neutron transitions		R_0	δ
	$\lvert\langle n'\lvert\mathbf{s}\rvert 0'\rangle_p\rvert^2$	$\Delta E_{n'}$ (MeV)	$\lvert\langle n'\lvert\mathbf{s}\rvert 0\rangle'_n\rvert^2$	$\Delta E_{n'}$ (MeV)	(fm)	
^{138}Ba	18/25	2.7	170/121	5.3	6.20	0.09
	2/25	4.1	200/121	5.4		
	28/81	4.3	30/121	5.5		
	56/81	4.4	136/121	5.9		
	16/81	4.5	56/121	6.0		
	8/9	4.6	60/121	6.2		
	8/81	5.2	8/121	6.5		
^{206}Pb	10/11	4.5	72/169	6.1	7.09	0.03
	162/121	4.6	462/169	6.2		
	98/121	4.7	318/169	6.3		
	250/121	4.8	132/169	6.4		
	32/121	5.0	100/169	6.5		
	8/121	5.1	6/169	6.7		
			2/169	6.9		
			2/3	1.4		
			10/9	2.0		
^{208}Pb	10/11	4.5	72/169	6.1	7.11	0.05
	162/121	4.6	462/169	6.2		
	98/121	4.7	318/169	6.3		
	250/121	4.8	132/169	6.4		
	32/121	5.0	100/169	6.5		
	8/121	5.1	6/169	6.7		
			2/169	6.9		

Table 7.3: Nuclear radii R_0, deformation parameters δ, matrix elements $|\langle n'|\mathbf{s}|0'\rangle_{p,n}|^2$ and the corresponding energies $\Delta E_{n'}$ of M1 spin-flip transitions in some spherical nuclei of interest.

In conclusions of this subsection we discuss the accuracy of our estimates of matrix elements and corresponding energies presented in Tables 7.3 and 7.4. For this purpose, it is convenient to consider the reduced transition probability of M1 spin-flip transition, $B_0 \equiv \sum_{n'} B(M1, 0' \to n')$. Using the data from Table 7.4, we find this quantity for ^{232}Th, $B_0 = 14.8\mu_0$, and for ^{172}Yb, $B_0 = 14.6\mu_0$. These values may be compared with the corresponding quantities presented in Ref. [52] obtained on the basis of sophisticated Hartree-Fock plus RPA nuclear calculation: $B_0 = 14.9\mu_0$ for ^{232}Th and $B_0 = 12.8\mu_0$ for ^{172}Yb. As a result we conclude that the simple single-particle nuclear shell model used in this paper allows us to determine the nuclear M1 matrix elements with error about 15% . Errors in nuclear energies are within 50%. It may be checked that the accuracy of nuclear calculations for other heavy nuclei considered in our paper is within this range. Therefore, we conclude that the errors in determining values of nuclear matrix elements and corresponding energies of spin-flip M1 transitions are under 50% for all nuclei. This level of accuracy is acceptable for the goals of this work, although a better accuracy may be achieved with the use of more sophisticated nuclear models.

7.B Evaluation of electronic matrix elements

In this appendix, we provide the details for the numerical calculation of the electronic matrix element (7.17c). For convenience, we use the spherical basis $(\mathbf{e}_+, \mathbf{e}_-, \mathbf{e}_0)$. The components of vectors in this basis will be labeled by the $(+, -, 0)$ subscripts. Due to spherical symmetry, Eq. (7.17c) may be rewritten in terms of the '0'-component of the operators $\mathbf{D}$ and $\mathbf{M}$ introduced in Eqs. (7.16),

$$M(\Delta E_{n'}) = \frac{\alpha}{c_{s_{1/2}} c_{p_{1/2}}} \sum_n \frac{\langle p_{1/2}| M_0 |n\rangle \langle n| D_0 |s_{1/2}\rangle}{\Delta E_n + \mathrm{sgn}(E_n)\Delta E_{n'}} + (s_{1/2} \leftrightarrow p_{1/2})\,. \tag{7.40}$$

In Eq. (7.40), the sum is taken over all excited electron states $|n\rangle$ with energies E_n, including those from the discrete and continuous spectra. As discussed in Sect. 7.5, the states from the discrete spectrum give negligible contributions to the electronic matrix elements. Therefore, in what follows, we will consider

	Proton transitions		Neutron transitions		R_0 (fm)	δ
	Transition	$\Delta E_{n'}$ (MeV)	Transition	$\Delta E_{n'}$ (MeV)		
^{172}Yb	$\|523\frac{7}{2}\rangle \to \|523\frac{5}{2}\rangle$	4.5	$\|651\frac{3}{2}\rangle \to \|651\frac{1}{2}\rangle$	3.9	6.67	0.31
	$\|532\frac{5}{2}\rangle \to \|532\frac{3}{2}\rangle$	4.0	$\|642\frac{5}{2}\rangle \to \|642\frac{3}{2}\rangle$	4.5		
	$\|541\frac{3}{2}\rangle \to \|541\frac{1}{2}\rangle$	4.5	$\|633\frac{7}{2}\rangle \to \|633\frac{5}{2}\rangle$	5.0		
	$\|404\frac{9}{2}\rangle \to \|404\frac{7}{2}\rangle$	4.1	$\|505\frac{11}{2}\rangle \to \|505\frac{9}{2}\rangle$	5.1		
			$\|514\frac{9}{2}\rangle \to \|514\frac{7}{2}\rangle$	4.6		
^{174}Yb	$\|523\frac{7}{2}\rangle \to \|523\frac{5}{2}\rangle$	4.5	$\|651\frac{3}{2}\rangle \to \|651\frac{1}{2}\rangle$	3.9	6.70	0.31
	$\|532\frac{5}{2}\rangle \to \|532\frac{3}{2}\rangle$	4.0	$\|642\frac{5}{2}\rangle \to \|642\frac{3}{2}\rangle$	4.5		
	$\|541\frac{3}{2}\rangle \to \|541\frac{1}{2}\rangle$	4.5	$\|633\frac{7}{2}\rangle \to \|633\frac{5}{2}\rangle$	5.0		
	$\|404\frac{9}{2}\rangle \to \|404\frac{7}{2}\rangle$	4.1	$\|505\frac{11}{2}\rangle \to \|505\frac{9}{2}\rangle$	5.1		
			$\|514\frac{9}{2}\rangle \to \|514\frac{7}{2}\rangle$	4.6		
			$\|512\frac{5}{2}\rangle \to \|512\frac{3}{2}\rangle$	2.4		
^{176}Yb	$\|523\frac{7}{2}\rangle \to \|523\frac{5}{2}\rangle$	4.5	$\|651\frac{3}{2}\rangle \to \|651\frac{1}{2}\rangle$	4.2	6.72	0.29
	$\|532\frac{5}{2}\rangle \to \|532\frac{3}{2}\rangle$	4.1	$\|642\frac{5}{2}\rangle \to \|642\frac{3}{2}\rangle$	4.5		
	$\|541\frac{3}{2}\rangle \to \|541\frac{1}{2}\rangle$	4.5	$\|633\frac{7}{2}\rangle \to \|633\frac{5}{2}\rangle$	5.0		
	$\|404\frac{9}{2}\rangle \to \|404\frac{7}{2}\rangle$	4.0	$\|505\frac{11}{2}\rangle \to \|505\frac{9}{2}\rangle$	5.2		
			$\|512\frac{5}{2}\rangle \to \|512\frac{3}{2}\rangle$	2.4		
^{178}Hf	$\|523\frac{7}{2}\rangle \to \|523\frac{5}{2}\rangle$	4.4	$\|505\frac{11}{2}\rangle \to \|505\frac{9}{2}\rangle$	4.2	6.75	0.26
	$\|532\frac{5}{2}\rangle \to \|532\frac{3}{2}\rangle$	4.1	$\|512\frac{5}{2}\rangle \to \|512\frac{3}{2}\rangle$	2.4		
	$\|541\frac{3}{2}\rangle \to \|541\frac{1}{2}\rangle$	4.1	$\|633\frac{7}{2}\rangle \to \|633\frac{5}{2}\rangle$	5.0		
	$\|402\frac{5}{2}\rangle \to \|402\frac{3}{2}\rangle$	1.9	$\|642\frac{5}{2}\rangle \to \|642\frac{3}{2}\rangle$	4.6		
	$\|411\frac{3}{2}\rangle \to \|411\frac{1}{2}\rangle$	1.4	$\|631\frac{3}{2}\rangle \to \|631\frac{1}{2}\rangle$	7.8		
^{180}Hf	$\|523\frac{7}{2}\rangle \to \|523\frac{5}{2}\rangle$	4.4	$\|505\frac{11}{2}\rangle \to \|505\frac{9}{2}\rangle$	4.2	6.80	0.25
	$\|532\frac{5}{2}\rangle \to \|532\frac{3}{2}\rangle$	4.1	$\|512\frac{5}{2}\rangle \to \|512\frac{3}{2}\rangle$	2.4		
	$\|541\frac{3}{2}\rangle \to \|541\frac{1}{2}\rangle$	4.1	$\|624\frac{9}{2}\rangle \to \|624\frac{7}{2}\rangle$	5.3		
	$\|402\frac{5}{2}\rangle \to \|402\frac{3}{2}\rangle$	1.9	$\|633\frac{7}{2}\rangle \to \|633\frac{5}{2}\rangle$	5.0		
	$\|411\frac{3}{2}\rangle \to \|411\frac{1}{2}\rangle$	1.4	$\|642\frac{5}{2}\rangle \to \|642\frac{3}{2}\rangle$	4.6		
			$\|631\frac{3}{2}\rangle \to \|631\frac{1}{2}\rangle$	7.8		
^{226}Ra	$\|523\frac{7}{2}\rangle \to \|523\frac{5}{2}\rangle$	4.3	$\|624\frac{9}{2}\rangle \to \|624\frac{7}{2}\rangle$	5.0	7.31	0.20
	$\|514\frac{9}{2}\rangle \to \|514\frac{7}{2}\rangle$	4.4	$\|615\frac{11}{2}\rangle \to \|615\frac{9}{2}\rangle$	5.0		
	$\|505\frac{11}{2}\rangle \to \|505\frac{9}{2}\rangle$	4.4	$\|606\frac{13}{2}\rangle \to \|606\frac{11}{2}\rangle$	5.6		
			$\|761\frac{3}{2}\rangle \to \|761\frac{1}{2}\rangle$	4.3		
^{232}Th	$\|651\frac{3}{2}\rangle \to \|651\frac{1}{2}\rangle$	4.5	$\|752\frac{5}{2}\rangle \to \|752\frac{3}{2}\rangle$	4.1	7.37	0.25
	$\|505\frac{11}{2}\rangle \to \|505\frac{9}{2}\rangle$	4.2	$\|761\frac{3}{2}\rangle \to \|761\frac{1}{2}\rangle$	4.0		
	$\|514\frac{9}{2}\rangle \to \|514\frac{7}{2}\rangle$	4.0	$\|631\frac{3}{2}\rangle \to \|631\frac{1}{2}\rangle$	1.0		
	$\|523\frac{7}{2}\rangle \to \|523\frac{5}{2}\rangle$	3.7	$\|624\frac{9}{2}\rangle \to \|624\frac{7}{2}\rangle$	5.0		
			$\|615\frac{11}{2}\rangle \to \|615\frac{9}{2}\rangle$	4.8		
			$\|606\frac{13}{2}\rangle \to \|606\frac{11}{2}\rangle$	5.4		

Table 7.4: Nuclear radii R_0, deformation parameters δ and energies $\Delta E_{n'}$ of M1 spin-flip transitions in some deformed nuclei of interest.

only intermediate states $|n\rangle$ from the continuum, including both positive and negative energy solutions of the Dirac equation.

For further computation of the matrix element (7.40) the electron wave functions need to be specified.

7.B.1 The $s_{1/2}$ and $p_{1/2}$ wave functions

The valence electron $s_{1/2}$ and $p_{1/2}$ wave functions may be expressed in terms of the spherical spinors $\Omega_\mu^\kappa(\hat{\mathbf{R}})$ (see, e.g., Ref. [75]) where μ is the magnetic quantum number and $\kappa = (l-j)(2j+1)$ as

$$|s_{1/2}\rangle = c_{s_{1/2}} \begin{pmatrix} f_{s_{1/2}}(R)\Omega_\mu^{-1}(\hat{\mathbf{R}}) \\ ig_{s_{1/2}}(R)\Omega_\mu^{1}(\hat{\mathbf{R}}) \end{pmatrix}, \tag{7.41a}$$

$$|p_{1/2}\rangle = c_{p_{1/2}} \begin{pmatrix} f_{p_{1/2}}(R)\Omega_\mu^{1}(\hat{\mathbf{R}}) \\ ig_{p_{1/2}}(R)\Omega_\mu^{-1}(\hat{\mathbf{R}}) \end{pmatrix}, \tag{7.41b}$$

where the radial wave functions $f_{s,p_{1/2}}$ and $g_{s,p_{1/2}}$ are well approximated in the region $R_0 < R \ll a_B/Z^{1/3}$ by the Bessel functions of the first kind $J_\nu(x)$ (see, e.g., [51]),

$$f_{s_{1/2}}(R) = \frac{1}{R}\left[(-1+\gamma)J_{2\gamma}\left(\sqrt{\frac{8ZR}{a_B}}\right) - \frac{1}{2}\sqrt{\frac{8ZR}{a_B}}J_{2\gamma-1}\left(\sqrt{\frac{8ZR}{a_B}}\right)\right], \tag{7.42a}$$

$$f_{p_{1/2}}(R) = \frac{1}{R}\left[(1+\gamma)J_{2\gamma}\left(\sqrt{\frac{8ZR}{a_B}}\right) - \frac{1}{2}\sqrt{\frac{8ZR}{a_B}}J_{2\gamma-1}\left(\sqrt{\frac{8ZR}{a_B}}\right)\right], \tag{7.42b}$$

$$g_{s_{1/2}}(R) = g_{p_{1/2}}(R) = \frac{1}{R}Z\alpha J_{2\gamma}\left(\sqrt{\frac{8ZR}{a_B}}\right). \tag{7.42c}$$

Note that the wave functions (7.42) are the zero-energy solutions of the Dirac-Coulomb equations for a point-like nucleus. For an extended nucleus, the corresponding solution is complicated. At the current level of accuracy, it suffices to use Eqs. (7.42) as an approximation to the wave functions. For the region inside the nucleus, $0 \le R \le R_0$, the radial wave functions $f_{s,p_{1/2}}$ and $g_{s,p_{1/2}}$ may be continued as follows

$$f_{s_{1/2}}(R) = \frac{1}{R_0}\left[(-1+\gamma)J_{2\gamma}\left(\sqrt{\frac{8ZR_0}{a_B}}\right) - \frac{1}{2}\sqrt{\frac{8ZR_0}{a_B}}J_{2\gamma-1}\left(\sqrt{\frac{8ZR_0}{a_B}}\right)\right], \tag{7.43a}$$

$$f_{p_{1/2}}(R) = \frac{R}{R_0^2}\left[(1+\gamma)J_{2\gamma}\left(\sqrt{\frac{8ZR_0}{a_B}}\right) - \frac{1}{2}\sqrt{\frac{8ZR_0}{a_B}}J_{2\gamma-1}\left(\sqrt{\frac{8ZR_0}{a_B}}\right)\right], \tag{7.43b}$$

$$g_{s_{1/2}}(R) = \frac{R}{R_0}Z\alpha J_{2\gamma}\left(\sqrt{\frac{8ZR_0}{a_B}}\right), \tag{7.43c}$$

$$g_{p_{1/2}}(R) = \frac{1}{R_0}Z\alpha J_{2\gamma}\left(\sqrt{\frac{8ZR_0}{a_B}}\right). \tag{7.43d}$$

Note that these functions are the approximate solutions (containing only leading terms at small distance) of the Dirac equation inside the nucleus with constant density.

Note also that since $8ZR_0/a_B \ll 1$, the Bessel functions in Eqs. (7.43) may be series expanded over their arguments. For computing radial integrals inside the nucleus it is sufficient to keep the leading terms of these expansions as in Eqs. (7.5).

7.B.2 Excited electronic states of the continuous spectrum

The excited electronic states $|n\rangle$ in the continuous spectrum may be labeled by the quantum number $\kappa = (l-j)(2j+1)$ and the energy E, $|n\rangle \equiv |E\kappa\rangle$. In spherical coordinates, these functions read (see, e.g., Refs. [77, 78]):

$$|n\rangle \equiv |E\kappa\rangle = \begin{pmatrix} f_\kappa^E(R)\Omega_\mu^\kappa(\hat{\mathbf{R}}) \\ ig_\kappa^E(R)\Omega_\mu^{-\kappa}(\hat{\mathbf{R}}) \end{pmatrix}, \tag{7.44}$$

with

$$f^E_\kappa(R) = \frac{(2pR)^\gamma e^{\pi y/2}\,|\Gamma(\gamma+iy)|\,\sqrt{|E+m_e|}}{R\sqrt{\pi p}\Gamma(2\gamma+1)}\mathrm{Re}[e^{-ipR+i\eta}{}_1F_1(\gamma+1+iy,2\gamma+1,2ipR)]\,, \tag{7.45a}$$

$$g^E_\kappa(R) = -\mathrm{sgn}(E)\frac{(2pR)^\gamma e^{\pi y/2}\,|\Gamma(\gamma+iy)|\,\sqrt{|E-m_e|}}{R\sqrt{\pi p}\Gamma(2\gamma+1)}\mathrm{Im}[e^{-ipR+i\eta}{}_1F_1(\gamma+1+iy,2\gamma+1,2ipR)]\,. \tag{7.45b}$$

Here $p=\sqrt{E^2-m_e^2}$ is the electron's momentum, $y=Z\alpha E/p$, $e^{i\eta}=\sqrt{-\frac{\kappa-iym_e/E}{\gamma+iy}}$ and ${}_1F_1(a,b,z)$ is the confluent hypergeometric function of the first kind. Note that the wave functions (7.44) are normalized as $\langle E'\kappa|E\kappa\rangle=\delta(E'-E)$.

The functions (7.45) solve for the Dirac equation with a point-like nucleus. Therefore, we will only use them for outside of the nucleus, $R>R_0$. For the inside of the nucleus, $0\le R\le R_0$, we will consider the following continuation of these functions

$$f^E_\kappa(R)=b_1R^l\,,\qquad g^E_\kappa(R)=b_2R^{\tilde l}\,, \tag{7.46}$$

where $l=|\kappa+1/2|-1/2$ is the orbital angular momentum corresponding to κ, $\tilde l=|-\kappa+1/2|-1/2$ is the orbital angular momentum corresponding to $-\kappa$. The values of the coefficients b_1 and b_2 are determined by matching Eqs. (7.45) and (7.46) on the boundary of the nucleus. The wave functions (7.46) are, to the leading order, solutions to the Dirac equation inside a nucleus of a constant density.

We stress that the extension of the electronic wave functions to the inside region of the nucleus (7.46) is an approximation which is acceptable at our level of accuracy. We checked the validity of this approximation by computing the Lamb shift in heavy atoms due to nuclear polarizability. Within this approximation, we have 95% agreement with the exact results presented in Refs. [47–49].

7.B.3 Results of calculation of electronic matrix element

Substituting the wave functions (7.41) and (7.44) into Eq. (7.40) and performing the integration over angular variables, we obtain

$$M(\Delta E_{n'})=-\frac{2\alpha}{9}\int_{m_e}^{\infty}\frac{T(E)dE}{E-E_{s_{1/2}}+\Delta E_{n'}}-\frac{2\alpha}{9}\int_{-\infty}^{-m_e}\frac{T(E)dE}{E-E_{s_{1/2}}-\Delta E_{n'}}\,, \tag{7.47}$$

where

$$T(E)=R^{(1)}_s(E)R^{(1)}_p(E)-R^{(-2)}_s(E)R^{(-2)}_p(E)-S^{(-1)}_s(E)S^{(-1)}_p(E)+S^{(2)}_s(E)S^{(2)}_p(E)\,, \tag{7.48}$$

and the radial integrals $R^{(\kappa)}_{s,p}(E)$ and $S^{(\kappa)}_{s,p}(E)$ are defined by

$$R^{(\kappa)}_s(E)\equiv\int_0^\infty\left(f_{s_{1/2}}f^E_\kappa+g_{s_{1/2}}g^E_\kappa\right)f(R)R^2dR\,, \tag{7.49a}$$

$$R^{(\kappa)}_p(E)\equiv\int_0^\infty\left(f_{p_{1/2}}g^E_\kappa+g_{p_{1/2}}f^E_\kappa\right)f(R)R^2dR\,, \tag{7.49b}$$

$$S^{(\kappa)}_s(E)\equiv\int_0^\infty\left(f_{s_{1/2}}g^E_\kappa+g_{s_{1/2}}f^E_\kappa\right)f(R)R^2dR\,, \tag{7.49c}$$

$$S^{(\kappa)}_p(E)\equiv\int_0^\infty\left(f_{p_{1/2}}f^E_\kappa+g_{p_{1/2}}g^E_\kappa\right)f(R)R^2dR\,. \tag{7.49d}$$

Here, the radial function $f(R)$ takes into account the radial dependence of the operators (7.16),

$$f(R)=\theta(R-R_0)\frac{1}{R^2}+\theta(R_0-R)\frac{R}{R_0^3}\,. \tag{7.50}$$

Note that Eq. (7.48) involves only the terms with $\kappa=\pm1,\pm2$ which are allowed by the selection rules for transitions from $s_{1/2}$ and $p_{1/2}$ bound electron states.

With the radial wave functions (7.42), (7.43), (7.45) and (7.46), the radial integrals (7.49) may be computed numerically for any specific electron energy E and nuclear energy $\Delta E_{n'}$. For all values of $\Delta E_{n'}$

	Spherical			Deformed						
	^{138}Ba	^{206}Pb	^{208}Pb	^{172}Yb	^{174}Yb	^{176}Yb	^{178}Hf	^{180}Hf	^{226}Ra	^{232}Th
$\frac{M_p}{a_B}$	11.1	94.1	94.0	69.3	69.3	69.2	121	121	156	244
$\frac{M_n}{a_B}$	16.5	143	95.7	83.4	106	88.7	96.8	114	196	385

Table 7.5: Numerical values for the electronic matrix elements M_p and M_n for several atoms of interest.

presented in Appendix 7.A, numerical analysis showed that for $|E| > 500m_e$, $T(E)/(E_{s_{1/2}} - E \pm \Delta E_{n'})$ is effectively zero, so the energy integrals in Eqs. (7.47) may be cut off at $|E| = 500m_e$. We also point out that the dominant contributions to the energy integrals (7.47) come from the region where $E \sim 50m_e$, which is larger than the values of $\Delta E_{n'}$ considered in Appendix 7.A. As a result, the function $M(\Delta E_{n'})$ has weak energy dependence.

The energy integrals in Eqs. (7.47) are computed numerically, giving $M(\Delta E_{n'})$ for all values of $\Delta E_{n'}$ presented in Appendix 7.A. The resulting numerical values of the electronic factors M_p and M_n introduced in Eqs. (7.21) are presented in Table. 7.5.

Bibliography

[1] N. Cabibbo, Phys. Rev. Lett. **10**, 531 (1963).

[2] M. Kobayashi and T. Maskawa, Prog. Theor. Phys. **49**, 652 (1973).

[3] R. D. Peccei and H. R. Quinn, Phys. Rev. Lett. **38**, 1440 (1977).

[4] S. Weinberg, Phys. Rev. Lett. **40**, 223 (1978).

[5] F. Wilczek, Phys. Rev. Lett. **40**, 279 (1978).

[6] N. Yamanaka, B. Sahoo, N. Yoshinaga, T. Sato, K. Asahi, and B. Das, Eur. Phys. J. A **53**, 54 (2017).

[7] T. E. Chupp, P. Fierlinger, M. J. Ramsey-Musolf, and J. T. Singh, Rev. Mod. Phys. **91**, 015001 (2019).

[8] W. C. Griffith, M. D. Swallows, T. H. Loftus, M. V. Romalis, B. R. Heckel, and E. N. Fortson, Phys. Rev. Lett. **102**, 101601 (2009).

[9] C. A. Baker, D. D. Doyle, P. Geltenbort, K. Green, M. G. D. van der Grinten, P. G. Harris, P. Iaydjiev, S. N. Ivanov, D. J. R. May, J. M. Pendlebury, et al., Phys. Rev. Lett. **97**, 131801 (2006).

[10] J. J. Hudson, D. M. Kara, I. Smallman, B. E. Sauer, M. R. Tarbutt, and E. A. Hinds, Nature **473**, 493 (2011).

[11] J. Baron, W. C. Campbell, D. DeMille, J. M. Doyle, G. Gabrielse, Y. V. Gurevich, P. W. Hess, N. R. Hutzler, E. Kirilov, I. Kozyryev, et al., Science **343**, 269 (2014).

[12] R. H. Parker, M. R. Dietrich, M. R. Kalita, N. D. Lemke, K. G. Bailey, M. Bishof, J. P. Greene, R. J. Holt, W. Korsch, Z.-T. Lu, et al., Phys. Rev. Lett. **114**, 233002 (2015).

[13] J. M. Pendlebury et al., Phys. Rev. D **92**, 092003 (2015).

[14] B. Graner, Y. Chen, E. G. Lindahl, and B. R. Heckel, Phys. Rev. Lett. **116**, 161601 (2016).

[15] G. E. Harrison, P. G. H. Sandars, and S. J. Wright, Phys. Rev. Lett. **23**, 274 (1969).

[16] E. A. Hinds and P. G. H. Sandars, Phys. Rev. A **21**, 480 (1980).

[17] D. A. Wilkening, N. F. Ramsey, and D. J. Larson, Phys. Rev. A **29**, 425 (1984).

[18] D. Schropp, D. Cho, T. Vold, and E. A. Hinds, Phys. Rev. Lett. **59**, 991 (1987).

[19] D. Cho, K. Sangster, and E. A. Hinds, Phys. Rev. A **44**, 2783 (1991).

[20] T. G. Vold, F. J. Raab, B. Heckel, and E. N. Fortson, Phys. Rev. Lett. **52**, 2229 (1984).

[21] T. E. Chupp, R. J. Hoare, R. L. Walsworth, and B. Wu, Phys. Rev. Lett. **72**, 2363 (1994).

[22] R. E. Stoner, M. A. Rosenberry, J. T. Wright, T. E. Chupp, E. R. Oteiza, and R. L. Walsworth, Phys. Rev. Lett. **77**, 3971 (1996).

[23] D. Bear, T. E. Chupp, K. Cooper, S. DeDeo, M. Rosenberry, R. E. Stoner, and R. L. Walsworth, Phys. Rev. A **57**, 5006 (1998).

[24] M. A. Rosenberry and T. E. Chupp, Phys. Rev. Lett. **86**, 22 (2001).

[25] M. V. Romalis, W. C. Griffith, J. P. Jacobs, and E. N. Fortson, Phys. Rev. Lett. **86**, 2505 (2001).

[26] M. Bishof, R. H. Parker, K. G. Bailey, J. P. Greene, R. J. Holt, M. R. Kalita, W. Korsch, N. D. Lemke, Z.-T. Lu, P. Mueller, et al., Phys. Rev. C **94**, 025501 (2016).

[27] H. Loh, K. C. Cossel, M. C. Grau, K.-K. Ni, E. R. Meyer, J. L. Bohn, J. Ye, and E. A. Cornell, Science **342**, 1220 (2013).

[28] S. Eckel, P. Hamilton, E. Kirilov, H. W. Smith, and D. DeMille, Phys. Rev. A **87**, 052130 (2013).

[29] W. B. Cairncross, D. N. Gresh, M. Grau, K. C. Cossel, T. S. Roussy, Y. Ni, Y. Zhou, J. Ye, and E. A. Cornell, Phys. Rev. Lett. **119**, 153001 (2017).

[30] P. Aggarwal, H. L. Bethlem, A. Borschevsky, M. Denis, K. Esajas, P. A. Haase, Y. Hao, S. Hoekstra, K. Jungmann, T. B. Meijknecht, et al., Eur. Phys. J. D **72**, 197 (2018).

[31] V. Andreev, D. G. Ang, D. DeMille, J. M. Doyle, G. Gabrielse, J. Haefner, N. R. Hutzler, Z. Lasner, C. Meisenhelder, B. R. O'Leary, et al. (ACME), Nature **562**, 355 (2018).

[32] V. Flambaum, M. Pospelov, A. Ritz, and Y. Stadnik, Phys. Rev. D **102**, 035001 (2020).

[33] T. S. Roussy et al., arXiv:2006.15787 (2020).

[34] P. W. Graham and S. Rajendran, Phys. Rev. D **84**, 055013 (2011).

[35] L. I. Schiff, Phys. Rev. **132**, 2194 (1963).

[36] O. P. Sushkov, V. V. Flambaum, and I. B. Khriplovich, Zh. Eksp. Teor. Fiz **87**, 1521 (1984).

[37] V. V. Flambaum, I. B. Khriplovich, and O. P. Sushkov, Nucl. Phys. A **449**, 750 (1986).

[38] V. V. Flambaum, Phys. Lett. B **320**, 211 (1994).

[39] V. A. Dzuba, V. V. Flambaum, P. G. Silvestrov, and O. P. Sushkov, Phys. Lett. A **118**, 177 (1986).

[40] V. V. Flambaum, Phys. Rev. A **98**, 043408 (2018).

[41] H. B. Tran Tan, V. V. Flambaum, and I. B. Samsonov, Phys. Rev. A **99**, 013430 (2019).

[42] V. V. Flambaum and I. B. Samsonov, Phys. Rev. A **98**, 053437 (2018).

[43] V. V. Flambaum and I. B. Samsonov, Phys. Rev. Res. **2**, 023042 (2020).

[44] V. V. Flambaum, J. S. M. Ginges, and G. Mititelu, arXiv:nucl-th/0010100 (2000).

[45] V. V. Flambaum and I. B. Khriplovich, Zh. Eksp. Theor. Fiz **89**, 1505 (1985).

[46] J. Bsaisou, U.-G. Meißner, A. Nogga, and A. Wirzba, Annals Phys. **359**, 317 (2015).

[47] G. Plunien, B. Müller, W. Greiner, and G. Soff, Phys. Rev. A **43**, 5853 (1991).

[48] K. Pachucki, D. Leibfried, and T. W. Hänsch, Phys. Rev. A **48**, R1 (1993).

[49] G. Plunien and G. Soff, Phys. Rev. A **51**, 1119 (1995).

[50] S. G. Nilsson, Dan. Mat. Fys. Medd. **29**, 1 (1955).

[51] I. B. Khriplovich, *Parity nonconservation in atomic phenomena* (Gordon and Breach Science Publishers, 1991).

[52] P. Sarriguren, E. Moya de Guerra, and R. Nojarov, Phys. Rev. C **54**, 690 (1996).

[53] T. Fleig and M. Jung, J. High Energy Phys. **2018**, 12 (2018).

[54] M. Pospelov and A. Ritz, Ann. Phys. **318**, 119 (2005), special Issue.

[55] R. J. Crewther, P. Di Vecchia, G. Veneziano, and E. Witten, Phys. Let. B **88**, 123 (1979).

[56] W. Hockings and U. van Kolck, Phys. Lett. B **605**, 273 (2005).

[57] K. Ottnad, B. Kubis, U.-G. Meissner, and F.-K. Guo, Phys. Lett. B **687**, 42 (2010).

[58] F.-K. Guo and U.-G. Meissner, J. High Energy Phys. **12**, 097 (2012).

[59] M. Pospelov and A. Ritz, Phys. Rev. Lett. **83**, 2526 (1999).

[60] V. V. Flambaum, D. DeMille, and M. G. Kozlov, Phys. Rev. Lett. **113**, 103003 (2014).

[61] M. Pospelov and A. Ritz, Phys. Rev. D **63**, 073015 (2001).

[62] F. Abusaif et al., arXiv:1912.07881 (2019).

[63] J. de Vries, E. Mereghetti, and A. Walker-Loud, Phys. Rev. C **92**, 045201 (2015).

[64] J. Bsaisou, J. de Vries, C. Hanhart, S. Liebig, U.-G. Meißner, D. Minossi, A. Nogga, and A. Wirzba, J. High Energy Phys. **2015**, 104 (2015).

[65] J. de Vries and U.-G. Meißner, Int. J. Mod. Phys. E **25**, 1641008 (2016).

[66] J. Bsaisou, C. Hanhart, S. Liebig, U.-G. Meißner, A. Nogga, and A. Wirzba, Eur. Phys. J. A **49**, 1 (2013).

[67] C. Abel, S. Afach, N. J. Ayres, C. A. Baker, G. Ban, G. Bison, K. Bodek, V. Bondar, M. Burghoff, E. Chanel, et al., Phys. Rev. Lett. **124**, 081803 (2020).

[68] V. V. Flambaum and V. A. Dzuba, Phys. Rev. A **101**, 042504 (2020).

[69] B. K. Sahoo, Phys. Rev. D **95**, 013002 (2017).

[70] N. Sachdeva, I. Fan, E. Babcock, M. Burghoff, T. E. Chupp, S. Degenkolb, P. Fierlinger, S. Haude, E. Kraegeloh, W. Kilian, et al., Phys. Rev. Lett. **123**, 143003 (2019).

[71] F. Allmendinger, I. Engin, W. Heil, S. Karpuk, H.-J. Krause, B. Niederländer, A. Offenhäusser, M. Repetto, U. Schmidt, and S. Zimmer, Phys. Rev. A **100**, 022505 (2019).

[72] M. Tanabashi et al. (Particle Data Group), Phys. Rev. D **98**, 030001 (2018).

[73] S. Ban, J. Dobaczewski, J. Engel, and A. Shukla, Phys. Rev. C **82**, 015501 (2010).

[74] H. Loh, K. C. Cossel, M. C. Grau, K.-K. Ni, E. R. Meyer, J. L. Bohn, J. Ye, and E. A. Cornell, Science **342**, 1220 (2013).

[75] R. Szmytkowski, J. Math. Chem. **42**, 397 (2007).

[76] A. Bohr and B. R. Mottelson, *Nuclear Structure*, vol. 2 (World Scientific, Singapore, 1998).

[77] V. B. Berestetskii, E. M. Lifshitz, and L. P. Pitaevskii, *Quantum electrodynamics*, vol. 4 (Butterworth-Heinemann, 1982).

[78] W. Greiner, *Relativistic quantum mechanics: Wave Equations*, vol. 2 (Springer, 2000).

Chapter 8

Effects of CP-violating internucleon interactions in paramagnetic molecules

8.1 Overview

In chapter 7, I showed that nucleon EDMs can induce atomic EDM via the combined electric and magnetic electron-nucleon interaction. In this chapter, I demonstrate that CP-odd internucleon forces can have similar effects: when coupled with electron-nucleon electric and magnetic interaction, they induce measurable atomic EDMs.

As a result of my research, I have published the following paper:

1. V. V. Flambaum, I. B. Samsonov and H. B. Tran Tan
   Effects CP-violating internucleon interactions in paramagnetic molecules
   Phys. Rev. D 102, 115036 (2020), DOI: 10.1103/PhysRevD.102.115036, arXiv:2009.07992.

8.2 Abstract

We demonstrate that electron electric dipole moment (eEDM) experiments with molecules in paramagnetic state are sensitive to P,T-violating nuclear forces and other CP-violating parameters in the hadronic sector. These experiments, in particular, measure the coupling constant C_{SP} of the CP-odd contact semileptonic interaction. We establish relations between C_{SP} and different CP-violating hadronic parameters including strength constants of the CP-odd nuclear potentials, CP-odd pion-nucleon interactions, quark-chromo EDM and QCD vacuum angle. These relations allow us to find limits on various CP-odd hadronic parameters.

8.3 Introduction

The existence of non-vanishing electric dipole moments (EDMs) of elementary particles was conjectured nearly seventy years ago [1–4], but they have not been observed so far. Their discovery would be a crucial step in the study of charge and parity (CP) violations. On the one hand, the Standard Model of elementary particles predicts non-vanishing values for the EDMs of the electron and nucleons, but these values are so minuscule that they are practically unobservable in current experiments. On the other hand, it is known that the CP-violation is needed to explain the apparent matter-antimatter asymmetry in the universe [5]. It is therefore an important challenge for experimental physics to measure the EDMs of elementary particles as well as EDMs of composite objects such as nucleons, nuclei and atoms.

In the last decade or so, tremendous progress has been achieved in the experiments with paramagetic molecules which measure the electron EDM through specific energy level shifts [6, 7] (see also Refs. [8, 9] for reviews). As was demonstrated in the recent works [10, 11], these experiments are also sensitive to the CP-violating interactions in the hadronic sector, which originate, in particular, from the nucleon EDMs. The aim of the current work is to extend the results of the papers [10, 11] and to study the sensitivity of paramagnetic EDM experiments to P,T-violating nuclear forces.

It is a well-known fact that the CP-violating effects are significantly enhanced in heavy atoms [12]. In this paper, we consider a single-particle nuclear model in which the open-shell nucleon interacts with a heavy nuclear core through a nuclear potential $U(\mathbf{r})$. The P,T-violating nuclear forces are taken into account by the phenomenological interaction Hamiltonian $H_{\rm odd} = \xi\boldsymbol{\sigma}\cdot\nabla U(\mathbf{r})$, where $\boldsymbol{\sigma}/2$ is the nucleon spin operator and ξ is the coupling constant of dimension of length. This coupling constant will be denoted by ξ_p for proton and ξ_n for neutron. The authors of Ref. [13] demonstrated that the leading contributions to this interaction arise due to π meson exchange between the open-shell nucleon and the nuclear core. In general, however, this interaction may arise due to the CP-violating πNN, ηNN, three-pion and four-nucleon interactions. The last two interactions were considered, in particular, in Ref. [14].

In this paper, we will focus on the contributions to the atomic EDM arising due to the P,T-odd nuclear force with the Hamiltonian $H_{\rm odd}$ regardless of the underlying fundamental interaction. In principle, experimental limits on the phenomenological parameters $\xi_{p,n}$ may be converted into limits on the parameters of more fundamental hadronic interactions. We stress that the interaction $H_{\rm odd}$ considered in this work is an independent source of CP violating effects, separate from the contributions due to nucleon EDMs considered in Refs. [10, 11].

The most stringent experimental constraint on the electron EDM was obtained by the ACME collaboration [6] which measured specific energy level shifts in the ^{232}ThO molecule. Based on theoretical calculations [15, 16], this experiment also placed a limit on the CP-odd electron-nucleon interaction coupling constant (90% C.L.),

$$|C_{SP}|_{\rm Th} < 7.3\times10^{-10}\,. \tag{8.1}$$

In a heavy, spinless nucleus with Z protons and $N = A - Z$ neutrons this coupling constant is a linear combination of independent electron couplings to protons (C_{SP}^p) and neutrons (C_{SP}^n), $C_{SP} = C_{SP}^p Z/A + C_{SP}^n N/A$. The latter two coupling constants correspond to the following CP-odd semileptonic operators

$$\mathcal{L} = \frac{iG_F}{\sqrt{2}}C_{SP}^p\,\bar e\gamma_5 e\,\bar p p + \frac{iG_F}{\sqrt{2}}C_{SP}^n\,\bar e\gamma_5 e\,\bar n n\,, \tag{8.2}$$

where G_F is the Fermi coupling constant, e, p and n are respectively the electron, proton and neutron fields. Note that the subscript 'SP' denotes the nucleon-scalar and electron pseudoscalar two-fermion bilinears.[1]

Our goal is to establish the leading-order relation between the coupling constant C_{SP} and the parameters of the P,T-odd internucleon interaction ξ_p and ξ_n, $C_{SP} = C_{SP}(\xi_p,\xi_n)$. This will allow us to find limits on these couplings originating from the experimental constraint (8.1). Then, using known relations between the constants ξ_p,ξ_n and more fundamental CP-violating hadronic parameters, we will establish leading-order relation between C_{SP} and CP-odd pion-nucleon couplings $\bar g_{\pi NN}^{(0,1,2)}$, quark-chromo EDMs $\tilde d_{u,d}$ and QCD vacuum angle $\bar\theta$.

Note that this problem involves the third order perturbation theory in the nuclear part and second order in the electron-nucleus interaction. To get through these complications we have to make some approximations in the nuclear part of the problem where we perform the calculations analytically. While all these approximations are common and justifiable, we cannot pretend that the accuracy of our results is better than a factor of two [12, 13, 17]. However, this accuracy is comparable to that in other calculations of the hadronic contributions to atomic EDM where the limits on the CP-violating parameters are often presented on the logarithmic scale. For instance, current limit on QCD vacuum angle reads $|\bar\theta| < 10^{-10}$, see, e.g., reviews [8, 9] and updated limits presented in Ref. [18].

The rest of the paper is organized as follows. In Sect. 8.4, we present an estimate for the atomic EDM arising from the CP-odd nuclear forces. In Sect. 8.5, we compare this contribution to the atomic EDM with that of the contact electron-nucleon interaction and the nucleon permanent EDMs and find relations between the constant C_{SP} and CP-violating hadronic parameters. In Sect. 8.6 we give a summary of our results and provide some comments on assumptions and precision. Technical details of calculations of electronic and nuclear matrix elements are collected in appendices.

Throughout this paper we use natural units with $c = \hbar = 1$.

[1] In general, there are also nucleon-pseudoscalar and electron-scalar ('PS') as well as tensor-tensor ('TT') CP-violating semileptonic interactions. These interactions play subleading role in atoms with spinless nuclei and, therefore, they will be ignored in this paper.

8.4 Contributions to the atomic EDM from P,T-odd nuclear forces

In this section, we determine the contributions to the atomic EDM arising due to nuclear P,T-odd interactions. In Sect. 8.4.1 we start with a review of the P,T-perturbed nuclear wave functions, which were found in Ref. [13]. These wave functions will be used in Sect. 8.4.2 for the computation of the nuclear matrix elements contributing to the atomic EDM.

8.4.1 Nuclear wave functions perturbed by P,T-odd nuclear interactions

The nucleons in a nucleus can exhibit different P,T-odd interactions originating both from the Standard Model and beyond. Independently of their nature, in the non-relativistic limit, these short-range interactions may be taken into account by the following phenomenological single-particle Hamiltonian [13]

$$H_{\rm odd} = \frac{G_F}{\sqrt{2}}\frac{\eta}{2m_p}\boldsymbol{\sigma}\cdot\nabla\rho(\mathbf{r})\,, \tag{8.3}$$

where $\boldsymbol{\sigma}/2$ is the spin of the open-shell non-relativistic nucleon, $\rho(\mathbf{r})$ is the density of the nuclear core, η is the effective coupling constant and m_p is the proton mass.

In a heavy nucleus, the nuclear core creates an effective nuclear potential $U(\mathbf{r})$ in which the open-shell nucleon moves. In the short-range approximation, this potential is proportional to the density of the nuclear core, $\rho(\mathbf{r}) = U(\mathbf{r})\rho(0)/U(0)$. Taking this into account, the Hamiltonian (8.3) may be represented as

$$H_{\rm odd} = \xi\boldsymbol{\sigma}\cdot\nabla U(\mathbf{r})\,, \tag{8.4}$$

where [13]

$$\xi = \eta\frac{G_F}{2\sqrt{2}m_p}\frac{\rho(0)}{U(0)} \approx -2\times10^{-21}\eta\cdot\mathrm{cm}\,. \tag{8.5}$$

The total potential for the open-shell nucleon is thus given by

$$\tilde{U} = U + H_{\rm odd} = U + \xi\boldsymbol{\sigma}\cdot\nabla U \approx U(\mathbf{r}+\xi\boldsymbol{\sigma})\,. \tag{8.6}$$

Now let $\psi_{n'}(\mathbf{r})$ be unperturbed single-nucleon wave function labeled by some quantum numbers n'. This function is supposed to solve for the Schrödinger equation with the potential $U(\mathbf{r})$. Equation (8.6) suggests that the wave function perturbed by the P,T-odd interaction (8.3) may be represented as

$$\tilde{\psi}_{n'}(\mathbf{r}) = \psi_{n'}(\mathbf{r}+\xi\boldsymbol{\sigma}) \approx (1+\xi\boldsymbol{\sigma}\cdot\nabla)\psi_{n'}(\mathbf{r})\,, \tag{8.7}$$

or, more generally, generalizing to all nucleons

$$\tilde{\psi}_{n'}(\mathbf{r}_1,...,\mathbf{r}_A) = \left(1+\sum_{\tau=1}^{A}\xi_\tau\boldsymbol{\sigma}_\tau\cdot\nabla_\tau\right)\psi_{n'}(\mathbf{r}_1,...,\mathbf{r}_A)\,, \tag{8.8}$$

where $\tilde{\psi}_{n'}(\mathbf{r}_1,...,\mathbf{r}_A)$ and $\psi_{n'}(\mathbf{r}_1,...,\mathbf{r}_A)$ are multi-palrticle nuclear wave functions. Note that the constants ξ_τ are different for proton ($\xi_\tau = \xi_p$) and neutron ($\xi_\tau = \xi_n$).

According to Eq. (8.8), the matrix elements of an operator $\mathcal{O}$ may be written up to the first order in coupling constant ξ as

$$\langle\tilde{m}'|\mathcal{O}|\tilde{n}'\rangle = \langle m'|\mathcal{O}|n'\rangle - \sum_{\tau=1}^{A}\xi_\tau\langle m'|[\boldsymbol{\sigma}_\tau\cdot\nabla_\tau,\mathcal{O}]|n'\rangle\,, \tag{8.9}$$

where $|n'\rangle$ and $|\tilde{n'}\rangle$ are the kets corresponding to the wave functions $\psi_{n'}(\mathbf{r}_1,...,\mathbf{r}_A)$ and $\tilde{\psi}_{n'}(\mathbf{r}_1,...,\mathbf{r}_A)$, respectively.

The P,T-perturbed wave functions (8.8) were found in Ref. [13]. In the next subsection we will use these wave functions to compute the nuclear matrix elements contributing to the atomic EDM.

8.4.2 Electron-nucleon interaction Hamiltonian

Let us consider a valence electron of charge $-e$ and position vector $\mathbf{R}$ interacting with nucleons of charge q_τ located at the point $\mathbf{r}_\tau$. The interaction Hamiltonian considered in this paper is a combination of the electric (q) and magnetic (μ) terms,

$$H_{\rm int} = -\sum_{\tau=1}^{A}(H^q_\tau + H^\mu_\tau)\,, \tag{8.10a}$$

$$H^q_\tau = \frac{eq_\tau}{|\mathbf{R}-\mathbf{r}_\tau|}\,, \tag{8.10b}$$

$$H^\mu_\tau = \frac{e\,\boldsymbol{\mu}_\tau\cdot[(\mathbf{R}-\mathbf{r}_\tau)\times\boldsymbol{\alpha}]}{|\mathbf{R}-\mathbf{r}_\tau|^3}\,, \tag{8.10c}$$

where

$$\boldsymbol{\mu}_\tau = \mu_0(g^l_\tau \mathbf{l}_\tau + g^s_\tau \mathbf{s}_\tau) \tag{8.11}$$

is the nucleon's magnetic moment operator, μ_0 is the nuclear magneton, g^l_τ and g^s_τ are the orbital and spin g-factors of the nucleon. Note that $\mathbf{s}_\tau = \boldsymbol{\sigma}_\tau/2$ is the nucleon spin operator while $\boldsymbol{\alpha} = \left(\begin{smallmatrix} 0 & \boldsymbol{\sigma} \\ \boldsymbol{\sigma} & 0 \end{smallmatrix}\right)$ are the Dirac matrices acting on electron's states. We point out that since we consider spinless nuclei in this paper, the interaction (7.7a) does not arise if the nucleus is treated as a pointlike object.

The interaction Hamiltonian (8.10) as a function of $\mathbf{R}$ and $\mathbf{r}_\tau$ may be expanded into a multipole series. In particular, the leading terms in the expansion of the electric interaction Hamiltonian (8.10b) are

$$H^q_\tau = eq_\tau\left(\frac{1}{R}+\frac{\mathbf{R}\cdot\mathbf{r}_\tau}{R^3}\right)\theta(R-r_\tau) + eq_\tau\left(\frac{1}{r}+\frac{\mathbf{R}\cdot\mathbf{r}_\tau}{r^3_\tau}\right)\theta(r_\tau-R)+\ldots\,, \tag{8.12}$$

where the ellipsis stand for terms with higher multipolarity. In this expansion, the term $\theta(R-r_\tau)/R + \theta(r_\tau-R)/r_\tau$, after averaging with the nuclear charge density $\rho(\mathbf{r})$, gives rise to the Coulomb interaction of the electron with the extended nucleus. This interaction is assumed to have already been taken into account by the unperturbed electronic wave functions.

The term $(\mathbf{R}\cdot\mathbf{r}_\tau)[\theta(R-r_\tau)/R^3 + \theta(r_\tau-R)/r^3_\tau]$ in Eq. (8.12) is the leading dipole one on which we will focus our attention[2]. Evidently, at a distance from the nucleus, this term falls off as $1/R^2$. To find the effective electron-nucleon interaction Hamiltonian inside the nucleus, one needs to average this term over the normalized nuclear density, which, in the leading approximation, may be taken as constant inside the sphere of radius R_0 and vanishing outside, $\rho(r) = 3\theta(R_0-r)/R^3_0$. Since $\rho(r)$ is only needed for the calculation of electronic matrix elements, where dominant contribution comes from outside the nucleus, this approximation does not greatly affect our results. Indeed, a computation which uses a more realistic Woods-Saxon model for the nuclear density only gives a difference of about 3%. The constant density approximation has the advantage of giving analytical form for the regularized potentials. In fact, it was used in the calculation of Lamb shift due to nuclear polarizability [19–22] and hyperfine structure which gave perfect agreement with experiments.

Using this prescription, one may obtain the following continuation of the $1/R^2$ function to small distance

$$f(R) \equiv \int_0^\infty \rho(r)\left[\frac{1}{R^2}\theta(R-r)+\frac{1}{r^2}\theta(r-R)\right]r^2dr = \frac{1}{R^2}\theta(R-R_0)+\frac{3R_0-2R}{R^3_0}\theta(R_0-R)\,, \tag{8.13}$$

with which the regularized dipole interaction operator (8.12) takes the form

$$\bar{H}^q_\tau \equiv eq_\tau(\hat{\mathbf{R}}\cdot\mathbf{r}_\tau)f(R)\,, \tag{8.14}$$

where $\hat{\mathbf{R}} \equiv \mathbf{R}/R$.

The magnetic interaction operator (8.10c) also behaves as $1/R^2$ at large distances from the nucleus and may also be extended to the short-distance region inside the nucleus according to the prescription (8.13),

$$\bar{H}^\mu_\tau \equiv e\boldsymbol{\mu}_\tau\cdot(\hat{\mathbf{R}}\times\boldsymbol{\alpha})f(R)\,. \tag{8.15}$$

[2] This expansion is needed to describe the interaction between the nucleus and the electron. The contribution inside the nucleus is relatively small, the dominant contribution comes from the region outside the nucleus. This justifies the use of the dipole term for the electronic variables.

Thus, the dipole part of the interaction (8.10a) which is regularized at short distances reads

$$\bar{H}_{\rm int} = -\sum_{\tau=1}^{A}(\bar{H}^q_\tau + \bar{H}^\mu_\tau)\,, \tag{8.16}$$

with $\bar{H}^q_\tau$ and $\bar{H}^\mu_\tau$ given by Eqs. (8.14) and (8.15).

According to Eq. (8.9), to take into account the P,T-perturbed nuclear wave functions one has to consider the commutators of the operator $\boldsymbol{\sigma}_\tau\cdot\nabla_\tau$ with the interaction Hamiltonians (8.14) and (8.15),

$$[\boldsymbol{\sigma}_\tau\cdot\nabla_\tau, \bar{H}^q_\tau] = eq_\tau(\boldsymbol{\sigma}_\tau\cdot\hat{\mathbf{R}})f(R)\,, \tag{8.17a}$$

$$[\boldsymbol{\sigma}_\tau\cdot\nabla_\tau, \bar{H}^\mu_\tau] = ie\mu_0(g^s_\tau - g^l_\tau)f(R)(\hat{\mathbf{R}}\times\boldsymbol{\alpha})\cdot(\boldsymbol{\sigma}_\tau\times\nabla_\tau)\,. \tag{8.17b}$$

In deriving Eq. (8.17b) we have applied the following commutator identities: $[\sigma_i,\sigma_j] = 2i\varepsilon_{ijk}\sigma_k$ and $[\nabla_i, l_j] = i\varepsilon_{ijk}\nabla_k$.

8.4.3 Atomic EDM due to P,T-odd nuclear forces

The unperturbed atomic states will be denoted by $|nn'\rangle = |n\rangle|n'\rangle$, where $|n\rangle$ and $|n'\rangle$ are electronic and nuclear states, respectively. In what follows, the nuclear quantum numbers will be distinguished from the electronic ones with the apostrophe. As in Sect. 8.4, the P,T-perturbed nuclear wave functions (8.8) are denoted as $|\tilde{n}'\rangle$. Electronic and nuclear ground states are denoted as $|0\rangle$ and $|\tilde{0}'\rangle$ (or $|0'\rangle$ for unperturbed state), respectively.

The atomic EDM arising from the mixed interaction $H_{\rm int}$ may be calculated in perturbation theory. The first-order contribution to the atomic EDM vanishes for spinless nuclei which we consider in this paper,

$$\sum_{n\neq 0}\frac{\langle 0|-e\mathbf{R}|n\rangle\langle n\tilde{0}'|\bar{H}_{\rm int}|\tilde{0}'0\rangle}{E_0-E_n} = 0\,. \tag{8.18}$$

Indeed, it may be shown that $\langle\tilde{0}'|\bar{H}_{\rm int}|\tilde{0}'\rangle \propto \langle 0'|\mathbf{s}|0'\rangle$=0, where $\mathbf{s}\equiv\sum_{\tau=1}^{A}\mathbf{s}_\tau$ is the nuclear spin operator.

The leading non-vanishing contributions to the atomic EDM thus arise in the second-order perturbation theory,

$$\begin{aligned}\mathbf{d} = 2\sum_{m\neq 0, n\tilde{n}'\neq 0\tilde{0}'}&\frac{\langle 0|-e\mathbf{R}\,|m\rangle\,\langle m\tilde{0}'|\,\bar{H}_{\rm int}\,|\tilde{n}'n\rangle\,\langle n\tilde{n}'|\,\bar{H}_{\rm int}\,|\tilde{0}'0\rangle}{(E_m-E_0)\,[E_n-E_0+{\rm sgn}(E_n)(E_{\tilde{n}'}-E_{\tilde{0}'})]}\\ +\sum_{m\neq 0, n\tilde{n}'\neq 0\tilde{0}'}&\frac{\langle 0\tilde{0}'|\bar{H}_{\rm int}|\tilde{n}'n\rangle\langle n|-e\mathbf{R}|m\rangle\langle m\tilde{n}'|\bar{H}_{\rm int}|\tilde{0}'0\rangle}{[E_n-E_0+{\rm sgn}(E_n)(E_{\tilde{n}'}-E_{\tilde{0}'})][E_m-E_0+{\rm sgn}(E_m)(E_{\tilde{n}'}-E_{\tilde{0}'})]}\,,\end{aligned} \tag{8.19}$$

where the ${\rm sgn}(E_n)$ in the denominators is needed to correctly account for the negative energy electronic states. Indeed, the negative energy electronic states contribute with opposite sign of the nuclear energy because they may be viewed as blocking contributions which prevent the valence electron from directly transitioning into such states which are supposed to be completely occupied in the Dirac sea picture.

The term in the second line in Eq. (8.19) may be neglected in comparison with the other one because it is suppressed by higher power of nuclear energy in the denominator. Moreover, we assume that the leading contributions to the atomic EDM arise from the matrix elements with $|0\rangle = |s_{1/2}\rangle$ and $|m\rangle = |p_{1/2}\rangle$ electronic states because these wave functions are significantly enhanced in the vicinity of a heavy nucleus. Taking this into account, Eq. (8.19) may be cast in the form

$$\mathbf{d} \approx 2\frac{\langle s_{1/2}|e\mathbf{R}|p_{1/2}\rangle\langle p_{1/2}|H_{\rm eff}|s_{1/2}\rangle}{E_{p_{1/2}}-E_{s_{1/2}}}\,, \tag{8.20}$$

where we have introduced the effective interaction Hamiltonian

$$H_{\rm eff} \equiv \sum_{n\tilde{n}'\neq 0\tilde{0}'}\frac{|m\rangle\langle m\tilde{0}'|\bar{H}_{\rm int}|\tilde{n}'n\rangle\langle n\tilde{n}'|\bar{H}_{\rm int}|\tilde{0}'0\rangle\langle 0|}{\Delta E_n + {\rm sgn}(E_n)\Delta E_{\tilde{n}'}}\,. \tag{8.21}$$

Here $\Delta E_n = E_n - E_0$ and $\Delta E_{\tilde{n}'} = E_{\tilde{n}'} - E_{\tilde{0}'}$. Our goal is to calculate the matrix element $\langle p_{1/2}|H_{\rm eff}|s_{1/2}\rangle$ which is responsible for the leading-order contributions to the atomic EDM.

Using the identity (8.9), one may single out the part of the matrix element of the effective Hamiltonian (8.21) which is linear in the P,T-odd nuclear interaction coupling ξ

$$\langle p_{1/2}|H_{\rm eff}|s_{1/2}\rangle = -\sum_{\tau=1}^{A}\sum_{nn'\neq 00'}\frac{\langle p_{1/2}0'|[\xi_\tau\boldsymbol{\sigma}_\tau\cdot\nabla_\tau,\bar{H}_{\rm int}]|n'n\rangle\langle nn'|\bar{H}_{\rm int}|0's_{1/2}\rangle}{\Delta E_n+{\rm sgn}(E_n)\Delta E_{n'}}+(s_{1/2}\leftrightarrow p_{1/2})\,. \quad (8.22)$$

Substituting Eq. (8.16) into Eq. (8.22), we express this matrix element in terms of the operators (8.14) and (8.15),

$$\langle p_{1/2}|H_{\rm eff}|s_{1/2}\rangle = \sum_{\tau=1}^{A}\sum_{nn'\neq 00'}\frac{\xi_\tau\left(\mathcal{M}^{1\tau}_{nn'}+\mathcal{M}^{2\tau}_{nn'}\right)}{\Delta E_n+{\rm sgn}(E_n)\Delta E_{n'}}\,, \quad (8.23)$$

where

$$\mathcal{M}^{1\tau}_{nn'} \equiv \langle p_{1/2}0'|[\boldsymbol{\sigma}_\tau\cdot\nabla_\tau,\bar{H}^q_\tau]|n'n\rangle\langle nn'|\bar{H}^\mu_\tau|0's_{1/2}\rangle\,, \quad (8.24a)$$

$$\mathcal{M}^{2\tau}_{nn'} \equiv \langle p_{1/2}0'|[\boldsymbol{\sigma}_\tau\cdot\nabla_\tau,\bar{H}_\mu]|n'n\rangle\langle nn'|\bar{H}^q_\tau|0's_{1/2}\rangle\,. \quad (8.24b)$$

These matrix elements will be calculated in the next subsection.

8.4.4 Calculation of matrix elements

Consider the matrix elements in Eq. (8.24a). Using the identities (8.15) and (8.17a), one may separate its electronic and nuclear components as

$$\mathcal{M}^{1\tau}_{nn'} = e^2q_\tau\langle 0'|\boldsymbol{\sigma}_\tau|n'\rangle\langle n'|\boldsymbol{\mu}_\tau|0'\rangle\langle p_{1/2}|f(R)\hat{\mathbf{R}}|n\rangle\langle n|f(R)\hat{\mathbf{R}}\times\boldsymbol{\alpha}|s_{1/2}\rangle\,. \quad (8.25)$$

Note that in the product of the nuclear matrix elements we may single out the scalar term which gives dominant contribution in spinless nuclei,

$$\langle 0'|\sigma^i_\tau|n'\rangle\langle n'|\mu^j_\tau|0'\rangle = \frac{1}{3}\delta_{ij}\langle 0'|\boldsymbol{\sigma}_\tau|n'\rangle\langle n'|\boldsymbol{\mu}_\tau|0'\rangle+\dots\,, \quad (8.26)$$

where the ellipsis stands for the tensor terms which we omit in further calculations. With the use of the definition (8.11), the expression $\langle 0'|\boldsymbol{\sigma}_\tau|n'\rangle\langle n'|\boldsymbol{\mu}_\tau|0'\rangle$ reduces to the nuclear spin-flip matrix element

$$\langle 0'|\boldsymbol{\sigma}_\tau|n'\rangle\langle n'|\boldsymbol{\mu}_\tau|0'\rangle = 2\mu_0(g^s_\tau-\epsilon g^l_\tau)|\langle 0'|\mathbf{s}_\tau|n'\rangle|^2\,, \quad (8.27)$$

where In Eq. (8.27), we have taken into account the fact that for spherical nuclei, the states are usually represented in the lj-basis in which $\langle 0'|\mathbf{s}|n'\rangle\langle n'|\mathbf{j}|0'\rangle=0$ while the states of deformed nuclei are usually represented in the ls-basis with $\langle 0'|\mathbf{s}|n'\rangle\langle n'|\mathbf{l}|0'\rangle=0$.

With the use of Eqs. (8.26) and (8.27) the matrix element (8.25) may now be cast in the form

$$\mathcal{M}^{1\tau}_{nn'} = \frac{2}{3}\mu_0(g^s_\tau-\epsilon g^l_\tau)e^2q_\tau|\langle 0'|\mathbf{s}_\tau|n'\rangle|^2\langle p_{1/2}|f(R)\hat{\mathbf{R}}|n\rangle\langle n|f(R)\hat{\mathbf{R}}\times\boldsymbol{\alpha}|s_{1/2}\rangle\,. \quad (8.28)$$

Similarly, one may write the expression (8.24b) for $\mathcal{M}^2_{nn'}$ as

$$\mathcal{M}^{2\tau}_{nn'} = \frac{i}{3}e^2q_\tau\mu_0(g^s_\tau-g^l_\tau)\langle 0'|\boldsymbol{\sigma}_\tau\times\nabla_\tau|n'\rangle\langle n'|\mathbf{r}_\tau|0'\rangle\langle p_{1/2}|f(R)\hat{\mathbf{R}}\times\boldsymbol{\alpha}|n\rangle\langle n|f(R)\hat{\mathbf{R}}|s_{1/2}\rangle\,. \quad (8.29)$$

Here $\langle n'|\mathbf{r}_\tau|0'\rangle$ is the E1 nuclear transition matrix element which may be considered within the giant dipole resonance model. Effectively, this means that the sum over n' is dominated by the matrix elements $\langle n'|\mathbf{r}_\tau|0'\rangle$ which constitute the giant electric dipole resonance with the excitation energy $\Delta\bar{E}$. Then having fixed the nuclear energy in the denominator of Eq. (8.23), one might use the completeness relation for the nuclear states, $|n'\rangle\langle n'|=1$, to reduce the nuclear matrix elements in Eq. (8.29) to the expectation value of the $\mathbf{l}_\tau\cdot\mathbf{s}_\tau$ operator,

$$\langle 0'|\boldsymbol{\sigma}_\tau\times\nabla_\tau|n'\rangle\langle n'|\mathbf{r}_\tau|0'\rangle \approx -2i\langle 0'|\mathbf{l}_\tau\cdot\mathbf{s}_\tau|0'\rangle \equiv -2i\langle\mathbf{l}_\tau\cdot\mathbf{s}_\tau\rangle\,. \quad (8.30)$$

With this expression for the nuclear matrix element, Eq. (8.29) simplifies to

$$\mathcal{M}^{2\tau}_{nn'} \approx \frac{2}{3}e^2q_\tau\mu_0(g^s_\tau-g^l_\tau)\langle 0'|\mathbf{l}_\tau\cdot\mathbf{s}_\tau|0'\rangle\langle p_{1/2}|f(R)\hat{\mathbf{R}}\times\boldsymbol{\alpha}|n\rangle\langle n|f(R)\hat{\mathbf{R}}|s_{1/2}\rangle\,. \quad (8.31)$$

Substituting Eqs. (8.28) and (8.31) into Eq. (8.23), one may represent the matrix element of the effective operator (8.21) in the compact form

$$\langle p_{1/2}|H_{\rm eff}|s_{1/2}\rangle = 2\sum_{\tau=1}^{A}\xi_\tau q_\tau\mu_0\left[\sum_{n'}(g_\tau^s-\epsilon g_\tau^l)M(E_{n'})|\langle 0'|\mathbf{s}_\tau|n'\rangle|^2+(g_\tau^s-g_\tau^l)M(\Delta\bar{E})\langle 0'|\mathbf{l}_\tau\cdot\mathbf{s}_\tau|0'\rangle\right], \tag{8.32}$$

where

$$M(E)\equiv\frac{e^2}{3}\sum_n\frac{\langle p_{1/2}|f(R)\hat{\mathbf{R}}|n\rangle\langle n|f(R)\hat{\mathbf{R}}\times\boldsymbol{\alpha}|s_{1/2}\rangle}{\Delta E_n+{\rm sgn}(E_n)E}+(s_{1/2}\leftrightarrow p_{1/2})\,. \tag{8.33}$$

Note that the sum in Eq. (8.32) contains only single-particle nucleon excitations. It is instructive to separate proton (p) and neutron (n) contributions with nuclear excitation energies denoted by ΔE_p and ΔE_n as

$$\langle p_{1/2}|H_{\rm eff}|s_{1/2}\rangle = 2\mu_0\sum_{i=p,n}\xi_i q_i\left[(g_i^s-\epsilon g_i^l)M_i+(g_i^s-g_i^l)\bar{M}\langle\mathbf{l}\cdot\mathbf{s}\rangle_i\right], \tag{8.34}$$

where

$$M_p\equiv\sum_{\Delta E_p}|\langle 0'|\mathbf{s}|n'\rangle_p|^2M(\Delta E_p)\,, \tag{8.35}$$

$$M_n\equiv\sum_{\Delta E_n}|\langle 0'|\mathbf{s}|n'\rangle_n|^2M(\Delta E_n)\,, \tag{8.36}$$

$$\bar{M}\equiv M(\Delta\bar{E})\,. \tag{8.37}$$

We recall that for a free nucleon, the g-factors are $g_p^l=1$, $g_p^s=5.586$ for proton and $g_n^l=0$, $g_n^s=-3.826$ for neutron. In a nuclear medium, the g-factors should be reduced by about a factor of 0.7. The effective nucleon charge is modified by the recoil effect: $q=q_p\equiv eN/A$ for proton and $q=q_n\equiv -eZ/A$ for neutron.

8.4.5 Matrix elements of the effective Hamiltonian for some heavy atoms

In this section, we present the results of numerical calculation of the matrix element (8.34) for different heavy atoms of experimental interest including ^{138}Ba, ^{206}Pb, ^{208}Pb, ^{172}Yb, ^{174}Yb, ^{176}Yb, ^{178}Hf, ^{180}Hf, ^{226}Ra, ^{232}Th. These atoms, as parts of various paramagnetic molecules, have been considered or are proposed for consideration in recent and future eEDM experiments.

The expression (8.34) depends on different nuclear matrix elements and corresponding energies of nuclear transitions. In particular, $\langle 0'|\mathbf{s}|n'\rangle_p$ and $\langle 0'|\mathbf{s}|n'\rangle_n$ are matrix elements for nuclear spin-flip proton and neutron transitions with energies ΔE_p and ΔE_n, respectively. Since the nuclear operators we use are single-particle operators, these matrix elements and energies may be estimated within the Nilsson nuclear model [23] which takes into account single-particle excitations only. This model allows one to estimate also the expectation value of the $\mathbf{l}\cdot\mathbf{s}$ operator for proton $\langle\mathbf{l}\cdot\mathbf{s}\rangle_p$ and neutron $\langle\mathbf{l}\cdot\mathbf{s}\rangle_n$ states. The details of calculation of these matrix elements and the corresponding energies are given in Appendix 8.A, see Tables 8.5 and 8.6. These tables contain also the energies of giant dipole resonance $\Delta\bar{E}$ which enter in the last term in Eq. (8.34).

The sum over the intermediate electronic states in Eq. (8.34) is taken into account with the function (8.33) which should be evaluated for each nuclear energy. This function involves electronic bound states $|s_{1/2}\rangle$ and $|p_{1/2}\rangle$, as well as intermediate excited electronic states $|n\rangle$, which include those from the discrete spectrum and both negative and positive continua.

Owing to the fact that the function $f(R)$ peaks at the surface of the nucleus where the overlap between different bound states is small, matrix elements that involve intermediate bound states are typically orders of magnitude smaller than those coming from intermediate continuum states. The nuclear energy $\Delta E_{n'}$ (in MeV range) in the denominator of Eq. (8.23) provides further suppression of the contribution from discrete states. As a result, in the computation below, the intermediate electronic states are restricted to the continual spectra as in Refs. [19, 21]. This is in contrast with the situation in Ref. [24], where contributions of the discrete states are significantly enhanced due to small electronic energy denominators (eV range).

Note that the operators in the matrix elements in Eq. (8.34) are short-range because the function (8.13) falls off as $1/R^2$ outside the nucleus. Therefore, these matrix elements receive their main contributions from the region $0<R\ll a_B/Z^{1/3}$, where a_B is the Bohr radius. In this region, the inter-electron

interaction and screening are negligible as compared with the electron-nucleus Coulomb interaction. Therefore, the states $|s_{1/2}\rangle$ and $|p_{1/2}\rangle$ may be described by the unscreened Dirac-Coulomb wave functions which are appropriately regularized inside the nucleus; see Appendix 8.B.1 for further details.

The intermediate electronic states $|n\rangle$ in Eq. (8.33) are given by the Dirac-Coulomb wave functions in the continuous spectrum (see Appendix 8.B.2). Using these wave functions, we calculate numerically the radial integrals in the matrix elements (8.33) for each particular nuclear energy (see Appendix 8.B.3). The results of these calculations are collected in Table 8.1.

	Spherical			Deformed						
	^{138}Ba	^{206}Pb	^{208}Pb	^{172}Yb	^{174}Yb	^{176}Yb	^{178}Hf	^{180}Hf	^{226}Ra	^{232}Th
M_p/a_B	11.1	94.1	94.0	69.3	69.3	69.2	121	121	156	244
M_n/a_B	16.5	143	95.7	83.4	106	88.7	96.8	114	196	385
$\bar{M}/a_B$	1.83	10.7	10.7	4.83	4.83	4.74	5.53	5.54	16.0	18.3

Table 8.1: Numerical values for the electronic matrix elements M_p, M_n and $\bar{M}$ for several atoms of interest.

We observe that the values of $M_{p,n}$ and $\bar{M}$ generally increases with increasing nuclear charge Z. This is due to the fact that the electronic matrix element (8.33) receives the most contribution in the region near the nucleus, as can be seen from the behaviour of the function $f(R)$ in Eq. (8.13). For large Z, $Z\alpha \sim 1$ and the electronic Coulomb wave function near the nucleus is significantly enhanced due to relativistic effects, thus making $M(E)$ large.

Using the values of the nuclear matrix elements from Tables 8.5 and 8.6, and the values of the electronic matrix elements from Table 8.1, we find the matrix element (8.34) for various atoms,

$$\langle p_{1/2}|H_{\rm eff}|s_{1/2}\rangle = 2c_{s_{1/2}}c_{p_{1/2}}\frac{e\mu_0}{a_B}(\tilde{\lambda}_p\xi_p + \tilde{\lambda}_n\xi_n)\,, \tag{8.38}$$

where $c_{s_{1/2}}$ and $c_{p_{1/2}}$ are the normalization coefficients of the wave functions (8.56) and

$$\tilde{\lambda}_p = \frac{A-Z}{A}[(g_p^s - \epsilon g_p^l)M_p + (g_p^s - g_p^l)\bar{M}\langle \mathbf{l}\cdot\mathbf{s}\rangle_p]\,, \tag{8.39}$$

$$\tilde{\lambda}_n = -\frac{Z}{A}[(g_n^s - \epsilon g_n^l)M_n + (g_n^s - g_n^l)\bar{M}\langle \mathbf{l}\cdot\mathbf{s}\rangle_n]\,. \tag{8.40}$$

Numerical values of these coefficients are given in Table 8.2. Equation (8.38) represents one of the main results on this paper as it specifies the leading-order dependence of the atomic EDM (8.20) on the P,T-odd coupling constants ξ_p and ξ_n.

	^{138}Ba	^{206}Pb	^{208}Pb	^{172}Yb	^{174}Yb	^{176}Yb	^{178}Hf	^{180}Hf	^{226}Ra	^{232}Th
$\tilde{\lambda}_p/100$	0.65	7.0	7.1	3.6	3.6	3.6	5.4	5.4	11	15
$\tilde{\lambda}_n/100$	0.68	5.8	4.8	2.4	2.9	2.3	2.6	3.2	6.7	11

Table 8.2: Results of numerical calculations of coefficients $\tilde{\lambda}_p$ and $\tilde{\lambda}_n$ which specify the leading-order dependence of the matrix element (8.38) on P,T-odd coupling constants ξ_p and ξ_n.

8.5 Comparison with the contact CP-odd electron-nucleon interaction

In this section, we will compare the matrix element (8.38) with that of the contact interaction (8.2). This will allow us to determine the dependence of the coupling constant C_{SP} on the P,T-odd nuclear force coupling constants ξ_p and ξ_n. Then, employing the experimental constraint (8.1) we will determine the limits on ξ_p and ξ_n originating from the EDM experiments with paramagnetic atoms and molecules.

8.5.1 Limits on P,T-odd nuclear interaction couplings

In an atom, the contact interaction (8.2) yields the following interaction Hamiltonian between a valence electron and a nucleus [25]

$$H_{\rm cont} = \frac{iG_F}{\sqrt{2}} A C_{SP} \gamma_0 \gamma_5 \rho(\mathbf{R}) \,, \tag{8.41}$$

where γ_0 and γ_5 are the Dirac matrices and $\rho(\mathbf{R})$ is the normalized nuclear charge density. The matrix element of this operator with the $s_{1/2}$ and $p_{1/2}$ states was calculated in Ref. [11],

$$\langle p_{1/2}| H_{\rm cont} |s_{1/2}\rangle = -c_{s_{1/2}} c_{p_{1/2}} \frac{G_F C_{SP}}{10\sqrt{2}\pi} \frac{1+4\gamma}{\Gamma(2\gamma+1)^2} \frac{AZ\alpha}{R_0^2} \left(\frac{2ZR_0}{a_B}\right)^{2\gamma} , \tag{8.42}$$

where $\gamma = \sqrt{1-Z^2\alpha^2}$ is the relativistic factor.

We stress that at the atomic level the operator (8.41) describes a general contact CP-odd interaction which may originate from different fundamental CP-violating sources, such as the direct electron-nucleus interaction due to exchange by a heavy intermediate boson, nucleon EDM, QCD vacuum angle, P,T-odd nuclear forces, etc. Although contributions from different sources to the atomic EDM may partly cancel each other, complete 'accidental cancellation' does not seem to be an attractive hypothesis since the scales of such interactions are different in any reasonable model. Therefore, in this paper, we use the traditional approach in EDM studies based on the 'single-source assumption' and consider a contribution to the coupling constant C_{SP} of the interaction (41) originating from the CP-violating internucleon interaction with the Hamiltonian (3). In principle, different sources of CP-violation may be disentangled by measurements on several systems with significantly different sensitivities to distinct CP-violating parameters, see, e.g., Ref. [24].

The goal of this section is to determine the leading-order dependence of the contact interaction constant C_{SP} on the P,T-odd nuclear interaction couplings ξ_p and ξ_n. This relation appears upon equating the matrix elements (8.38) and (8.42), $\langle p_{1/2}| H_{\rm cont} |s_{1/2}\rangle = \langle p_{1/2}| H_{\rm eff} |s_{1/2}\rangle$. As a result, we find

$$C_{SP} = (\lambda_p \xi_p + \lambda_n \xi_n) \times 10^{13} {\rm cm}^{-1} \,, \tag{8.43}$$

where the dimensionless coefficients $\lambda_{p,n}$ are

$$\lambda_{p,n} = -\frac{e\mu_0}{a_B} \frac{20\sqrt{2}\pi}{G_F} \frac{\Gamma(2\gamma+1)^2}{1+4\gamma} \frac{R_0^2}{AZ\alpha} \left(\frac{a_B}{2ZR_0}\right)^{2\gamma} \tilde{\lambda}_{p,n} \times 10^{-13} {\rm cm} \,. \tag{8.44}$$

The numerical values of these coefficients may be found from the corresponding values for $\tilde{\lambda}_{p,n}$ listed in Table 8.2. We present them in Table 8.3 below.

The relation (8.43) may be used to derive limits on the couplings $\xi_{p,n}$ which follow from the experimental constraints (8.1), yielding

$$|\xi_p| < 2.2 \times 10^{-23} {\rm cm} \,, \qquad |\xi_n| < 3.0 \times 10^{-23} {\rm cm} \,. \tag{8.45}$$

Similar limits on $\xi_{p,n}$ obtained from the $^{180}{\rm HfF}^+$ experiment [26] are about an order of magnitude weaker, $|\xi_p| < 2.6 \times 10^{-22}$cm, $|\xi_n| < 4.5 \times 10^{-22}$cm.

To summarize, we have presented a mean to relate the experimentally measured quantity C_{SP} with the phenomenological parameters of the CP-odd nuclear interaction. We now proceed to express this relation in terms of the coupling constants of more fundamental CP-odd nuclear forces.

8.5.2 Relation between C_{SP} and CP-odd pion-nucleon coupling constants

The tree-level pion exchange in known to give dominant contribution to the CP-odd internucleon interaction (8.3). The authors of Refs. [13, 27] established the leading-order dependence of the constants ξ_p and ξ_n on the CP-odd pion-nucleon couplings $\bar{g}^{(0)}_{\pi NN}$, $\bar{g}^{(1)}_{\pi NN}$ and $\bar{g}^{(2)}_{\pi NN}$ as

$$\xi_p = -\xi_n = 10^{-14} g (\bar{g}^{(1)}_{\pi NN} + 0.4 \bar{g}^{(2)}_{\pi NN} - 0.2 \bar{g}^{(0)}_{\pi NN}) \, {\rm cm} \,, \tag{8.46}$$

where $g \approx 13.6$ is the strong interaction constant. Substituting this relation into Eq. (8.43) allows us to find the leading-order relation between the constant C_{SP} and CP-violating pion-nucleon couplings

$$C_{SP} = \lambda_0 \bar{g}^{(0)}_{\pi NN} + \lambda_1 \bar{g}^{(1)}_{\pi NN} + \lambda_2 \bar{g}^{(2)}_{\pi NN} \,, \tag{8.47}$$

where the numerical values of the coefficients $\lambda_0 = -0.272(\lambda_p - \lambda_n)$, $\lambda_1 = 1.36(\lambda_p - \lambda_n)$ and $\lambda_2 = 0.544(\lambda_p - \lambda_n)$ are collected in Table 8.3 for various paramagnetic atoms.

8.5.3 Relation between C_{SP} and quark chromo-EDM

In this subsection, we consider the chromo-EDM of up and down quarks denoted by $\tilde{d}_u$ and $\tilde{d}_d$, respectively. Assuming that these quantities are the only sources of CP-violating internucleon forces, the authors of Refs. [27–30] established the following relations:

$$g\bar{g}^{(0)}_{\pi NN} = 0.8\times 10^{15}(\tilde{d}_u+\tilde{d}_d)\text{cm}^{-1}\,, \tag{8.48a}$$

$$g\bar{g}^{(1)}_{\pi NN} = 4.0\times 10^{15}(\tilde{d}_u-\tilde{d}_d)\text{cm}^{-1}\,. \tag{8.48b}$$

We substitute these relations into Eqs. (8.46) and (8.47) and ignore the last term $\propto \bar{g}^{(2)}_{\pi NN}$ because its relation to the quark chromo-EDMs is not known. As a result, we find the leading-order dependence of C_{SP} on $\tilde{d}_u$ and $\tilde{d}_p$,

$$C_{SP} = (\lambda_u\tilde{d}_u+\lambda_d\tilde{d}_d)\times 10^{14}\text{cm}^{-1}\,. \tag{8.49}$$

Numerical values of the coefficients $\lambda_u = 3.84(\lambda_p-\lambda_n)$ and $\lambda_d = -4.16(\lambda_p-\lambda_n)$ are given in Table 8.3 below.

8.5.4 Relation between C_{SP} and QCD vacuum angle

The pion-nucleon coupling constants $\bar{g}^{(0)}_{\pi NN}$ and $\bar{g}^{(1)}_{\pi NN}$ may be expressed via the QCD vacuum angle $\bar{\theta}$ as (see, e.g., Refs. [8, 30–32])

$$\bar{g}^{(0)}_{\pi NN} = -15.5\times 10^{-3}\,\bar{\theta}\,, \tag{8.50a}$$

$$\bar{g}^{(1)}_{\pi NN} = 3.4\times 10^{-3}\,\bar{\theta}\,. \tag{8.50b}$$

Substituting these relations into Eq. (8.47), we may represent C_{SP} in terms of $\bar{\theta}$ as

$$C_{SP} = \lambda_\theta\times 10^{-2}\bar{\theta}\,, \tag{8.51}$$

where the value of the constant $\lambda_\theta = 0.88(\lambda_p-\lambda_n)$ is given in Table 8.3 for different atoms. In particular, with the use of the corresponding value for ^{232}Th, the experimental constraint on C_{SP} (8.1) implies

$$|\bar{\theta}| < 9\times 10^{-8}\,. \tag{8.52}$$

This constraint is almost three orders of magnitude weaker than the currently accepted one [33] which is based on the neutron EDM [34] and Hg EDM [35] experiments. However, it is comparable to the constraint on QCD vacuum angle originating from the ^{129}Xe EDM experiments [36, 37] and from constraints on the nucleon EDM [10, 11] derived from the experiments with paramagnetic molecules. This demonstrates the importance of contributions from the P,T-odd nuclear forces to the atomic EDM. For reference, we collect the limits on $\xi_{p,n}$, $\bar{g}^{(0,1,2)}_{\pi NN}$, $\tilde{d}_{u,d}$ and $\bar{\theta}$ in Table 8.4.

		λ_p	λ_n	λ_0	λ_1	λ_2	λ_u	λ_d	λ_θ
Spherical	$^{138}_{56}$Ba	-4.1	-4.3	-0.053	0.26	0.11	0.74	-0.80	0.17
	$^{206}_{82}$Pb	-3.4	-2.8	0.17	-0.83	-0.33	-2.3	2.5	-0.54
	$^{208}_{82}$Pb	-3.4	-2.3	0.29	-1.5	-0.58	-4.1	4.5	-0.95
Deformed	$^{172}_{70}$Yb	-5.6	-3.7	0.50	-2.5	-1.0	-7.1	7.7	-1.6
	$^{174}_{70}$Yb	-5.6	-4.5	0.31	-1.6	-0.62	-4.4	4.8	-1.0
	$^{176}_{70}$Yb	-5.5	-3.5	0.56	-2.8	-1.1	-7.9	8.6	-1.8
	$^{178}_{72}$Hf	-3.9	-2.2	0.47	-2.4	-0.94	-6.7	7.2	-1.5
	$^{180}_{72}$Hf	-6.9	-4.0	0.77	-3.8	-1.5	-11	-12	-2.5
	$^{226}_{88}$Ra	-2.9	-1.8	0.29	-1.4	0.58	-4.1	4.4	-0.94
	$^{232}_{90}$Th	-3.3	-2.4	0.25	-1.2	-0.50	-3.5	3.8	-0.81

Table 8.3: The results of numerical computations of λ-coefficients in Eqs. (8.43), (7.31), (7.33) and (7.36).

$\frac{\lvert\xi_p\rvert}{10^{-23}\text{cm}}$	$\frac{\lvert\xi_n\rvert}{10^{-23}\text{cm}}$	$\frac{\bar{g}^{(0)}_{\pi NN}}{10^{-9}}$	$\frac{\bar{g}^{(1)}_{\pi NN}}{10^{-9}}$	$\frac{\bar{g}^{(2)}_{\pi NN}}{10^{-9}}$	$\frac{\tilde{d}_u}{10^{-24}\text{cm}}$	$\frac{\tilde{d}_d}{10^{-24}\text{cm}}$	$\frac{\bar{\theta}}{10^{-8}}$
2.2	3.0	2.9	0.6	1.5	2.1	1.9	9

Table 8.4: Limits on $\xi_{p,n}$, $\bar{g}^{(0,1,2)}_{\pi NN}$, $\tilde{d}_{u,d}$ and $\bar{\theta}$ obtained from the ThO limit on $|C_{SP}| < 7.3 \times 10^{-10}$.

8.6 Conclusions

In this paper, we demonstrated that the eEDM experiments with paramagnetic molecules are also sensitive to the P,T-violating nuclear forces, as well as to other sources of CP violation in the hadronic sector. We considered P,T-violating internucleon interaction described by the Hamiltonian (8.4) with coupling constants $\xi_{p,n}$. We established the leading-order relation (8.43) between these couplings and the constant C_{SP} of the contact semileptonic interaction (8.2). This relation contains atom-specific coefficients $\lambda_{p,n}$ calculated numerically and presented in Table 8.3. We used this relation to place independent limits (8.45) on the coupling constants $\xi_{p,n}$ originating from the experimental constraint (8.1).

The P,T-odd nuclear interaction is described by the phenomenological Hamiltonian which may originate from different fundamental interactions. In particular, it is known [13] that this interaction may appear due to the π meson exchange between nucleons. In this case, the parameters $\xi_{p,n}$ may be expressed via the CP-odd pion-nucleon couplings as in Eq. (8.46). Then, using the known relations between the pion couplings and the quark-chromo EDMs (8.48) as well as QCD $\bar{\theta}$ angle (8.50) we relate the parameters $\xi_{p,n}$ to $\tilde{d}_{u,d}$ and to $\bar{\theta}$ as in Eqs. (8.49) and (8.51), respectively. This allows us to place limits on $\tilde{d}_{u,d}$ and $\bar{\theta}$ originating from the experimental constraint (8.1).

We stress that the limits on $\bar{g}^{(0,1,2)}_{\pi NN}$, $\tilde{d}_{u,d}$ and $\bar{\theta}$ obtained in this paper are independent from similar constraints established in our recent paper [11] because the latter were found by taking into account nucleon EDM while in this paper we consider the P,T-odd nuclear force as the origin for these relations. It is useful to compare these two results. For example, the limit on the CP-odd pion-nucleon coupling constant $\bar{g}^{(2)}_{\pi NN}$ is obtained in the present paper only, the limits on u-quark chromo-EDM $\tilde{d}_u$ are approximately the same in both papers while the constraint on $\bar{\theta}$ in Eq. (8.52) is six times weaker than the analogous one found in Ref. [11], but it is comparable to the constraint on QCD vacuum angle originating from ^{129}Xe EDM experiment [36, 37]. Of course, all these constraints on $\bar{\theta}$ are not competitive with currently accepted strongest limit $|\bar{\theta}| < 10^{-10}$ [33], obtained on the neutron EDM [34] and Hg EDM [35] experiments (see also discussion in Ref. [18]).

It is pertinent to make some comments about the accuracy of our results. All our results are based on numerical calculations of the coefficients (8.39) listed in Table 8.2. These coefficients involve both nuclear and electronic matrix elements as well as nuclear excitation energies. The electronic matrix elements in Eq. (8.33) contain radial integrals which are calculated numerically with some details given in Appendix 8.B.3. To estimate the accuracy of our numerical integration methods, we calculated similar radial integrals which are responsible for atomic energy level shifts (contributions to the Lamb shifts) due to nuclear polarizability and compared these shifts with calculated earlier values in Refs. [19, 21]. This allows us to conclude that the error in numerical calculation of electronic matrix elements does not exceed 5%. However, the main source of uncertainty is represented by nuclear matrix elements and nuclear excitation energies. In this paper, we use the single-particle nuclear shell model to estimate M1 spin-flip matrix elements and corresponding energies in heavy nuclei listed in Appendix 8.A. Using these quantities we calculated reduced transition probabilities for M1 spin-flip transitions for some nuclei (ytterbium and thorium). The results have been compared with analogous quantities calculated using sophisticated many-body methods in Ref. [38]. On the basis of this comparison we estimate the error in nuclear transition energies and matrix elements to be under 45-50%.

To conclude, we stress that the EDM-like experiments with molecules in paramagnetic state are sensitive to hadronic CP-violating parameters such as CP-odd pion-nucleon couplings, quark-chromo EDMs and QCD vacuum angle. We expect that results from the next generation of these experiments will significantly improve the limits on these parameters.

Acknowledgements

This work was supported by the Australian Research Council Grants No. DP190100974 and DP200100150 and the Gutenberg Fellowship.

8.A Nuclear energies and matrix elements

These appendices follow our calculation in Ref. [11] and are presented here to provide the reader with the details facilitating the understanding of the current paper. In the first appendix we estimate the matrix elements and corresponding energies of the nuclear M1 spin-flip single-particle transitions. The details of these computations slightly differ for (nearly) spherical and deformed nuclei. Therefore, we consider these two cases separately.

8.A.1 Spherical nuclei

In this section, we focus on the ^{208}Pb, ^{206}Pb and ^{138}Ba nuclei, which are nearly spherical, i.e., they have deformation $\delta < 0.1$. For these nuclei, proton and neutron single-particle states may be labeled as $|n, l, j, m\rangle$, where n is the oscillator quantum number, l and j are the orbital and total momentum numbers, m is magnetic quantum number. In this basis, the nuclear spin operator $\mathbf{s} = \sum_{\tau=1}^{A} \mathbf{s}_\tau$ provides transitions between fine structure doublets.

In the ^{208}Pb nucleus, the non-vanishing matrix elements of the spin operator are $\langle 5h\frac{9}{2}m|\mathbf{s}|5h\frac{11}{2}m'\rangle$ for protons and $\langle 6i\frac{11}{2}m|\mathbf{s}|6i\frac{13}{2}m'\rangle$ for neutrons (henceforth, the ground state will be put on the right side of the operator $\mathbf{s}$). The isotope ^{206}Pb receives additional contributions from the $\langle 5p\frac{1}{2}m|\mathbf{s}|5p\frac{3}{2}m'\rangle$ neutron matrix elements. For ^{138}Ba, non-vanishing proton contributions arise from the matrix elements $\langle 4d\frac{3}{2}m|\mathbf{s}|4d\frac{5}{2}m'\rangle$ and $\langle 4g\frac{9}{2}m|\mathbf{s}|4g\frac{7}{2}m'\rangle$ whereas neutron contributions come from $\langle 5h\frac{9}{2}m|\mathbf{s}|5h\frac{11}{2}m'\rangle$. All these matrix elements may be calculated using the properties of spherical spinors (see, e.g., Ref. [39]). The energies of all these transitions may be estimated with the use of Fig. 5 in Ref. [23].

In Table 8.5 below, we collect the values of reduced matrix elements squared $|\langle n'||s||0'\rangle|^2$ and the transition energies for proton and neutron transitions in ^{208}Pb, ^{206}Pb and ^{138}Ba nuclei. The matrix element with the initial magnetic quantum number m' summed over $|\langle n'|\mathbf{s}|0'\rangle|^2 \equiv \sum_{m'} |\langle n, l, j, m|\mathbf{s}|n, l, j', m'\rangle|^2$ may be calculated with the help of Wigner-Eckart theorem. The transition energy depends on the final quantum number m. When the energies are (nearly) degenerate, we give the sum over m of the matrix elements corresponding to the same energy.

The values for the nuclear radii R_0 and the energy of giant dipole resonance are calculated according to the empirical formulas:

$$R_0 = 1.2A^{1/3}\,\mathrm{fm}\,, \tag{8.53}$$

$$\Delta\bar{E} = 95A^{-1/3}(1 - A^{-1/3})\,\mathrm{MeV}\,. \tag{8.54}$$

For reference, the values of the deformation parameter δ are also presented [40, 41].

8.A.2 Deformed nuclei

For deformed heavy nuclei with $\delta > 0.1$, it is convenient to use the Nilsson basis [23, 42], wherein proton and neutron single-particle states are labeled with $|n_3, n_\perp, \Lambda, \Omega\rangle$, where n_3 and $n_\perp$ are the oscillator quantum numbers, Λ and Ω are the projections of angular and total momenta on the deformation axis. Note that $\Omega = \Lambda + \Sigma$ where Σ is the projection of the nucleon's spin on the deformation axis. The dependence of the energy levels on the deformation parameter δ in this model may be inferred from Fig. 5 in Ref. [23]. From such dependence, one may estimate the energies of the spin-flip transitions. Note that in the basis $|n_3, n_\perp, \Lambda, \Omega\rangle$, each M1 spin-flip matrix element is $\langle m'|\, s_+ \,|0'\rangle = 1$, and the corresponding energy level is doubly degenerate since each quantum number Σ corresponds to $\pm\Lambda$.

The single-nucleon spin-flip transition energies $\Delta E_{n'}$, the energies the of giant dipole resonance $\Delta\bar{E}$, the deformation parameters δ and the nuclear radii R_0 for several nuclei of interest are presented in Table 8.6.

8.B Evaluation of electronic matrix elements

In this appendix, we provide the details for the numerical calculation of the electronic matrix element (8.33). For convenience, we use the spherical basis $(\mathbf{e}_+, \mathbf{e}_-, \mathbf{e}_0)$. The components of the vectors in this basis will be labeled by the $(+, -, 0)$ subscripts. Due to spherical symmetry, Eq. (8.33) may be rewritten in terms of the '0'-component of the operators $\hat{\mathbf{R}}$ and $\hat{\mathbf{R}} \times \boldsymbol{\alpha}$

$$M(\Delta E_{n'}) = \frac{\alpha}{c_{s_{1/2}} c_{p_{1/2}}} \sum_n \frac{\langle p_{1/2}|\, f(R)\hat{\mathbf{R}}_0\, |n\rangle\, \langle n|\, f(R)(\hat{\mathbf{R}} \times \boldsymbol{\alpha})_0\, |s_{1/2}\rangle}{\Delta E_n + \mathrm{sgn}(E_n)\Delta E_{n'}} + (s_{1/2} \leftrightarrow p_{1/2})\,. \tag{8.55}$$

For further computation of the matrix elements in Eq. (7.40) the electron wave functions need to be specified.

8.B.1 The $s_{1/2}$ and $p_{1/2}$ wave functions

The valence electron $s_{1/2}$ and $p_{1/2}$ wave functions may be expressed in terms of the spherical spinors $\Omega_\mu^\kappa(\hat{\mathbf{R}})$ where μ is the magnetic quantum number and $\kappa = (l-j)(2j+1)$ as

$$|s_{1/2}\rangle = c_{s_{1/2}} \begin{pmatrix} f_{s_{1/2}}(R)\Omega_\mu^{-1}(\hat{\mathbf{R}}) \\ ig_{s_{1/2}}(R)\Omega_\mu^{1}(\hat{\mathbf{R}}) \end{pmatrix}, \tag{8.56a}$$

$$|p_{1/2}\rangle = c_{p_{1/2}} \begin{pmatrix} f_{p_{1/2}}(R)\Omega_\mu^{1}(\hat{\mathbf{R}}) \\ ig_{p_{1/2}}(R)\Omega_\mu^{-1}(\hat{\mathbf{R}}) \end{pmatrix}, \tag{8.56b}$$

where the radial wave functions $f_{s,p_{1/2}}$ and $g_{s,p_{1/2}}$ are well approximated in the region $R_0 < R \ll a_B/Z^{1/3}$ by the Bessel functions of the first kind $J_\nu(x)$ (see, e.g., [12]),

$$f_{s_{1/2}}(R) = \frac{(-1+\gamma)J_{2\gamma}(x) - \frac{x}{2}J_{2\gamma-1}(x)}{R}, \tag{8.57a}$$

$$f_{p_{1/2}}(R) = \frac{(1+\gamma)J_{2\gamma}(x) - \frac{x}{2}J_{2\gamma-1}(x)}{R}, \tag{8.57b}$$

$$g_{s_{1/2}}(R) = g_{p_{1/2}}(R) = \frac{Z\alpha J_{2\gamma}(x)}{R}, \tag{8.57c}$$

where $x \equiv \sqrt{8ZR/a_B}$.

Note that the wave functions (8.57) are the zero-energy solutions of the Dirac-Coulomb equations for a point-like nucleus. For an extended nucleus, the corresponding solution is complicated. At the current level of accuracy, it suffices to use Eqs. (7.42) as an approximation to the wave functions. For the region inside the nucleus, $0 \le R \le R_0$, the radial wave functions $f_{s,p_{1/2}}$ and $g_{s,p_{1/2}}$ may be continued as follows

$$f_{s_{1/2}}(R) = \frac{(-1+\gamma)J_{2\gamma}(x_0) - \frac{x_0}{2}J_{2\gamma-1}(x_0)}{R_0}, \tag{8.58a}$$

$$f_{p_{1/2}}(R) = \frac{R\left[(1+\gamma)J_{2\gamma}(x_0) - \frac{x_0}{2}J_{2\gamma-1}(x_0)\right]}{R_0^2}, \tag{8.58b}$$

$$g_{s_{1/2}}(R) = \frac{R}{R_0} Z\alpha J_{2\gamma}(x_0), \tag{8.58c}$$

$$g_{p_{1/2}}(R) = \frac{1}{R_0} Z\alpha J_{2\gamma}(x_0), \tag{8.58d}$$

where $x_0 \equiv \sqrt{8ZR_0/a_B}$.

Note that these functions are the approximate solutions (containing only leading terms at small distance) of the Dirac equation inside the nucleus with constant density.

8.B.2 Excited electronic states of the continuous spectrum

The excited electronic states $|n\rangle$ in the continuous spectrum may be labeled by the quantum number $\kappa = (l-j)(2j+1)$ and the energy E, $|n\rangle \equiv |E\kappa\rangle$. In spherical coordinates, these functions read (see, e.g., Refs. [43, 44]):

$$|n\rangle \equiv |E\kappa\rangle = \begin{pmatrix} f_\kappa^E(R)\Omega_\mu^\kappa(\hat{\mathbf{R}}) \\ ig_\kappa^E(R)\Omega_\mu^{-\kappa}(\hat{\mathbf{R}}) \end{pmatrix}, \tag{8.59}$$

with

$$f_\kappa^E(R) = \frac{(2pR)^\gamma e^{\pi y/2}\left|\Gamma(\gamma+iy)\right|\sqrt{|E+m_e|}}{R\sqrt{\pi p}\,\Gamma(2\gamma+1)} \mathrm{Re}[e^{-ipR+i\eta}{}_1F_1(\gamma+1+iy, 2\gamma+1, 2ipR)], \tag{8.60a}$$

$$g_\kappa^E(R) = -\mathrm{sgn}(E)\frac{(2pR)^\gamma e^{\pi y/2}\left|\Gamma(\gamma+iy)\right|\sqrt{|E-m_e|}}{r\sqrt{\pi p}\,\Gamma(2\gamma+1)} \mathrm{Im}[e^{-ipR+i\eta}{}_1F_1(\gamma+1+iy, 2\gamma+1, 2ipR)]. \tag{8.60b}$$

Here $p = \sqrt{E^2 - m_e^2}$ is the electron's momentum, $y = Z\alpha E/p$, $e^{i\eta} = \sqrt{-\frac{\kappa - iym_e/E}{\gamma + iy}}$ and ${}_1F_1(a, b, z)$ is the confluent hypergeometric function of the first kind. Note that the wave functions (8.59) are normalized as $\langle E'\kappa|E\kappa\rangle = \delta(E' - E)$.

The functions (8.60) solve for the Dirac equation with a point-like nucleus. Therefore, we will only use them for outside of the nucleus, $R > R_0$. For the inside of the nucleus, $0 \le R \le R_0$, we will consider the following continuation of these functions

$$f_\kappa^E(R) = b_1 R^l\,, \qquad g_\kappa^E(R) = b_2 R^{\tilde{l}}\,, \tag{8.61}$$

where $l = |\kappa + 1/2| - 1/2$ is the orbital angular momentum corresponding to κ, $\tilde{l} = |-\kappa + 1/2| - 1/2$ is the orbital angular momentum corresponding to $-\kappa$. The values of the coefficients b_1 and b_2 are determined by matching Eqs. (8.60) and (8.61) on the boundary of the nucleus. The wave functions (7.46) are, to the leading order, solutions to the Dirac equation inside a nucleus of a constant density.

We stress that the extension of the electronic wave functions to the inside region of the nucleus (8.61) is an approximation which is acceptable at our level of accuracy. We checked the validity of this approximation by computing the Lamb shift in heavy atoms due to nuclear polarizability. Within this approximation, we have agreement within 5% of the known results presented in Refs. [19–21].

8.B.3 Results of calculation of electronic matrix element

Substituting the wave functions (8.56) and (8.59) into Eq. (7.40) and performing the integration over angular variables, we obtain

$$M(\Delta E_{n'}) = -\frac{2\alpha}{9}\int_{m_e}^{\infty}\frac{T(E)dE}{E - E_{s_{1/2}} + \Delta E_{n'}} - \frac{2\alpha}{9}\int_{-\infty}^{-m_e}\frac{T(E)dE}{E - E_{s_{1/2}} - \Delta E_{n'}}\,, \tag{8.62}$$

where

$$T(E) = R_s^1(E)R_p^1(E) - R_s^{-2}(E)R_p^{-2}(E) - S_s^{-1}(E)S_p^{-1}(E) + S_s^2(E)S_p^2(E)\,, \tag{8.63}$$

and the radial integrals $R_{s,p}^\kappa(E)$ and $S_{s,p}^\kappa(E)$ are defined by

$$R_s^\kappa(E) \equiv \int_0^\infty \left(f_{s_{1/2}} f_\kappa^E + g_{s_{1/2}} g_\kappa^E\right) f(R) R^2 dR\,, \tag{8.64a}$$

$$R_p^\kappa(E) \equiv \int_0^\infty \left(f_{p_{1/2}} g_\kappa^E + g_{p_{1/2}} f_\kappa^E\right) f(R) R^2 dR\,, \tag{8.64b}$$

$$S_s^\kappa(E) \equiv \int_0^\infty \left(f_{s_{1/2}} g_\kappa^E + g_{s_{1/2}} f_\kappa^E\right) f(R) R^2 dR\,, \tag{8.64c}$$

$$S_p^\kappa(E) \equiv \int_0^\infty \left(f_{p_{1/2}} f_\kappa^E + g_{p_{1/2}} g_\kappa^E\right) f(R) R^2 dR\,. \tag{8.64d}$$

Here the radial function $f(R)$ is given by Eq. (8.13). Note that Eq. (8.63) involves only the terms with $\kappa = \pm 1, \pm 2$ which are allowed by the selection rules for transitions from $s_{1/2}$ and $p_{1/2}$ bound electron states.

With the radial wave functions (8.57), (8.58), (8.60) and (8.61), the radial integrals (8.64) may be computed numerically for any specific electron energy E and nuclear energy $\Delta E_{n'}$ or $\Delta\bar{E}$. For all values of $\Delta E_{n'}$ and $\Delta\bar{E}$ presented in Appendix 8.A, numerical analysis showed that for $|E| > 500m_e$, $T(E)/(E_{s_{1/2}} - E \pm \Delta E_{n'})$ is effectively zero, so the energy integrals in Eqs. (7.47) may be cut off at $|E| \approx 500m_e$. We also point out that the dominant contributions to the energy integrals (7.47) come from the region where $E \sim 50m_e$, which is larger than the values of $\Delta E_{n'}$ or $\Delta\bar{E}$ considered in Appendix 8.A. As a result, $M(\Delta E_{n'})$ is a slowly varying function of energy.

The energy integrals in Eqs. (7.47) are computed numerically, giving $M(\Delta E_{n'})$ for all values of $\Delta E_{n'}$ and $\Delta\bar{E}$ presented in Appendix A. The resulting numerical values of the electronic factors M_p, M_n and $M(\Delta\bar{E})$ are presented in Table 8.1 below.

Bibliography

[1] E. M. Purcell and N. F. Ramsey, Phys. Rev. **78**, 807 (1950).

[2] T.-D. Lee and C. N. Yang, Tech. Rep., Brookhaven National Lab., Upton, NY (1957).

[3] L. Landau, Sov. Phys. - JETP **5**, 336 (1957).

[4] L. Landau, Nuclear Physics **3**, 127 (1957).

[5] A. D. Sakharov, Sov. Phys. Usp. **34**, 392 (1991).

[6] V. Andreev, D. G. Ang, D. DeMille, J. M. Doyle, G. Gabrielse, J. Haefner, N. R. Hutzler, Z. Lasner, C. Meisenhelder, B. R. O'Leary, et al. (ACME), Nature **562**, 355 (2018).

[7] H. Loh, K. C. Cossel, M. C. Grau, K.-K. Ni, E. R. Meyer, J. L. Bohn, J. Ye, and E. A. Cornell, Science **342**, 1220 (2013).

[8] N. Yamanaka, B. Sahoo, N. Yoshinaga, T. Sato, K. Asahi, and B. Das, Eur. Phys. J. A **53**, 54 (2017).

[9] T. E. Chupp, P. Fierlinger, M. J. Ramsey-Musolf, and J. T. Singh, Rev. Mod. Phys. **91**, 015001 (2019).

[10] V. V. Flambaum, M. Pospelov, A. Ritz, and Y. V. Stadnik, Phys. Rev. D **102**, 035001 (2020).

[11] V. V. Flambaum, I. B. Samsonov, and H. B. Tran Tan, arXiv:2004.10359 (2020).

[12] I. B. Khriplovich, *Parity nonconservation in atomic phenomena* (Gordon and Breach Science Publishers, 1991).

[13] O. P. Sushkov, V. V. Flambaum, and I. B. Khriplovich, Zh. Eksp. Teor. Fiz **87**, 1521 (1984).

[14] J. Bsaisou, U.-G. Meißner, A. Nogga, and A. Wirzba, Annals Phys. **359**, 317 (2015).

[15] M. Denis and T. Fleig, J. Chem. Phys. **145**, 214307 (2016).

[16] L. V. Skripnikov, J. Chem. Phys. **145**, 214301 (2016).

[17] V. V. Flambaum, I. B. Khriplovich, and O. P. Sushkov, Nucl. Phys. A **449**, 750 (1986).

[18] V. V. Flambaum and V. A. Dzuba, Phys. Rev. A **101**, 042504 (2020).

[19] G. Plunien, B. Müller, W. Greiner, and G. Soff, Phys. Rev. A **43**, 5853 (1991).

[20] K. Pachucki, D. Leibfried, and T. W. Hänsch, Phys. Rev. A **48**, R1 (1993).

[21] G. Plunien and G. Soff, Phys. Rev. A **51**, 1119 (1995).

[22] A. V. Nefiodov, L. N. Labzowsky, G. Plunien, and G. Soff, Phys. Lett. A **222**, 227 (1996).

[23] A. Bohr and B. R. Mottelson, *Nuclear Structure*, vol. 2 (World Scientific, Singapore, 1998).

[24] T. Fleig and M. Jung, J. High Energy Phys. **2018**, 12 (2018).

[25] V. V. Flambaum and I. B. Khriplovich, Zh. Eksp. Theor. Fiz **89**, 1505 (1985).

[26] W. B. Cairncross, D. N. Gresh, M. Grau, K. C. Cossel, T. S. Roussy, Y. Ni, Y. Zhou, J. Ye, and E. A. Cornell, Phys. Rev. Lett. **119**, 153001 (2017).

[27] V. V. Flambaum, D. DeMille, and M. G. Kozlov, Phys. Rev. Lett. **113**, 103003 (2014).

[28] M. Pospelov and A. Ritz, Phys. Rev. Lett. **83**, 2526 (1999).

[29] M. Pospelov and A. Ritz, Phys. Rev. D **63**, 073015 (2001).

[30] M. Pospelov and A. Ritz, Ann. Phys. **318**, 119 (2005), special Issue.

[31] J. de Vries, E. Mereghetti, and A. Walker-Loud, Phys. Rev. C **92**, 045201 (2015).

[32] J. Bsaisou, C. Hanhart, S. Liebig, U.-G. Meissner, A. Nogga, and A. Wirzba, Eur. Phys. J. A **49**, 31 (2013).

[33] M. Tanabashi et al. (Particle Data Group), Phys. Rev. D **98**, 030001 (2018).

[34] C. Abel, S. Afach, N. J. Ayres, C. A. Baker, G. Ban, G. Bison, K. Bodek, V. Bondar, M. Burghoff, E. Chanel, et al., Phys. Rev. Lett. **124**, 081803 (2020).

[35] B. Graner, Y. Chen, E. G. Lindahl, and B. R. Heckel, Phys. Rev. Lett. **116**, 161601 (2016).

[36] N. Sachdeva, I. Fan, E. Babcock, M. Burghoff, T. E. Chupp, S. Degenkolb, P. Fierlinger, S. Haude, E. Kraegeloh, W. Kilian, et al., Phys. Rev. Lett. **123**, 143003 (2019).

[37] F. Allmendinger, I. Engin, W. Heil, S. Karpuk, H.-J. Krause, B. Niederländer, A. Offenhäusser, M. Repetto, U. Schmidt, and S. Zimmer, Phys. Rev. A **100**, 022505 (2019).

[38] P. Sarriguren, E. Moya de Guerra, and R. Nojarov, Phys. Rev. C **54**, 690 (1996).

[39] R. Szmytkowski, J. Math. Chem. **42**, 397 (2007).

[40] S. Raman, C. Nestor, and P. Tikkanen, At. Data Nucl. Data Tables **78**, 1 (2001).

[41] N. Stone, At. Data Nucl. Data Tables **90**, 75 (2005).

[42] S. G. Nilsson, Dan. Mat. Fys. Medd. **29**, 1 (1955).

[43] V. B. Berestetskii, E. M. Lifshitz, and L. P. Pitaevskii, *Quantum electrodynamics*, vol. 4 (Butterworth-Heinemann, 1982).

[44] W. Greiner, *Relativistic quantum mechanics: Wave Equations*, vol. 2 (Springer, 2000).

	Proton transitions		$\lvert\langle n'\rvert\rvert s\rvert\rvert 0'\rangle\rvert_p^2$	Neutron transitions		$\lvert\langle n'\rvert\rvert s\rvert\rvert 0'\rangle\rvert_n^2$	$\langle \mathbf{l}\cdot\mathbf{s}\rangle_p$	$\langle \mathbf{l}\cdot\mathbf{s}\rangle_n$	R_0 (fm)	$\Delta\bar{E}$ (MeV)	δ
	$[m', m]$	$\Delta E_{n'}$ (MeV)		$[m', m]$	$\Delta E_{n'}$ (MeV)						
^{138}Ba	$\lvert 4g\frac{9}{2}m'\rangle \rightarrow \lvert 4g\frac{7}{2}m\rangle$		160/9	$\lvert 5h\frac{11}{2}m'\rangle \rightarrow \lvert 5h\frac{9}{2}m\rangle$		336/13	15	21	7.11	13.3	0.05
	$\left[\frac{9}{2}, \frac{7}{2}\right], \left[\frac{7}{2}, \frac{5}{2}\right]$	4.4		$\left[\frac{5}{2}, \frac{3}{2}\right], \left[\frac{7}{2}, \frac{5}{2}\right]$ $\left[\frac{9}{2}, \frac{7}{2}\right], \left[\frac{11}{2}, \frac{9}{2}\right]$	5.3						
	$\left[\frac{5}{2}, \frac{5}{2}\right]$	4.8									
	$\left[\frac{7}{2}, \frac{7}{2}\right], \left[\frac{3}{2}, \frac{5}{2}\right]$	5.2		$\left[\frac{3}{2}, \frac{1}{2}\right]$	5.6						
	$\left[\frac{5}{2}, \frac{7}{2}\right]$	5.5		$\left[\frac{5}{2}, \frac{5}{2}\right]$	5.7						
	$\lvert 4d\frac{5}{2}m'\rangle \rightarrow \lvert 4d\frac{3}{2}m\rangle$		48/5	$\left[\frac{3}{2}, \frac{3}{2}\right], \left[\frac{7}{2}, \frac{7}{2}\right]$ $\left[\frac{9}{2}, \frac{9}{2}\right]$	5.9						
	$\left[\frac{1}{2}, \frac{1}{2}\right], \left[\frac{1}{2}, \frac{-1}{2}\right]$	2.7									
	$\left[\frac{1}{2}, \frac{3}{2}\right]$	4.0		$\left[\frac{1}{2}, \frac{1}{2}\right], \left[\frac{1}{2}, \frac{-1}{2}\right]$ $\left[\frac{5}{2}, \frac{7}{2}\right]$	6.2						
				$\left[\frac{1}{2}, \frac{3}{2}\right]$	6.3						
				$\left[\frac{3}{2}, \frac{5}{2}\right], \left[\frac{7}{2}, \frac{9}{2}\right]$	6.4						
^{206}Pb	$\lvert 5h\frac{11}{2}m'\rangle \rightarrow \lvert 5h\frac{9}{2}m\rangle$		240/11	$\lvert 6i\frac{13}{2}m'\rangle \rightarrow \lvert 6i\frac{11}{2}m\rangle$		336/13	15	22	7.09	13.3	0.03
	$\left[\frac{11}{2}, \frac{9}{2}\right]$	4.5		$\left[\frac{5}{2}, \frac{3}{2}\right]$	6.1						
	$\left[\frac{9}{2}, \frac{7}{2}\right], \left[\frac{7}{2}, \frac{5}{2}\right]$	4.6		$\left[\frac{9}{2}, \frac{7}{2}\right], \left[\frac{7}{2}, \frac{5}{2}\right]$ $\left[\frac{3}{2}, \frac{1}{2}\right], \left[\frac{1}{2}, \frac{1}{2}\right]$ $\left[\frac{1}{2}, \frac{-1}{2}\right], \left[\frac{3}{2}, \frac{3}{2}\right]$	6.2						
	$\left[\frac{5}{2}, \frac{3}{2}\right], \left[\frac{3}{2}, \frac{1}{2}\right]$	4.7									
	$\left[\frac{1}{2}, \frac{-1}{2}\right], \left[\frac{1}{2}, \frac{1}{2}\right]$ $\left[\frac{3}{2}, \frac{3}{2}\right], \left[\frac{5}{2}, \frac{5}{2}\right]$ $\left[\frac{7}{2}, \frac{7}{2}\right], \left[\frac{9}{2}, \frac{9}{2}\right]$	4.8		$\left[\frac{13}{2}, \frac{11}{2}\right], \left[\frac{11}{2}, \frac{9}{2}\right]$ $\left[\frac{1}{2}, \frac{3}{2}\right]$	6.3						
	$\left[\frac{1}{2}, \frac{3}{2}\right], \left[\frac{3}{2}, \frac{5}{2}\right]$	5.0		$\left[\frac{5}{2}, \frac{5}{2}\right], \left[\frac{7}{2}, \frac{7}{2}\right]$	6.4						
	$\left[\frac{5}{2}, \frac{7}{2}\right], \left[\frac{7}{2}, \frac{9}{2}\right]$	5.1		$\left[\frac{3}{2}, \frac{5}{2}\right], \left[\frac{5}{2}, \frac{7}{2}\right]$ $\left[\frac{9}{2}, \frac{9}{2}\right], \left[\frac{11}{2}, \frac{11}{2}\right]$	6.5						
				$\left[\frac{7}{2}, \frac{9}{2}\right]$	6.7						
				$\left[\frac{9}{2}, \frac{11}{2}\right]$	6.9						
				$\lvert 5p\frac{3}{2}m'\rangle \rightarrow \lvert 5p\frac{1}{2}m\rangle$		16/3					
				$\left[\frac{3}{2}, \frac{-1}{2}\right]$	1.4						
				$\left[\frac{1}{2}, \frac{1}{2}\right], \left[\frac{1}{2}, \frac{-1}{2}\right]$	2.0						
^{208}Pb	$\lvert 5h\frac{11}{2}m'\rangle \rightarrow \lvert 5h\frac{9}{2}m\rangle$		240/11	$\lvert 6i\frac{13}{2}m'\rangle \rightarrow \lvert 6i\frac{11}{2}m\rangle$		336/13	15	21	7.11	13.3	0.05
	$\left[\frac{11}{2}, \frac{9}{2}\right]$	4.5		$\left[\frac{5}{2}, \frac{3}{2}\right]$	6.1						
	$\left[\frac{9}{2}, \frac{7}{2}\right], \left[\frac{7}{2}, \frac{5}{2}\right]$	4.6		$\left[\frac{9}{2}, \frac{7}{2}\right], \left[\frac{7}{2}, \frac{5}{2}\right]$ $\left[\frac{3}{2}, \frac{1}{2}\right], \left[\frac{1}{2}, \frac{1}{2}\right]$ $\left[\frac{1}{2}, \frac{-1}{2}\right], \left[\frac{3}{2}, \frac{3}{2}\right]$	6.2						
	$\left[\frac{5}{2}, \frac{3}{2}\right], \left[\frac{3}{2}, \frac{1}{2}\right]$	4.7									
	$\left[\frac{1}{2}, \frac{-1}{2}\right], \left[\frac{1}{2}, \frac{1}{2}\right]$ $\left[\frac{3}{2}, \frac{3}{2}\right], \left[\frac{5}{2}, \frac{5}{2}\right]$ $\left[\frac{7}{2}, \frac{7}{2}\right], \left[\frac{9}{2}, \frac{9}{2}\right]$	4.8		$\left[\frac{13}{2}, \frac{11}{2}\right], \left[\frac{11}{2}, \frac{9}{2}\right]$ $\left[\frac{1}{2}, \frac{3}{2}\right]$	6.3						
	$\left[\frac{1}{2}, \frac{3}{2}\right], \left[\frac{3}{2}, \frac{5}{2}\right]$	5.0		$\left[\frac{5}{2}, \frac{5}{2}\right], \left[\frac{7}{2}, \frac{7}{2}\right]$	6.4						
	$\left[\frac{5}{2}, \frac{7}{2}\right], \left[\frac{7}{2}, \frac{9}{2}\right]$	5.1		$\left[\frac{3}{2}, \frac{5}{2}\right], \left[\frac{5}{2}, \frac{7}{2}\right]$ $\left[\frac{9}{2}, \frac{9}{2}\right], \left[\frac{11}{2}, \frac{11}{2}\right]$	6.5						
				$\left[\frac{7}{2}, \frac{9}{2}\right]$	6.7						
				$\left[\frac{9}{2}, \frac{11}{2}\right]$	6.9						

Table 8.5: Nuclear radii R_0, deformation parameters δ, nucleon spin-orbit expectation values $\langle \mathbf{l}\cdot s\rangle_{p,n}$, E1 giant resonance energies $\Delta\bar{E}$ and reduced matrix elements $|\langle n'||\mathbf{s}||0'\rangle_{p,n}|^2$ and energies $\Delta E_{n'}$ of M1 spin-flip transitions in some spherical nuclei of interest. The pair $[m', m]$ represents the magnetic quantum numbers of the initial and final states of the transitions. For each pair $[m', m]$, there is another pair $[-m', -m]$ with the same transition energy.

	Proton transitions		Neutron transitions		$\langle \mathbf{l}\cdot\mathbf{s}\rangle_p$	$\langle \mathbf{l}\cdot\mathbf{s}\rangle_n$	R_0 (fm)	$\Delta\bar{E}$ (MeV)	δ
	Transition	$\Delta E_{n'}$ (MeV)	Transition	$\Delta E_{n'}$ (MeV)					
^{172}Yb	$\|523\frac{7}{2}\rangle \to \|\frac{5}{2}\rangle$	4.5	$\|651\frac{3}{2}\rangle \to \|\frac{1}{2}\rangle$	3.9	10	15	6.67	14.0	0.31
	$\|532\frac{5}{2}\rangle \to \|\frac{3}{2}\rangle$	4.0	$\|642\frac{5}{2}\rangle \to \|\frac{3}{2}\rangle$	4.5					
	$\|541\frac{3}{2}\rangle \to \|\frac{1}{2}\rangle$	4.5	$\|633\frac{7}{2}\rangle \to \|\frac{5}{2}\rangle$	5.0					
	$\|404\frac{9}{2}\rangle \to \|\frac{7}{2}\rangle$	4.1	$\|505\frac{11}{2}\rangle \to \|\frac{9}{2}\rangle$	5.1					
			$\|514\frac{9}{2}\rangle \to \|\frac{7}{2}\rangle$	4.6					
^{174}Yb	$\|523\frac{7}{2}\rangle \to \|\frac{5}{2}\rangle$	4.5	$\|651\frac{3}{2}\rangle \to \|\frac{1}{2}\rangle$	3.9	10	17	6.70	14.0	0.31
	$\|532\frac{5}{2}\rangle \to \|\frac{3}{2}\rangle$	4.0	$\|642\frac{5}{2}\rangle \to \|\frac{3}{2}\rangle$	4.5					
	$\|541\frac{3}{2}\rangle \to \|\frac{1}{2}\rangle$	4.5	$\|633\frac{7}{2}\rangle \to \|\frac{5}{2}\rangle$	5.0					
	$\|404\frac{9}{2}\rangle \to \|\frac{7}{2}\rangle$	4.1	$\|505\frac{11}{2}\rangle \to \|\frac{9}{2}\rangle$	5.1					
			$\|514\frac{9}{2}\rangle \to \|\frac{7}{2}\rangle$	4.6					
			$\|512\frac{5}{2}\rangle \to \|\frac{3}{2}\rangle$	2.4					
^{176}Yb	$\|523\frac{7}{2}\rangle \to \|\frac{5}{2}\rangle$	4.5	$\|651\frac{3}{2}\rangle \to \|\frac{1}{2}\rangle$	4.2	10	13	6.72	13.9	0.29
	$\|532\frac{5}{2}\rangle \to \|\frac{3}{2}\rangle$	4.1	$\|642\frac{5}{2}\rangle \to \|\frac{3}{2}\rangle$	4.5					
	$\|541\frac{3}{2}\rangle \to \|\frac{1}{2}\rangle$	4.5	$\|633\frac{7}{2}\rangle \to \|\frac{5}{2}\rangle$	5.0					
	$\|404\frac{9}{2}\rangle \to \|\frac{7}{2}\rangle$	4.0	$\|505\frac{11}{2}\rangle \to \|\frac{9}{2}\rangle$	5.2					
			$\|512\frac{5}{2}\rangle \to \|\frac{3}{2}\rangle$	2.4					
^{178}Hf	$\|523\frac{7}{2}\rangle \to \|\frac{5}{2}\rangle$	4.4	$\|505\frac{11}{2}\rangle \to \|\frac{9}{2}\rangle$	4.2	9	13	6.75	13.8	0.26
	$\|532\frac{5}{2}\rangle \to \|\frac{3}{2}\rangle$	4.1	$\|512\frac{5}{2}\rangle \to \|\frac{3}{2}\rangle$	2.4					
	$\|541\frac{3}{2}\rangle \to \|\frac{1}{2}\rangle$	4.1	$\|633\frac{7}{2}\rangle \to \|\frac{5}{2}\rangle$	5.0					
	$\|402\frac{5}{2}\rangle \to \|\frac{3}{2}\rangle$	1.9	$\|642\frac{5}{2}\rangle \to \|\frac{3}{2}\rangle$	4.6					
	$\|411\frac{3}{2}\rangle \to \|\frac{1}{2}\rangle$	1.4	$\|631\frac{3}{2}\rangle \to \|\frac{1}{2}\rangle$	7.8					
^{180}Hf	$\|523\frac{7}{2}\rangle \to \|\frac{5}{2}\rangle$	4.4	$\|505\frac{11}{2}\rangle \to \|\frac{9}{2}\rangle$	4.2	9	17	6.80	13.8	0.25
	$\|532\frac{5}{2}\rangle \to \|\frac{3}{2}\rangle$	4.1	$\|512\frac{5}{2}\rangle \to \|\frac{3}{2}\rangle$	2.4					
	$\|541\frac{3}{2}\rangle \to \|\frac{1}{2}\rangle$	4.1	$\|624\frac{9}{2}\rangle \to \|\frac{7}{2}\rangle$	5.3					
	$\|402\frac{5}{2}\rangle \to \|\frac{3}{2}\rangle$	1.9	$\|633\frac{7}{2}\rangle \to \|\frac{5}{2}\rangle$	5.0					
	$\|411\frac{3}{2}\rangle \to \|\frac{1}{2}\rangle$	1.4	$\|642\frac{5}{2}\rangle \to \|\frac{3}{2}\rangle$	4.6					
			$\|631\frac{3}{2}\rangle \to \|\frac{1}{2}\rangle$	7.8					
^{226}Ra	$\|523\frac{7}{2}\rangle \to \|\frac{5}{2}\rangle$	4.3	$\|624\frac{9}{2}\rangle \to \|\frac{7}{2}\rangle$	5.0	12	16	7.31	13.0	0.20
	$\|514\frac{9}{2}\rangle \to \|\frac{7}{2}\rangle$	4.4	$\|615\frac{11}{2}\rangle \to \|\frac{9}{2}\rangle$	5.0					
	$\|505\frac{11}{2}\rangle \to \|\frac{9}{2}\rangle$	4.4	$\|606\frac{13}{2}\rangle \to \|\frac{11}{2}\rangle$	5.6					
			$\|761\frac{3}{2}\rangle \to \|\frac{1}{2}\rangle$	4.3					
^{232}Th	$\|651\frac{3}{2}\rangle \to \|\frac{1}{2}\rangle$	4.5	$\|752\frac{5}{2}\rangle \to \|\frac{3}{2}\rangle$	4.1	13	19	7.37	12.9	0.25
	$\|505\frac{11}{2}\rangle \to \|\frac{9}{2}\rangle$	4.2	$\|761\frac{3}{2}\rangle \to \|\frac{1}{2}\rangle$	4.0					
	$\|514\frac{9}{2}\rangle \to \|\frac{7}{2}\rangle$	4.0	$\|631\frac{3}{2}\rangle \to \|\frac{1}{2}\rangle$	1.0					
	$\|523\frac{7}{2}\rangle \to \|\frac{5}{2}\rangle$	3.7	$\|624\frac{9}{2}\rangle \to \|\frac{7}{2}\rangle$	5.0					
			$\|615\frac{11}{2}\rangle \to \|\frac{9}{2}\rangle$	4.8					
			$\|606\frac{13}{2}\rangle \to \|\frac{11}{2}\rangle$	5.4					

Table 8.6: Nuclear radii R_0, deformation parameters δ, nucleon spin-orbit expectation values $\langle \mathbf{l}\cdot\mathbf{s}\rangle_{p,n}$, E1 giant resonance energies $\Delta\bar{E}$ and matrix elements $|\langle n'|s|0'\rangle_{p,n}|^2$ and energies $\Delta E_{n'}$ of M1 spin-flip transitions in some deformed nuclei of interest.

Chapter 9

Time- and parity-violating effects of nuclear Schiff moment in molecules and solids

9.1 Overview

As mentioned in Sect. 1.2.2, experiments searching for CP-violation in atoms and molecules often attempt to measure the nuclear Schiff moment, which only arises from CP-odd nuclear forces and nucleon EDMs in a finite-sized nucleus. Experimentally, the molecular energy shifts $\Delta E \sim W_S S$ due to the Schiff moment S are measured and the value of S may be computed if the quantity W_S, which characterizes the interaction between the Schiff moment and the molecular electrons, is known. In this chapter, I present a simple method through which existing molecular computations of W_S may be refined, which will lead to more precise constraints on the nuclear Schiff moment.

As the result of my research, I have published this paper:

1. V. V. Flambaum, V. A. Dzuba and H. B. Tran Tan
   Time- and parity-violating effects of nuclear Schiff moment in molecules and solids
   Phys. Rev. A **101**, 042501 (2020), DOI: 10.1103/PhysRevA.101.042501, arXiv:1912.10620.

9.2 Abstract

We show that existing calculations of the interaction between nuclear Schiff moments and electrons in molecules use an inaccurate operator which gives rise to significant errors. By comparing the matrix elements of the accurate and imprecise Schiff moment operators, we calculated the correction factor as a function of the nuclear charge Z and presented corrected results for the T,P-violating interaction of the nuclear spin with the molecular axis in the TlF, PbO, RaO, TlCN, AcF molecules and in the ferroelectric solid $PbTiO_3$.

9.3 Introduction

The search for new interactions which violate both the time-reversal (T) and parity (P) invariances is of fundamental importance for the study of Physics beyond the Standard Model. It is well known that, among other phenomena, P,T-odd nuclear interactions give rise to the nuclear Schiff moment [1–4], which may interact with electrons and cause measurable shifts in atomic and molecular spectra.

Currently, all calculations of the interaction of nuclear Schiff moments with electrons in molecules use an operator which is only approximately correct [2, 5–11]. Although a more accurate form for this operator do exist [12], its use has not been widely adopted. In this paper, we demonstrate that the imprecise operator may lead to significant inaccuracy of the results and suggest a simple way to amend the situation.

The rest of the paper will be organized as follows. In Sect. 9.4, we give a brief review of the various forms of interaction and the problems associated with them. We will also introduce scaling factors, which

are the ratios between the matrix elements of the correct and imprecise operators. These factors may be used to correct the published results obtained from the imprecise operator. In Sect. 9.5 and 9.6, we present the analytical and numerical results for these scaling factors. Sect. 7.7 contains a short summary of our findings.

9.4 The different forms of interaction

For a pointlike nucleus, the electro-static potential produced by the Schiff moment is presented in the form [1, 3] [1]

$$\varphi_0(\mathbf{R}) = 4\pi \mathbf{S}\cdot\nabla\delta(\mathbf{R}) \,, \tag{9.1}$$

where $\mathbf{R}$ is the electron position vector from the center of the nucleus, $\delta(\mathbf{R})$ is the delta function and $\mathbf{S}$ is the nuclear Schiff moment.

Let us consider the matrix element of $-e\varphi_0$ between the electronic s and p states, which reads

$$M_0^{sp} = 4\pi \mathbf{S}\cdot\left(\nabla\psi_s^\dagger\psi_p\right)_{R\to 0} \,, \tag{9.2}$$

where $\psi_{s,p}$ are the s and p wavefunction for an electron in the potential of a point-like nucleus.

We note that although the quantity $\left(\nabla\psi_s^\dagger\psi_p\right)_{R\to 0}$ tends toward a constant value for a non-relativistic electron, it becomes infinite for a relativistic electron. This issue is resolved by considering a finite-size instead of a point-like nucleus. One solution is to simply cut off the point-like-nucleus relativistic electron wavefunction at the surface of the nucleus, obtaining

$$M_1^{sp} = 4\pi \mathbf{S}\cdot\left(\nabla\psi_s^\dagger\psi_p\right)_{R\to R_N} \,, \tag{9.3}$$

where R_N is the radius of the nucleus. However, since the variation of $\nabla\psi_s^\dagger\psi_p$ inside the nucleus is of the order of $Z^2\alpha^2$ where Z is the nuclear charge and α is the fine-structure constant, formula (9.3) does not give reliable results in the case of a heavy nucleus.

Another approach is to use, for the wavefunctions $\psi_{s,p}$, the correct solutions to the Dirac equation with the potential from a finite-size nucleus. Although in this case, the quantity $\left(\nabla\psi_s^\dagger\psi_p\right)_{R\to 0}$ is finite, using Eq. (9.2) to calculate the matrix element is logically inconsistent (since Eq. (9.2) corresponds to the Schiff moment being placed at the center of the nucleus) and may give imprecise results. Unfortunately, this approach in used in all molecular calculations of the effects of nuclear Schiff moments.

A more accurate formula for the potential produced by the nuclear Schiff moment was derived in Ref. [12]

$$\varphi_2(\mathbf{R}) = \frac{3\mathbf{S}\cdot\mathbf{R}}{B} n(R) \,, \tag{9.4}$$

where $B = \int n(R)\, R^4 dR \approx R_N^5$ and $n(R)$ is nuclear charge density. This formula correspond to a constant electric field $\mathbf{E} = -\nabla\varphi_2$ produced by the Schiff moment at the center of the nucleus and zero field outside the nucleus. Here, we see that the actual interaction with the Schiff moment potential vanishes at the center of the nucleus which explains why placing the Schiff moment at the center of the nucleus as in Eq. (9.2) is not reasonable. However, all molecular calculations used Eq. (9.2).

The corresponding matrix element of $-e\varphi_2$ between s and p waves is given by

$$M_2^{sp} = \frac{3\mathbf{S}}{B}\cdot\int \psi_s^\dagger \mathbf{R}\psi_p n(R)\, d^3R \,, \tag{9.5}$$

where $\psi_{s,p}$ is the electron wavefunction corresponding to a finite-size nucleus.

As we will show below, compared to the correct formula (9.5), Eqs. (9.2) and (9.3) give rise to errors as large as 20%, which may compromise the reliability of otherwise very accurate atomic and molecular calculations. In this paper, we present a solution to this problem. We provide the numerical values for the ratios of the matrix elements

$$r^{sp}_{\text{center}} = \left|\frac{M_0^{sp}}{M_2^{sp}}\right| \quad \text{and} \quad r^{sp}_{\text{surface}} = \left|\frac{M_1^{sp}}{M_2^{sp}}\right| \,, \tag{9.6}$$

which can be used to simply rescale any result involving the matrix elements (9.2) and (9.3) to the correct value which involves the matrix element (9.5).

[1] Ref. [1] considered the effects of proton electric dipole moment whereas Ref. [3] consider the effects of P,T-odd nuclear forces which give a bigger contribution to the Schiff moment.

9.5 Analytical results

The matrix element (9.2) may be written as [12]

$$M^{sp}_{\text{center}} = 3e\mathbf{S}\cdot\langle s|\,\mathbf{n}\,|p\rangle\,\frac{U_{sp}(R)}{R}\bigg|_{R\to 0}\,, \tag{9.7}$$

where $\mathbf{n}=\mathbf{R}/R$, $\langle s|\,\mathbf{n}\,|p\rangle = \int \Omega_s^\dagger \mathbf{n}\Omega_p \sin\theta d\theta d\phi$ and $U_{sp}(R) = f_s(R)\,f_p(R) + g_s(R)\,g_p(R)$. Here, $f_{s,p}$ and $g_{s,p}$ are the upper and lower component of the electron wave function.

Similarly, the matrix element (9.3) may be written as

$$M^{sp}_{\text{surface}} = 3e\mathbf{S}\cdot\langle s|\,\mathbf{n}\,|p\rangle\,\frac{U_{sp}(R)}{R}\bigg|_{R\to R_N}\,, \tag{9.8}$$

and the matrix element (9.5) as

$$M^{sp}_{\text{body}} = \frac{15\mathbf{S}}{R_N^5}\cdot\langle s|\,\mathbf{n}\,|p\rangle\int U_{sp}nR^3dR\frac{15\mathbf{S}}{R_N}\cdot\langle s|\,\mathbf{n}\,|p\rangle\int_0^1 U_{sp}(x)\,x^3dx\,, \tag{9.9}$$

where we have, for simplicity, assumed that the nucleus has a sharp surface, i.e., $n(R-R_N)=\theta(R_N-R)$ where θ is the Heaviside function. A more accurate numerical calculation will be performed in the next section. We found that the difference is insignificant.

Using Eqs. (9.7), (9.3) and (9.5), we may write

$$r^{sp}_{\text{center}} = \frac{U_{sp}(R)/R|_{R\to 0}}{\frac{5}{R_N}\int_0^1 U_{sp}(x)\,x^3dx}\,, \tag{9.10a}$$

$$r^{sp}_{\text{surface}} = \frac{U_{sp}(R)/R|_{R\to R_N}}{\frac{5}{R_N}\int_0^1 U_{sp}(x)\,x^3dx}\,. \tag{9.10b}$$

The analytical form of the functions $U_{sp_{1/2}}$ and $U_{sp_{3/2}}$ for a finite nucleus may be taken from Ref. [12]. They read[2]

$$U_{sp_{1/2}}(x) \sim R_N x\left\{1-\frac{3}{5}(Z\alpha)^2x^2\left[1-\frac{3}{14}x^2+\frac{2}{135}x^4\right]+\frac{81}{560}(Z\alpha)^4x^4\right\}\,, \tag{9.11a}$$

$$U_{sp_{3/2}}(x) \sim x\left\{1-\frac{9}{20}(Z\alpha)^2x^2\left[1-\frac{69}{315}x^2+\frac{1}{63}x^4\right]+\frac{243}{2800}(Z\alpha)^4x^4\right\}\,, \tag{9.11b}$$

which, upon insertion into Eqs. (9.10a) and (9.10b), give

$$r^{sp_{1/2}}_{\text{Center}} \approx \frac{1}{1-0.361(Z\alpha)^2+0.08(Z\alpha)^4}\,, \tag{9.12a}$$

$$r^{sp_{1/2}}_{\text{Surface}} \approx \frac{1-0.480(Z\alpha)^2+0.145(Z\alpha)^4}{1-0.361(Z\alpha)^2+0.08(Z\alpha)^4}\,, \tag{9.12b}$$

$$r^{sp_{3/2}}_{\text{Center}} \approx \frac{1}{1-0.270(Z\alpha)^2+0.05(Z\alpha)^4}\,, \tag{9.12c}$$

$$r^{sp_{3/2}}_{\text{Surface}} \approx \frac{1-0.359(Z\alpha)^2+0.09(Z\alpha)^4}{1-0.270(Z\alpha)^2+0.05(Z\alpha)^4}\,. \tag{9.12d}$$

The plots of these ratios as functions of the nuclear charge Z are shown in Fig. 9.1.

As can be observed from these plots, for small Z, the ratio r^{sp}_{center} and r^{sp}_{surface} tend to unity which indicates that formulae (9.2) and (9.3) give reasonable estimates of the correct matrix elements. However, for large Z, the formula (9.2) presented an overestimate whereas the formula (9.3) presents an underestimate of the result.

[2] Because we calculate ratios of the matrix elements, the normalization of these functions is not important. These functions are calculated to the fourth order of $Z\alpha$, which provides sufficient accuracy, as can be seen from numerical calculations described in the next section.

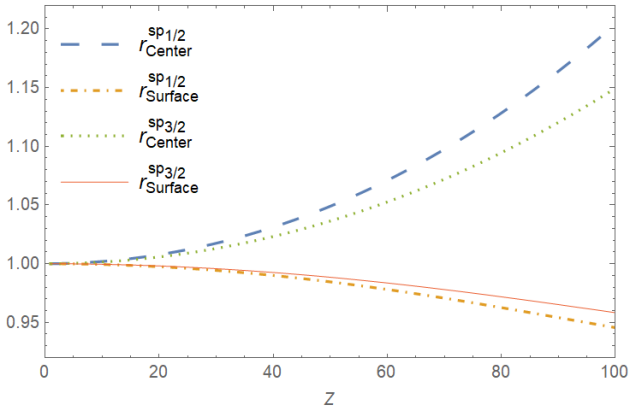

Figure 9.1: Ratios of the matrix elements of at-the-center (9.2), on-the-surface (9.3) and finite-size (9.5) nucleus Schiff moment potentials as functions of the nuclear charge Z. The results are presented separately for $sp_{1/2}$ and $sp_{3/2}$ matrix elements.

Also, the approximation (9.3) which corresponds to placing the Schiff moment on the surface of the nucleus appears to have a better accuracy (error $\leq 5\%$) than the approximation (9.2) which places the Schiff moment at the center of the nucleus (error may be as large as 20%). The surface formula (9.3) give a better accuracy since the accurate potential (9.4) is zero at the center of the nucleus and has a maximum closer to the nuclear surface.

9.6 Numerical calculation

In this section, we provide the numerical results of our calculations for the ratio $r^{sp}_{\rm center}$ in several atoms and molecules of interest. Since the surface formula (9.3) is not commonly used in molecular calculations, and since the inaccuracy associated with it is not severe (less than 5%), we do not evaluate the correction factor $r^{sp}_{\rm surface}$. We use the obtained $r^{sp}_{\rm center}$ ratios to adjust the existing results of the interaction constant W_S for the effective T,P-odd interaction in molecules defined by

$$H^{T,P}_{\rm eff} = W_S \mathbf{S}\cdot\hat{\mathbf{n}} \tag{9.13}$$

where $\hat{\mathbf{n}}$ is the unit vector along the molecular axis[3].

For numerical calculations we use a standard Fermi distribution for $n\,(R)$ [13, 14]

$$n\,(R) = \frac{a}{1+\exp\frac{R-R_N}{\delta}}. \tag{9.14}$$

where a is a normalization constant chosen fixed by the condition $\int n dV = Z$ and δ is the nuclear skin thickness, $\delta \approx \delta_0/4\ln 3$, δ_0 =2.3 fm.

Note that a good compromise between (9.1) and (9.4) can be achieved if the delta function in (9.1) is replaced by Fermi distribution (9.14). The difference in the results in this case is reduced to just a few percent.

Numerical calculations of the correction factors may be done at the relativistic Hartree-Fock-Dirac (HFD) level. At this level the matrix elements of the Schiff moment operator for higher waves (beyond s and p) are practically zero. All many-body corrections may be formally expressed as (infinite) sums of the HFD matrix elements.

To check the role of the many-body effects we use the so-called random-phase approximation (RPA). The RPA equations present a linear response of the Hartree-Fock-Dirac atomic states to a perturbation by an external field. They can be written in a form

$$(H_0-\epsilon_c)\delta\psi_c = -(F+\delta V^F)\psi_c. \tag{9.15}$$

Here H_0 is the relativistic Hartree-Fock-Dirac Hamiltonian, ψ_c is the HFD electron state in the core, $\delta\psi_c$ is the correction to the HFD state in the core induced by the external field F given by (9.1) or (9.4),

[3]Some older molecular calculations presented the constant $X = W_S/6$.

Z	Atom	$r^{sp_{1/2}}_{\rm center}$ (n.)	$r^{sp_{1/2}}_{\rm center}$ (a.)	$r^{sp_{3/2}}_{\rm center}$ (n.)	$r^{sp_{3/2}}_{\rm center}$ (a.)
70	Yb	1.11	1.10	1.09	1.07
81	Tl	1.15	1.13	1.11	1.10
80	Pb	1.15	1.13	1.12	1.09
88	Ra	1.18	1.16	1.13	1.12
89	Ac	1.18	1.16	1.14	1.12
90	Th	1.19	1.16	1.14	1.12

Table 9.1: Numerical values (n.) of the ratios of the sp matrix elements with operators (9.1) and (9.4); $r^{sp_{1/2}}_{\rm center} = \left|\langle s_{1/2}|\,\phi_0\,|p_{1/2}\rangle\,/\,\langle s_{1/2}|\,\phi_2\,|p_{1/2}\rangle\right|$ and $r^{sp_{3/2}}_{\rm center} = \left|\langle s_{1/2}|\,\phi_0\,|p_{3/2}\rangle\,/\,\langle s_{1/2}|\,\phi_2\,|p_{3/2}\rangle\right|$. For comparison, the values obtained from the analytical (a.) formulae (9.12a) and (9.12c) are also presented.

Molecule	W_S (p.)	Ref.	$\bar{r}^{sp}$	W_S (c.)
$PbTiO_3$	30270	[10]	1.14	26670
PbO	44400	[10]	1.14	39119
TlF	14000	[2]	1.13	12400
TlF	46458	[5]	1.13	41113
TlF	52482	[6]	1.13	46444
TlF	45810	[7]	1.13	40539
AcF	160000	[15]	1.16	140000
RaO	45192	[8, 9]	1.16	39127
ThO	45000	[15]	1.17	39000
TlCN	7150	[11]	1.13	6327

Table 9.2: The interaction constants $W_S = 6X$ between the nuclear Schiff moment and the molecular axis. Published values (p.) were obtained with the (9.1) operator. Corrected values (c.) are obtained by dividing the published results by the factor $\bar{r}^{sp} = \left(r^{sp_{1/2}}_{\rm center} + r^{sp_{3/2}}_{\rm center}\right)/2$. All values of W_S are given in a.u.

δV^F is the correction to the self-consistent HFD potential due to the corrections to all core states. Index c numerates states in the core. RPA equations (9.15) are solved self-consistently for all states in the core. It turns our that in spite of the fact that the RPA corrections increase matrix elements significantly, their ratio for the operators (9.1) and (9.4) in Hartree-Fock-Dirac and RPA approximations is practically the same.

9.6.1 Results of atomic calculations

The results of atomic calculations for the ratios $r^{sp_{1/2}}_{\rm center}$ and $r^{sp_{3/2}}_{\rm center}$ are presented in Table 9.1. For comparison, the values obtained from Eqs. (9.12a) and (9.12c) are also presented. It is observed that the analytical formulae (9.12) give results which are in good agreement with numerical calculations.

The published and corrected values for the interaction constant W_S of the effective T,P-odd interaction between the molecular electrons and the nuclear Schiff moments for several molecules are presented in Table 9.2. Note that we have taken the scaling factor as an average of $r^{sp_{1/2}}_{\rm center}$ and $r^{sp_{3/2}}_{\rm center}$, $\bar{r}^{sp} = \left(r^{sp_{1/2}} + r^{sp_{3/2}}\right)/2$. Indeed, the expansion of molecular orbitals over atomic orbitals centered at a heavy atom contains both $p_{1/2}$ and $p_{3/2}$ components. Because the factors $r^{sp_{1/2}}$ and $r^{sp_{3/2}}$ are close in value, the exact values of the weighting coefficients before the two components are not important.

9.7 Conclusion

We showed in this paper how the use of an imprecise form for the interaction between the nuclear Schiff moment and the atomic and molecular electrons overestimates the results of molecular calculations up to 20%. We provided the analytical formulae tested by the numerical calculations for the ratio between the electronic matrix elements using the correct and imprecise operators. We presented the corrected results for all existing molecular calculations. Our scaling factors may be used to obtain correct results in future molecular calculations using existing computer codes.

Acknowledgements

This work was supported by the Australian Research Council and the Gutenberg Fellowship.

Bibliography

[1] P. G. H. Sandars, Phys. Rev. Lett. **19**, 1396 (1967).

[2] E. A. Hinds and P. G. H. Sandars, Phys. Rev. A **21**, 471 (1980).

[3] O. Sushkov, V. Flambaum, and I. Khriplovich, Sov. Phys. - JETP **60**, 1521 (1984).

[4] V. Flambaum, I. Khriplovich, and O. Sushkov, Nucl. Phys. A **449**, 750 (1986), ISSN 0375-9474.

[5] F. A. Parpia, J. Phys. B **30**, 3983 (1997).

[6] H. M. Quiney, J. K. Laerdahl, K. Fægri, and T. Saue, Phys. Rev. A **57**, 920 (1998).

[7] A. N. Petrov, N. S. Mosyagin, T. A. Isaev, A. V. Titov, V. F. Ezhov, E. Eliav, and U. Kaldor, Phys. Rev. Lett. **88**, 073001 (2002).

[8] V. V. Flambaum, Phys. Rev. A **77**, 024501 (2008).

[9] A. D. Kudashov, A. N. Petrov, L. V. Skripnikov, N. S. Mosyagin, A. V. Titov, and V. V. Flambaum, Phys. Rev. A **87**, 020102 (2013).

[10] L. V. Skripnikov and A. V. Titov, J. Chem. Phys. **145**, 054115 (2016).

[11] A. V. Kudrin, A. Zaitsevskii, T. A. Isaev, D. E. Maison, and L. V. Skripnikov, Atoms **7** (2019).

[12] V. V. Flambaum and J. S. M. Ginges, Phys. Rev. A **65**, 032113 (2002).

[13] R. Hofstadter, H. R. Fechter, and J. A. McIntyre, Phys. Rev. **92**, 978 (1953).

[14] B. Hahn, D. G. Ravenhall, and R. Hofstadter, Phys. Rev. **101**, 1131 (1956).

[15] V. V. Flambaum and V. A. Dzuba, arXiv:1912.03598 (2019).

Chapter 10

Conclusions

In this thesis, I explored two new methods for detecting axions in a laboratory, which is important for the direct detection of Dark Matter.

I demonstrated that by using the axion-photon interference in resonant absorption by atoms and molecules, one may achieve axion signals that are linear in the axion-normal matter coupling constants. This is in stark contrast with conventional Dark Matter searches whose signals are quadratic or quartic in the underlying coupling constants. As a result, the projected sensitivity of the proposed scheme is at least an order of magnitude better than those of existing laboratory-based axion experiments.

I also considered a scheme which uses the forward scattering of photons on atoms in media to produce axions. The axion production rate of this method is proportional to the axion-electron coupling constant squared, g_{aee}^2, in contrast with conventional photon-axion conversion process, e.g., ALPS and ALPS-II, whose rate is proportional to the axion-photon coupling constant squared, $g_{a\gamma\gamma}^2$. This gives a possibility to measure a different coupling constant.

I also investigated several different methods to circumvent the Schiff's screening theorem and gain direct access to the electric dipole moments of nuclei. This is particularly useful since direct measurements of nuclear electric dipole moments provide information about CP-violation in the hadronic section, the knowledge of which will, in turn, contribute to solving the apparent matter-antimatter asymmetry in the universe.

A static external electric field is completely screened by atomic electrons from reaching the atomic nucleus. I studied the mechanism which allows the penetration of an external oscillating electric field inside atom or molecule. If the field's frequency is not in resonance with any atomic or molecular level, the field is only partially screened. On the other hand, if resonance happens then there is a strong enhancement of the field on the nucleus.

I then considered the effects produced by oscillating CP-odd nuclear moments in atoms and molecules. In particular, I showed that an oscillating nuclear electric dipole moment, when coupled with an oscillating electric field with the same frequency can give rise to observable nuclear spin precession. I also showed that oscillating nuclear electric dipole moments, Schiff moments and magnetic quadrupole moments can induce observable transitions in atoms and molecules. This provides a method for studying axion Dark Matter.

Finally, I studied the effect of the combined electric and magnetic electron-nucleon interaction, which gives rise to atomic and molecular EDMs. As a result, I was able to place independent constraints on various hadronic CP-violating parameters including the nucleon electric dipole moments, the coupling constants of the CP-odd nuclear forces, the CP-odd pion-nucleon coupling constants, the quark chromo-EDMs as well as the QCD vacuum angle.